



UNIVERSIDAD DE CHILE
FACULTAD DE CIENCIAS FÍSICAS Y MATEMÁTICAS
DEPARTAMENTO DE GEOLOGÍA

**STRATIGRAPHY, SEDIMENTOLOGY AND GEOCHRONOLOGY OF THE TONEL,
PURILACTIS AND BARROS ARANA FORMATIONS IN THE SALAR DE ATACAMA
BASIN (22°30'-23°S), CHILE**

TESIS PARA OPTAR AL GRADO DE MAGÍSTER EN CIENCIAS MENCIÓN GEOLOGÍA

MEMORIA PARA OPTAR AL TÍTULO DE GEÓLOGO

SEBASTIÁN ANDRÉS BASCUÑÁN HUGHES

PROFESOR GUÍA:
JACOBUS PHILIPPUS LE ROUX

MIEMBROS DE LA COMISIÓN:
CÉSAR ARRIAGADA ORTEGA
REYNALDO CHARRIER GONZÁLEZ
FERNANDO BARRA PANTOJA

SANTIAGO DE CHILE
MAYO 2014

Resumen

La Cuenca del Salar de Atacama, ubicada en la Región de Antofagasta, en el norte de Chile, posee un registro estratigráfico y estructural completo desde el Cretácico Tardío hasta el presente. Aunque se han realizado bastantes trabajos respecto a su sedimentología y estructura, las formaciones del Cretácico Tardío aún mantienen preguntas importantes respecto a sus orígenes y el alzamiento de la Cordillera de Domeyko y el desarrollo de la Fase Peruana.

En esta tesis, se realizaron cerca de 4000 m de columnas estratigráficas de alto detalle de las formaciones Tonel, Purilactis y Barros Arana, de manera de constreñir sus ambientes deposicionales y los pulsos tectónicos presentes durante su deposición. Once muestras fueron tomadas para análisis de conteo modal y siete para análisis U-Pb de circones detríticos.

La Formación Tonel presenta una transición desde sedimentos aluviales a flujos efímeros (Miembros Agua Salada y La Escalera) y evaporitas (Miembro Arcoiris), indicando denudación y erosión de sucesiones Permo-Triásicas, y un incremento progresivo de espacio de acomodamiento, relacionado a un incremento de subsidencia. La Formación Purilactis comienza con areniscas pertenecientes a llanuras de ríos trenzados distales y ríos de lechos arenosos (Miembro Los Cóndores). Le siguen conglomerados granocrecientes y areniscas de origen aluvial y fluvial proximal con un pequeño ciclo granodecreciente hacia su techo (Miembro Limón Verde). Posteriormente se observa un pequeño ciclo granocreciente, una sucesión granodecreciente y, hacia el techo, un ciclo granocreciente (Miembros Lampallar, Licán y Pajarito), que contienen areniscas de ríos de lechos arenosos y conglomerados de ríos trenzados. Los ciclos granocrecientes sugieren disminución del espacio de acomodamiento, debido a una menor actividad tectónica y progradación de abanicos, mientras que los ciclos granodecrecientes indican lo contrario. Un período de quiescencia tectónica y aridez está marcado por facies fluviales finas y facies eólicas (Miembro Vizcachita), mientras que los depósitos conglomerádicos y fluviales que le siguen (Miembros Seilao y Rio Grande) indican un breve retorno de actividad tectónica, seguido de denudación, y, finalmente, otro pulso tectónico. La sobreyacente Formación Barros Arana muestra menor espacio de acomodamiento y a la progradación de abanicos aluviales, con pequeños pulsos tectónicos. El tamaño promedio de los clastos aumenta en las unidades más jóvenes, indicando mayor cercanía a la fuente, lo que se confirma con la presencia de clastos de granitoides de grano grueso en las secciones superiores. Esto indica, junto a direcciones de paleocorrientes hacia el este-noreste, a la Cordillera de Domeyko como posible fuente. Los estudios de proveniencia de conteo modal muestran que la fuente es probablemente un arco magmático posiblemente asociado a una temprana presencia de basamento levantado.

Las dataciones U-Pb de circones detríticos de arrojan una edad entre 107 y 83.6 Ma para la Formación Tonel y parte inferior de la Formación Purilactis, y 79 a 65 Ma para la mayoría de la Formación Purilactis y la Formación Barros Arana. Las fuentes de sedimentos se encuentran más al oeste de lo que indicaban estudios anteriores, evidenciando la compresión del margen continental. Se observa que la Fase Peruana se subdivide en una fase “temprana”, con la deposición de la Formación Tonel y el Miembro Los Cóndores, que evidencia la deformación y levantamiento de la Cordillera de la Costa, y una fase “tardía”, reflejado en la deposición de las unidades restantes y un salto al este del frente de deformación al área de la Cordillera de Domeyko.

La falta de discordancias locales o regionales obvias, o deformación progresiva, indican que las formaciones estudiadas fueron posiblemente depositadas en una zona de ‘foredeep’ (¿proximal?) de una cuenca de antepaís, donde los distintos aportes son el resultado de la inversión de cuencas preexistentes. La subsidencia fue posiblemente el principal factor que controló la deposición de las gravas, y las facies reconocidas sugieren que el paleoclima fue árido a semi-árido, aunque definitivamente más húmedo que las condiciones actuales.

Debido a su aparente génesis en común, se propone crear el Grupo Muriacala para reunir las formaciones del Cretácico Superior.

Abstract

The Salar de Atacama Basin, located in the Antofagasta Region of northern Chile, has a complete stratigraphic and structural record from the Late Cretaceous to recent times. Although much work has been done with regard to its sedimentology and structure, the mid- to Late Cretaceous formations still present important questions about their origins, the uplift of the Cordillera de Domeyko and the unraveling of the Peruvian Phase.

In this thesis, high-resolution stratigraphic sections of the Tonel, Purilactis and Barros Arana Formations (around 4000 m) were measured in order to better constrain the depositional environment and tectonic regime during their deposition. Eleven samples were taken for point counting analysis and seven for U-Pb detrital zircon data.

The Tonel Formation presents a transition from alluvial sediments to ephemeral floods (Agua Salada and La Escalera Members) and evaporites (Arcoiris Member), indicating denudation and erosion of Permian-Triassic successions and an increase in accommodation space due to increased subsidence. The Purilactis Formation starts with sheetflood sandstones belonging to distal braid-plains and sand-bed rivers (Los Cóndores Member). It is followed by alluvial and proximal fluvial, coarsening-upward conglomerates and sandstones with a fining-upward cycle towards the top, which presents two small-scale cycles (Limón Verde Member). The column continues with a small coarsening-upward cycle, a fining-upward succession and another coarsening-upward cycle towards the top (Lampallar, Licán and Pajarito Members), containing sandstones related to sand-bed rivers and conglomerates deposited in braided rivers. The coarsening-upward cycles suggest a lack of accommodation space, related to decreased tectonic activity and fan progradation, whereas the fining-upward cycle shows the contrary. Eolian and fine-grained fluvial facies (Vizcachita Member) indicate tectonic quiescence and aridity, while conglomerates and distal, fluvial to lacustrine deposits (Seilao and Rio Grande Members) indicate brief tectonic renewal, followed by denudation, and finally a return of tectonic activity. The overlying Barros Arana Formation signals decreased accommodation space and alluvial fan progradation, with small tectonic pulses. The average clast size increases upward in the sections observed, indicating an overall closer proximity to the uplifted source. The increasing presence of coarse granitoid clasts in the upper sections also indicates deep exhumation of the source area; this, together with paleocurrent directions indicating an east-northeastward transport, confirms the Cordillera de Domeyko as the possible source for these sediments. The point counting provenance studies show a magmatic arc provenance for the samples, possibly mixed with early basement uplift.

The U-Pb detrital zircon data show that the Tonel Formation and the lower Purilactis Formation were deposited between 107-83.6 Ma, while the upper Purilactis and Barros Arana Formations were deposited between 79-65 Ma. The sources are located farther to the west than expected, and reflect compression of the entire margin. The Peruvian Phase can be split into an “early” phase, with deposition of the Tonel Formation and the Los Cóndores Member, showing the uplift of the Cordillera de la Costa area, and a “later” phase showing the deposition of the remaining units and an eastward jump of the deformation front to the Cordillera de Domeyko area.

The lack of obvious regional or local unconformities, or progressive deformation, indicates that the studied formations were probably deposited in the (proximal?) foredeep zone of a foreland basin, where the appearance of different sources is the result of the inversion of previous basins. Subsidence was probably the main controlling factor during gravel deposition, and the facies suggest that the paleoclimate was arid to semi-arid, though more humid than present-day conditions.

Due to their apparently related origin, the Group Muriacala is proposed for the Upper Cretaceous formations.

INDEX

I INTRODUCTION	1
I.1 Andean tectonics in northern Chile.....	2
I.2 Geological setting and Cretaceous stratigraphy of the Salar de Atacama Basin	5
I.3 Stratigraphic definition and age of the Tonel, Purilactis and Barros Arana Formations	12
I.4 Late Cretaceous basins in northern Chile	15
I.5 Remaining questions in the Barros Arana Syncline.....	15
I.6 Objectives of this thesis	16
I.7 Hypotheses.....	16
I.8 Proposed methodology.....	16
II METHODOLOGY	18
II.1 Sedimentology and stratigraphy	18
II.1.1 Lithofacies model	19
II.2 Tectonic cycle interpretation	21
II.3 Clast counts	22
II.4 Paleocurrent data	22
II.5 Sediment provenance.....	24
II.6 U-Pb detrital zircon geochronology.....	25
III RESULTS	27
III.1 Sedimentology and stratigraphy.....	27
III.2 Paleocurrent data.....	52
III.3 Conglomerate clast count.....	55
III.4 Sediment provenance	56
III.5. Detrital U-Pb geochronology	59
IV DISCUSSION	67
V CONCLUSIONS	77
VI REFERENCES	79

INDEX OF FIGURES

Figure I. 1. Summary and comparison of tectonic and sedimentary evolution proposed for the Salar de Atacama Basin and Cordillera de Domeyko Area.	4
Figure I. 2. Tectonic evolution of the Cordillera de Domeyko area (~23°S) since the Late Jurassic. Modified from Amilibia <i>et al.</i> (2008).	5
Figure I. 3. Regional pre-Neogene geological map for northern Chile. Modified from SERNAGEOMIN (2003) and Arriagada <i>et al.</i> (2003).	9
Figure I. 4: a) Map of the western margin of South America, showing the location of the simplified tectonic map. b) Morphotectonic domains after Amilibia <i>et al.</i> (2008). c) Geographic map, with stars showing towns and cities. Study area is enclosed in the white rectangle.....	10
Figure I. 5. Geological map of the study area, showing the location of the U-Pb samples and the columns profiled. Modified from Henríquez (in prep.).	11
Figure I. 6. Evolution of the stratigraphic knowledge and terminology of the Cretaceous to Paleogene successions of the Salar de Atacama area. Modified from Arriagada (1999).....	14
Figure II. 1. Facies and outcrops observed in this study: a) Planar cross-stratified conglomerates (Gpt). b) Imbricated, horizontally stratified conglomerates (Gch). c) Burrows found in laminated sandstones (Sh). e) Trough cross-stratified sandstones. f) Horizontally stratified, clast-supported conglomerates (Gch) intercalated with medium- to coarse-grained sandstones (Sl).....	18
Figure II. 2. Fluvial styles, showing facies and fining-upward cycles (shown by arrows), observed in this study. Numbers indicate bounding surface order, not discussed here (See Miall, 1985; 1996). Adapted from Miall (1996).....	20
Figure II. 3. Schematic summary of the basin-filling process. The evolution is from top to bottom; the red star indicates a fixed position within the basin. The cartoon shows how loading produces fine-grained deposits, while coarse-grained deposits are produced as a consequence of unloading or tectonic quiescence. An overall coarsening-upward style of the formations is produced by the eastward migration of the orogenic front. Partly modified from Yang (2011).	22
Figure II. 4. Summary of method II, for obtaining paleocurrent directions from 2-D exposures of trough and planar cross-stratified sandstones. Arrows indicate flow component to the left or right of the section; crosses indicate that the flow direction is into the section; points indicate the contrary. Points and crosses indicate that this information cannot be constrained. Adapted from DeCelles <i>et al.</i> (1983).	24

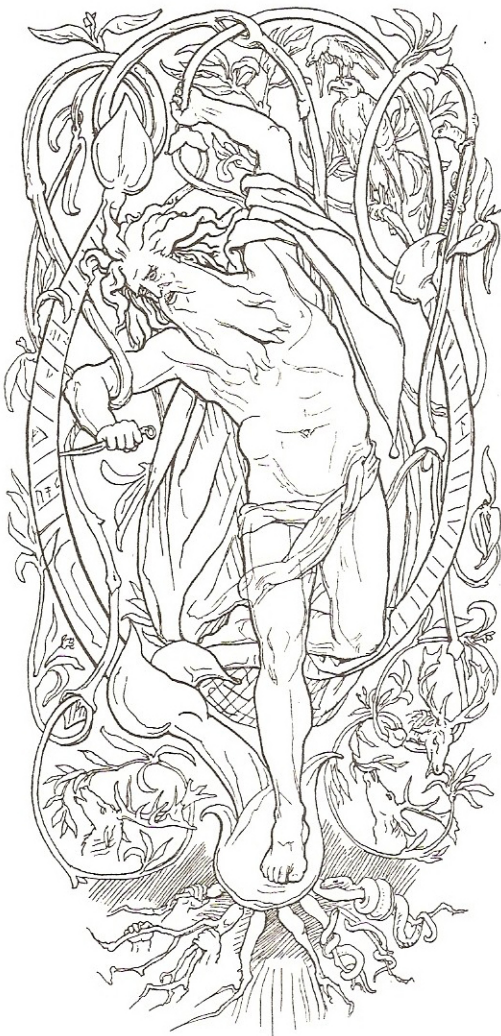
Figure III. 1. a) Compiled stratigraphic column, showing the changes in grain size. The equation in the upper-right corner represents a trend line for the column, showing an overall increase in grain size over the studied formations. b) General column of all three formations, showing covered areas which represent maximums obtained from Google Earth. Paleocurrent directions are also plotted.	28
Figure III. 2. Stratigraphic columns of the Tonel Formation, Limón Verde and Lampallar Members, showing grain-size change every 2 m. 1: Clay; 2: Silt; 3: Very fine sand; 4: Fine sand; 5: Medium sand; 6: Coarse sand; 7: Very coarse sand; 8: Granules; 9: Pebbles; 10: Cobbles; 11: Boulders.....	29
Figure III. 3. Stratigraphic columns of the Licán, Pajarito and Vizcachita Members, showing grain-size change every 2 m. 1: Clay; 2: Silt; 3: Very fine sand; 4: Fine sand; 5: Medium sand; 6: Coarse sand; 7: Very coarse sand; 8: Granules; 9: Pebbles; 10: Cobbles; 11: Boulders.	30
Figure III. 4. Stratigraphic columns of the Seilao, Río Grande Members and Barros Arana Formation, showing grain-size change every 2 m. 1: Clay; 2: Silt; 3: Very fine sand; 4: Fine sand; 5: Medium sand; 6: Coarse sand; 7: Very coarse sand; 8: Granules; 9: Pebbles; 10: Cobbles; 11: Boulders.....	31
Figure III. 5. Basal conglomerates of the Agua Salada Member.	32
Figure III. 6. Fine-grained, reddish brown sandstones of the La Escalera Member.	33
Figure III. 7. Contact between grey to green sandstones of the Limón Verde Member and red sandstones of the Los Cóndores Member, and evaporites of the Arcoiris Member.	35
Figure III. 8. Grey, medium-grained sandstones of the Limón Verde Member, showing isolated clasts....	36
Figure III. 9. Lithosomes of the Limón Verde Member. Jacob’s staff is 110 cm long.	37
Figure III. 10. Horizontally stratified conglomerate lenses interbedded between medium- to coarse-grained laminated sandstones of the Lampallar Member.....	38
Figure III. 11. Medium-grained sandstones showing a channel filled by massive, clast-supported conglomerates.	39
Figure III. 12. Outcrops of interbedded red and brown sandstones and conglomerates of the Licán Member.	40
Figure III. 13. Horizontally stratified conglomerates interbedded with coarse-grained sandstones.	41
Figure III. 14. Gradational contact between the Vizcachita and Pajarito Members.....	42

Figure III. 15. Outcrops of the Pajarito Member, showing diffuse, thin lenses with granule-sized grains, together with coarse-grained sandstones.....	43
Figure III. 16. Outcrops of the Vizcachita Member, showing large-scale cross-stratificated sandstones. Person shown as scale is 1.65 m tall.	45
Figure III. 17. Horizontally stratified conglomerates of the Seilao Member.	46
Figure III. 18. Fine- and coarse-grained outcrops of the Río Grande Member. Outcrops of the Barros Arana Formation are seen beyond the highway.	48
Figure III. 19. Outcrops and lithosomes of the Barros Arana Formation.....	50
Figure III. 20. Sandstones and planar cross-stratified gravels of the Barros Arana Formation.	51
Figure III. 21. Paleocurrent data obtained for the Tonel, Purilactis and Barros Arana Formations. Information plot with GeoRose 0.3.0 software. Data without rotation. Number of measurements shown inside the circle.	53
Figure III. 22. Rotated paleocurrent data.	54
Figure III. 23. Conglomerate clast-counts for the Tonel, Purilactis and Barros Arana Formations. Counts marked with * are qualitative in nature.	56
Figure III. 24. Sandstone petrographic data: a) Qt-F-L and b) Qm-F-Lt diagrams. Fields after Dickinson et al. (1983). 1: Craton Interior. 2: Transitional Continental. 3: Basement Uplift. 4: Quartzose Recycled. 5: Mixed. 6: Dissected Arc. 7: Transitional Arc. 8: Undissected Arc. 9: Lithic Recycled. 10: Transitional Recycled. c) Qp-Lv-Ls, d) Qt-F-L, e) Qm-F-Lt and f) Qm-P-K after Weltje (2006). A: Continental Block Provenance. B: Magmatic Arc Provenance. C: Recycled Orogen Provenance. g) Qp-Lv-Fp, after Ingersoll (2012). U: Undissected Arc. T: Transitional Arc. R: Recycled Orogen. B: Basement Uplift.	59
Figure III. 25. Sample location and U-Pb geochronology results for the a) La Escalera Member and b) Arcoiris Member. Map key found in Figure I.5.	60
Figure III. 26. Sample location and U-Pb geochronology results for samples a) SP3-90 and b) SP3-91 of the Limón Verde Member. Map key found in Figure I.5.....	61
Figure III. 27. Sample location and U-Pb geochronology results for the Licán Member. Map key found in Figure I.5.....	62

Figure III. 28. Sample location and U-Pb geochronology results for the Río Grande Member. Map key found in Figure I.5.....	63
Figure III. 29. Sample location and U-Pb geochronology results for the Barros Arana Formation. Map key found in Figure I.5.....	64
Figure III. 30. Relative probability plots of the samples discussed.....	65
Figure III. 31. Reduced relative probability plots of the aforementioned samples, only including zircons 550 Ma or younger.....	66
Figure IV. 1. Facies evolution of the Salar de Atacama Basin during the mid-Cretaceous to Paleogene. a) Sand-braided river and lacustrine deposits of the Tonel Formation and part of the Los Cóndores Member. b) Mainly sand-braided rivers of the Limón Verde, Lampallar, Licán and Pajarito Members. c) Eolian dunes representing the Vizcachita Member. d) Gravel-braided rivers of the Seilao Member. e) Fluvial and lacustrine deposits of the Río Grande Member. f) Deep, gravel-braided rivers of the Barros Arana Formation. Blue arrows indicate major paleocurrent directions. The Tuina Area (in dark grey) has been rotated 30° counterclockwise. Light grey area indicates the present-day western Cordillera de Domeyko outcrop limit. Light-stippled line shows the hypothetical foredeep section of the basin. Crosses indicate positive relief.....	68
Figure IV. 2. Basin inversion and compression in northern Chile. Modified from SERNAGEOMIN (2003).	73
Figure IV. 3. Schematic cross-section of northern Chile between 22°-23°S, showing basin and orogenic wedge evolution.	74

INDEX OF TABLES

Table 1. Lithofacies codes, with associated description and interpretation.	19
Table 2. Parameters for thin section point-counting	25



“Veit ek, at ek hekk
vindga meiði á
nætr allar níu,
geiri undaðr
ok gefinn Óðni,
sjalfr sjalfum mér,
á þeim meiði,
er manngi veit
hvers af rótum renn.

Við hleifi mik sældu
né við hornigi;
nýsta ek niðr,
nam ek upp rúnar,
æpandi nam,
fell ek aftr þaðan“

-Hávamál, 138-139.

Agradecimientos

Al proyecto de mapeo regional 1:100.000 de SERNAGEOMIN.

A los profesores de la comisión: Jacobus Le Roux, César Arriagada, Reynaldo Charrier, Fernando Barra. Otros profesores del departamento: Katja Deckart, Marcelo Farías, Luisa Pinto.

Al Laboratorio de Tectónica y Paleomagnetismo; Luis Acevedo, Juan Becerra, Susana Henríquez, Fernando “Pana” Martínez, Katherine “Tatanka” Narea, Matías “Ataxia” Peña, Juan Fernando Rubilar, Marco Vaccaris, Ricardo Valdivia, Sergio “Warrior” Villagrán.

A Maritza Acuña, Carlos Alvarado, Blanca Baccola, Rosa Flores, Carlos Gómez, William Godoy, Arnoldo Quilodrán y María Rosa Rocco.

A mis amigos/as y compañeros/as de Geología: Pablo Acevedo, Catalina Carreño, María Angélica Contreras, Nicolás Correa, Javier Cortés, Álvaro Espinoza, Valeska Farías, Iván Gómez, Sebastián Herrera, Tomás Iglesias, Pablo Molina, Moyra Montes, Cristián Morales, Javiera Morandé, Hugo Quinteros, Rodrigo Quiroga, Irene del Real, Pablo Sepúlveda, Yerko Simicic, Basilio San Juan, María Fernanda Soto, Ignacio Valenzuela, Vladimir Vicencio, Valeria Zavala. En general, mi curso entero; perdón si olvidé incluirlos.

A mis amigos del colegio: Mauricio Cornejo, Juan José Cornejo, Emilio González, Andrés Guzmán, Felipe Lobos, Juan Ignacio Montes, Daniel Rebolledo, Javier Salinas, Camilo Silva, Pedro Streeter, Juan Andrés Yolin. Gracias también a Sofia, Vale, Maida, Pacita y Patty.

Al Kru Juan Carlos “Huracán” Coria, Daniela Callejas y la escuela de Muay Thai Kai Muay Chile.

Esta tesis está dedicada a: Armando Bascañán, Veronica Hughes, José Manuel Bascañán, Alex Loyer (& Marilú), Pedro Urrutia; without whose support I would have never accomplished this. Mis abuelas: Rina Bustamante & Ellen Ulfeldt. Mis tías: María Angélica Bascañán, Isabel Hughes, Patricia Marchant. Mis tíos: James Hughes, Juan Pablo Urrutia. También: Caro, Ignacio, Flo, Santi, Andrés, Alan & brothers, Pato, Gigio.

Muchas gracias a mi polola, Leonie Kausel por el apoyo y comprensión durante este tiempo. Muchas gracias también a los Kausels.

También va para: Chuck Schuldiner, Layne Staley, Quorthon, Ronnie James Dio, Mike Starr, Cliff Burton, Dimebag Darrell, and most forms of metal as well.

Till next we meet

I INTRODUCTION

The evolution of the Chilean Precordillera between 22° and 24°S has been the focus of diverse studies over the last years, which have characterized the style and timing of the deformation of its diverse constituents (Ramírez & Gardeweg, 1982; Marinovic & Lahsen, 1984; Charrier & Reutter, 1994; Maksaev & Zentilli, 1999; Mpodozis *et al.*, 2005; Arriagada *et al.*, 2006a; Amilibia *et al.*, 2008; Henríquez, 2012). These authors have shown that uplift and shortening were more important during the Eocene-Early Oligocene and the Neogene, although tenuous evidence of deformation during the Cretaceous has also been recorded. The latter event ('Peruvian Phase'; Steinman, 1929) has been identified along most of the western margin of South America (Cobbold & Rosello, 2003; Jaillard *et al.*, 2005; Jaimes & De Freitas, 2006; Cobbold *et al.*, 2006; Tunik *et al.*, 2010), including detailed studies regarding its temporality and subdivisions in Peru (Jaillard, 1992; Jaillard, 1993; Noblet *et al.*, 1996). However, investigations concerning its effects and/or timing in the Chilean northern Central Andes are scarce.

The Salar de Atacama Basin, located in northern Chile, has an important geological record from Late Cretaceous to recent times (Brüggen, 1934; 1942; 1950; Arriagada, 1999; Ramírez & Gardeweg, 1982; Marinovic & Lahsen, 1984; Mpodozis *et al.*, 2005; Arriagada *et al.*, 2006a). Although much work has been done with regard to its stratigraphy, sedimentology (Brüggen, 1942; Dingman, 1967; Hartley *et al.*, 1989; Hartley *et al.*, 1992) and structure (Macellari *et al.*, 1991; Muñoz *et al.*, 2002; Arriagada, 1999; Pananont *et al.*, 2004; Mpodozis *et al.*, 2005; Arriagada *et al.*, 2006a; Reutter *et al.*, 2006), the Late Cretaceous-Paleogene Tonel, Purilactis and Barros Arana Formations (former Purilactis Group) still pose important questions about their origin, tectonic setting(s) and, inextricably, about the uplift of the Cordillera de Domeyko Range during the Late Cretaceous. The absence of fossils, tuff layers or other indicators has made dating of these units problematic; the only ages available have been obtained through Ar⁴⁰-Ar³⁹ analysis in mostly weathered, pyroxene samples (Flint *et al.*, 1989) or in samples south of the syncline, from Maastrichtian or younger units (Ramírez & Gardeweg, 1982; Hartley *et al.*, 1992; Hammerschmidt *et al.*, 1992; Charrier & Reutter, 1994; Mpodozis *et al.*, 2005). Thus, the time span of these formations remains doubtful.

Although arid to semi-arid conditions have been already established for most of the units (Hartley *et al.*, 1988; Hartley *et al.*, 1992), more detailed studies could also reveal information about the climatic changes that occurred during the evolution of the Salar de Atacama Basin.

In this thesis, almost 4000 m of high-resolution stratigraphic sections of the former Purilactis Group were measured, in order to establish the relation between the depositional environments and concomitant tectonic pulses. This, in turn, aids in clarifying the tectonic setting and climatic conditions prevailing from Late Cretaceous to Paleogene times. Eleven samples were taken for provenance (point counting) analysis and U-Pb detrital zircon geochronological dating on seven samples was also carried out to better constrain its age of deposition and source rocks.

The following subchapters (I.1-I.4) were written to summarize previous investigations and questions regarding the geology of the studied area and the stratigraphic definitions developed over the years.

I.1 Andean tectonics in northern Chile

The present configuration of the Andean Cordillera in northern Chile started during the late stages of the Early Jurassic age, when subduction was renewed at the western margin of South America, due to the break-up of Gondwana and subsequent continental drift (Jokat *et al.*, 2003; Cobbold *et al.*, 2006, Charrier *et al.*, 2007). This stage, uninterrupted to the present day, is called the Andean Cycle (Coira *et al.*, 1982; Charrier *et al.*, 2007). In this cycle, Charrier *et al.* (2007) recognized three stages; the first, ranging from the late Early Jurassic to the late Early Cretaceous, is characterized by the development of a N-S oriented magmatic arc, located in the present-day Coastal Cordillera, and an extensional back-arc basin to its east. This extensional episode is interpreted as a product of low coupling between plates, which produced a westward rollback of the subduction margin. This stage came to an end with an intense deformation episode, named the Peruvian Phase (Steinmann, 1929; Cobbold *et al.*, 2006; Ramos, 2010), where back-arc deposits were heavily inverted and deformed between approximately 100-90 Ma. The second stage, between the early Late Cretaceous and the early Paleogene, was characterized by an eastward migration of the magmatic arc, the development of a foreland basin to its east, and the presence of a wide fore-arc zone towards its west. The deposits of this stage were inverted during a Late Cretaceous-early Paleogene event, denominated the “K-T” event (Cornejo *et al.*, 2003). Another depositional event followed, which ended with the Incaic Phase during the Eocene-Early Oligocene (Noble *et al.*, 1979; Charrier *et al.*, 2007; 2009). The third stage of the Andean Cycle, maintained from the late Paleogene to the present day, saw the uplift of the Andes to its present elevation, erosion of the Incaic Cordillera and migration of the volcanic arc to its present position.

The changes observed during the Andean Cycle occurred due to variations of different parameters of the subducting plate and the resulting coupling; in this regard, Scheuber *et al.* (1994) proposed a high obliquity angle (around 60°) and NW-SE movement direction between the Aluk (Phoenix) and South American Plates during the first stage of the Andean Cycle, which is consistent with a left lateral strike-slip system. In contrast, the second stage of the Andean Cycle showed a configuration where the angle between the subducting plates was less than 45°; this was associated with a compressive regime, with possible extensional episodes. The subducting plate had a WSW-ENE direction, making the lateral strike-slip component dextral in nature. Compressive events were then a product of an increase of the convergence rates between plates, while extensional episodes, if present, were related to stages with lower convergence rates and reduced coupling. This overall configuration was kept until Miocene times, where the Nazca Plate showed an almost orthogonal convergence direction (Somoza & Ghidella, 2005). However, recent reconstructions of the western margin of South America show that it is likely that this orthogonal convergence could have started earlier (Arriagada *et al.*, 2008).

Arriagada (1999), Mpodozis *et al.* (2005) and Arriagada *et al.* (2006) (Figure I.1) recognized different compressive events in the El Bordo Escarpment, located at the eastern border of the Cordillera de Domeyko. There, they identified synorogenic structures related to a Cretaceous compressive event (possible Peruvian Phase). A Late Cretaceous-Paleocene stage, responsible for the deposition of the Naranja Formation was also recorded, together with an Eocene-Early Oligocene event (Incaic Phase) related to gravels of the Loma Amarilla Formation.

Thus, for the Cordillera de Domeyko and the present fore-arc, Amilibia *et al.* (2008), proposed (Figure I.1, I.2) (1) an important extensional event during the Late Jurassic and Early Cretaceous (Tarapacá-Domeyko Basin) (2) a compressional episode around 90 Ma, related to inversion of the previous basin and generation of a foreland basin and (3) another compressive event, which involved thin- and thick-skinned deformation, together with clockwise rotations, which they related to the Incaic Phase; this phase shows the most important exhumation of the Cordillera de Domeyko (Maksaev & Zentilli, 1999). On the other hand, Reutter *et al.* (2006), proposed a scheme (Figure I.1) where the Salar de Atacama represents the westernmost prolongation of the Salta Rift Basin, in which only slight uplift around 65 Ma in the Cerro Quimal zone is recorded (Andriessen & Reutter, 1994).

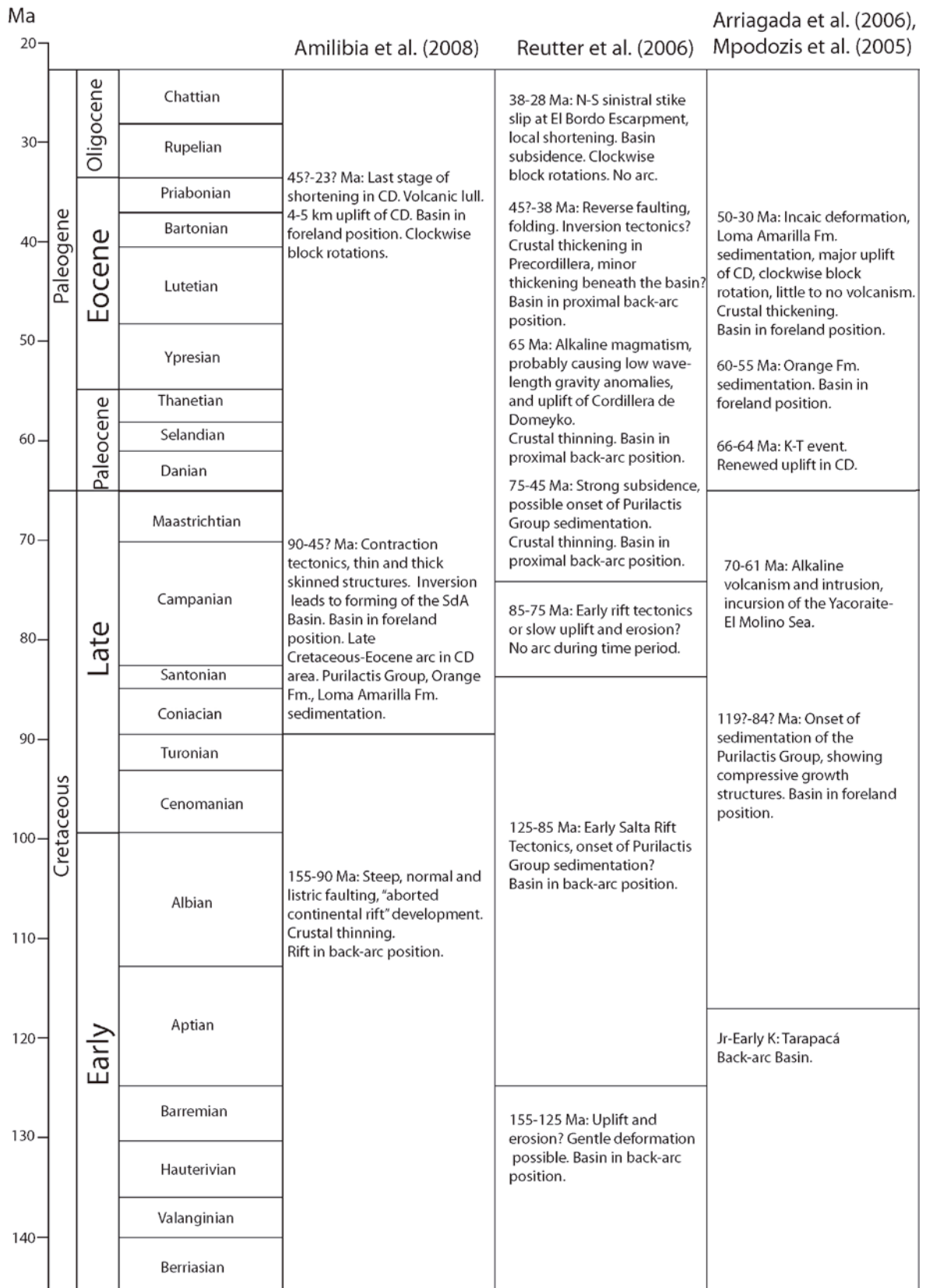


Figure I. 1. Summary and comparison of tectonic and sedimentary evolution proposed for the Salar de Atacama Basin and Cordillera de Domeyko Area.

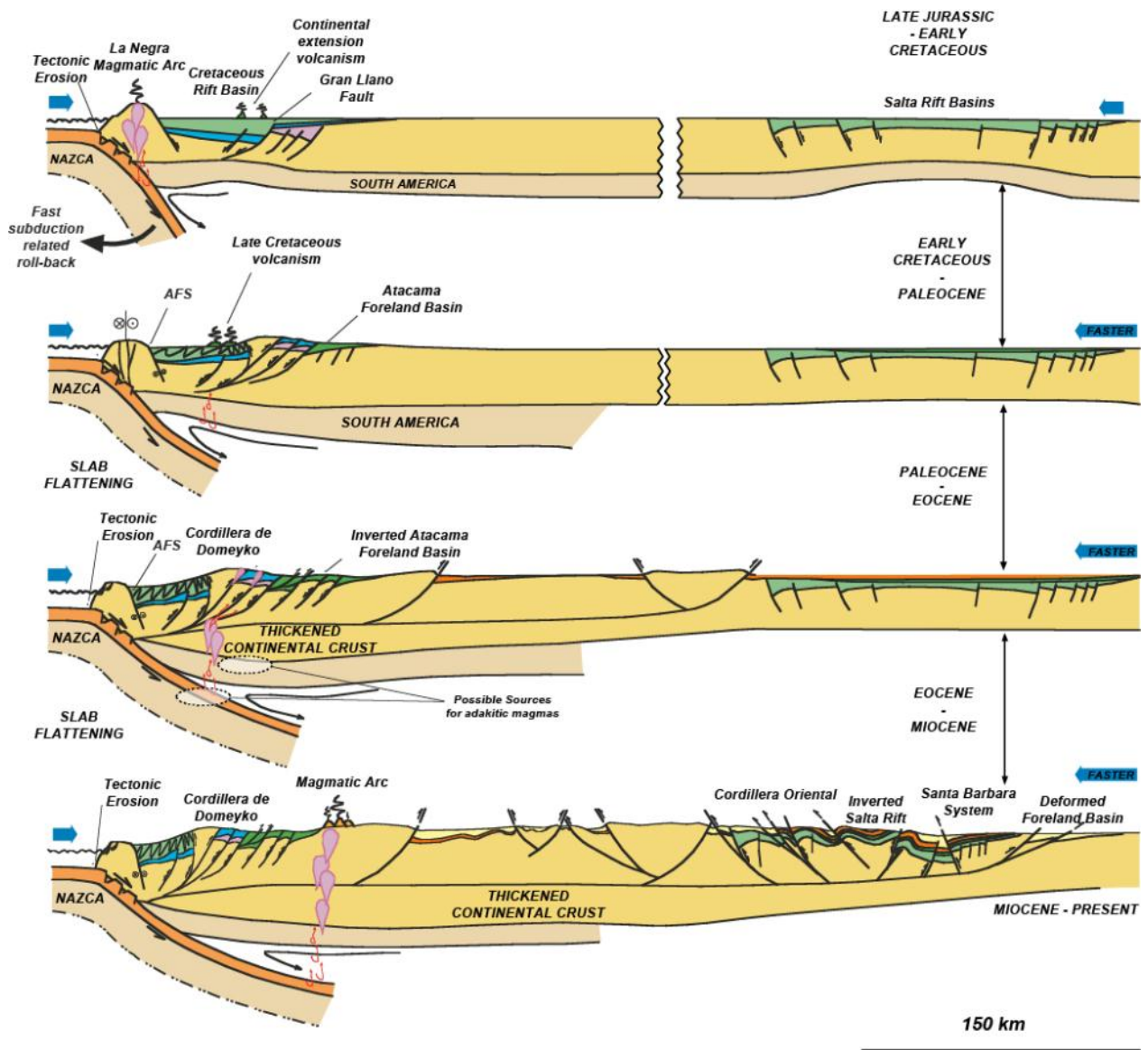


Figure I. 2. Tectonic evolution of the Cordillera de Domeyko area (~23°S) since the Late Jurassic. Modified from Amilibia *et al.* (2008).

I.2 Geological setting and Cretaceous stratigraphy of the Salar de Atacama Basin

The study area, located between 22°30'-23°S (Figure I.3, I.4 and I.5), presents several distinct, first-order morphostructural units, which are the product of various processes acting at the western margin of South America (Charrier *et al.*, 2007). According to Charrier *et al.* (2007), from W to E, these are: the Coastal Cordillera, constituted mainly by Cretaceous volcanics and intrusives (Oliveros *et al.*, 2006); the Central Depression or Longitudinal Valley; the Precordillera, or also Cordillera de Domeyko in this area; the Salar's Depression, which is only found in northern Chile, between 21°-27°30'S, here represented by the Salar de Atacama Basin;

the Western Cordillera, which holds the current magmatic arc, and the Altiplano-Puna Plateau, which corresponds to the most important depression observed in the Andean Cordillera, and one of the world's greatest plateaus (Isacks, 1988). Further E, in Argentina, the morphostructural units found are the Eastern Cordillera and the Sub-Andean Ranges, followed by the actual foreland (Ramos *et al.*, 2004; Charrier *et al.*, 2007).

The Salar de Atacama Basin is the most recognizable topographic anomaly in the Western Cordillera of the Central Andes (Figure I.3, I.4 and I.5) (Isacks, 1988; Allmendinger *et al.*, 1997; Jordan *et al.*, 2002; Götze & Krause, 2002; Yuan *et al.*, 2002; Arriagada *et al.*, 2006a). It is located between 22°30'S and 24°30'S, being 150 km long (N-S) and 80 km wide (E-W), with its lowest point at 2300 m a.s.l. (Mpodozis *et al.*, 2005). It lies east of the Cordillera de Domeyko (Precordillera) and west of the magmatic arc, which here shows a 60 km displacement to the east (Mpodozis *et al.*, 2005).

The Cordillera de Domeyko is a well-defined tectonic terrain about 500 km long (N-S), divided into different units whose cores are composed of basement blocks bounded by high-angle faults (Amilibia *et al.*, 2008). In the Salar de Atacama area the Cordillera de Domeyko can reach ~3000 m a.s.l., where it is constituted of Paleozoic to Mesozoic ignimbrites and rhyolitic domes associated with basaltic and andesitic rocks, intruded by lesser granitoids between 200-300 My (Davidson *et al.*, 1985; Breitzkreutz & Van Schmus, 1996; Arriagada *et al.*, 2006a). Although the range contains evidence that an important period of exhumation occurred during the Eocene, possibly related to the Incaic Event (Ramírez & Gardeweg, 1982; Charrier & Reutter, 1994; Makshev & Zentilli, 1999; Muñoz *et al.*, 2002), syntectonic structures found in Cretaceous rocks point to an even earlier event of uplift and erosion (Mpodozis *et al.*, 2005; Arriagada *et al.*, 2006a; Amilibia *et al.*, 2008). The eastern limit of the range coincides with the El Bordo Escarpment, which exhibits outcrops of Mesozoic and Cenozoic rocks (Arriagada, 1999; Charrier & Muñoz, 1994; Mpodozis *et al.*, 2005; Arriagada *et al.*, 2006a). To the NNE, in the area of the Barros Arana Pass, Mesozoic formations are folded into the Barros Arana syncline, 80 km long (NE-SW) and 16 km wide (NW-SE) (Hartley *et al.*, 1988; Hartley *et al.*, 1992; Arriagada, 1999; Mpodozis *et al.*, 2005; Arriagada *et al.*, 2006a). The western flank of the syncline borders the Paleozoic to Triassic basement of the Tuina Formation (Rackzyński, 1973; Marinovic & Lahsen, 1984).

East of the El Bordo Escarpment lies the Llano de la Paciencia, a sub-basin 80 km long (N-S) and 8 km wide (E-W), which is filled primarily by Quaternary alluvial fans (Marinovic & Lahsen, 1984; Jolley *et al.*, 1990; Arriagada, 1999; Mpodozis *et al.*, 2005). It borders to the east with the Cordillera de la Sal, a SSW-NNE structure 5 to 10 km wide, reaching ~200 m above the basin floor, composed of highly folded Oligocene to Pliocene evaporate-rich sedimentary units (Flint *et al.*, 1993; Jordan *et al.*, 2002; Arriagada *et al.*, 2006a). The present salt pan (salar) is located east of the Cordillera de la Sal, where it developed on Cretaceous to Neogene rocks (Macellari *et al.*, 1991; Muñoz *et al.*, 1997; Arriagada *et al.*, 2006a) and contains a Quaternary alluvial and evaporitic fill (Ramírez & Gardeweg, 1982; Marinovic & Lahsen, 1984; Jordan *et al.*, 2002; Lowenstein *et al.*, 2003).

The Salar de Atacama Basin presents an increasing volume of ignimbrites of Miocene and Pleistocene age towards its eastern border with the current magmatic arc and its deposits (Rámirez & Gardeweg, 1982; Marinovic & Lahsen, 1984). The basin is bounded to the south by the Western Cordillera (Arriagada, 1999; Arriagada *et al.*, 2006a) and with the Cordón de Lila Range, composed of igneous and sedimentary rocks of Ordovician-Carboniferous age (Niemeyer, 1984; Coira *et al.*, 2009).

Cretaceous rocks in the Salar de Atacama Basin are contained within the former Purilactis Group (*sensu* Mpodozis *et al.*, 2005), which includes the Tonel, Purilactis, Barros Arana and Cerro Totola Formations. The Tonel Formation is divided into three members (Arriagada, 1999; Mpodozis *et al.*, 2005), starting with ~60 m of basal breccias and medium-grained conglomerates with andesitic, rhyolitic and sedimentary clasts (Mpodozis *et al.*, 2005), derived from proximal alluvial fans and valley-fills (Hartley *et al.*, 1992). The middle member is composed of 400 to 1000 m of brown to red, horizontally-laminated sandstones at times alternating with gypsum layers, followed by a top member of unknown thickness containing deformed anhydrite deposits. The last two members display paleocurrent directions indicating a western provenance (Mpodozis *et al.*, 2005), and the depositional setting is interpreted as a playa-lake or continental sabkha environment (Hartley *et al.*, 1992). The contact between the Tonel and Purilactis Formations is frequently faulted (detached) (Hartley *et al.*, 1988; Arriagada, 1999; Mpodozis *et al.*, 2005; Arriagada *et al.*, 2006a).

The Purilactis Formation has five members reaching a total thickness of about 3000 m according to Hartley *et al.* (1992) and subsequent researchers (*e.g.* Arriagada, 1999; Mpodozis *et al.*, 2005; Arriagada *et al.*, 2006a). The basal unit is represented by the Limón Verde Member, containing 420 m of sandstones and brownish-reddish conglomerates, interpreted as proximal alluvial fan deposits, which grade into fine playa-lake deposits towards its upper 40 m, where it shows a transition into the Licán Member (Hartley *et al.*, 1992; Arriagada, 1999; Mpodozis *et al.*, 2005). The latter contains about 700 m of sandstones and red mudstones, interbedded with conglomerates and evaporites, which are interpreted as representing channelized medial to proximal fluvial deposits with distal sheetfloods and playa-lakes (Hartley *et al.*, 1988; Hartley *et al.*, 1992; Arriagada, 1999). The Vizcachita Member overlies the Licán Member with a sharp contact, displaying predominantly eolian facies, with a greater percentage of fluviually reworked deposits in the western outcrops, while finer-grained eolian sandsheets and barchans up to 30 m high dominate the eastern deposits. The fluvial rocks show a western provenance, while the dunes indicate paleocurrent directions from the south (Hartley *et al.*, 1992; Arriagada, 1999). The change to eolian facies may be due to a cessation of tectonic activity, which would have starved the basin of fluvial input until deposition of the Seilao Member (Hartley *et al.*, 1992). Andesitic flows are found in some locations at the contact between the Seilao and Vizcachita Members (Quebrada Seilao, Hartley *et al.*, 1988; Hartley *et al.*, 1992). The Seilao Member shows a return to predominantly alluvial facies, with the presence of poorly confined conglomeratic sheetflood and high-density flood deposits, either fining upward into or grading from sandflat and playa deposits. Some fluvial deposits can be found as small-scale, fining-upward cycles (Hartley *et al.*, 1992), probably representing meandering streams. The Seilao Member fines upward into the 250

m thick Río Grande Member, which contains sandstones, siltstones and varved mudstones, evidencing a possibly permanent, shallow lake subject to alluvial flooding and deposition of distal sheetflood sands (Hartley *et al.*, 1988; Hartley *et al.*, 1992; Arriagada, 1999).

The Río Grande Member represents the last unit of the Purilactis Formation, conformably underlying the Barros Arana Formation (Arriagada, 1999). According to Hartley *et al.* (1992), the latter is composed of thick alluvial fan deposits, with clasts up to 20 cm in diameter, derived mostly from Paleozoic granitoids and rhyolites with minor andesites and limestones to the west. The dominant facies are laterally amalgamated, proximal channelized streamflow and sheetflood deposits, together with some high-density flood and debris flow deposits. The large percentage of basement-derived clasts, as compared to the Purilactis Formation, suggests an important degree of deep exhumation of the Cordillera de Domeyko Range during its deposition (Mpodozis *et al.*, 2005).

The Purilactis Group (*sensu* Arriagada, 1999) ends with the Totola Formation (Estratos Cerros de Totola of Arriagada, 1999 and Mpodozis *et al.*, 1999), which is mainly composed of andesites, basaltic andesites and fewer dacites, interbedded with welded rhyolitic tuffs and some sandstones and red volcanoclastic conglomerates (Arriagada, 1999). This formation unconformably overlies deposits of the Tonel Formation and the Licán Member and is currently interpreted as being younger in age than the Barros Arana Formation (Arriagada, 1999; Mpodozis *et al.*, 1999; Mpodozis *et al.*, 2005).

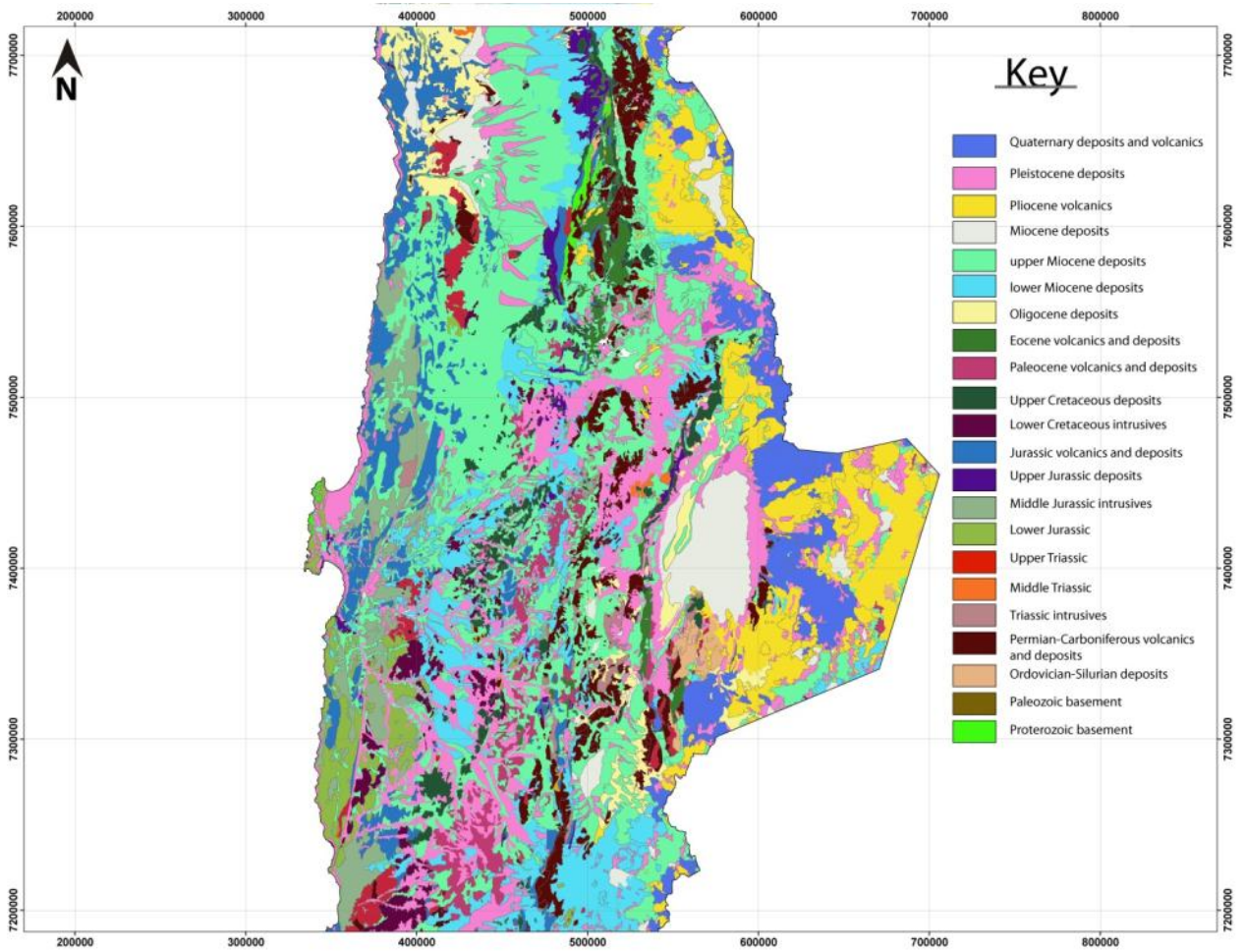


Figure I. 3. Regional pre-Neogene geological map for northern Chile. Modified from SERNAGEOMIN (2003) and Arriagada et al. (2003).

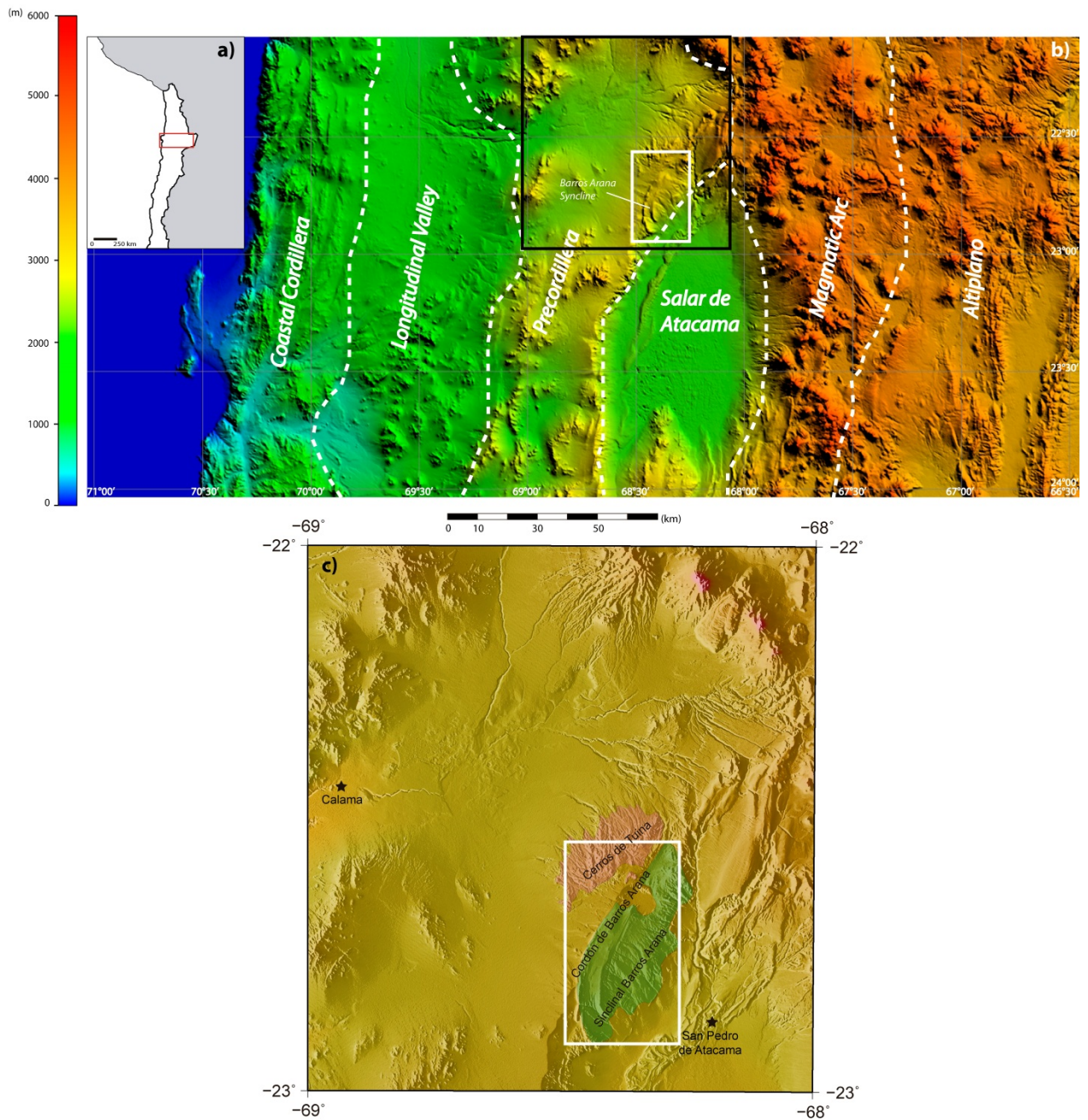


Figure I. 4: a) Map of the western margin of South America, showing the location of the simplified tectonic map. b) Morphotectonic domains after Amilibia et al. (2008). c) Geographic map, with stars showing towns and cities. Study area is enclosed in the white rectangle.

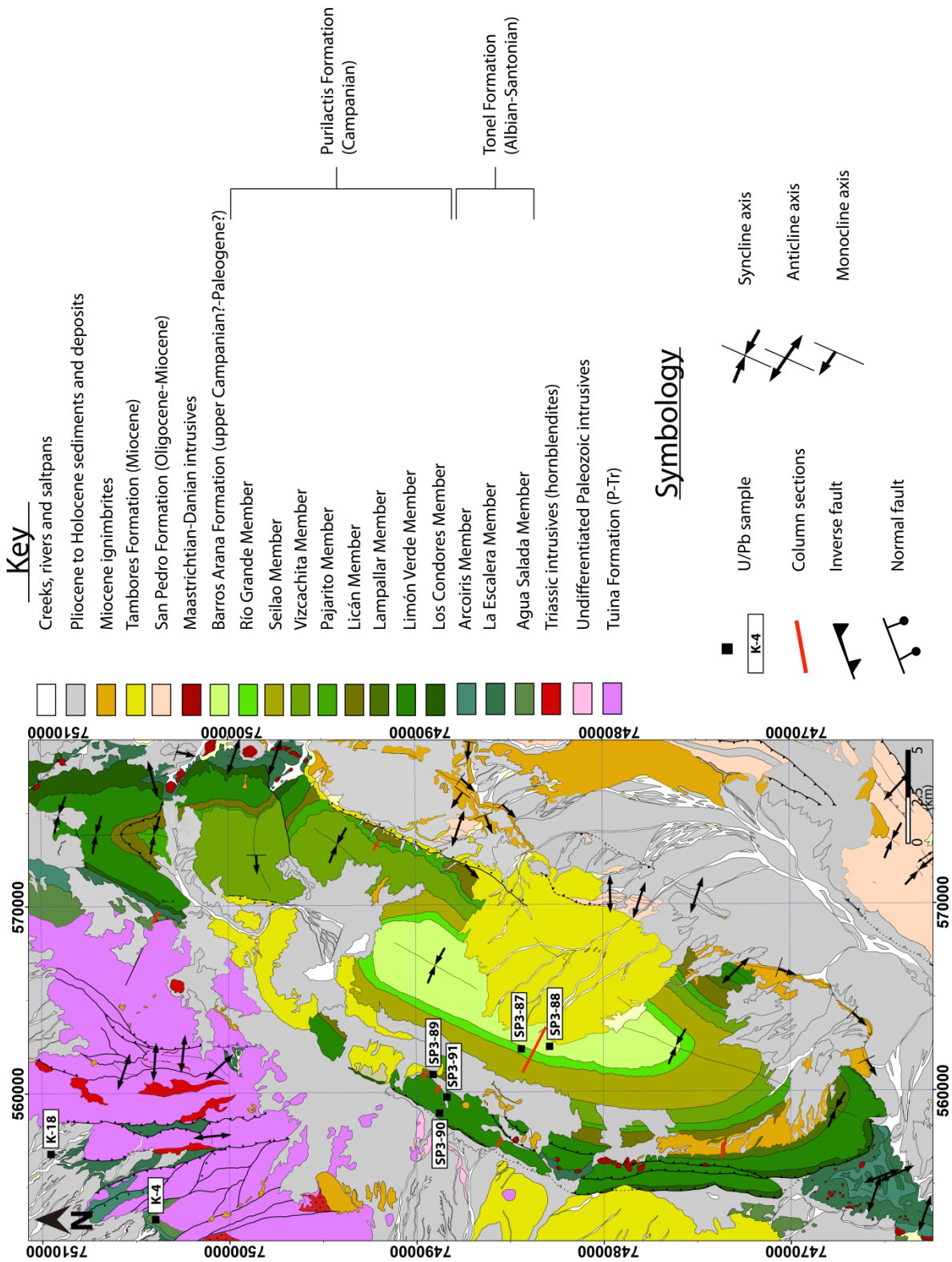


Figure I. 5. Geological map of the study area, showing the location of the U-Pb samples and the columns profiled. Modified from Henríquez (in prep.).

I.3 Stratigraphic definition and age of the Tonel, Purilactis and Barros Arana Formations

The first studies of the Purilactis and Tonel Formations and their ages were realized by Brüggén (1934, *in* Ramírez & Gardeweg, 1982; 1942, 1950), who assigned an Early Cretaceous age to the Purilactis Formation based on the finding of reworked fossils of Jurassic age (Felsch (1933) *in* Brüggén, 1942; 1950) and the presence of a *Pucalitus* fossil within the Salina de Purilactis Formation. Dingman (1963, 1967) suggested a Cretaceous age for the Purilactis Formation utilizing the same criteria as previous authors, and considered the Tonel Formation, an equivalent of the previously defined Salinas de Purilactis Formation, as Jurassic in age, based on its stratigraphic location beneath the Purilactis Formation. This is reinforced by the presence of hornblendite clasts in the Purilactis Formation, which were derived from dykes that intruded the Tonel Formation.

Ramírez & Gardeweg (1982) included the Tonel Formation within the Purilactis Formation, and considered its age in the Late Jurassic-Cretaceous range, based on Middle Jurassic reworked fossils (*Vaugonia v. l. gottschei* (Moericke), *Perisphinctes* sp.) found throughout the formation. The formation is also intruded, near the Cerro Quimal area, by monzonites and tonalites with ages between 66.4 ± 1.4 Ma and 64.6 ± 1.1 Ma (K-Ar). Marinovic & Lahsen (1984) present a similar nomenclature, but restrict the age of the formation to the Cretaceous, considering the time needed to deform and uplift the Jurassic rocks which provided the reworked fossils to the Purilactis Formation.

Hartley *et al.*, (1988, 1992) returned to the nomenclature proposed by Dingman (1963, 1967), and assigned a Late Jurassic age to the Tonel Formation, and a Cretaceous-Paleogene age to the Purilactis Formation. This is supported by an Ar^{40} - Ar^{39} age of 64 ± 10 Ma (Danian) obtained from an andesitic bed found in the Vizcachita Member of the Purilactis Formation (Flint *et al.*, 1989; Hartley *et al.*, 1992). A Late Eocene age is defined as the minimum age of the formation, based on a K-Ar age of 39.9 ± 3 Ma obtained from basal lavas attributed to the Cinchado Formation, located unconformably over the Purilactis Formation (Ramírez & Gardeweg, 1982).

Almost simultaneously, Charrier & Reutter (1990, 1994) defined the Purilactis Group, including the Cinchado Formation of Ramírez & Gardeweg (1982). They also included the lower-middle part of the Purilactis Formation *sensu* Hartley *et al.*, (1992) into the Tonel Formation. The Formación Yesífera Superior was added as the group's youngest formation. ^{39}Ar - ^{40}Ar ages of 44.0 ± 0.9 Ma and 43.8 ± 0.5 Ma from pyroclastic beds found at the base of the newly redefined Purilactis Formation (Döbel, 1989 *in* Charrier & Reuter, 1990) define a Middle to Late Eocene age, similar to the ages obtained by Ramírez & Gardeweg (1982) for the Cinchado Formation. They also questioned the age presented by Flint *et al.* (1989), and reinterpreted its Ar release spectra; the reinterpretation shows an age more similar to that proposed by them.

Arriagada (1999) and Mpodozis *et al.* (1999), besides changing the definition of the Purilactis Group, gave new K-Ar ages of 68 ± 2 Ma y 61 ± 3 Ma from dykes intruding the lower units of the group. According to their studies, and similar ages and interpretations obtained by

Macellari *et al.* (1991), these ages could show Ar loss due to weathering, which would make the intrusives older. This fact, together with ages between 71-60 Ma from lava beds that cover the Purilactis Formation in the Cerro Totola area (Cerro Totola Beds), led the authors to assign a mid-Cretaceous age to the Tonel Formation and the lower members of the Purilactis Formation. This is in concordance with paleomagnetic data presented by Arriagada (1999) and Arriagada *et al.* (2000), which show that these lower units only present normal polarity, associated with the Cretaceous normal polarity superchron, which ranges between 119-84 Ma. The upper members of the Purilactis Formation would be of Late Cretaceous age. The same authors also included the Barros Arana and Cerro Totola beds into the group (both part of the Cinchado Formation of Ramírez & Gardeweg, (1982) and Hartley *et al.* (1992); upper part of the Purilactis Group *sensu* Charrier & Reutter (1988, 1990)). They assigned a Late Cretaceous age to the former and a Maastrichtian age to the latter, without observing a direct contact between them. Other Paleogene units are included in the group, which is extended to the Eocene-Oligocene limit.

Mundaca (2002) also studied the Purilactis and Tonel Formations in the Barros Arana area, supporting the Cretaceous age of the Tonel Formation, and used a stratigraphic scheme similar to the one proposed by Brüggén (1942), dividing the Purilactis Formation into three members. He assigned a Paleocene-Eocene age to this formation, utilizing similar reasoning to that of Charrier & Reutter (1990, 1994).

Mpodozis *et al.* (2005) and Arriagada *et al.* (2006) changed the denomination of the Cerro Totola and Barros Arana Beds to formations, and excluded all units younger than Danian from the Purilactis Group. They also presented K-Ar ages between 61.0 ± 2.0 Ma and 70.2 ± 2.0 Ma for the Cerro Totola Formation and related intrusives found in the lower units of the Purilactis Group. The age of the Cerro Totola Formation is similar to values obtained from the Lomas Negras Formation (Marinovic & Lahsen, 1984), further NE along the strike of the Barros Arana syncline (Hammerschmidt *et al.*, 1992).

Figure I.6 presents a summary of the evolution of the stratigraphic knowledge related to the Late Cretaceous formations over the last 25 years.



Figure I. 6. Evolution of the stratigraphic knowledge and terminology of the Cretaceous to Paleogene successions of the Salar de Atacama area. Modified from Arriagada (1999).

I.4 Late Cretaceous basins in northern Chile

Continental deposits of similar age found further northwest (Figure I.5) comprise the Cerro Empexa, Tolar and Tambillo Formations (Marinovic & García, 1999; Tomlinson *et al.*, 2001; Mpodozis *et al.*, 2005). The last two formations show continental sediments and volcanics with coarsening-upward profiles, with paleocurrents derived from the NE and W, respectively, while the Cerro Empexa Formation shows mostly volcanic rocks and minor continental sediments derived from a western magmatic arc (Tomlinson *et al.*, 2001).

Directly west of the Salar de Atacama Basin, the Quebrada Mala Formation, comprising more than 3700 m of sandstones and conglomerates of Late Cretaceous age, has been usually attributed to deposition in an extensional setting (Sierra del Buitre Fault, Marinovic & García, 1999), which would have undergone inversion in Paleocene times.

Between 24°S and 27°S, Upper Cretaceous formations are found in the Pedernales-Maricunga Basin; here, the continental Leoncito Formation shows a coarsening-upward profile, and a strong angular unconformity with the Lower Cretaceous Quebrada Monardes Formation; mafic dykes found throughout the formation yield K/Ar ages of 64 Ma (Cornejo *et al.*, 1993, 1998; Mpodozis & Clavero, 2002; Mpodozis *et al.*, 2005).

Further south, between the Copiapó River and Donkey Creek valleys, the Upper Cretaceous formations show, at first, around 4000 m of conglomeratic and volcanic beds, deposited in a post-rift tectonic setting (Cerrillos Formation), followed by 1000 m of sedimentary and volcanic successions evidencing synorogenic deposition (Hornitos Formation) during the K-T event (Martínez *et al.*, 2012; 2013).

I.5 Remaining questions in the Barros Arana Syncline

It can be seen from the previous sections that, although much work has been done on the mid-Cretaceous successions of the Salar de Atacama Basin and the Depression of the Salars due south of the Salar de Atacama, many issues remain open. The tectonic setting during the deposition of these successions has not been completely understood, nor has a complete relation between the sedimentary facies and tectonism been proposed. A better understanding of the stratigraphy could also shed more light on the paleoclimate of the study area.

The source areas have been shown to lie west of the study area (see above), but more precise locations, or the maximum distance from which these sediments could have arrived have not been proposed.

Another issue involved is the position and tectonic setting of the sediments during their deposition: more precisely, their location following the foreland basin system model proposed by DeCelles & Gilles (1996). What evidence is needed to conclusively resolve this aspect is also a relevant discussion topic.

However, one of the most critical problems regarding the successions is their age; this information is key to understanding what was occurring during the mid-Cretaceous and later in northern Chile and, possibly, elsewhere. As a matter of fact, answering this question alone could by itself solve many of the remaining concerns.

I.6 Objectives of this thesis

The main objective of this thesis is to understand the tectonic setting and factors that controlled the deposition of the Upper Cretaceous units found in the Barros Arana Syncline, namely the Tonel, Purilactis and Barros Arana Formations.

In order to complete this objective, the following specific objectives are proposed:

- Review the stratigraphy of the study area, in order to understand the sedimentary processes involved in the deposition of the mid-Cretaceous units, and comprehend the relation between these units and the tectonic activity.
- Identify the possible sources for the studied units, which will aid in understanding their tectonic history (unroofing, uplift, erosion, etc...) as well as the history of the basin itself.
- Define the age of these deposits in order to comprehend their relation with the compressive phases identified at the western margin of South America.

I.7 Hypotheses

The hypotheses postulated are:

- a) The formations represent compression at the western margin of South America between the mid-Cretaceous and Paleocene.
- b) The different tectonic cycles and pulses recorded are directly related to the tectonic regime, and can show both their provenance and their position in the depositional basin.
- c) The paleoclimate and its variations can be derived from the studied units.

I.8 Proposed methodology

The following methodologies are proposed to address the mentioned issues:

1. Detailed, centimeter-to meter-scale measurements of the Upper Cretaceous successions following the recent mapping by Henríquez (in prep.), together with the recording of clast-counts and paleocurrent data.
2. Provenance studies from 11 samples, in order to expand the information provided by previous studies, and to locate other possible sediment source areas.
3. U-Pb detrital zircon geochronology to constrain the ages and to define new source areas.

The results are shown in Chapter III and discussed in Chapter IV. A detailed methodological chapter (II), where the different methods are explained, is also presented. Finally, a new stratigraphic scheme is proposed.

II METHODOLOGY

II.1 Sedimentology and stratigraphy

Stratigraphic columns, measured on a centimeter to meter scale, and lithological information were collected from different sections throughout the Barros Arana Syncline, in accordance to the regional mapping of Henríquez (in prep.). Partial sections were obtained from most of the formations and members involved, with the sole exception of the Los Cóndores Member. For this unit, the information provided by Arriagada (1999) was utilized to establish its sedimentary environment. A Jacob's staff together with a 5 m measuring tape were utilized to obtain true stratal thicknesses. Afterwards, several meter-scale columns with detailed grain-size information were drawn using Adobe Illustrator CS5.1 (See Supplementary Material A); the grain-size scale chosen was the same as that of Carrapa *et al.* (2012). These columns were then rescaled by recording the grain size every 2 m. Then, using an Excel worksheet, these points were averaged every for 10 m. The results are shown in Chapter III.1.

To analyze the sedimentary environment, the different facies observed (e.g., Figure II.1) were summarized in a facies code (Table 1) which is partly modified from Miall (1996), Nalpas *et al.* (2008), Carrapa *et al.* (2011; 2012), Siks and Horton (2011), and DeCelles *et al.* (2011). Sedimentological analysis and depositional environment interpretation are based both on the data acquired in this research and that of Hartley *et al.* (1988; 1992), Arriagada (1999) and Mpodozis *et al.* (2005).

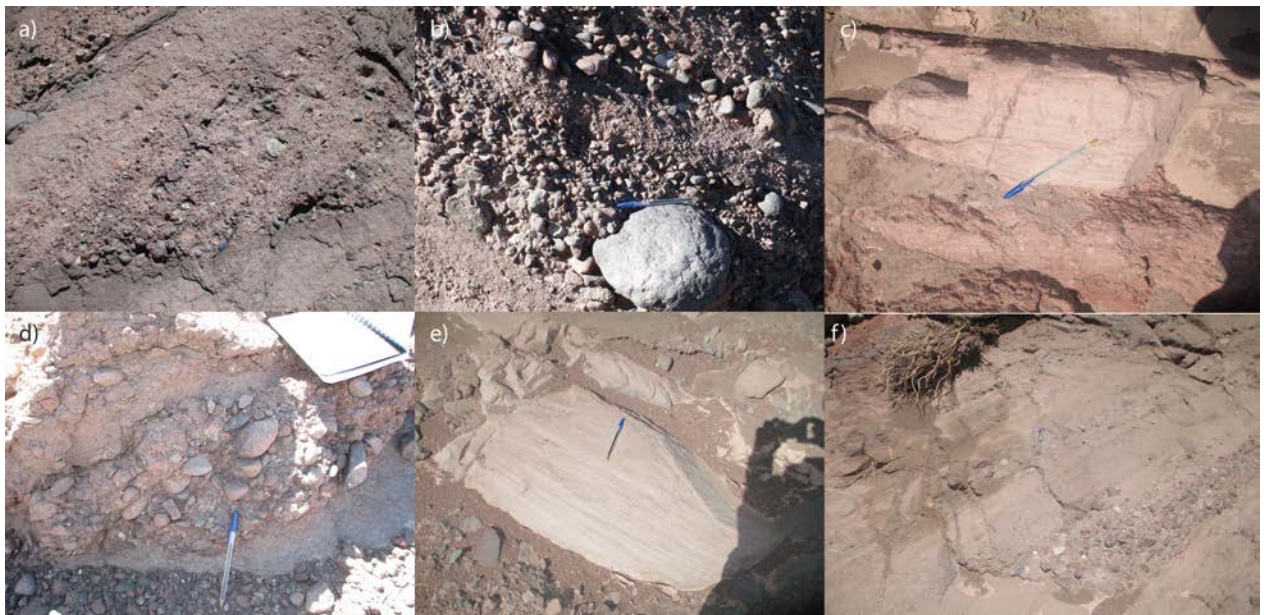


Figure II. 1. Facies and outcrops observed in this study: a) Planar cross-stratified conglomerates (Gpt). b) Imbricated, horizontally stratified conglomerates (Gch). c) Burrows found in laminated sandstones (Sh). e) Trough cross-stratified sandstones. f) Horizontally stratified, clast-supported conglomerates (Gch) intercalated with medium- to coarse-grained sandstones (Sl)

Table 1. Lithofacies codes, with associated description and interpretation.

Code	Description	Interpretation
Sh	Medium- to fine-grained sandstones with horizontal lamination.	Subcritical to supercritical flow transition.
Sp	Fine- to very fine-grained sandstones with planar cross lamination.	2-D dune migration under low regime conditions.
Sl	Medium- to very coarse-grained sandstone with low angle (<10°) cross-bedding.	Deposition over inclined surfaces or low angle dune migration.
St	Medium- to very-coarse grained sandstones with trough cross-bedding.	3-D dune migration under lower regime conditions.
Gmm	Matrix-supported, massive, structureless conglomerate.	Plastic, high-strength debris flow.
Gmg	Matrix-supported conglomerate, with inverse or normal grading.	Pseudoplastic, low-strength debris flow.
Gch	Clast-supported conglomerates with stratification or imbrication.	Rapid downstream gravel transport; longitudinal bedforms.
Gcm	Clast-supported, massive, structureless conglomerate.	Pseudoplastic debris flow; hyper-concentrated flows.
Gp	Clast-supported conglomerates with planar stratification.	Slow downstream gravel transport; transverse bedforms.
Fm	Mud and silt with dessication marks and small-scale ripples.	Deposition from suspension and/or weak traction- currents and dessication .

II.1.1 Lithofacies model

In order to determine which kind of river or fluvial style corresponds to the deposits observed, they are correlated with one of the lithofacies shown in Table 1. Only the categories relevant to this study are shown. However, more information, such as the presence of burrows, the color of the deposits, the geometry of the lithosomes and others are just as important to obtain a correct classification.

Once this information is processed, a facies model can be utilized to classify the deposits. Here, the models proposed by Miall (1985; 1996) are chosen, based on their demonstrated usefulness and flexibility with regard to incorporating different factors.

However, it must be noted that, as with any other model, the interpretations obtained from it are not necessarily definitive, and any transition between two end-members is valid. Also, new, not-yet-described styles may be incorporated into the model.

Each fluvial style as described by Miall (1996) and used in this thesis is briefly summarized below (Figure II.2):

1.- Gravel braided with sediment-gravity flows: Deposited mainly by distributary fluvial systems that form the deposits of alluvial fans. This style incorporates sediment-gravity flow deposits, such as matrix-supported conglomerates and some massive, clast-supported conglomerates related to high-energy stream flow. Minor thicknesses of fine-grained deposits are also present. The Trollheim fan in Death Valley, California, serves as a modern example.

2.- Shallow gravel braided (“Scott type”): Corresponds to proximal gravel-bed rivers and braid deltas in which sediment-gravity flows are rare to absent. They show different gravel bedforms deposited in unstable, low-sinuosity channels. These channels are usually around 1 m deep, and channel margins are difficult to identify. Most lithosomes found consist of tabular bodies with minor internal erosion surfaces, and assemblages of clast-supported gravels, with minor sandy bedforms. The most characteristic model example is that of the Scott River in Alaska.

3.- Deep gravel braided (“Donjek type”): Consists of braided rivers with different, recognizable topographic levels. These may include major and minor channels, bar surfaces and floodplains. Typical lithofacies found are similar to the previous case, but some examples of lateral or downstream accretion can be seen. Cycles are more readily observed than in the last case; their scale can vary from meters to tens of meters, representing different kinds of events. The case example for this fluvial style is the Donjek River in Canada.

4.- Gravel-sand meandering river: This style includes bed-load streams, in which the channel and macroform sediments consist of sand and pebbly sand, or sand with a lag of gravel. Abandoned channels and meander scars are also common. The primary components readily found in these rivers are point-bar deposits, representing different channel fills. The lithofacies observed are thus, mostly, stratified, clast-supported conglomerates and sandy bedforms, up to fine-grained facies; however, the typical cycle is not necessarily observed over the whole river system. A classic example is the South Saskatchewan River, Canada.

5.- Distal, sheetflood, sand-bed river: Corresponds to sheets, lenses and wedges of sandy lithofacies, with scarce flood cycles a few meters deep. Fine-grained facies are less common. These facies are common on distal braid plains in arid regions, where channels are ephemeral and poorly defined. Eolian sand dunes may be intercalated with these deposits. The Kayenta and Navajo Formations in Arizona, U.S.A, are ancient examples of this style.

6.- Flashy, ephemeral, sheetflood, sand-bed river: Similar to the previous fluvial style, distinguished from it by the preferential deposition of transitional to upper flow-regime beds, like plane-laminated sand and low-angle cross-bedded sand. They are deposited as sheets in poorly defined channels during flood events. Parts of the Kayenta Formation in Arizona, and the Bijou Creek in Colorado, show this facies assemblage.

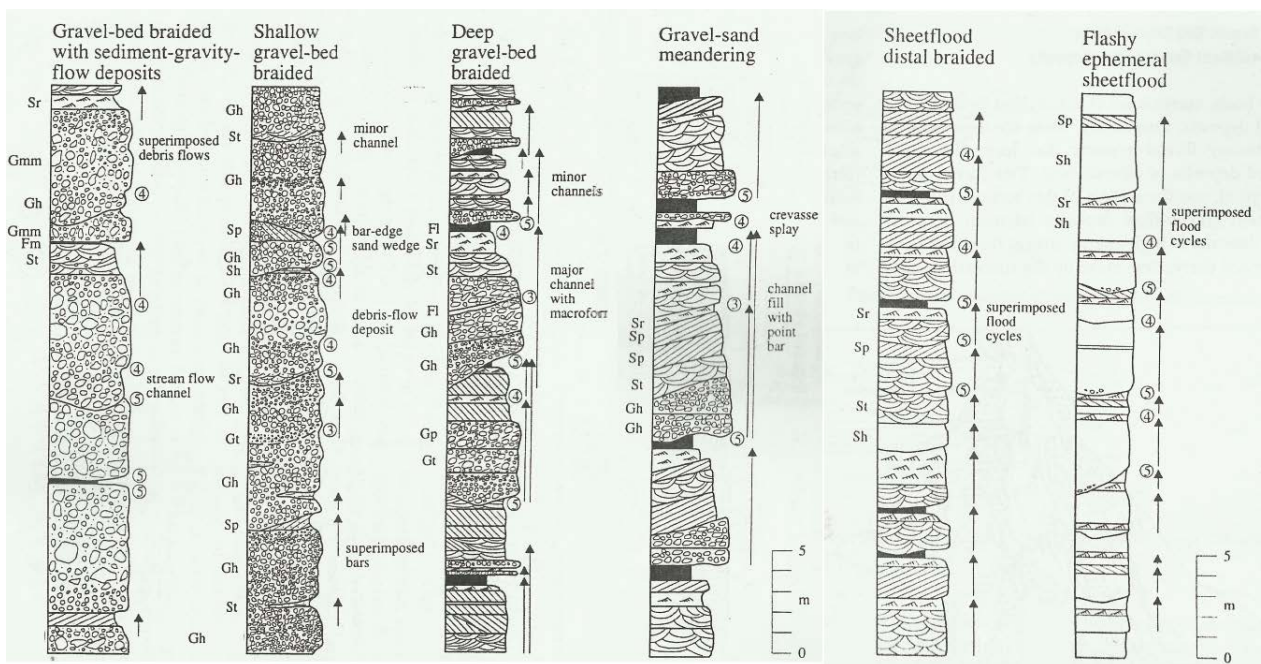


Figure II. 2. Fluvial styles, showing facies and fining-upward cycles (shown by arrows), observed in this study. Numbers indicate bounding surface order, not discussed here (See Miall, 1985; 1996). Adapted from Miall (1996).

II.2 Tectonic cycle interpretation

The model used here for interpreting clastic deposits (Figure II.3) is based on the work of Blair & Bilodeau (1988), in which they interpret the change from coarse-grained to fine-grained deposits as evidence of tectonic activity, in opposition to previous views which reflected the inverse situation ('theory of Davis', Davis (1899) *in* Blair & Bilodeau, 1988). One of the main arguments is that the association of fine-grained facies to tectonic quiescence implies that there must be a long-term rise in lake or sea level of hundreds of meters in the previous scenario, which would be geomorphologically inconsistent, as low-gradient fluvial environments are maintained for long periods of time in the lowest parts of any given sedimentary basin. It would also imply that the source area is eliminated during tectonism, hence explaining why deposits become finer-grained. Also, they show that tectonic uplift in modern orogenic belts can be as much as 8 times higher than denudation rates, even 117 times higher in regions with <100 cm of annual precipitation, which makes large-scale fan progradation during tectonism difficult.

Miall (1996) also mentions that, in the particular case of foreland basins, which are the product of crustal loading by overriding thrust sheets, which in turn generates syntectonic subsidence of proximal parts of the basin, the immediate basin response would be the incursion of low energy sediments, with ponding of coarse-grained deposits toward the basin margin. Yang & Miall (2010) and Yang (2011) developed a similar model, albeit specifically for foreland basins.

In this regard, Armitage *et al.* (2011) use forward model simulations to show that the response to a tectonic regime change may be less straightforward than previously thought; in particular, an increase in uplift may result in the deposition of larger grains at proximal sites, and a reduction of grain size in distal sites.

As to the influence of climate, Hartley *et al.* (1992) ascribed the regularity of the cycles larger than 100 m observed to be more likely a consequence of tectonic activity. Studies carried out by Armitage *et al.* (2013) show that Milankovitch-scale cycles are likely to be filtered in the long run by mountain and alluvial/fluvial dynamics. Also, their geometry and extent seem to be different, and less smooth than in tectonic events (Armitage *et al.*, 2011).

The 'anti-tectonic' gravel model has been used, tested and/or opposed (with different results) in several other research papers (e.g., Burbank *et al.*, 1988; Hartley *et al.*, 1988; Flemings & Jordan, 1990; Hartley *et al.*, 1992; Heller & Paola, 1992; Smith, 1994; Bridge, 2003; Marzo & Steel, 2000). Extreme caution must be exercised to analyze every factor which may produce results opposite to the model described above (e.g., Burbank *et al.*, 1988).

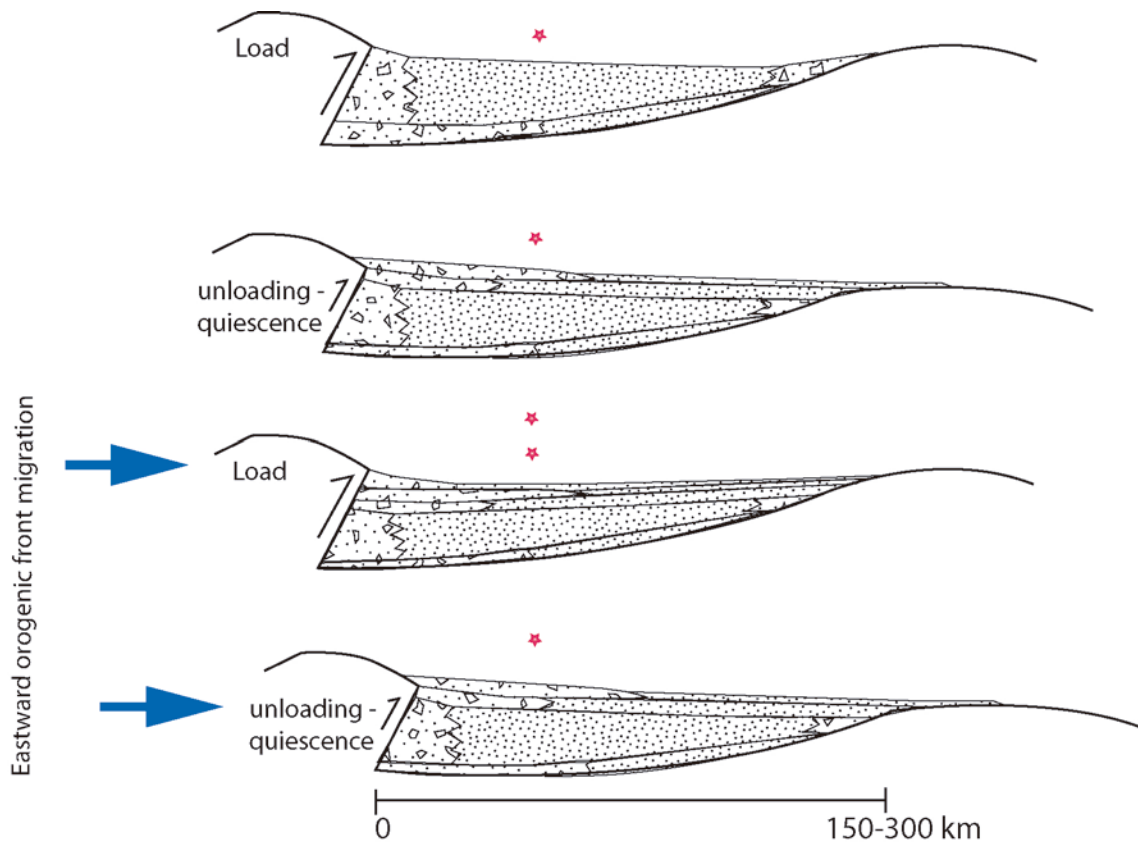


Figure II. 3. Schematic summary of the basin-filling process. The evolution is from top to bottom; the red star indicates a fixed position within the basin. The cartoon shows how loading produces fine-grained deposits, while coarse-grained deposits are produced as a consequence of unloading or tectonic quiescence. An overall coarsening-upward style of the formations is produced by the eastward migration of the orogenic front. Partly modified from Yang (2011).

II.3 Clast counts

Conglomerate clast counts were performed on at least 100 clasts in selected areas, where similar clast-sizes were found. On some occasions, qualitative counts were performed; this occurred mainly where one clast type was effectively predominant over any other. Clast counts were performed on the Tonel Formation (Agua Salada Member), the Limón Verde, Pajarito and Seilao Members of the Purilactis Formation and the Barros Arana Formation. This information was then compared with data previously published by Hartley *et al.* (1988; 1992).

II.4 Paleocurrent data

Data for paleocurrent analysis was obtained primarily from paleochannels and parting lineations found throughout the study area, following method II of DeCelles *et al.* (1983) (see below); in the case of scalars, the direction assumed was the same as that of the closest vectors obtained from other structures, like imbricated clast orientations, planar cross-stratification and 3-

D expositions of trough cross-strata. These measurements were taken from the Agua Salada and La Escalera Members of the Tonel Formation, the Limón Verde, Lampallar, Licán, Pajarito (the last three grouped together), Vizcachita and Seilao Members of the Purilactis Formation and the Barros Arana Formation. The data was then tilt-corrected with ROTDIR (Le Roux, 1991), and rotated according to Arriagada *et al.* (2000). The paleocurrent information was also compared with the studies performed by Hartley *et al.* (1988; 1992).

The method of DeCelles *et al.* (1983) devised to obtain paleocurrent directions from 2-D expositions of trough or planar cross-stratified sandstones is shown in Figure II.3. The authors drew numerous, hypothetical cross-sections of cylindrical and scoop-shaped troughs to examine the amount of information possible to extract from any given section. Thus, the approximate direction is obtained from: a) observing the geometry of the sets and the symmetry of the trough and b) observing the bedding/cut relationship. The degree of error varies between 10° in transverse-oblique directions, 25° in oblique-oblique exposures, and 45° overall. The method assumes a symmetric filling of troughs, and that most exposures seen are from cylindrical troughs; in the case of scoop-shaped troughs, oblique-oblique cuts from an already asymmetric trough makes it impossible to discern the component related to the bedding; the direction of the foresets can still be easily obtained.


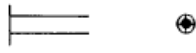

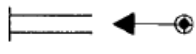

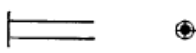

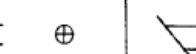












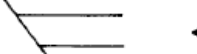

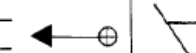
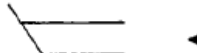


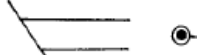

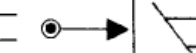
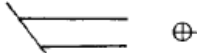
CUT TYPE	EXPOSURE	BEDDING/CUT RELATIONSHIPS & RESPECTIVE PALEOCURRENT COMPONENT INTERPRETATIONS	
TRANSVERSE-VERTICAL	1 		
	2 		
OBLIQUE-VERTICAL	3 		
	4 		
TRANSVERSE-OBLIQUE	5 		
	6 		
	7 		
OBLIQUE-OBLIQUE	8 		
	9 		
	10 		
	10 		

Figure II. 4. Summary of method II, for obtaining paleocurrent directions from 2-D exposures of trough and planar cross-stratified sandstones. Arrows indicate flow component to the left or right of the section; crosses indicate that the flow direction is into the section; points indicate the contrary. Points and crosses indicate that this information cannot be constrained. Adapted from DeCelles *et al.* (1983).

II.5 Sediment provenance

Sediment provenance (point counting) analyses were performed on 11 medium- to coarse-grained sandstones. Of these, one was taken from the Tonel Formation (La Escalera Member), nine from the Purilactis Formation and one from the Barros Arana Formation. These samples were obtained from different sections of the syncline, from which some the samples used for U-Pb detrital zircon geochronology were also taken. Around 400 to 500 grains exceeding 0.0625 mm in diameter were counted utilizing a Swift point counter and a petrographic microscope, following the Gazzi-Dickinson method (Dickinson, 1970; Dickinson & Suczek, 1979; Dickinson *et al.*, 1983; Ingersoll *et al.*, 1984; Dickinson, 1985). The parameters used are listed in Table 2.

The results were plotted on different ternary diagrams, following Dickinson (1985), Weltje (2006) and Ingersoll (2012), and partly using an electronic spreadsheet developed by Zahid & Barbeau (2011). Results are shown in Chapter III.4 and Appendix B.

Table 2. Parameters for thin section point-counting

Symbol	Description
Qm	Monocrystalline quartz
Qp	Polycrystalline quartz
Qt	Total quartz (Qp+Qm+C)
K	Potassium feldspar
Fp	Plagioclase
F	Total feldspar
Ch	Chert
C	Carbonate
St	Sandstone/siltstone fragment
Ls	Total sedimentary fragments (St+C)
Lm	Metamorphic fragment
Lv	Volcanic fragment
M	Matrix and cement
D	Iron oxides and other accessory minerals, including biotite, muscovite and epidote
Hb	Hornblende
Ol	Olivine

II.6 U-Pb detrital zircon geochronology

Due to the lack of beds and deposits suitable for more detailed geochronology studies, U-Pb detrital geochronology analyses were used to constrain the age of these deposits. Three samples were taken from the Limón Verde and Licán Members of the Purilactis Formation, one from the Río Grande Member and one from the Barros Arana Formation (Figure I.5). Two samples taken by Narea (in prep.) from outcrops in the Tuina area to the northwest of the syncline were also included (La Escalera and Arcoiris Members; samples K-4 and K18 in Figure I.5). Fine- to coarse-grained samples were chosen for the analysis.

Zircon separation was performed at the Sample Preparation Laboratory (Laboratorio de Preparación de Muestras) of the Universidad de Chile, under the supervision of J. Vargas using the Gemeni table, Frantz magnetic separator and heavy liquid procedures. They were then manually separated from other minerals using a magnifying glass. The zircon mineral separates were sent to the Laboratorio de Estudios Isotópicos (LEI), Geoscience Center, Universidad Nacional Autónoma de México (UNAM), Mexico, where 100 randomly chosen grains were analyzed. The analytical work was undertaken by using a *Resonetics Resolution M50* 193 nm

laser *Excimer* connected to a *Thermo Xii Series Quadrupole Mass Spectrometer* following analytical procedures and technical details after Solari *et al.* (2010). The employed laser diameter for ablation was of 23 μm . The best age was defined using the $\text{Pb}^{206}/\text{U}^{238}$ and $\text{Pb}^{207}/\text{Pb}^{206}$ ratios, with an 800 Ma cutoff. Average ages were calculated using *Isoplot v. 3.7* (Ludwig, 2008); they represent the youngest populations ($n \geq 3$) for each of the seven analyzed zircon samples. The maximum depositional age for each sample locality is given by this age. Age peaks and populations were also calculated using the Excel spreadsheet Age Pick, provided by the LaserChron Center at the University of Arizona. The Excel spreadsheet Normalized Age Probability Plots was used to summarize the relative probability plots of the different samples. The results are shown in Chapter III.5 and Appendix C, and discussed in Chapter IV.

III RESULTS

III.1 Sedimentology and stratigraphy

The measured columns are plotted, following the method described in Chapter II.1. Figure III.1 shows the compiled column, identifying each section with each proposed member, following the regional mapping by Henríquez (in prep.).

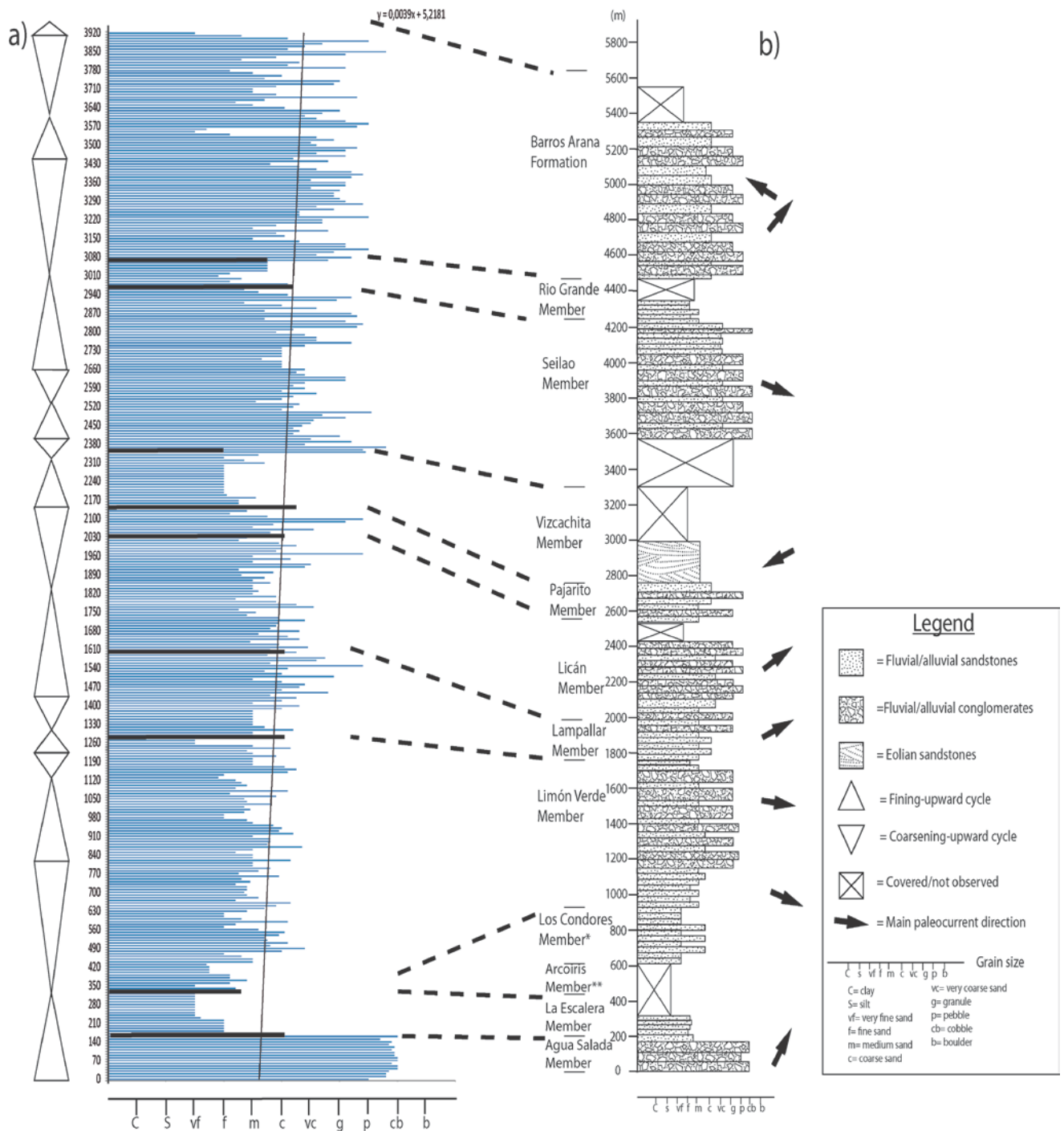


Figure III. 1. a) Compiled stratigraphic column, showing the changes in grain size. The equation in the upper-right corner represents a trend line for the column, showing an overall increase in grain size over the studied formations. b) General column of all three formations, showing covered areas which represent maximums obtained from Google Earth. Paleocurrent directions are also plotted.

Figures III.2, III.3 and III.4 show the 2 m resolution (when possible) for each member and formation measured. These are described below.

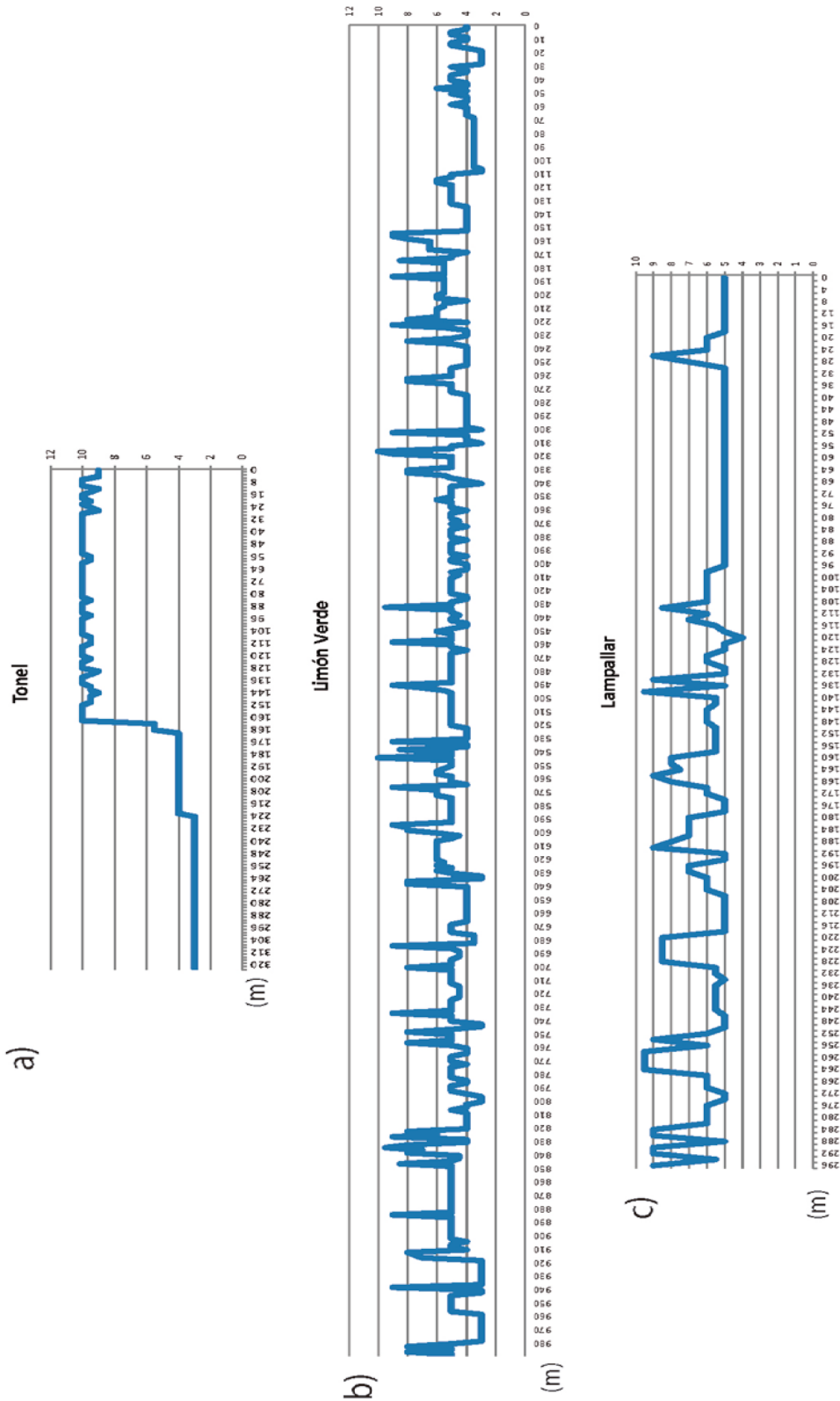


Figure III. 2. Stratigraphic columns of the Tonel Formation, Limón Verde and Lampallar Members, showing grain-size change every 2 m. 1: Clay; 2: Silt; 3: Very fine sand; 4: Fine sand; 5: Medium sand; 6: Coarse sand; 7: Very coarse sand; 8: Granules; 9: Pebbles; 10: Cobbles; 11: Boulders.

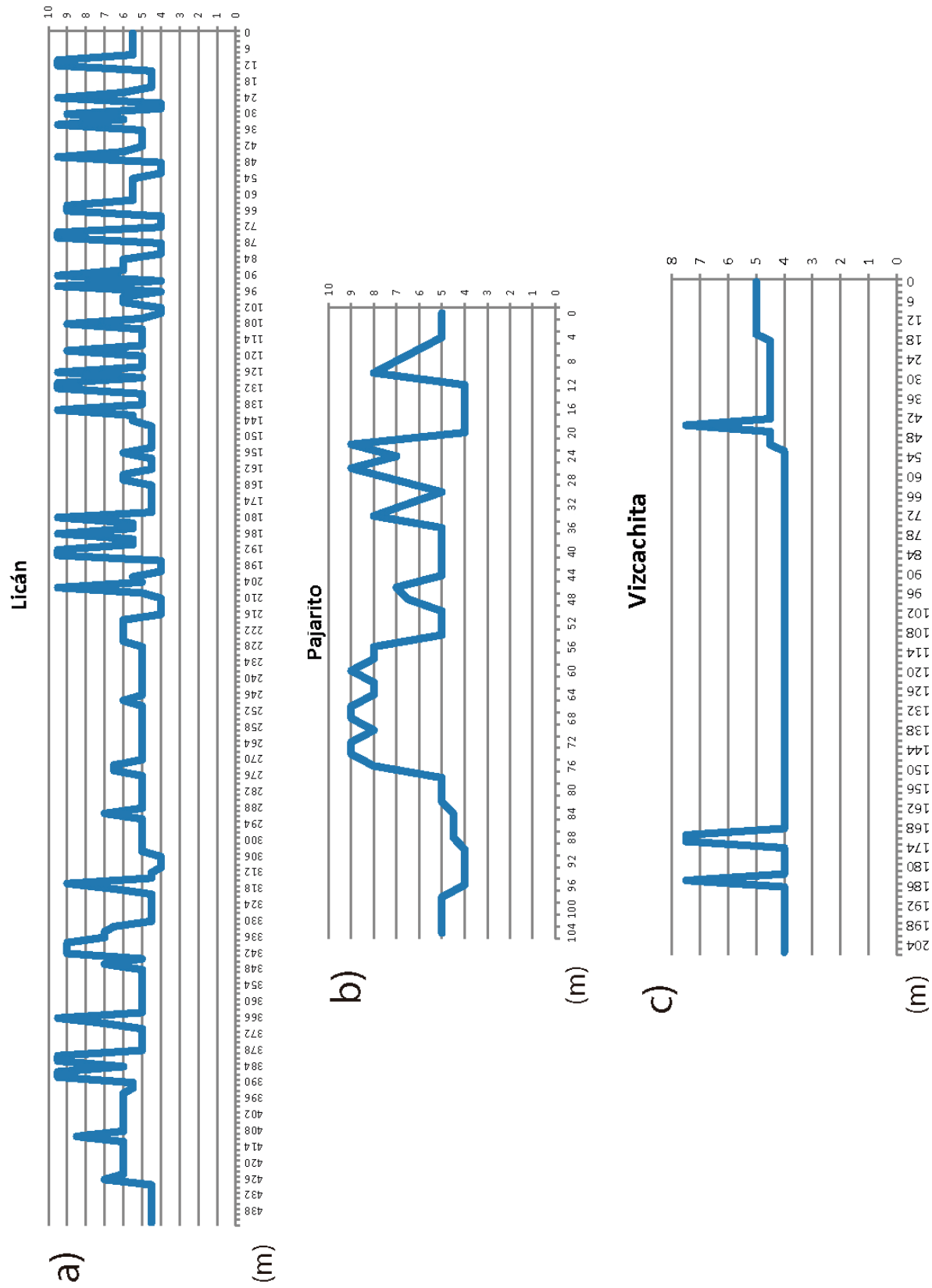


Figure III. 3. Stratigraphic columns of the Licán, Pajarito and Vizcachita Members, showing grain-size change every 2 m. 1: Clay; 2: Silt; 3: Very fine sand; 4: Fine sand; 5: Medium sand; 6: Coarse sand; 7: Very coarse sand; 8: Granules; 9: Pebbles; 10: Cobbles; 11: Boulders.

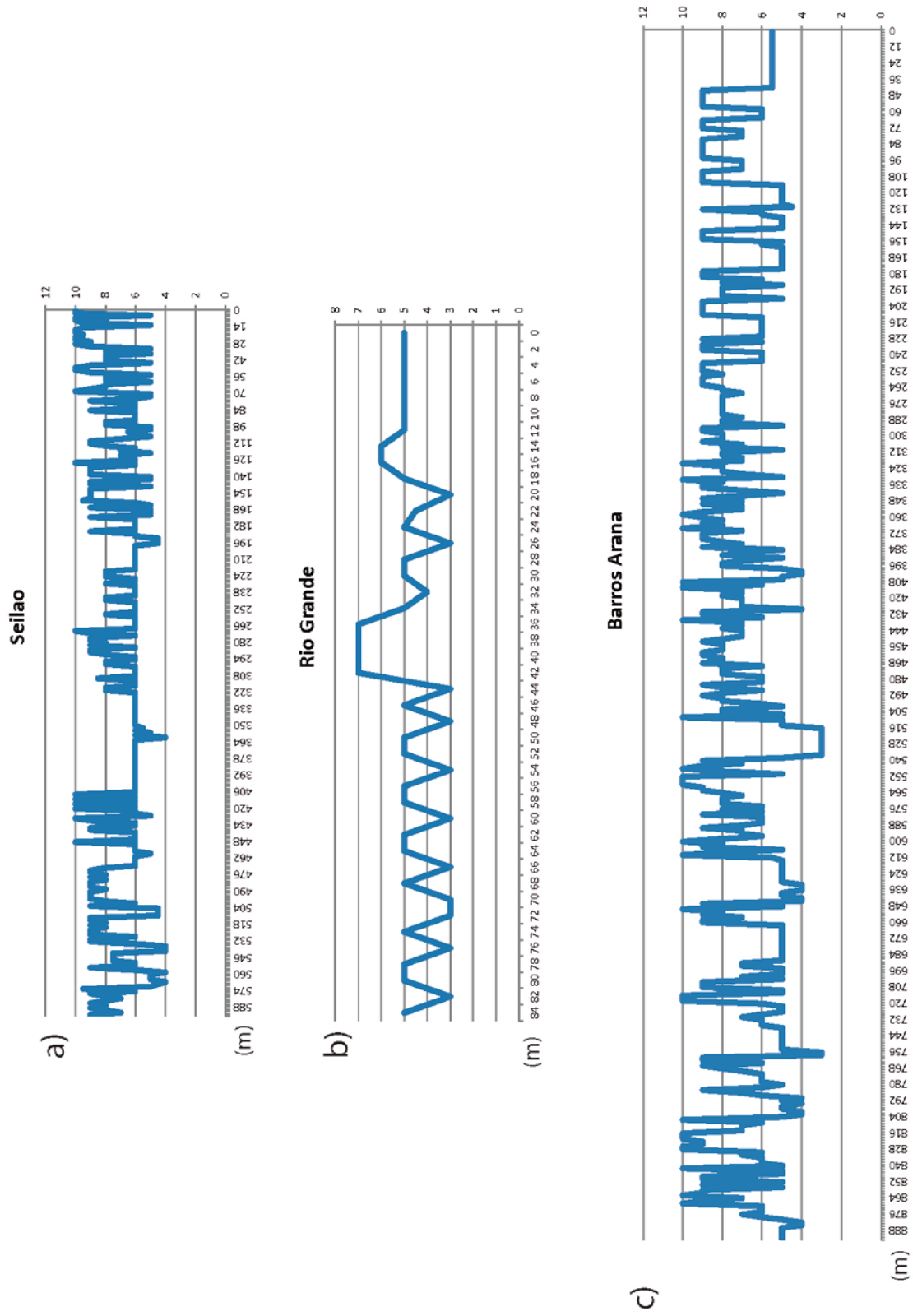


Figure III. 4. Stratigraphic columns of the Seilao, Río Grande Members and Barros Arana Formation, showing grain-size change every 2 m. 1: Clay; 2: Silt; 3: Very fine sand; 4: Fine sand; 5: Medium sand; 6: Coarse sand; 7: Very coarse sand; 8: Granules; 9: Pebbles; 10: Cobbles; 11: Boulders.

Tonel Formation

Agua Salada Member

The Agua Salada Member was studied in the northwestern part of the syncline (Figure I.5), where it overlies andesitic and tuffaceous rocks of the Tuina Formation with a slight angular unconformity. Here, this member (Figure III.2a, Appendix A.1) starts with ca. 168 m of light brown, laminated to crudely stratified clast-supported conglomerates (Gch), with clast sizes predominantly in the pebble range, although some isolated clasts up to 40 cm in diameter occur. (Figure III.5). The clasts are usually poorly sorted and subrounded to angular in shape, while the matrix is composed of an equally poorly sorted, subangular, coarse-grained sandstone. Beds may be hard to distinguish, although they are usually 15-30 cm thick when evident, forming 5 to 15 m thick units. The contacts between lithosomes are slightly erosive to non-erosive. The conglomerates are generally poorly channelized, but sometimes show lenses a few cm thick and a meter or so wide, between ca. 76 m and ca. 106 m of this section. These lenses are predominantly massive, pebble- to cobble-sized, clast-supported conglomerates, although matrix-supported conglomerates are locally present (Gcm and Gmm, respectively).

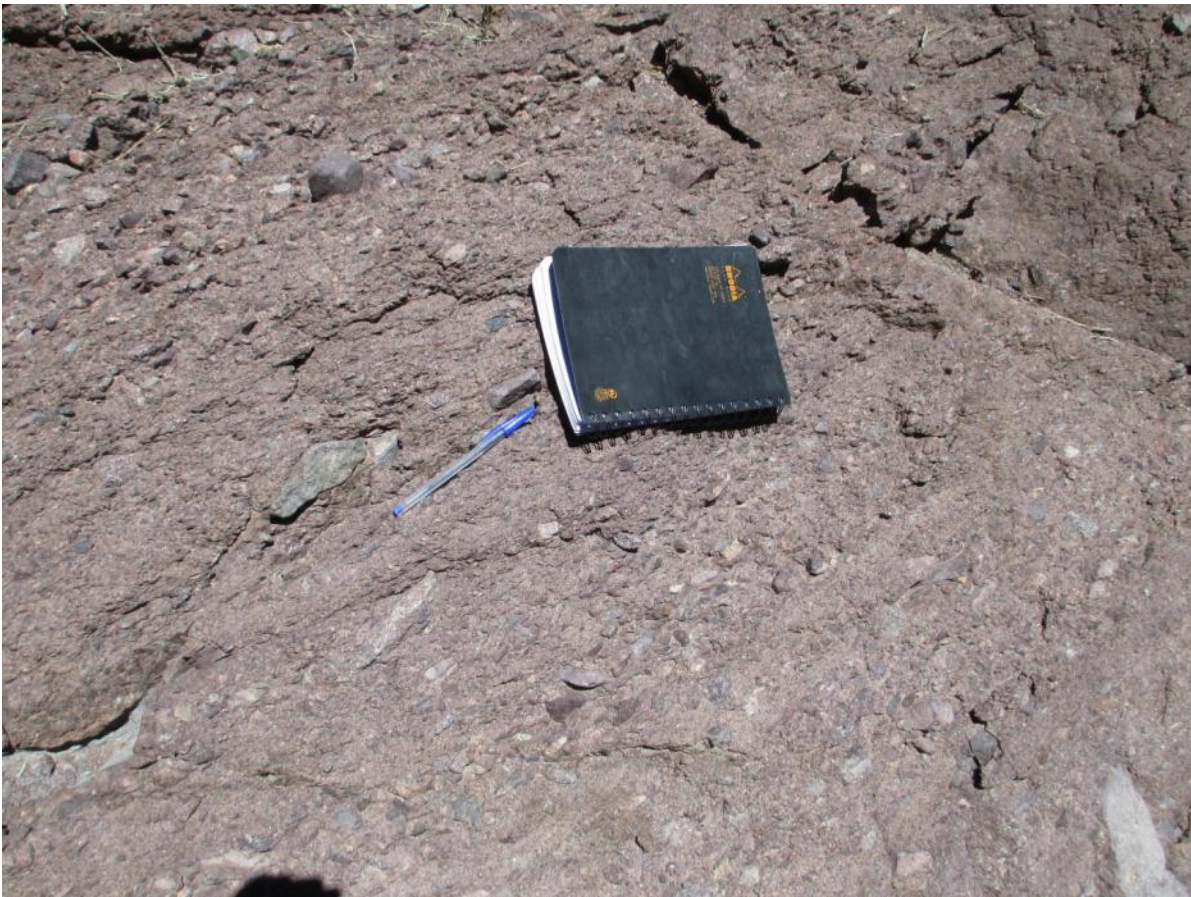


Figure III. 5. Basal conglomerates of the Agua Salada Member.

The Agua Salada Member has characteristics reminiscent of the shallow, gravel-bed, braided rivers of Miall (1985; 1996), such as a dominance of clast-supported, stratified conglomerates (Gch) with no channelization, arranged in multi-storey units. Their low thickness suggests unchanneled flooding on the lower reaches of alluvial fans (Nemec & Steel, 1984).

La Escalera Member

This unit was found in the same section as the Agua Salada Member. A conformable, non-erosive contact with laminated sandstones (Sh) is found at ca. 168 m (Figure III.2a, Appendix A.1), where there is a transition showing a medium- to coarse-grained sandstone containing conglomerate lenses with basal scouring and isolated clasts. These grade into mainly red to reddish brown, fine-grained sandstones, with scarce medium-grained sandstone beds (Figure III.6). Each bed is approximately 15 to 20 cm thick, showing sharp, non-erosional contacts between them. From ca. 230 m, the outcrops become partly covered; the sandstones here are dark brown and very fine-grained, with rare yellowish siltstone beds (Fm). No outcrops are present above ca. 322 m.

The change to fine- and very-fine grained, laminated sandstones (Sh) and siltstone beds (Fm) observed in this member represents a transition to a more distal environment, possibly lacustrine and/or overbank facies.



Figure III. 6. Fine-grained, reddish brown sandstones of the La Escalera Member.

Arcoiris Member

This member, which corresponds to the top and last subdivision of the Tonel Formation, was not observed in this study. It lies underneath the Purilactis Formation (Los Cóndores Member), showing a marked detachment in the southern part of the syncline (Figure III.7). According to the description of Henríquez (in prep.), it is constituted by an intercalation of siltstones, orange, fine-grained sandstones and light-grey evaporites (gypsum and halite) outcropping at the southern end of the syncline, on the eastern flank and in the Tuina area. Due to its intensely-folded structure, its thickness is hard to determine, though it ranges between 50 to 300 m.

The characteristics of the Tonel Formation closely resemble that described by Hartley et al. (1988; 1992), Arriagada (1999) and Mpodozis *et al.* (2005). The Agua Salada Member is correlated with the lower member of the Tonel Formation (T1) as defined by Mpodozis *et al.* (2005), which, however, is only 60 m thick; the differences are possibly due to along-strike variations in basin depth, or tectonic erosion of the basin fill. The La Escalera Member is partly equivalent to the middle member (T2) described by Mpodozis *et al.* (2005), and partly to the upper member described by Hartley *et al.* (1992); however, neither gypsum nor anhydrite were observed in this section. The Arcoiris Member (T3 of Mpodozis *et al.*, 2005) was not observed in this section, but may be present in the covered interval above 322 m.

Purilactis Formation

Los Cóndores Member

The Los Cóndores Member (Figure III.1), not measured in this study, corresponds to the first member of the Purilactis Formation (basal section of the Limón Verde Member *sensu* Arriagada, 1999; upper part of the Tonel Formation *sensu* Hartley *et al.*, 1992). The nature of the contact changes throughout the syncline; to the north, the contact is conformable with the Tonel Formation, as clearly seen on satellite images, while, to the south, it is detached from the evaporitic Arcoiris Member (Figure III.7). According to Arriagada (1999), it comprises ca. 320 m of reddish brown, fine- to coarse-grained, cross-stratified sandstones (St, Sl, Sh), found as beds 5 to 30 cm thick, occasionally interbedded with sparse matrix-supported conglomerates (Gmm) and siltstones (Fm). The conglomerates possess andesitic and rhyolitic clasts up to 5 cm in diameter.



Figure III. 7. Contact between grey to green sandstones of the Limón Verde Member and red sandstones of the Los Cóndores Member, and evaporites of the Arcoiris Member.

The description above points mostly to the generation of sandy bedforms (St facies) and scarce overbank fines (Fm) and/or gravity flows (Gmm), which, according to Miall (1996), could belong to a distal, sheetflood, sand bed-river with a high braiding index, which is characteristic of distal braid plains.

Limón Verde Member

The Limón Verde Member corresponds to the second member of the Purilactis Formation. It lies conformably upon the Los Cóndores Member, showing a sharp contact between them (Figure III.7), where an evident change in color is observed. The basal section of this member, studied on the western flank of the syncline (Fig. III.2b, Appendix A.2), shows mostly fine- to medium-grained, laminated green to grey sandstones (Sh) (Figure III.8), at times developing cycles with normal grading less than 1 m thick (i.e., between ca. 14 and ca. 28 m). They usually contain chemical concretions. Contacts are commonly non-erosive. These sandstones may contain isolated clasts of andesitic origin up to 10 cm in diameter. Towards ca. 110 m, coarse-grained, laminated sandstones (Sl) appear intercalated with medium-grained sandstones, or as thick bodies up to 8 m thick. Conglomerate bodies (Gch and Gcm) make a rare appearance between ca. 152-186 m. Scouring surfaces, showing an erosional nature and basal lag, are also seen. Channelization is not observed in this part.



Figure III. 8. Grey, medium-grained sandstones of the Limón Verde Member, showing isolated clasts.

Past ca. 186 m, the middle and upper parts of this member, studied next to the former section and further north along the western flank of the syncline (Figure I.5), show an overall coarser profile. The measured column starts with medium- to coarse-grained, laminated (S1), grey to red sandstones, containing isolated clasts and diffuse, clast-supported conglomerate lenses. The sandstone lithosomes may show either normal or inverse grading, with sharp contacts between them. Above ca. 222 m, clast-supported, horizontally stratified conglomerates (Gch) appear, at times showing erosive basal contacts. They are commonly found as intercalated deposits less than 1 m thick that may show normal grading, between ca. 259-265 m, ca. 314-336 m. Trough cross-stratified sandstones (St) are also found as lithosomes 1 to 6 m thick. Between ca. 414-708 m, an important presence of horizontally stratified and/or laminated conglomerates (Gch) is seen, with poor to moderate sorting and subangular clasts, normally as cycles with normal grading up to 8 m thick. The clast size is in the granule-pebble range, although they may be locally of cobble size, especially in basal conglomerates. Conglomerates are also found as diffuse lenses within sandstone lithosomes. Erosive surfaces are clearly seen at the base of these cycles. The sandstones here are grey, laminated and medium- to fine-grained (Sh). Fine- to very fine-grained sandstones show the same structures, but present a reddish-brown color. Trough cross-stratified sandstones (St) are present as lithosomes less than 3 m thick (Figure III.9). Cycles become less recognizable between ca. 708-936 m. Here, the conglomerates show clast sizes mostly in the granule range, and are also thicker (around 1 m) overall, although they become

thinner towards the top. Contacts between lithosomes are mostly sharp, and medium- to fine-grained sandstones (Sh) are abundant. Isolated clasts can reach up to 30 cm in diameter. This subdivision grades into mostly reddish sandstones and conglomerates of the Licán Member. The contact is more clearly appreciated in the field in the southern portions of the syncline.



Figure III. 9. Lithosomes of the Limón Verde Member. Jacob's staff is 110 cm long.

The predominance of laminated sandstone facies in the first ca. 185 m of the Limón Verde Member leads to its interpretation as reflecting distal, braided, sand-dominated rivers, or flashy, ephemeral sheetfloods; both are similar, though the latter presents a smaller variety of sandstone facies (Miall, 1996). In any case, they represent distal braid plains with little to no channelization, in mostly arid regions with shallow channel depths (Miall, 1996). Past ca. 185 m, the section shows a more varied array of lithofacies, with clear development of 3-D dunes and cycles indicating channels up to 8 m deep. Between ca. 186-414 m and ca. 708-936 m, the column possibly represents ephemeral sheetflood deposits, where laminated facies (Sl/Sh) are ubiquitous, which is also supported by a partial column measured on the southwestern flank of the syncline. The latter interval could also represent sandy, braided rivers. The abundance of conglomerates between ca. 414-708 m point to a gravel-sand meandering river or a deep, gravel-bed braided river (Miall, 1996).

Hartley *et al.* (1988; 1992) interpreted the Limón Verde Member as proximal to medial alluvial fan deposits, presenting laterally amalgamated stacked sandstone/pebble conglomerate packages, with poor to no channelization, where sandstone sheetfloods are the predominant facies

type. However, according to Miall (1996), it is reasonable to interpret these sheetfloods as deposits of more distal environments, which does not conflict with an alluvial origin. The coarse-grained section indicates a more proximal (possibly medial) environment, represented in the development of the deeper cycles observed (see above).

Lampallar Member

Outcrops of this member were examined in a section on the southwestern flank of the syncline, where it rests conformably on the Limón Verde Member (Figure I.5). It is the first of the subdivisions for the Licán Member (*sensu* Hartley *et al.*, 1992) proposed by Henríquez (in prep.). The Lampallar Member (Figure III.2c, Appendix A.3) shows ca. 160 m of laminated, brown to dark brown, fine- to medium-grained sandstones (Sh), with some coarser-grained deposits (Sl). In both cases, the deposits show poor to no channelization. They possess good overall sorting, but may contain isolated clasts up to 20 cm in diameter. It is also common to find lenses and/or small channels filled with clast- and/or matrix-supported conglomerates, showing subrounded, granule- to pebble-sized clasts in a medium- to coarse-grained sandstone matrix (Figure III.10). Above ca. 160 m, the section shows an increasing occurrence of conglomerates together with laminated sandstones.



Figure III. 10. Horizontally stratified conglomerate lenses interbedded between medium- to coarse-grained laminated sandstones of the Lampallar Member.

These coarser facies may show slight channelization. Matrix-supported, graded conglomerates (Gmg) can be up to 8 m thick, showing either inverse or normal grading, whereas matrix-supported, massive conglomerates (Gmm) are found as 30 cm thick lenses, although some lithosomes may be up to 8 m thick. Clast-supported conglomerates, either stratified or massive (Gch and Gcm respectively), are observed primarily as compound units, with either erosive or sharp contacts (Figure III.11). They are predominant in the last 100 m of this section, where they are found as units 1 m thick, intercalated with laminated sandstones (Sl). Some lenses and minor channels (less than 2 m wide) present massive, clast-supported conglomerates (Gcm) with normal grading, which are abundant in this part of the section together with fine-grained, laminated sandstone lenses (Sh) less than a meter thick.



Figure III. 11. Medium-grained sandstones showing a channel filled by massive, clast-supported conglomerates.

The facies described above reflect a transition from coarse-grained, sandy bedforms to different conglomerate types, showing faint channelization which is better developed upward in the section, forming cycles and channels less than 1 m thick; this is consistent with a shallow, gravel braided river (“Scott type”; Miall, 1996), with scarce gravity flow intercalations, as shown by the matrix-supported conglomerates.

Licán Member

The Licán Member was observed on the same flank where the previous member was studied (Figure I.5), and it corresponds to the second subdivision of the former Licán Member

made by Henríquez (in prep.). This member (Figure III.3a, Appendix A.4) shows a gradual transition from the previous division, where a change to red sandstones marks the difference between both units (Figure III.12). Conglomerates become increasingly important in the first ca. 150 m, being mainly of the clast-supported, massive type (Gcm), in beds less than 1 m thick, intercalated with medium- to fine-grained laminated sandstones (Sh). Other conglomerate facies are less noticeable. Most conglomerates show moderate sorting and rounded to sub-rounded clasts. Above ca. 150 m, sandstones become the most prominent lithology, showing laminated and stratified facies (Sl and Sh) that may locally become very faint. Contacts are usually sharp and non-erosional. Trough cross-stratified sandstones (St) are also found on rare occasions, where they might reach up to 2 m in thickness. Conglomerates found in this part of the section are clast-supported, either massive or stratified (Gcm and Gch), and occasionally matrix-supported (Gmm). They are found as lithosomes 1 m thick that are interbedded with laminated sandstones (Sl/Sh), forming discrete units a few m thick (Figure III.13).



Figure III. 12. Outcrops of interbedded red and brown sandstones and conglomerates of the Licán Member.



Figure III. 13. Horizontally stratified conglomerates interbedded with coarse-grained sandstones.

The interpretation for this member is quite similar to that for the Lampallar Member, though with a fining-upward trend. More reddish beds could also indicate increased subaerial exposure, which is also reflected by the presence of burrows toward the top of the section. Also, gravity flow deposits are scarcer than in the previous member.

Pajarito Member

The third subdivision of the former Licán Member (*sensu* Hartley *et al.*, 1992) was observed in the western flank of the syncline, where it conformably underlies the Vizcachita Member (Figure III.14); it also lies conformably on the Licán Member. The Pajarito Member (Figure III.3b, Appendix A.5) shows brown to reddish brown sandstones and conglomerates, grading from reddish sandstones of the previous subdivision. The dominant facies present are medium- to very coarse-grained, brown to dark grey, laminated sandstones (SI), containing at times isolated clasts up to 8 cm in diameter and diffuse, thin conglomerate lenses (Figure III.15). They are present as lithosomes 1 to 10 m thick, showing mostly sharp contacts with previous deposits. Beds, when clearly identified, are less than 50 cm thick, and sometimes show normal grading. Fine-grained, reddish sandstones are less noticeable (i.e., between ca. 14-21 m, 91-100 m). Conglomerates are mostly found as laminated or horizontally stratified, clast-supported lithosomes (Gch) less than 1 m thick, showing erosional basal surfaces. Cycles are not clearly

developed, although an upward-fining motif can be seen in certain instances, where these conglomerates alternate with progressively finer-grained sandstones and conglomerates (i.e., between ca. 9-14 m, 34-36 m, 46-48 m). Locally, the conglomerates form compound units intercalated with coarse-grained sandstones (i.e., between ca. 60-76 m). Planar cross-stratified conglomerates and massive conglomerates (Gpt and Gcm) are also found (i.e., between ca. 21-24 m, 34-36 m). Towards the top of the column (from ca. 76 m upward) laminated sandstones (Sl and Sh) become predominant.

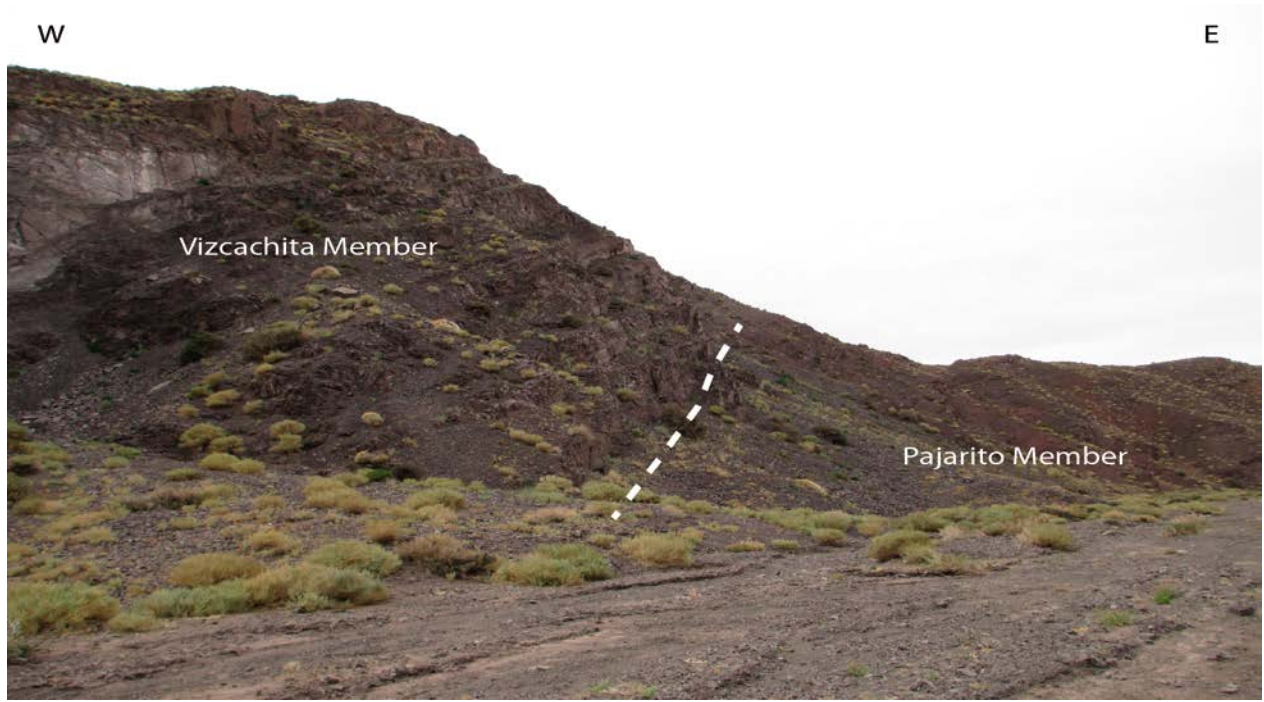


Figure III. 14. Gradational contact between the Vizcachita and Pajarito Members.



Figure III. 15. Outcrops of the Pajarito Member, showing diffuse, thin lenses with granule-sized grains, together with coarse-grained sandstones.

The Pajarito Member shows, in its first 76 m, lithofacies belonging to gravel-bed, probably shallow rivers, with a channel depth of ca. 1 m, while the upper portion of the column signals a change to ephemeral sheetflood, sand-bed rivers (Miall, 1996).

These three members have been previously identified as forming part of medial to distal cycles of alluvial fan progradation, with channelized sheetflood sandstones, red mudstones and minor conglomerates (Hartley *et al.*, 1988; Hartley *et al.*, 1992). The facies described above are partly consistent with this interpretation; conglomerates are much more abundant in these sections (particularly in the second division), and channelization is, in general, less evident. The gravity flow deposits also, though not predominantly, evidence a more proximal origin for the coarse-grained sections of this member. Evaporitic facies were not observed. The same authors described numerous coarsening-upward cycles 15-50 m thick; the conglomerates described here appear as intervals more than cycles, although the three members combined do show an overall coarsening-upward motif. Small-scale fining-upward cycles, as described by Hartley *et al.* (1992) have also been found.

Vizcachita Member

The Vizcachita Member was partly observed in the northeastern section of the Barros Arana Syncline (Figure I.5; Figure III.3c, Appendix A.6). It shows a transitional contact with the Pajarito Member (Figure III.14); though the color clearly changes on satellite images, similar facies are found in both members near their contact. This member comprises grey, medium to fine-grained lithic sandstones with horizontal lamination (Sh), good sorting and subrounded grains. It shows practically no variations throughout most of the measured section, except for a 2 m thick unit of poorly sorted, brown, coarse-grained sandstone (Sl) with isolated clasts up to 5 cm in diameter at ca. 43 m, and a couple of 2 m thick coarse, volcanoclastic intercalations in the upper half of the column (Sl). Lamination is faint in some instances; in higher parts of the column, both horizontal bedding and cross-lamination are clearly developed, showing beds around 30 cm thick. Above ca. 156 m, large scale-cross stratification is evident (St) (Figure III.16), with no evident change in textural maturity or composition. This member also presents an andesitic intercalation towards its top, in some places, marking the contact with the Seilao Member (Hartley *et al.*, 1992; Arriagada, 1999).

The deposits described above show an overwhelming occurrence of laminated sandstones (Sh) up to ca. 152 m, which leads to two possible interpretations, considering the important presence of large-scale cross-stratification higher up; either they correspond to ephemeral sheetflood sand-bed rivers (Miall, 1996), or eolian deposits (Kocurek 1981, 1991). Hartley *et al.* (1988) suggest a fluvial origin for some of these sandstones, although they also note that this member presents strong lateral variations into eolian dunes and eolian sand sheets. They also show that the eastern flank of the syncline presents a more abundant proportion of eolian sandsheets and dunes than the western flank, which is interpreted to have had a more important fluvial input. The presence of large scale cross-stratification and texturally mature sandstones above ca. 156 m is evidence of large dunes, up to 25 m high; Hartley *et al.* (1988; 1992) identified them as barchans, in places reaching up to 30 m high.



Figure III. 16. Outcrops of the Vizcachita Member, showing large-scale cross-stratificated sandstones. Person shown as scale is 1.65 m tall.

Seilao Member

The Seilao Member, studied on the western flank of the syncline (Figure I.5; Figure III.4a, Appendix A.7), shows a return to coarse facies, presenting brown, mainly horizontally laminated and/or stratified clast-supported conglomerates (Gch), with the clast size in the pebble-cobble range (Figure III.17). They alternate with laminated, medium-grained sandstones (SI/Sh). The clasts are usually subangular and spherical in shape; thicker deposits with cobble-sized clasts show poor sorting, and the matrix is usually coarse to very coarse, poorly sorted and texturally immature sand. Beds show poor channelization. Some conglomerates display normal grading, from cobble-pebble clast-supported conglomerates to medium-grained sandstones, which mainly fill channels 10 to 20 cm deep and 1 m wide. Most of the contacts between units are conformable and non-erosive, although some conglomerates show either basal scouring or minor channel infilling (e.g., between ca. 58 and ca. 74 m). Granule, clast-supported conglomerates are important above ca. 31 m. At ca. 74 m, coarse-grained sandstones (SI) become more relevant, and the conglomerates show a decrease in thickness and clast size, becoming less than 10 cm thick and having mainly granule-sized clasts. Contacts between the units also become more diffuse. From ca. 81 m to 125 m, laminated, coarse to very coarse-grained sandstones, with isolated clasts up to 30 cm in diameter, together with conglomerate lenses, become the dominant lithofacies in the section, although clast-supported conglomerates beds do occur (mainly between ca. 110 and 115 m). They may show a fining-upward trend from granule-sized clasts to coarse-grained sandstones. Clast-supported conglomerates become important once again at ca. 125 m, where they are also interbedded with coarse-grained, laminated sandstones (SI). Contacts are mostly non-erosive, and some units may fine upward. From ca. 174 m to ca. 269 m, the section presents

mainly laminated, coarse sandstones (SI), occasionally with isolated clasts and minor conglomerate beds less than 1 m thick, either massive or laminated (Gcm and Gch, respectively). The section here displays multiple clast-supported conglomerate beds, around 1 m thick, most of which are stratified (Gch). These beds have mostly sharp, non-erosional contacts, although some massive conglomerates show evidence of basal scouring. From ca. 326 to ca. 414 m, laminated, coarse-grained sandstones containing isolated clasts (SI) are found, along with scarce conglomerate lenses. Some of these sandstones appear as fining-upward cycles around 1 m thick, separated by a few cm of fine sandstone. Contacts between sandstone lithosomes may show basal scouring, along with rip-up clasts. Clast-supported conglomerates (mostly Gch) are found extensively after ca. 414 m, where they form bodies less than 2 m thick, at times interbedded with laminated, coarse-grained sandstones (SI). Contacts are mostly non-erosional, at times diffuse; however, some erosional surfaces exist between massive, clast-supported conglomerates (Gcm) and other lithosomes, where the former appear to erode the latter. Laminated sandstones (SI/Sh), although less prominent than the conglomerates, form most of the outcrops between ca. 548 m and ca. 576 m.



Figure III. 17. Horizontally stratified conglomerates of the Seilao Member.

According to Miall (1985; 1996), the deposits described above could represent, primarily, shallow, gravel-bed braided rivers, with intervals dominated by ephemeral sheetflood deposits (coarse-grained, laminated sandstones (SI)). The pattern of stratified conglomerates interbedded

with laminated sandstones is a common sight in braided stream conglomerates, where slight fluctuations in stream velocity may produce this alternation (Nemec & Steel, 1984). Finer-grained sandstones are equated to overbank deposits.

The coarse-grained nature of these deposits has been attributed to alluvial fan sedimentation with sheet and channel sandstones and conglomerate facies displaying large-scale coarsening-upward and fining-upward cycles (around 100 m thick), separated by small-scale cycles (3-15 m). While the coarsening-upward cycles show a change from playa and sandflat deposits to poorly confined conglomeratic sheetfloods and high-density flood deposits, the fining-upward cycles show the inverse succession (Hartley *et al.*, 1992). Although the transitions between these cycles are hard to observe in this section, coarse-grained and fine-grained intervals can be clearly discerned; these are not always separated by small-scale cycles. Overall, the description closely resembles that of previous authors (e.g., Hartley *et al.*, 1992; Mpodozis *et al.*, 2005; Arriagada *et al.*, 2006a).

Rio Grande Member

The Rio Grande Member was partly observed above the section described for the Seilao Member (Figure III.4b, Appendix A.8). The contact between both members is sharp, conformable, and traceable on satellite images. The section shows mostly laminated, brown to green, medium- to very fine-grained lithic sandstones (Sh) with scarce coarse- to very coarse-grained, laminated sandstones (Sl) containing isolated clasts up to 20 cm in diameter, and massive, clast-supported conglomerate lenses (Gcm). Some of the medium-grained sandstones display fining-upward cycles, such as those observed in the Seilao Member section (see above), between ca. 16 m and 36 m. This section is mostly covered towards the top (Figure III.18).



Figure III. 18. Fine- and coarse-grained outcrops of the Río Grande Member. Outcrops of the Barros Arana Formation are seen beyond the highway.

The section described above shows an abundance of lithofacies related to ephemeral, poorly confined sand-bed rivers (Miall, 1985; 1996), representing a transition to a more distal environment from the coarser, proximal to medial facies of the Seilao Member. Although they were not observed in this section, Hartley *et al.* (1988; 1992) found lacustrine siltstones and mudstones, together with green sandstones in this section, indicating frequent alluvial flooding and deposition of sheetflood sandstones. It is likely that this section represents the latter, coarser deposits.

Barros Arana Formation

The Barros Arana Formation was studied in a section directly east of the one described for the Río Grande Member (Figure III.4c Appendix A.9), where it forms the core of the Barros Arana Syncline. The section starts with ca. 42 m of green, medium- to coarse-grained laminated sandstones (SI) with isolated clasts less than 2 cm in diameter. A transition to pebble-sized, laminated, clast-supported conglomerates (Gch) is evidenced at this point, which are found as beds less than 1 m thick, interbedded with the sandstones described above (Figure III.19). The contacts between beds are mostly sharp and non-erosional. At ca. 114 m, laminated sandstones

become prominent over the conglomerates, which appear either as thin beds or lenses less than 1 m wide and a few cm thick. At ca. 150 m, the section shows a return to stratified conglomerates (Gch) exhibiting sharp contacts; some beds, however, do show basal scouring. Cross-stratified conglomerates (Gpt) (Figure III.20) are also found, together with stratified conglomerates (Gch) up to 2 m thick with granitic clasts reaching 30 cm in diameter. Laminated, medium-grained sandstones (Sl/Sh) overlie the latter deposits between ca. 160 and ca. 180 m, primarily as fining-upward cycles less than 1 m thick, with isolated clasts up to 7 cm in diameter. The section is more homogeneous from this point upward (ca. 180 m). It is formed by cycles 6 to 30 m thick, containing either a stratified or massive basal conglomerate (Gch or Gcm) showing basal scouring, slight channelization, poor to regular sorting and subangular, cobble- to pebble-sized clasts, followed by clast-supported conglomerate bodies around 1 m thick interbedded with medium- to very coarse-grained sandstones. The contacts between these lithosomes are non-erosional and diffuse. The sandstone portion varies from scarce to more than half of an individual cycle. The conglomerates are mostly stratified (Gch), sometimes massive (Gcm), and, on rare occasions, matrix-supported (Gmm); all of them show clast sizes mostly in the granule-pebble range, although they can be locally cobble-sized. The conglomerates can contain boulders up to 40 cm in diameter. These cycles end with coarse- to medium-grained, laminated sandstones (Sl) containing isolated clasts, with the top usually eroded by the subsequent cycle. Towards the upper half of this section (ca. 508 m), laminated, red to dark brown, very fine-grained sandstones (Sh) are found overlying coarse-grained sandstones and deposits of the previous cycles, up to ca. 539 m, where they are covered once again by conglomerate cycles. Similar deposits are also found between ca. 610 m and ca. 645 m, where they show grading from clast-supported, stratified conglomerates (Gch), up to laminated, medium- to fine-grained sandstones (Sh) with isolated clasts and conglomerate lenses. At ca. 662 m, medium and coarse-grained laminated sandstones (Sl) are found overlying these conglomerate cycles; they contain rare conglomerate lenses and isolated clasts up to 15 cm in diameter. A return to conglomerate facies is marked by basal erosion at ca. 699 m. The conglomerates are once again overlain by fine to very fine-grained, laminated sandstones (Sh) from ca. 738 m to ca. 758 m. Conglomerate cycles above this point show some individual clast-supported stratified beds (Gch) around 4 m thick. Above these cycles, at ca. 788 m, medium- to fine-grained laminated sandstones (Sh) are found up to ca. 806 m, and once again between ca. 880 and ca. 894 m; the former show well-developed bedding, while the latter have fainter contacts.

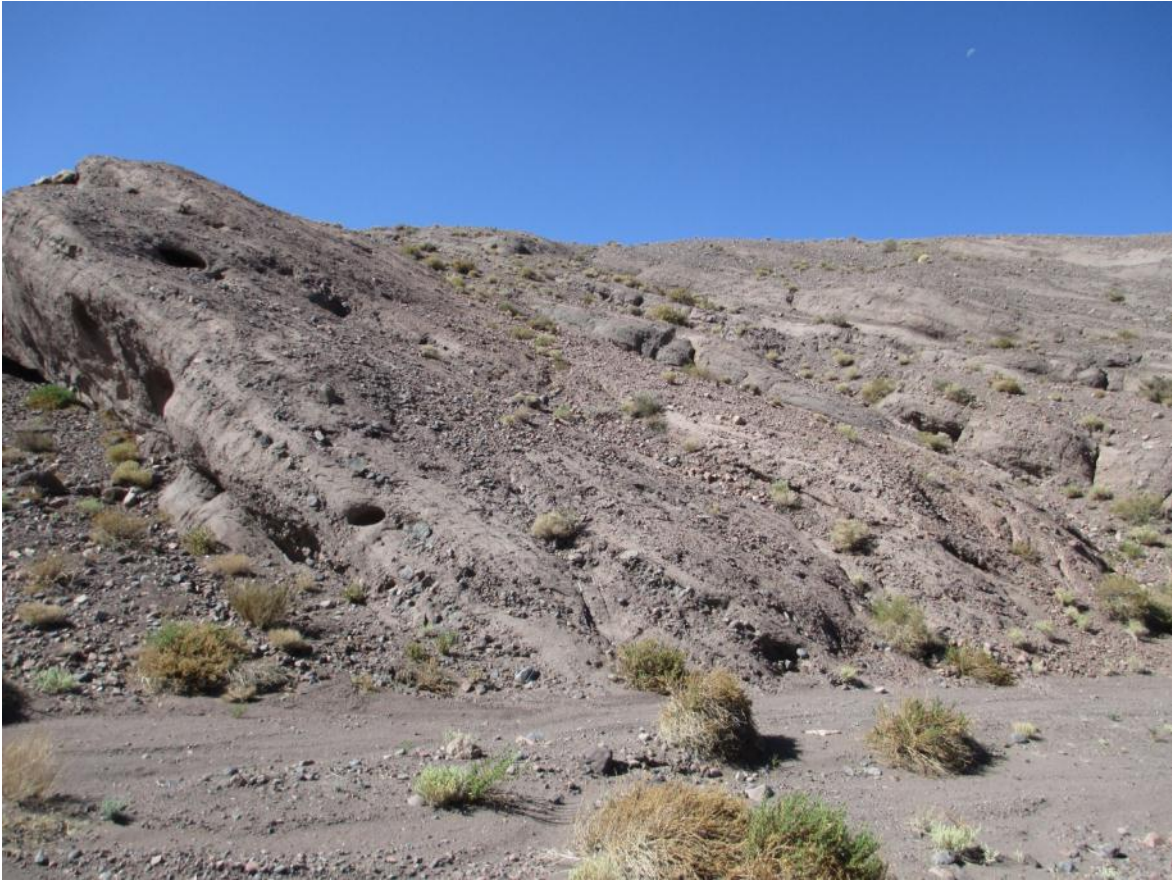


Figure III. 19. Outcrops and lithosomes of the Barros Arana Formation.



Figure III. 20. Sandstones and planar cross-stratified gravels of the Barros Arana Formation.

The dominance of conglomerate and minor sandstone cycles observed throughout this section is typical of gravel-bed braided rivers, either shallow or deep (Miall, 1996). A strong case is made for the second type by the development of cycles, which indicate deeper (at least > 1 m) channel depths (Miall, 1996). The cycles are similar to the turbulent sediment flows of Nemeč and Steel (1984), which are related to subaerial mass flows, possibly in environments with an important amount of water. The presence of extensive sandstone intervals could be related to overbank deposits, but it could also be argued that they are deposits belonging to ephemeral, poorly channelized sheetflood deposits, the product of flash floods in arid environments (“Bijou-Creek” type deposits; Miall, 1985; 1996).

Hartley *et al.* (1992), who did not extensively study this formation, proposed a proximal alluvial origin, based on the laterally amalgamated channelized streamflow and sheetflood deposits, interbedded with scarce high-density flood and debris flow deposits observed. This description is very similar to the section seen above.

III.2 Paleocurrent data

The results of the paleocurrent measurements are shown in Figures III.21 (not corrected for tectonic rotation) and III.22 (corrected). The Tonel Formation shows data indicating a predominantly NNE-trending flow, and fewer paleocurrents in the NW and ESE directions. The Limón Verde Member presents one main paleocurrent direction showing paleochannels and parting lineations towards the ESE, and another group of indicators pointing towards the NE. The Lampallar, Licán and Pajarito Members show a dominant transport to the E, recorded in many cross-stratified sandstones, with only a few structures pointing towards the NNW. The Vizcachita Member presents large paleodunes indicating sediment transport to the WSW (Figure III.16). Data from the Seilao Member show a clear ESE tendency, with some structures pointing to the ENE. The Barros Arana Formation shows a major component to the NE, and a second one to the WNW; the latter component could possibly reflect diagonal and/or point bar migration (Hein, 1984).

This information indicates a general west to east (NE-ESE) transport in most formations and members, with the exception of the mainly eolian Vizcachita Member showing westerly transport. The unrotated data is consistent with measurements taken by Hartley *et al.* (1988, 1992). This preferred direction is likely due to uplift of the Cordillera de Domeyko Range (Figures I.3, I.4, I.5), situated west of the study location, during the sedimentation of the three formations. In this regard, Mpodozis *et al.*, (2005) and Arriagada *et al.*, (2006a) found growth structures in strata belonging to the Tonel Formation, which indicate a compressional regime during their sedimentation in mid-Cretaceous times; the space available for sediment accumulation and the deformation observed would be partly due to an eastward-verging thrust system related to the Cordillera de Domeyko Range. The directions observed in the Vizcachita Member attest to the main wind direction during its deposition (Kocurek, 1981; 1991). Hartley *et al.* (1992) obtained paleowind directions to the north; this discrepancy could result from the interpretation of the structures observed in this member, where they could be either classified as tangential cross-laminated sets or one flank of a large trough formed by a barchan dune.

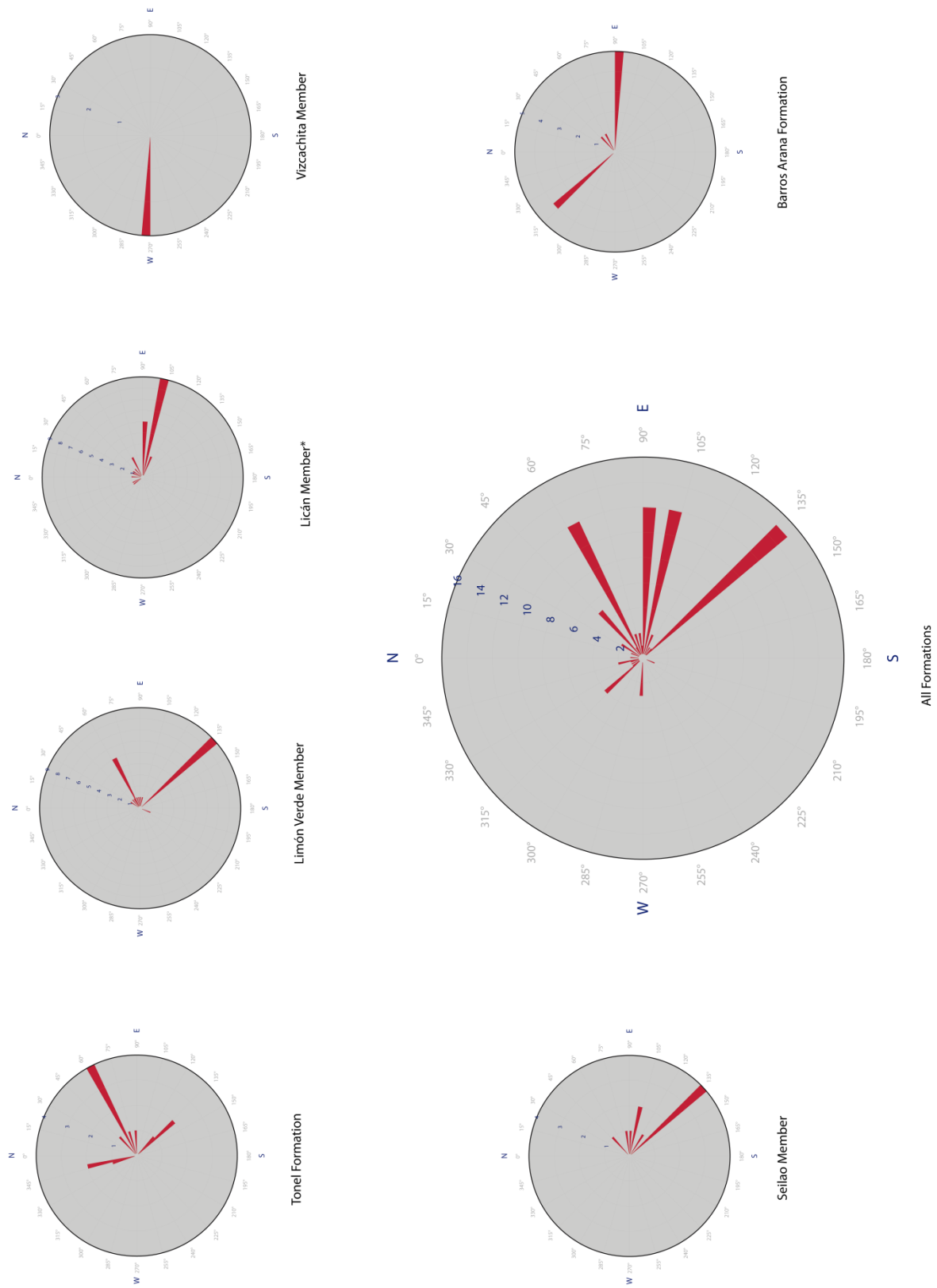
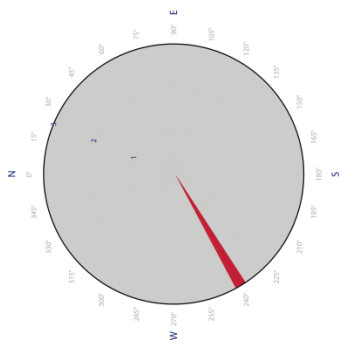
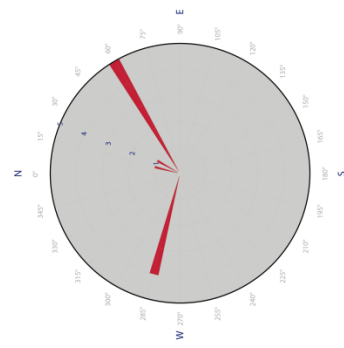


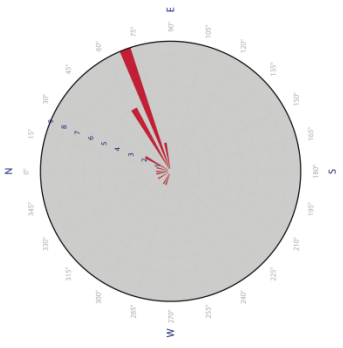
Figure III. 21. Paleocurrent data obtained for the Tonel, Purilactis and Barros Arana Formations. Information plot with GeoRose 0.3.0 software. Data without rotation. Number of measurements shown inside the circle.



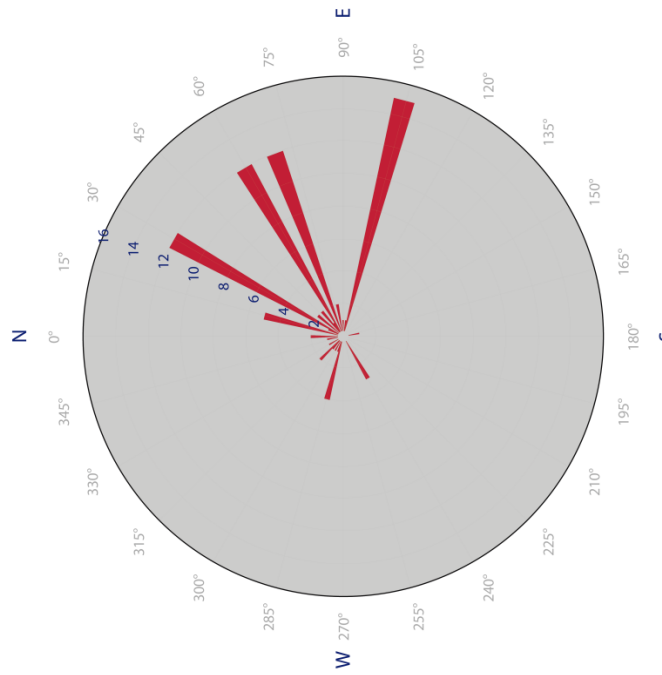
Vizcachita Member



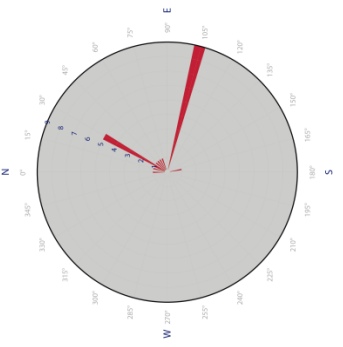
Barros Arana Formation



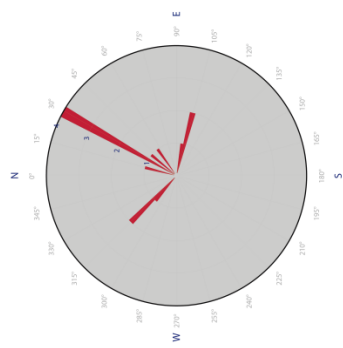
Licán Member*



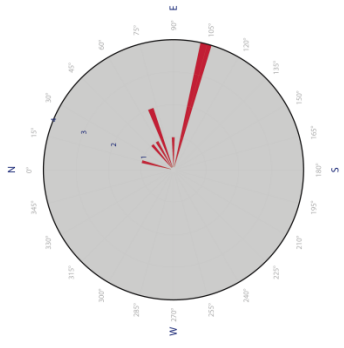
All Formations



Limón Verde Member



Tonel Formation



Seilao Member

Figure III. 22. Rotated paleocurrent data.

III.3 Conglomerate clast count

The conglomerate clast-counts are shown in Figure III.23. The Tonel Formation (Agua Salada Member) shows a predominance of andesitic and tuffaceous clasts, with only 10% of clasts being of sedimentary rock origin. These last are, most likely, a product of erosion within the same formation. The Limón Verde Member presents andesitic clasts as its key component, together with only a minor proportion of sedimentary clasts, and even fewer rhyolitic to dacitic tuff clasts. The observed siltstone and sandstone clasts are similar to the facies described for this member, making them a product of limited erosion or cannibalism. The Lampallar and Licán Members (only qualitatively observed) show clasts of andesitic origin, with few sandstone clasts in the former, while the Pajarito Member shows rhyolitic to dacitic tuff clasts together with andesitic clasts. The Seilao Member shows a prevalence of andesitic clasts, followed by granitic clasts, in a 3:1 ratio; this is reversed towards the top of this section. Finally, the Barros Arana Formation shows an increasing proportion of granitic vs. andesitic clasts, with only minor sandstone and limestone clasts.

The sections observed document an abundant presence of andesitic clasts, and a gradual increase of granitic, coarse-grained clasts over time; this is most evident in the Barros Arana Formation and Seilao Member sections, where granitic boulders can exceed 30 cm in diameter. These clasts are probably derived from granitoids that represent deep exhumation of the Cordillera de Domeyko area (Mpodozis *et al.*, 2005). The source of the andesitic clasts is most likely the Tuina Formation and/or exhumed levels of the Late Cretaceous-Eocene Arc (Hartley *et al.*, 1992).

Hartley *et al.* (1988; 1992) obtained similar clast compositions, with a higher percentage of limestone clasts in the Purilactis Formation; this is attributed to uplift of the Triassic-Lower Cretaceous back-arc basin fill, due west of the study area, which is consistent with observed paleocurrent bearings and growth structures (see above).

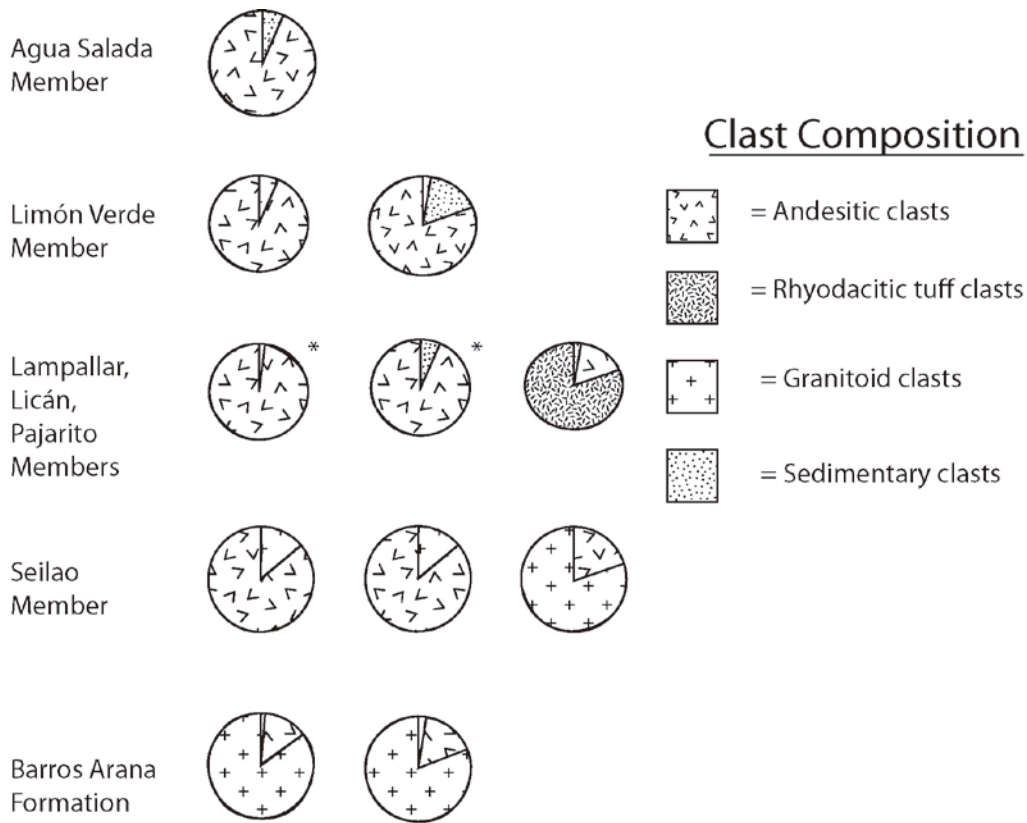


Figure III. 23. Conglomerate clast-counts for the Tonel, Purilactis and Barros Arana Formations. Counts marked with * are qualitative in nature.

III.4 Sediment provenance

The results of the point-counts performed are shown in Figure III.24. The La Escalera Member and one Limón Verde Member sample show an important amount of plagioclase, K-feldspar and quartz over lithic fragments; the quartz observed is mostly monocrystalline, while the lithics are mostly andesitic, microlithic fragments. Samples found higher in the stratigraphic record (upper Limón Verde Member and samples of the Licán Member *sensu* Hartley *et al.*, 1992) show a more important presence of lithic fragments and plagioclase over feldspar, occasionally containing red siltstone and minor quartz-feldspathic sandstone fragments. The sandstones of the Vizcachita Member show an overall lower percentage of quartz relative to other components, and a relevant presence of andesite fragments; plagioclase and quartz are again important in the Seilao Member, but are less commonly found in the Río Grande Member. The plotted average for the Purilactis Formation indeed shows that volcanic, lithic fragments are the most important constituent found, followed by plagioclase feldspar and monocrystalline quartz. Finally, the Barros Arana Formation sample shows monocrystalline quartz and plagioclase as major components. Some accessory minerals found throughout the section comprise opaque

minerals, micas, hornblende and, in some cases, broken, almost fresh pyroxene, particularly in the samples belonging to the Río Grande and Vizcachita Members.

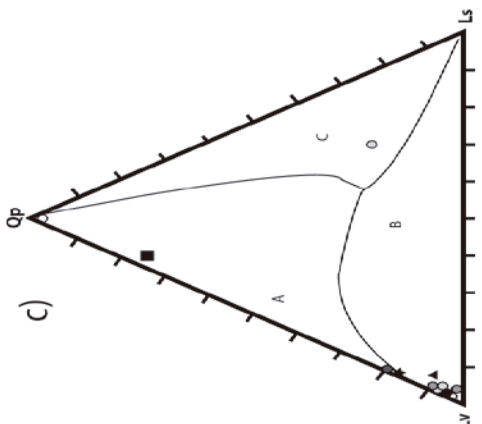
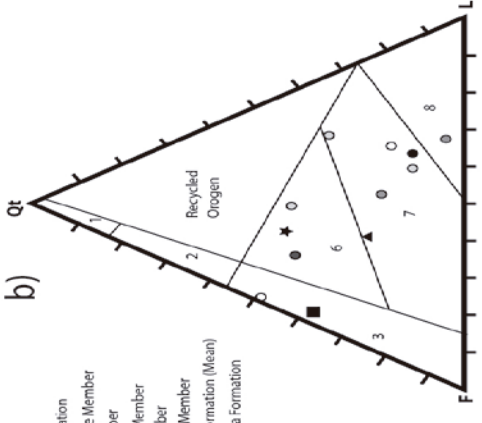
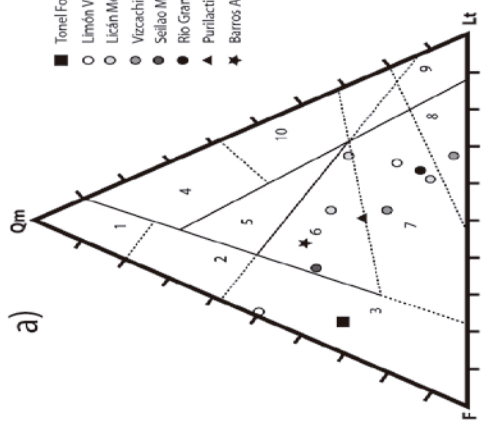
Source area classification of these sandstones is open to interpretation, partly because of the important amount of plagioclase found, which, in many cases, is overwhelmingly observed as very fine to fine sand-sized grains inside volcanic fragments. Though the traditional Gazzi-Dickinson method and other authors (see above) favor including these fragments in the feldspar group, we believe that, in this particular case, doing so would obscure the origin and nature of the formations.

When plagioclase in lithic fragments is considered as a volcanic fragment, most of the sandstones plot in the magmatic arc fields, though some samples may show some divergence when different diagrams are used. No clear temporary trend can be observed, although the two upper formations plot mostly in the volcanic arc fields, particularly the dissected to transitional arcs in the case of the Barros Arana and Purilactis Formations (Figure III.24, a, b). Only the La Escalera Member plots in the basement uplift field, which is the product of erosion of uplifted, deeply incised basement; however, Dickinson *et al.* (1983) concede that volcanic arcs can show similar compositions if they are intensively dissected, so that petrographic methods do not help in clarifying the tectonic regime if compositional overlap occurs.

Weltje (2006) tested the model proposed by the aforementioned authors, and produced modified ternary diagrams by means of statistical analysis. The diagrams are partitioned into three spaces separated by iso-density probability lines, where the grand means of each provenance association and their confidence regions are plotted. The efficiency of the partitioning and the predictive utility of these new diagrams were tested by stochastic simulations. The results show that probabilities of correct inference are: QpLvLs (78%), QFL (76%), QmFLt (74%) and QmPK (64%) (Figure III.24, c, d, e, f). Also, Ingersoll (2012), who worked on the Sierra Nevada and southern Cascade Magmatic arc, proposed a QpLvFp diagram (Figure III.24g) based on the discriminant analysis of modern sands shed from the arc. The latter shows a N-S trend, with more exhumation toward its southern end (basement uplift) than the north (undissected arc).

Following these diagrams (Figure III.24, c, d, e, f), the Tonel Formation falls in the basement uplift and continental block fields, though near to the magmatic arc field. The Purilactis Formation, as a whole, and the Barros Arana Formation plot mostly in the magmatic arc field. On the QpLvFp diagram (Figure III.24f), the sandstones of the Purilactis and Barros Arana Formations are closely located to the transitional arc field, while the Tonel Formation is closer to more uplifted, incised portions of the arc field.

Finally, in the case that the plagioclase found in lithic fragments were counted as feldspars, the sandstones would plot ambiguously between the basement uplift and transitional to dissected arc fields. This information can be reviewed in Appendix B.



- Tonel Formation
- Limón Verde Member
- Licán Member
- Vicachita Member
- Sellao Member
- Rio Grande Member
- ▲ Purilactis Formation (Mean)
- ★ Barros Arenas Formation

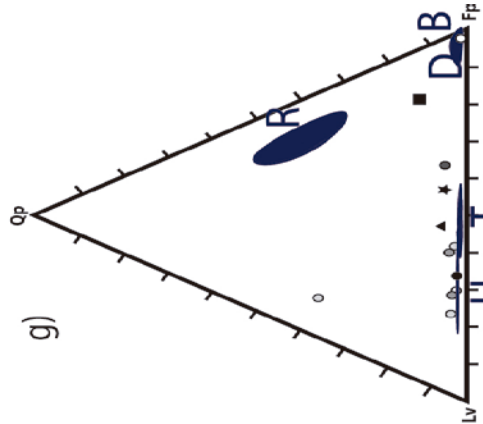
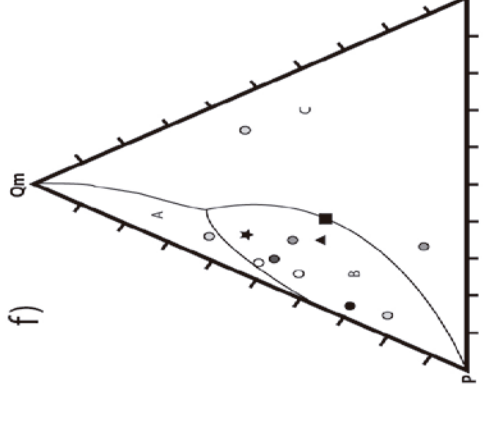
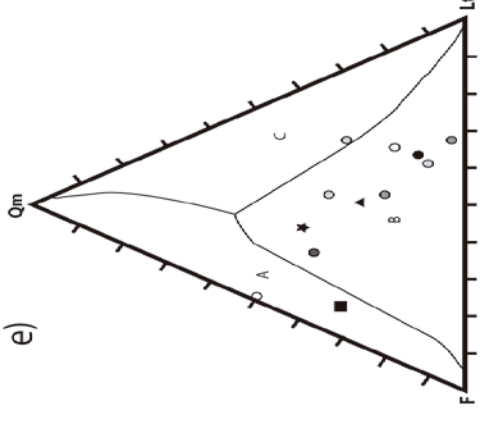
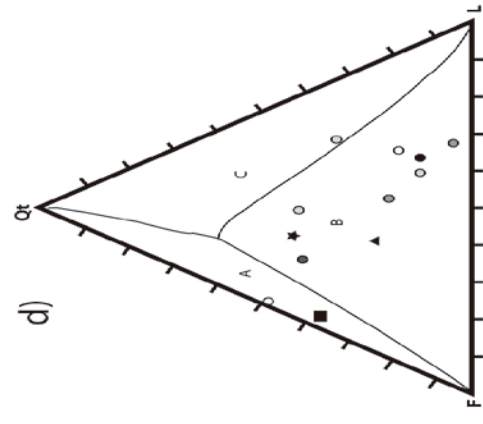


Figure III. 24. Sandstone petrographic data: a) Qt-F-L and b) Qm-F-Lt diagrams. Fields after Dickinson et al. (1983). 1: Craton Interior. 2: Transitional Continental. 3: Basement Uplift. 4: Quartzose Recycled. 5: Mixed. 6: Dissected Arc. 7: Transitional Arc. 8: Undissected Arc. 9: Lithic Recycled. 10: Transitional Recycled. c) Qp-Lv-Ls, d) Qt-F-L, e) Qm-F-Lt and f) Qm-P-K after Weltje (2006). A: Continental Block Provenance. B: Magmatic Arc Provenance. C: Recycled Orogen Provenance. g) Qp-Lv-Fp, after Ingersoll (2012). U: Undissected Arc. T: Transitional Arc. R: Recycled Orogen. B: Basement Uplift.

III.5. Detrital U-Pb geochronology

Tonel Formation

The two samples provided by Narea (in prep.) for the Tonel Formation (Figure I.5) show contrasting age populations. Sample K-4 (Figure III.25a), taken from the La Escalera Member, near the contact with the Agua Salada Member, presents $n = 42$ zircons in the Triassic, with $n = 5$ zircons around 211 Ma, $n = 7$ around 219 Ma and $n = 30$ around 230 Ma. These are followed by Permian-Triassic (252 Ma, $n = 19$), Permian-Carboniferous ($n = 8$ around 291 Ma and $n = 7$ around 299 Ma), mid to Early Cretaceous ($n = 5$, around 107 Ma) and Jurassic (153 Ma, $n = 4$) populations. The mean age obtained for the youngest population is 107 Ma, which corresponds to the sediment's maximum depositional age. The relative probability plot shows a high age peak around 252 Ma, followed by 230 Ma and 107 Ma peaks.

Sample K-18, taken from the Arcoiris Member (Figure III.25b) presents a maximum depositional age of 141 Ma. The largest populations found are of Ordovician ($n = 4$ around 459 Ma and $n = 7$ around 480 Ma) and Ediacaran ($n = 6$ around 566 Ma and $n = 4$ around 590 Ma) age. Other noteworthy populations are found (in decreasing order) in the Triassic ($n = 5$ around 228 Ma and $n = 4$ around 243), the Cambrian (566 Ma, $n = 6$), the Permian (260 Ma, $n = 5$), and the Early Cretaceous (142 Ma, $n = 5$). It is also worth noting that this sample has zircons in the Meso-Proterozoic (1000-1600 Ma), with $n = 10$ around 1125 Ma. The relative probability plot shows its most prominent peaks around 142 Ma and 228 Ma.

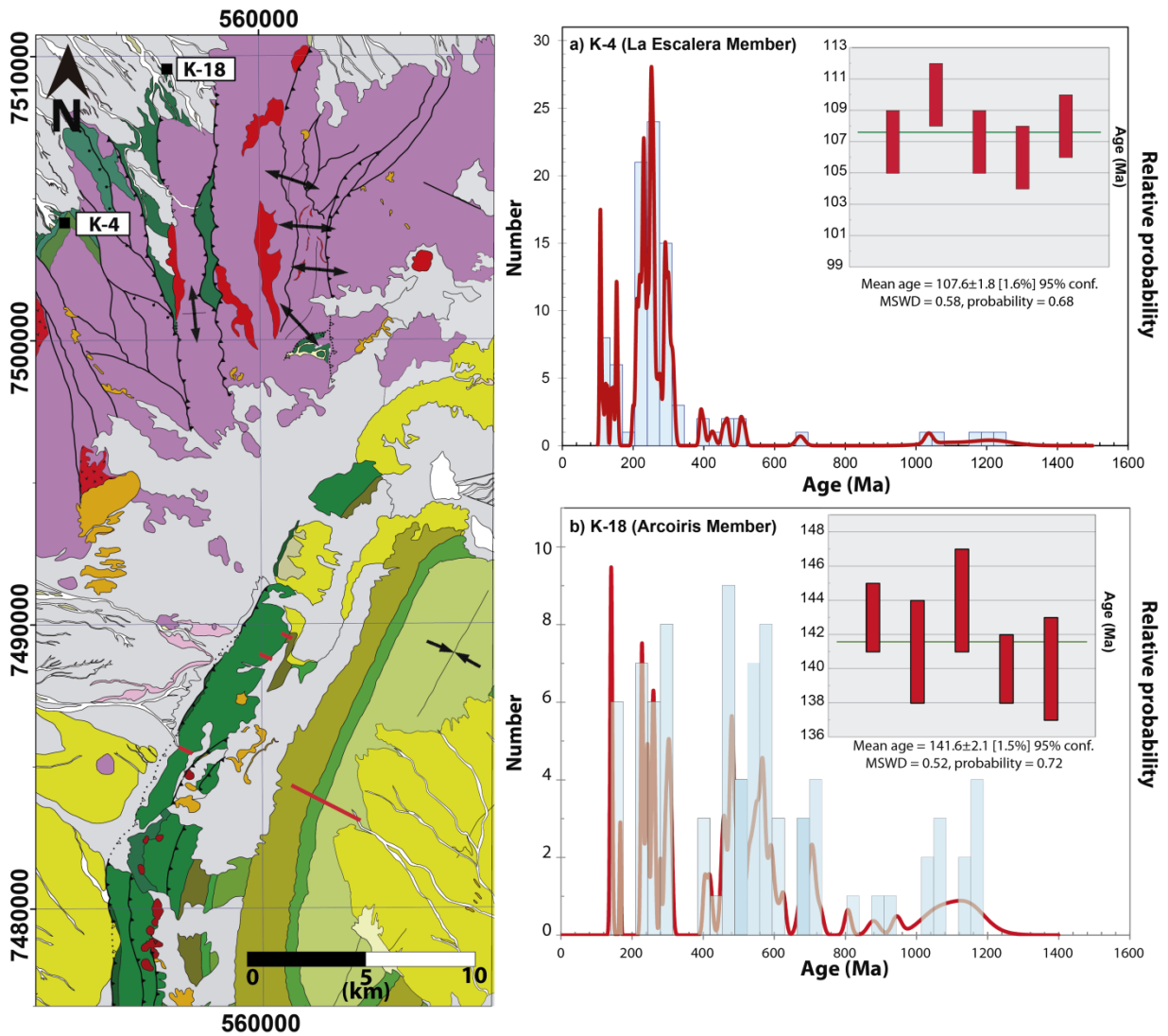


Figure III. 25. Sample location and U-Pb geochronology results for the a) La Escalera Member and b) Arcoiris Member. Map key found in Figure I.5.

Purilactis Formation

Limón Verde Member

The Limón Verde Member samples, taken near the Cordón de Barros Arana (Figure I.5), show similar ages, but present varying proportions of older zircons (Figure III.26). The basalmost sample (SP3-90, Figure III.26a) presents an important population (n = 13) around 81 Ma (Late Cretaceous); the maximum depositional age is 79 Ma. The second most important population is located in the Cambrian (n = 4 around 524 Ma and n = 5 around 538 Ma), followed by the Ordovician (n = 3 around 466 Ma and n = 5 around 480 Ma). Permian zircons (n = 5 around 293 Ma) also make an important contribution. Minor zircon populations found are: around 146 Ma (Early Cretaceous, n = 5); around 248 Ma (Triassic, n = 4), around 587 Ma and 621 Ma (Eldiacaran, n = 3 each), around 981 Ma (Tonian, n = 4), around 1050 Ma (n = 4, Stenian) and

around 1828 Ma (Orosirian, $n = 4$). The relative probability plot shows a prominent peak around 81 Ma.

On the other hand, sample SP3-91 (Figure III.26b), found higher up in the column, presents most of the zircons between 65-100 Ma (Late Cretaceous), concentrated around 83 Ma ($n = 24$) and 93 Ma ($n = 6$) and a mean age for the youngest zircon population of 80 Ma. Other important populations are found around 150 Ma (Jurassic, $n = 9$), around 296 Ma and around 313 Ma (Permian-Carboniferous, $n = 6$ and $n = 3$, respectively). Other important age peaks were obtained for the Early Cretaceous (102 Ma, $n = 3$) and the Carboniferous (321 Ma, $n = 3$). The relative probability plot has its highest peak around 83 Ma.

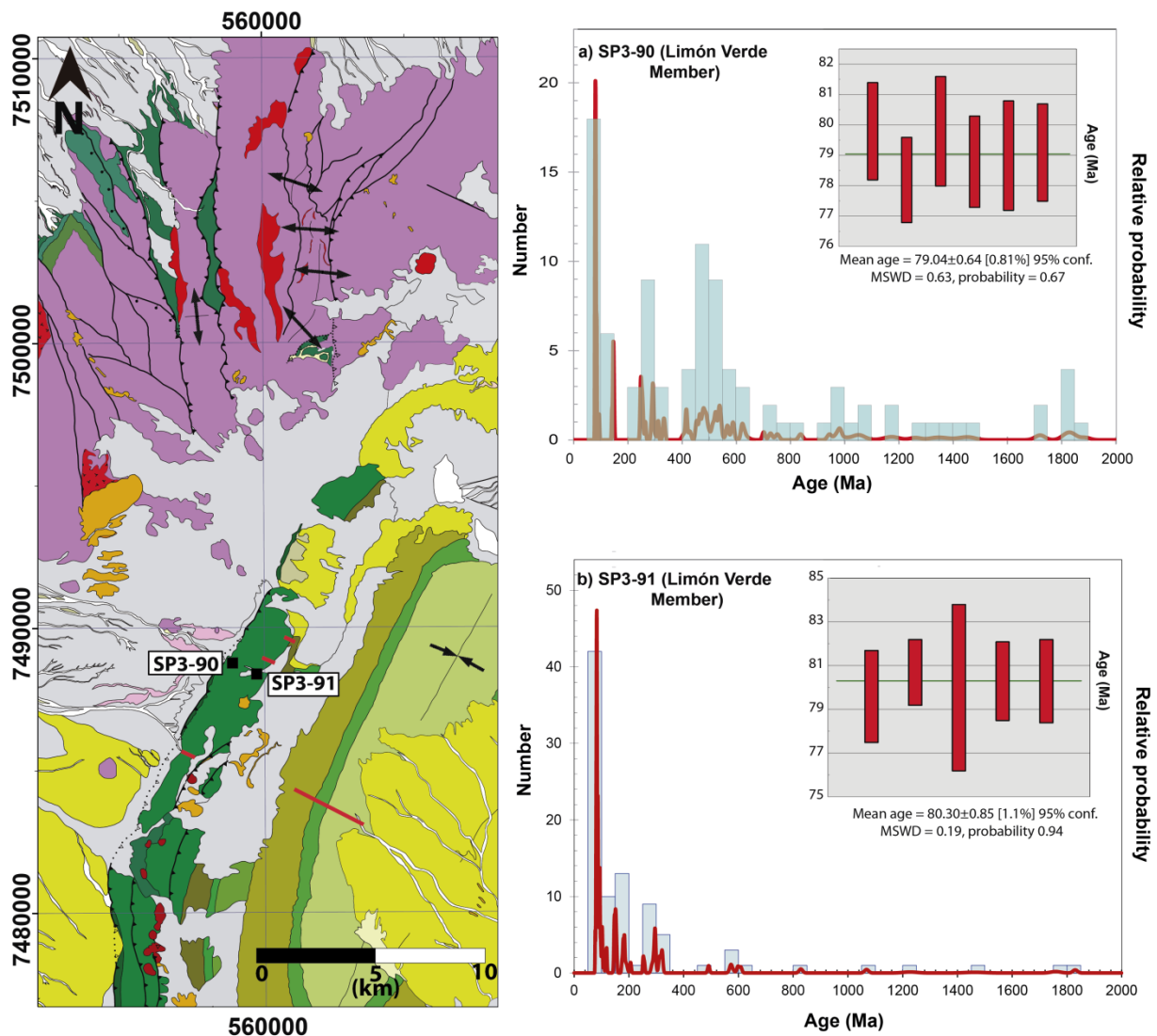


Figure III. 26. Sample location and U-Pb geochronology results for samples a) SP3-90 and b) SP3-91 of the Limón Verde Member. Map key found in Figure I.5.

Licán Member

The Licán Member (Sample SP3-89; Figure I.5) presents a maximum depositional age of 75 Ma. Its most important populations are in the Permian-Carboniferous range, with $n = 23$

around 298 Ma, $n = 10$ around 291 Ma and $n = 6$ around 309 Ma (Figure III.27); it is followed by a 65-100 Ma (Late Cretaceous, $n = 19$) age peak, with ages grouped around 80 Ma. Minor populations are found around 146 Ma (Early Cretaceous, $n = 7$), 202 Ma and 209 Ma (Triassic, $n = 4$ and $n = 3$, respectively). The relative probability plot shows the following age peaks, in decreasing order: 298 Ma, 146 Ma and 80 Ma.

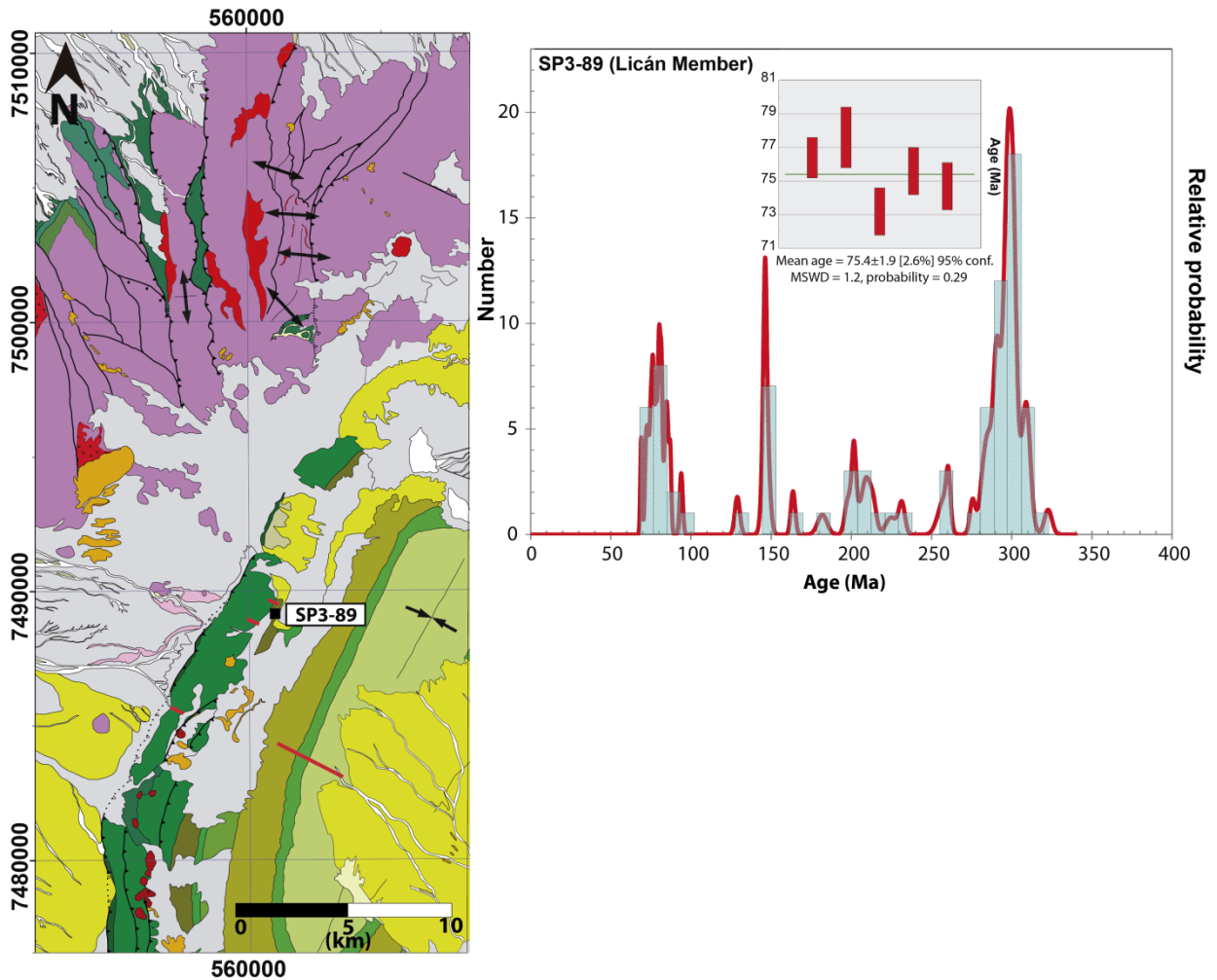


Figure III. 27. Sample location and U-Pb geochronology results for the Licán Member. Map key found in Figure I.5.

Río Grande Member

The sample obtained from the Río Grande Member (Sample SP3-87; Figure I.5) shows its largest population in the Permian-Carboniferous ($n = 51$), mainly around 289 Ma (Figure III.28). Late Cretaceous zircons ($n = 3$) are also found, grouped around 73 Ma. The maximum depositional age is 73 Ma. The relative probability plot shows a prominent, distinctive age peak at 289 Ma.

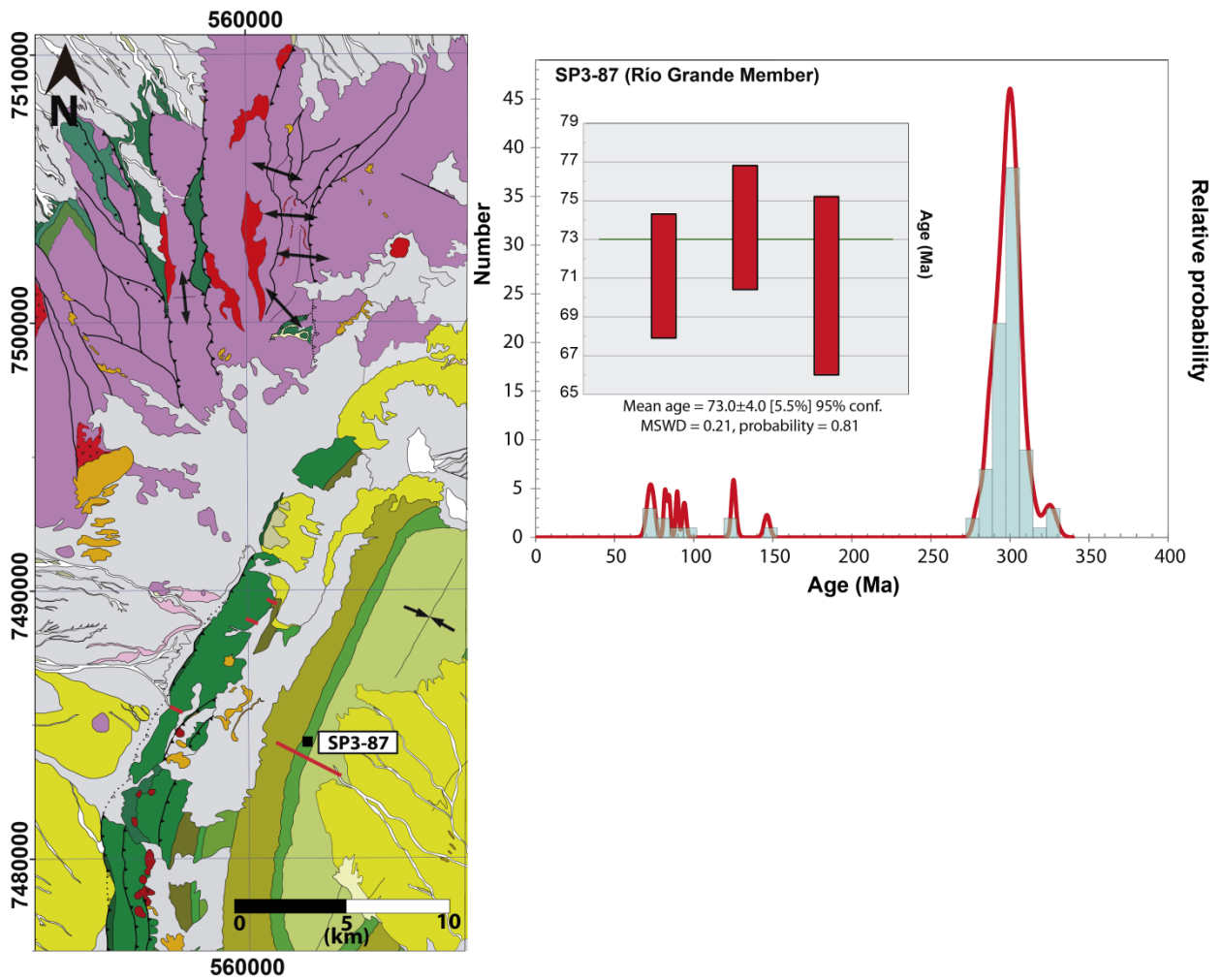


Figure III. 28. Sample location and U-Pb geochronology results for the Río Grande Member. Map key found in Figure I.5.

Barros Arana Formation

The Barros Arana Formation (Sample SP3-88; Figure I.5) has a dominant population in the Permian-Carboniferous ($n = 25$), distributed around 292 Ma. It is followed by other Permian populations around 278 Ma ($n = 7$) and 265 Ma ($n = 3$), numerous mid- to Late Cretaceous populations ($n = 4$ around 78 Ma, $n = 4$ around 84 Ma, $n = 9$ around 90 Ma and $n = 3$ around 97 Ma, for a total of $n = 20$) and an Early Cretaceous population around 137 Ma ($n = 5$). The mean age obtained for the youngest population is 78 Ma. The relative probability plot shows age peaks around 292 Ma, 90 Ma and 78 Ma.

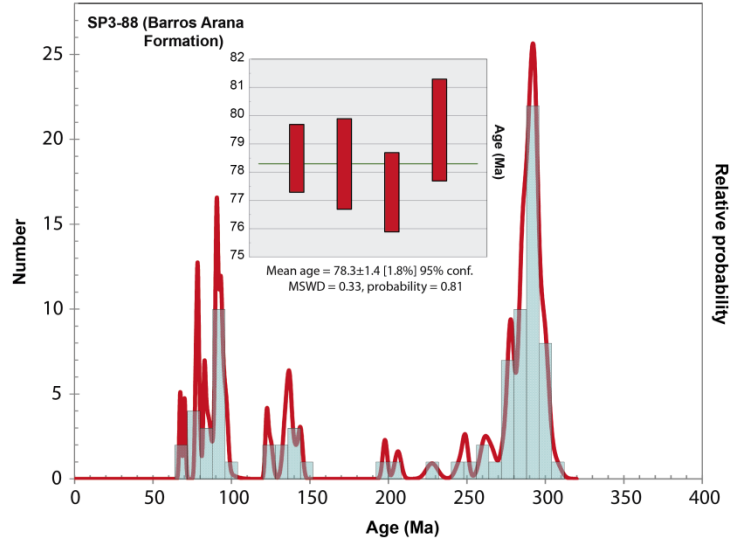
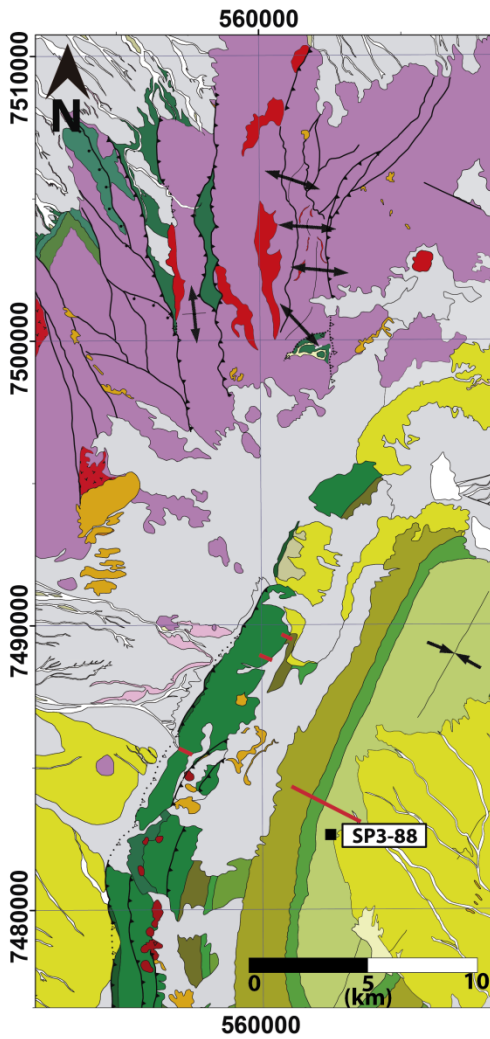


Figure III. 29. Sample location and U-Pb geochronology results for the Barros Arana Formation. Map key found in Figure I.5.

The relative probability plots of all samples are shown in Figures III.30 and III.31; the former shows all the ages obtained in these samples, while the latter shows data only from 550 Ma to recent times, in order to better inspect the changes in distributions and peaks. These figures are discussed in Chapter IV.

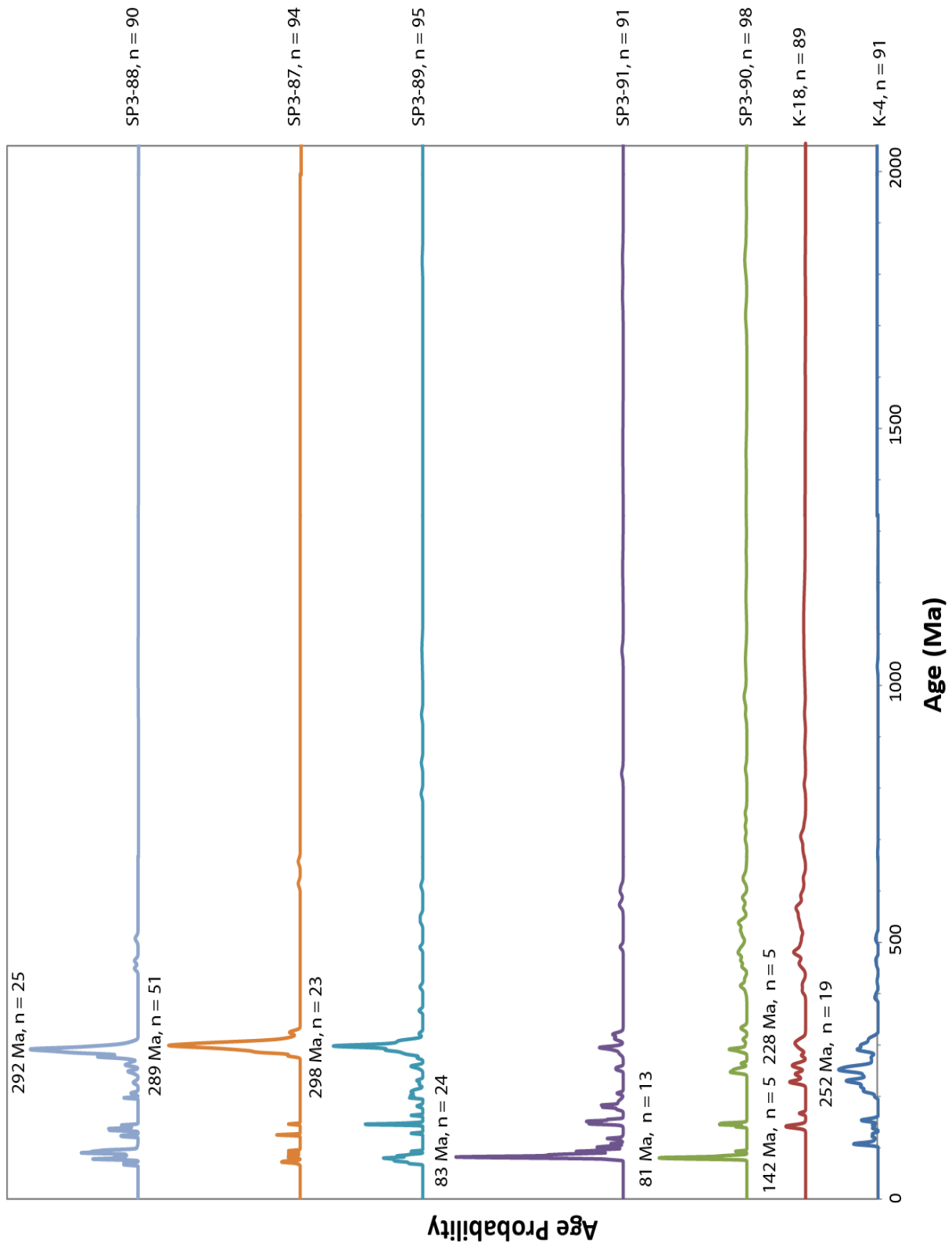


Figure III. 30. Relative probability plots of the samples discussed.

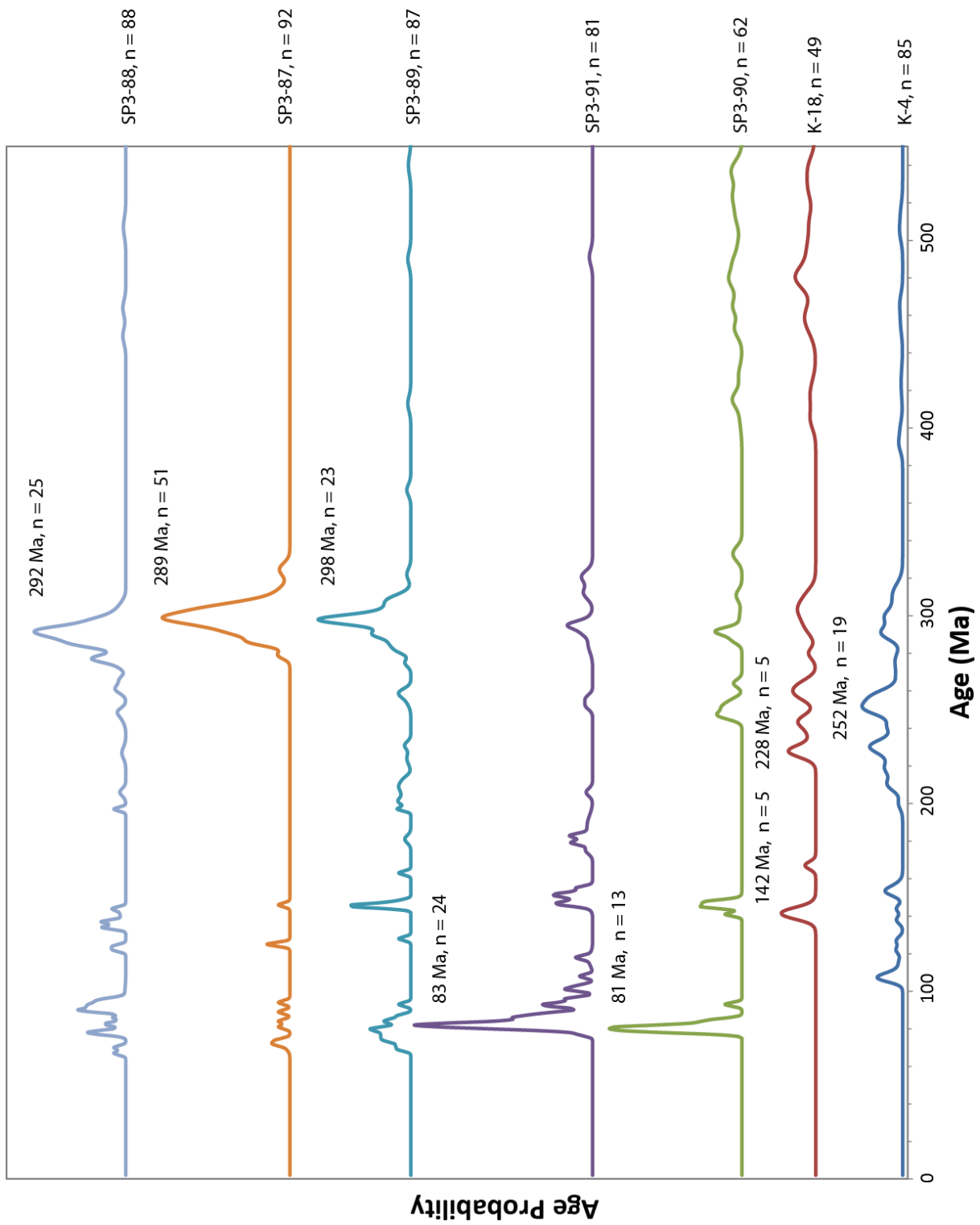


Figure III. 31. Reduced relative probability plots of the aforementioned samples, only including zircons 550 Ma or younger.

IV DISCUSSION

The high-resolution stratigraphic columns obtained from this study aid in understanding the tectonic evolution and sedimentation of the Salar de Atacama Basin since mid-Cretaceous times (Figure III.1, V.1). The Tonel Formation shows a fining-upward trend (Figures III.1, III.2a, IV.1a), from basal conglomerates derived from the El Bordo, Agua Dulce and Tuina Formations (Agua Salada Member), on which it unconformably lies, to medium- to fine-grained sandstones (La Escalera Member) and evaporitic deposits (Arcoiris Member) in some parts of the basin. This attests to increased subsidence and accommodation space in the Salar de Atacama area at the start of sedimentation, and orogenic loading in an underfilled basin (Yang & Miall, 2010; Yang, 2011), together with more distal deposition. The Limón Verde Member (Figures III.1, III.2b, IV.1b) shows, in its basal half, a coarsening-upward trend, followed by a fining-upward section; the first half can be interpreted as a consequence of reduced accommodation space and fan progradation, related to reduced tectonic activity, or early orogenic unloading in an underfilled period (Yang & Miall, 2010; Yang, 2011), while the latter shows the reverse. Smaller cycles seen at the top are probably also tectonic cycles, though less important than the former. In this context, the Los Cóndores Member represents the transition between the Tonel and Purilactis Formations. The Lampallar, Licán and Pajarito Members (Figures III.1, III.2c, III.3a, III.3b, and IV.1b) show a basal coarsening-upward profile, followed by a fining-upward trend for about ca. 400 m; it ends with another coarsening-upward section. These cycles can be explained by an important period of subsidence between two periods of tectonic quiescence. The Pajarito Member grades into the Vizcachita Member (Figures III.1, III.3c, and IV.1c), which mostly shows medium- to fine-grained sandstones, interpreted as eolian deposits (see above). Although Hartley *et al.* (1992) suggest abrupt, tectonically-induced basinwide sediment starvation as the reason for the facies change, the gradual transition from the Licán Member may imply that the change to a more arid environment could also be an explanation. The eolian facies coarsen upward in a short distance into the mainly alluvial to braided fluvial Seilao Member (Hartley *et al.*, 1992) (Figures III.1, III.4a, and IV.1d). It shows a small fining-upward trend, followed by a similarly thick coarsening-upward section, and then followed by a mostly fining-upward section that continues into the Río Grande Member (Figures III.1, III.4b, and IV.1e). Thus, these members show an increase of accommodation space, related to increased subsidence and tectonic activity, with one minor quiescent stage. Hartley (1993) also observed small-scale fining-upward cycles in the Seilao Member, interpreted as events of autocyclic fan lobe switching. Finally, the Barros Arana Formation (Figures III.1, III.4c, IV.1f) shows a predominantly coarsening-upward trend related to fan progradation, orogenic unloading and tectonic quiescence, interrupted by a 200 m thick fining-upward cycle in its midsection, and another, small-scale cycle (<100 m) at its top. The facies thus show that tectonic activity was, rather than one discrete pulse, the sum of alternating cycles of tectonism and quiescence.

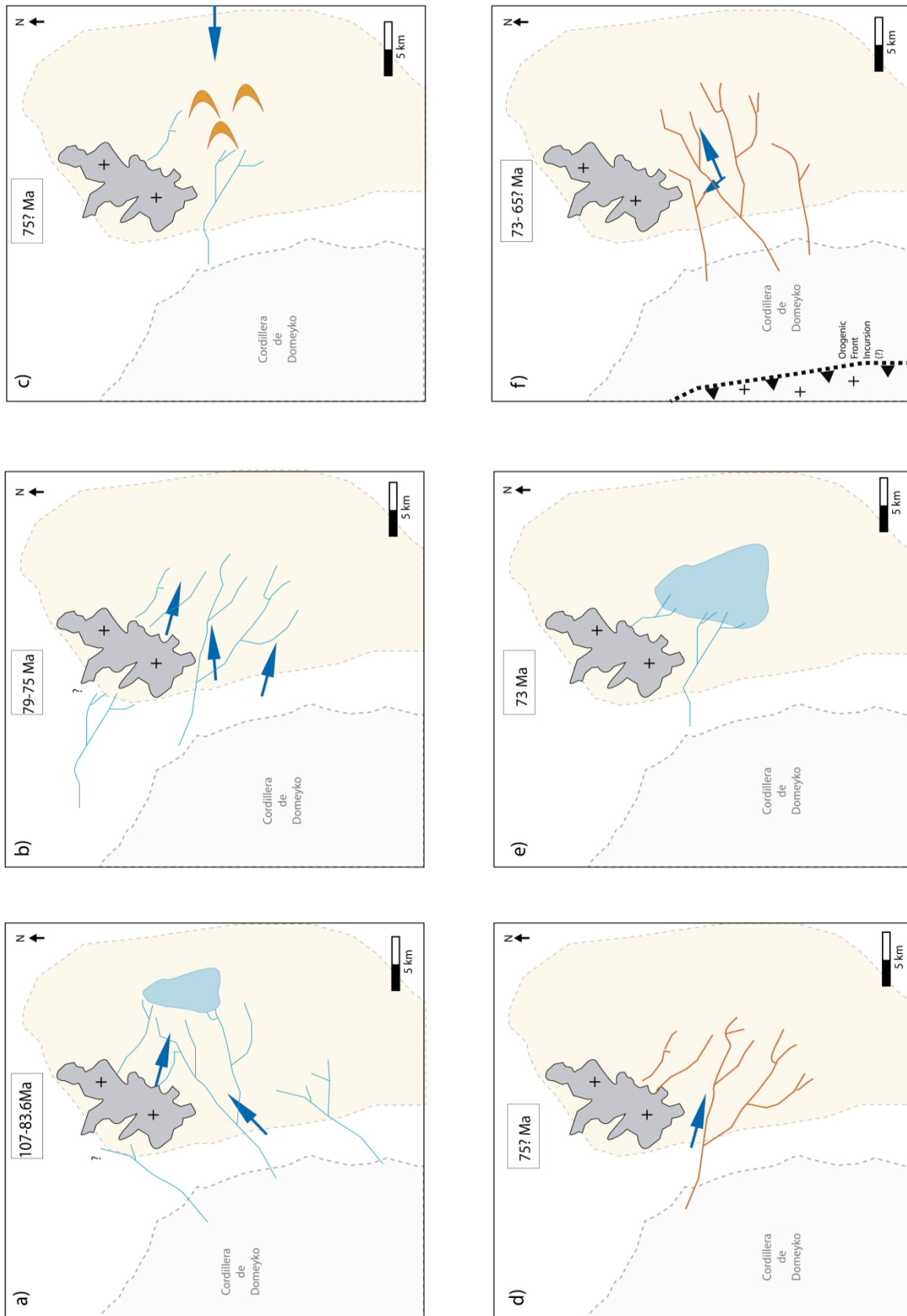


Figure IV. 1. Facies evolution of the Salar de Atacama Basin during the mid-Cretaceous to Paleogene. a) Sand-braided river and lacustrine deposits of the Tonel Formation and part of the Los Cóncores Member. b) Mainly sand-braided

rivers of the Limón Verde, Lampallar, Licán and Pajarito Members. c) Eolian dunes representing the Vizcachita Member. d) Gravel-braided rivers of the Seilao Member. e) Fluvial and lacustrine deposits of the Río Grande Member. f) Deep, gravel-braided rivers of the Barros Arana Formation. Blue arrows indicate major paleocurrent directions. The Tuina Area (in dark grey) has been rotated 30° counterclockwise. Light grey area indicates the present-day western Cordillera de Domeyko outcrop limit. Light-stippled line shows the hypothetical foredeep section of the basin. Crosses indicate positive relief.

The conglomerate clast counts (Figure III.23) obtained in this study and in previous research (Hartley *et al.*, 1992) attest to a progressive increase in crystalline, coarse-grained plutonic fragments from mostly andesitic, volcanic fragments, probably through an unroofing process. The provenance data (Figure III.24) indicate erosion of a transitional to dissected magmatic arc and, possibly, an uplifted crystalline basement; the paleocurrent data indicate that this source is most likely located to the west-southwest of the Salar de Atacama Basin (Figure III.21, III.22; Hartley *et al.*, 1992). This information, combined with the high-resolution columns profiled, shows a coarsening-upward profile, caused by increased progradation over time of alluvial fans or proximal braided rivers into the Salar de Atacama Basin (Figure III.1), and gradual proximity to the source region, owing to stages of tectonic activity (see above). The lack of obvious regional or local unconformities, or progressive deformation, with the exception of those found in the middle member of the Tonel Formation (Mpodozis *et al.*, 2005; Arriagada *et al.*, 2006a), indicates that the three formations were deposited in the (proximal?) foredeep zone of a foreland basin system (DeCelles & Giles, 1996). This lack of deformation between members, though more crude, is also seen in seismic sections (Figures 14, 15, Arriagada *et al.*, 2006a).

The U-Pb geochronological data obtained (Figures III.25, III.26, III.27, III.28, III.29, III.30 and III.31) yield new evidence to consider the age of the former Purilactis Group. Though the ages obtained for the formations are consistent with the chronostratigraphic chart presented by Mpodozis *et al.* (2005) and Arriagada *et al.* (2006), several assumptions must be contended; for instance, the accumulation of the lower Purilactis Formation cannot have happened entirely during the Late Cretaceous normal polarity superchron, owing to the presence of zircons younger than 85 Ma. The K/Ar ages obtained by Mpodozis *et al.* (2005) in dykes and intrusions in the lower Purilactis and Tonel Formations, together with the data presented here, show that sedimentation of the Tonel Formation might have begun near 107 Ma (Albian) and continued until around 83.6 Ma (Santonian); this coincides with the strong normal polarity displayed (Arriagada, 1999; Arriagada *et al.*, 2000). No data exists for the Los Cóndores Member, which could have been deposited in the same age range. Thus, the nature of the time gap between the Tonel and Purilactis Formations cannot be elicited. Sedimentation of the Limón Verde Member could have begun at 79 Ma (Campanian) and continued until no longer than 75 Ma, due to the ages obtained for the Licán Member (see above). For the same reasons, the Vizcachita Member cannot represent the magnetic inversion that ended the Late Cretaceous normal polarity superchron; it might record one of the various that occurred afterwards.

The age limit of the upper Purilactis (Seilao and Río Grande Members) and Barros Arana Formations is not clear; they are bound by the youngest mean zircon age found in the Río Grande Member (see above), which limits its maximum depositional age to the upper Campanian. The only clear geological constraint on the upper limit for the Barros Arana Formation is the presence of the unconformable Oligocene-Miocene Tambores Formation (Flint *et al.*, 1993; Naranjo *et al.*,

1994). A case could be made for their equivalence to the Naranja and/or Loma Amarilla Formations (Mpodozis *et al.*, 2005; Arriagada *et al.*, 2006), as their northern continuation; however, the age of the youngest population analyzed is older than the ages recorded for both the Totola and Naranja Formations (Mpodozis *et al.*, 2005). Thus, it can be assumed that the Barros Arana Formation might be, at least, older than 58.0±3 Ma (Naranja Formation), and possibly older than the Totola Formation, as envisioned by Mpodozis *et al.* (2005) and Arriagada *et al.* (2006).

In regard to the sources of these zircons, the mid-Cretaceous zircons probably come from the volcanic arc deposits and related intrusives found in the present day Central Valley, such as the Paradero del Desierto Formation (Cortés, 2000) and the Quebrada Mala Formation (Montaño, 1976; Marinovic & García, 1999). Early Cretaceous to Jurassic zircons were probably derived from the La Negra Arc, which is nowadays exposed in the Coastal Cordillera (Pichowiak *et al.*, 1990; Oliveros *et al.*, 2006). Permo-Triassic ages are found in the Tuina Formation, observed in the area of the same name (Marinovic & Lahsen, 1984; Henríquez, in prep.), where Narea (in prep.) obtained a U-Pb zircon age of 234.6±2.5 Ma from tuffs belonging to the upper member of the Tuina Formation. The El Bordo and Agua Dulce Formations (Ramírez & Gardeweg, 1982; Marinovic & Lahsen, 1984) are also possible sources of Permo-Triassic zircons. Other deposits of Permian age have been recorded at the eastern (Cas and Peine Formations; Ramírez & Gardeweg, 1982; Breitrkreuz, 1995) and southern edges of the Salar de Atacama (Zimmermann *et al.*, 2009; Niemeyer, in prep.).

The important Early Permian- Late Carboniferous zircon signal seen from the Licán Member upwards is probably related to the lower sections of the mentioned Permo-Triassic units and the intrusives seen in Cordillera de Domeyko, such as the multiple granodioritic intrusions found in the Sierra de Limón Verde (Complejo Intrusivo Limón Verde Indiferenciado; Marinovic & Lahsen, 1984; Morandé, in prep.) and the El Bordo and Agua Dulce Formations (Ramírez & Gardeweg, 1982; Breitrkreuz *et al.*, 1992; Basso & Mpodozis, 2012, Morandé, in prep.). This provenance is consistent with the conglomerate clast counts and paleocurrent data, which is also indicative of an unroofing process.

Early Carboniferous to Silurian zircons are scarcely found in these samples. Ordovician zircons are abundant in samples K-18 and SP3-90 (La Escalera Member and lower Limón Verde Member, respectively); they are probably derived from the Cordón de Lila Complex (Damm *et al.*, 1990; Zimmermann *et al.*, 2009; Niemeyer, in prep.). Similar ages are also found in the Sierra de Moreno Complex, at Quebrada Chojas, the Belén Metamorphic Complex and the Aguada de la Perdiz Formation; they probably represent equivalents to the Ordovician Ocloyic/Famatinian orogeny seen in northwestern Argentina (Charrier *et al.*, 2007; Hervé *et al.*, 2007). Morandé (in prep.) also found similar ages in low-grade, metasedimentary rocks belonging to the Estratos Pampa de Quenante and Estratos de Cerro Limón Verde, in the Sierra Limón Verde area. The samples also show Cambrian to Proterozoic detrital zircons.

The Cambrian-Neo Proterozoic populations seen in samples from the Tonel Formation and lower Limón Verde Member may represent the Pampean Orogeny of which the only close

representatives found in Chile are a cordierite-bearing gneiss in the Sierra Limón Verde of 777 ± 36.5 Ma (Damm *et al.*, 1990), and migmatites and schists of the same area (Skarmeta, 1983 in Hervé *et al.*, 2007). Similar ages are found further to the SE, in Argentina, in the Puncoviscana Formation (Lucassen *et al.*, 2000).

The zircon populations observed between 1000-1200 Ma can be related to the Grenvillian Event (Ramos, 2008; 2010). Rocks with these ages have been found in the Choja Metamorphic Complex (Damm *et al.*, 1990), as part of the Antofalla Terrane (Ramos, 2008; 2010). The diamictites of the Sierra Limón Verde also present detrital zircons of this age (Morandé *et al.*, 2012, Morandé, in prep.), as well as rocks of the El Toco Formation (Bahlburg *et al.*, 2009), which could indicate some form of recycling. Ages similar to the oldest ones found in the Tonel Formation and Limón Verde Member samples (Figures III.25, III.26, and III.30) have only been found far north, in the Belén Metamorphic Complex; they may correspond to the protolith of the Antofalla Terrane, as defined by Ramos (2008).

This information suggests that the Salar de Atacama Basin was receiving sediments from sources even farther to the west than the Cordillera de Domeyko, which also appears to have been uplifted, at least partly, earlier than expected (Maksaev & Zentilli, 1999); its western border was probably being uplifted during and after the mid-Cretaceous onwards (Figure IV.2 and IV.3), while the eastern border, near the southern end of the basin, was subject to tectonism during the K-T and Incaic Events (Arriagada *et al.*, 2006a; Henríquez, 2012). The multiple-source provenance is confirmed by the important variations seen in the Tonel Formation and Limón Verde Member samples, which may reflect influx from different tributaries to the system and/or catchment area variations.

The cycles observed in the sedimentary succession and the ages obtained show that the mid-Cretaceous compressive phase was not one event, but rather a long period formed by recurring compressive pulses, similar to the evolution proposed by Noblet *et al.* (1996) for the Central and Northern Andes, particularly for the Quechua and Incaic periods. Interestingly enough, the ages obtained so far are very similar to the ages of the compressive events identified at the Peruvian margin according to Jaillard (1992; 1993). The beginning of sedimentation of the Tonel Formation can be related to the Cenomanian-Albian, Turonian-early Coniacian or late Coniacian-Santonian events; more detailed sampling is required to properly define it. The Limón Verde and Licán Members could be related to the late Campanian event (77-75 Ma), which, according to Jaillard (1992; 1993), is the largest compressive event observed during the Peruvian Phase. Under this scheme, more than 3600 m of sediment accumulated as a result of the latter event, yielding a sedimentation rate of 0.36 mm/My for the Purilactis and Barros Arana Formations (not including the Los Cóndores Member). Though deposition of the Barros Arana Formation could be ascribed to the K-T event (Cornejo *et al.*, 2003), the presence of a well-identified K-T unconformity to the west of Calama (Somoza *et al.*, 2012), which is not present in the studied stratigraphic record, points to the contrary. Also, the ages obtained are older than the fission track ages found in the Cerro Quimal area by Andriessen & Reutter (1994), which shows slight uplift of the Cerro Quimal area.

Combining the U-Pb geochronological data with the regional geological information, a model can be proposed where the sediment and zircon sources are the product of inversion of earlier basins (Figure IV.2 and IV.3). The first of these inversions would have uplifted parts of the Jurassic-Lower Cretaceous magmatic arc found in the present-day coastal area (Pichowiak *et al.*, 1990; Oliveros *et al.*, 2006), which would explain the Early Cretaceous and Jurassic zircons found in the studied formations (particularly in the Tonel Formation, the Limón Verde and the Licán Members). This event would have also involved the Permian-Triassic formations mentioned above. The next step would have deformed the mid-Cretaceous deposits of the Central Valley and the western edge of the Cordillera de Domeyko; this signal is observed from the Limón Verde Member upward. This inversion would have also uplifted basement units in the Cordillera de Domeyko area, which is reflected in the abundant Carboniferous-Permian zircons observed from the Licán Member upwards. This process is similar to what has been recorded, though with different timings, in the Chañarcillo and Lautaro Basins (Martínez *et al.*, 2012; Martínez *et al.*, 2013).

These two steps effectively separate the Peruvian or mid-Cretaceous compressional phase into two different domains; the “early” Peruvian Phase (probably the same as the “Mochica” phase proposed by Mégard, 1984) involves strong compression and uplift of the present Coastal Cordillera area and had minor effects on other sectors close to the actual Salar de Atacama area, between 107 Ma and 83.6 Ma. This is reflected in the facies belonging to the Tonel Formation, which are less thick and finer-grained than the Purilactis and Barros Arana Formations, probably reflecting a more distal deposition. On the other hand, the “late” Peruvian Phase shows an eastward jump of the main deformation area, strongly involving the mid-Cretaceous arc units (see above) and the Cordillera de Domeyko area, reflected in the deposition of the Purilactis and Barros Arana Formations, from 79 Ma to 65 Ma. Sedimentation of the Barros Arana Formation is ended by the K-T event, shown by the deposition of the Totola Formation, the Naranja Formation, and then the Loma Amarilla Formation during the Incaic Event (Arriagada, 1999; Mpodozis *et al.*, 2005; Arriagada *et al.*, 2006; Henríquez, 2012).

Thus, it can be established that the Salar de Atacama Basin holds information regarding most of the tectonic phases observed at the western margin of South America during the Andean Cycle (*sensu* Charrier *et al.*, 2007).

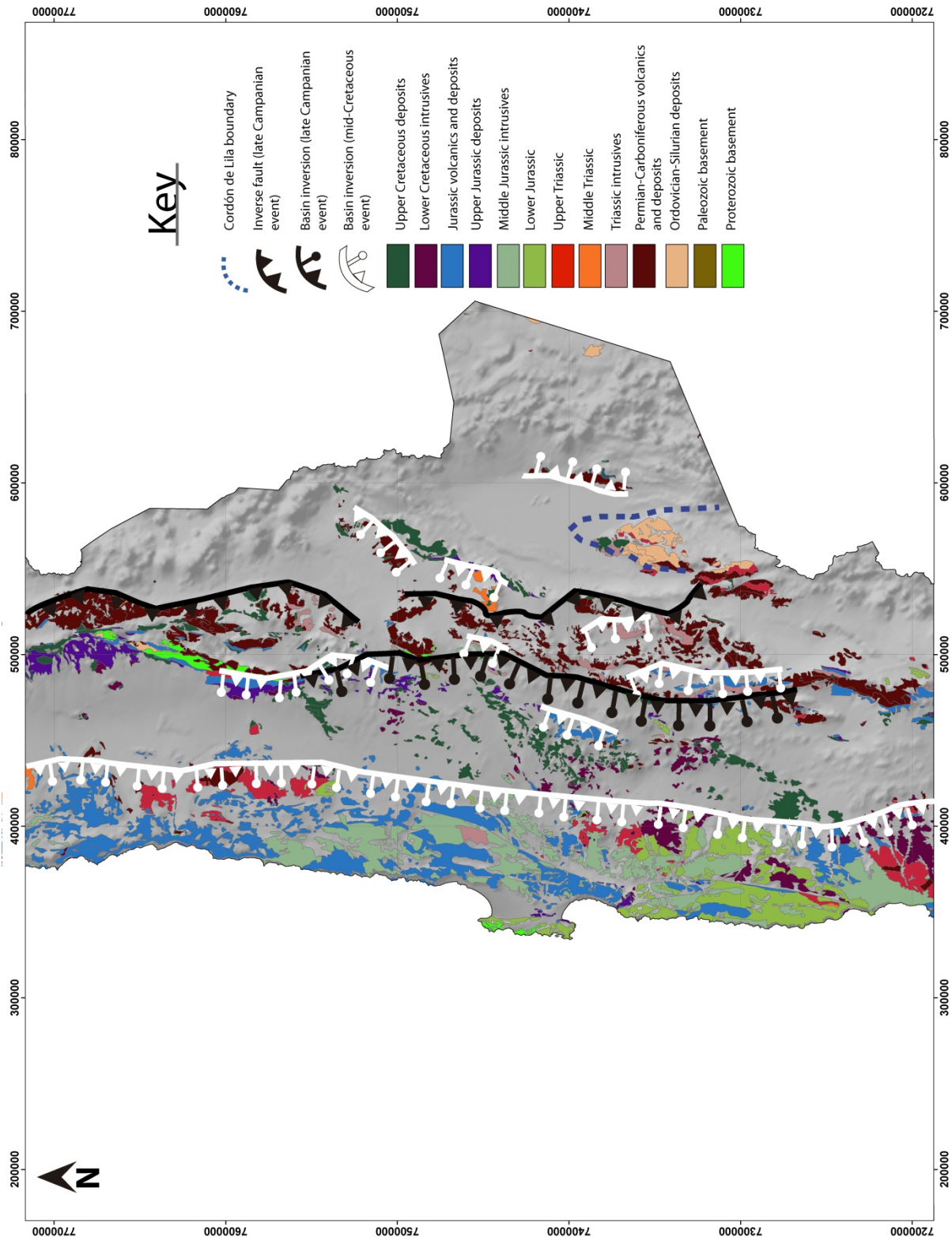


Figure IV. 2. Basin inversion and compression in northern Chile. Modified from SERNAGEOMIN (2003).

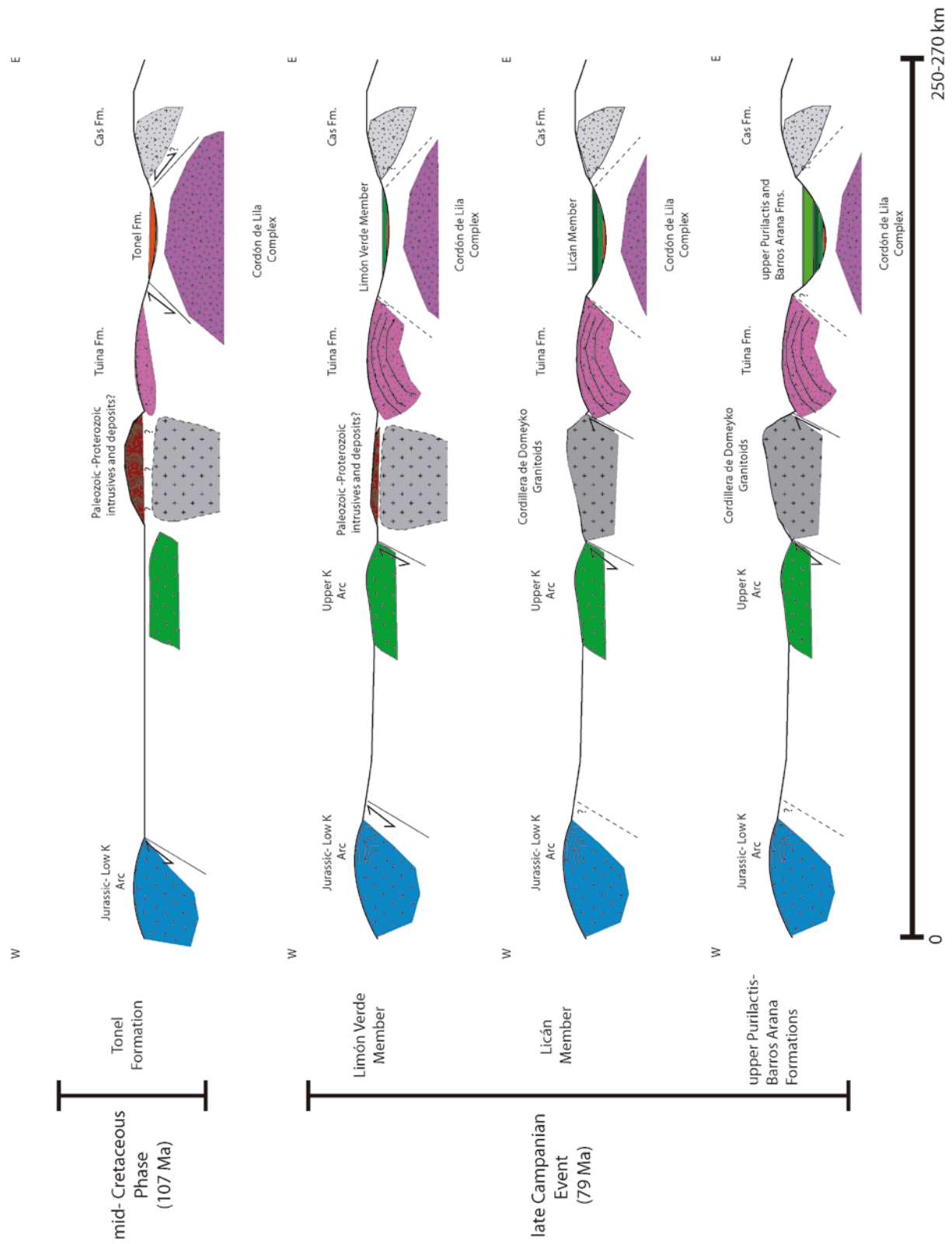


Figure IV. 3. Schematic cross-section of northern Chile between 22°-23°S, showing basin and orogenic wedge evolution.

It can be seen then that the Salar de Atacama Basin does not behave like a classic Foreland Basin System *sensu* DeCelles & Gilles (1996); instead of progressing continuously to the east, the orogenic wedge appears to have been broken several times during the Late Cretaceous. Though one could still consider all basement blocks west of the basin as part of the orogenic front, its internal structure is far more complicated. The Tolar and Tambillo Basins could be then considered as intra-montane (piggy-back?) basins, and part of the system as a whole.

More evidence for early uplift in this sector during mid-Cretaceous times has been found as far east as the Puna of NW Argentina, where apatite fission track (AFT) dating performed on the Eocene Geste Formation found AFT cooling ages between 88-112 Ma, which are explained as a distant signal coming from the Cordillera de Domeyko area (Carrapa & DeCelles, 2008). It is possible then that some formations interpreted to have been deposited in extensional basins, could in fact be compressive in nature; in the case of the Quebrada Mala Formation, the kinematics of the Sierra del Buitre Fault, which controls the deposition of the formation (Marinovic & García, 1999) are not distinctively clear. Andriessen & Reutter (1994) also pointed to the intrusion of the 80 Ma San Cristóbal Pluton in folded Jurassic-lower Cretaceous sediments as evidence of deformation in the Santonian. They also showed concordant fission track ages of 72 Ma obtained from granitoid stocks in Sierra de Navidad, which may indicate a tectonic event around that age; however, the results were not conclusive. In the case of the Cerrillos Formation, interpreted by Martínez *et al.* (2013) as a post-rift succession, Makshev *et al.* (2009) concluded that its coarse conglomeratic facies provide evidence of tectonic uplift during the middle to late Aptian. Close to this area, around 28°30'S, Merino *et al.* (2013) suggested tectonic unroofing of Lower Cretaceous units in the Coastal Cordillera between 90-85 Ma, reflected in the deposition of the Quebrada Seca Formation. It is interesting to note that the Tonel Formation is a time-equivalent of the Quebrada Seca and Cerrillos Formations, while the Hornitos Formation seems to be related to the Purilactis and Barros Arana Formations. Similar ages for the beginning of compression have been obtained for the Coastal Range of Central Chile, in the Caleu Pluton and the Las Chilcas Formation (Parada *et al.*, 2005); thus, a broader picture can be conceived, where the entire western margin was undergoing compression from mid-Cretaceous times onward.

The tectonic setting attributed to the Cretaceous deposits is in conflict with some of the previous interpretations given for other formations of northern Chile (See Chapter I.4), or the setting interpreted for northern Argentina at that time (Salta Rift; Monaldi *et al.*, 2008). Mpodozis *et al.* (2005) suggested that the coexistence of extensional and compressive basins could be due to oblique plate convergence, which would produce strike-slip motion, located in the thermally weakened arc, together with arc-orthogonal shortening and thrusting in the back-arc; Scheuber *et al.* (1994) also proposed a mechanism for alternations of compressive and extensional basins during the Cretaceous, though not exactly at the same precise time (See Chapter I.1). However, evidence has been obtained from the western margin of South America (e.g., Cobbold *et al.*, 2006; Figure 1 of Tunik *et al.*, 2010), which shows that the margin experienced an important compressive event during the mid- to Late Cretaceous, with the age varying from place to place, but ranging between 100-80 Ma. Also, reconstructions of the western margin of South America

for the Paleogene by Arriagada *et al.* (2008) indicate that the convergence was probably more orthogonal than previously thought; hence, a critical reexamination of previous theories must be realized.

With regard to the climatic conditions prevalent during deposition, the predominantly braided to alluvial facies observed indicate mostly semi-arid to arid conditions in most of the formations, with the exception of the evaporites present in the upper Tonel Formation and the Vizcachita Member, where more extreme desert conditions seem to have been prevalent. Almost fresh pyroxenes found in some members of the Purilactis Formation support this interpretation. Overall, this is consistent with existing models of Late Cretaceous climate (Sellwood & Valdes, 2006), which indicate that the Salar de Atacama area was most likely dry all year round, with the exception of a short wet season in February; temperatures were, on average, over 30°C. The concentration of evaporites in the western and southern portions of the Barros Arana Syncline could be considered as a paleoslope indicator. Semi-arid to arid conditions continued well into the Tertiary, though humid, pluvial phases are clearly observed (Le Roux, 2012).

Finally, the name ‘Muriacala Group’ is proposed, in conformity to the North American Stratigraphic Code (North American Commission on Stratigraphic Nomenclature, 2005), to encompass the studied formations, based on their common origin (in regard to basin development, lithologies and conformities) and somewhat continuous chronology. The name is taken from a valley (‘quebrada’ in Spanish) found at 22°44’06”S, 68°26’24”W, which displays good expositions of the lower members of the Purilactis Formation. It also does not conflict with existing names for the units observed, nor with other stratigraphic definitions found in northern Chile.

V CONCLUSIONS

The Tonel, Purilactis and Barros Arana Formations show a complete and diverse range of facies, accounting for almost 5500 m of sedimentation since the mid-Cretaceous, during the entire Peruvian Phase. The Tonel Formation shows shallow, gravel-bed, braided river facies (Agua Salada Member), which gradually change upward into fine-grained facies representing a transition to a more distal, possibly lacustrine or overbank environment (La Escalera and Arcoiris Members). The Los Cóndores Member shows sheetflood sandstones belonging to distal braidplains and sand-bed rivers. The Limón Verde Member presents distal, braided, sand-dominated river deposits, or ephemeral sheetflood sediments in mostly arid regions with shallow channel depths, with an upward manifestation of deeper, gravel-bed, braided river deposits. The Lampallar, Licán and Pajarito Members show laminated sandstones, related to slightly channelized, ephemeral, sand-bed rivers, and mostly clast-supported, stratified conglomerates probably deposited in shallow, gravel-bed braided rivers with scarce gravity flow deposits. It grades into the Vizcachita Member, dominated by eolian deposits. The Seilao Member shows a return to coarse facies, interpreted as shallow, gravel-bed braided rivers, with intervals dominated by ephemeral sheetflood deposits which grade into the Rio Grande Member, showing an abundance of lithofacies related to ephemeral, poorly confined sand-bed rivers and lacustrine deposits. Finally, the Barros Arana Formation exhibits facies typical of deep, gravel-bed braided rivers and flashflood deposits. Provenance data, conglomerate clast counts and the U-Pb detrital zircon geochronology show that the source of sediments was extremely diverse, reflecting the entire uplift of the arc and back-arc deposits. Sediment transport followed mainly a northeast-eastward direction. The age of these deposits ranges from 107 Ma (Albian) to 83.6 Ma (Santonian) for the Tonel Formation and, possibly, the Los Cóndores Member, and 79 Ma (Campanian) to 65 Ma (Paleocene) for the rest of the Purilactis and Barros Arana Formations.

The facies variations are intimately associated with the development of the Peruvian Phase; the “early” Peruvian Phase (around 107-83.6 Ma) encompassed deposition of the Tonel Formation and the Los Cóndores Member, while the “later” Peruvian Phase (79-65 Ma) witnessed deposition of the Purilactis and Barros Arana Formations. While the former event shows deformation and uplift of the Cordillera de la Costa area, the latter presents an eastward jump of the orogenic front to the present Cordillera de Domeyko area. The units were most likely deposited in a foredeep setting, with an increasing proximity to the orogenic front; the front itself is partly a result of the inversion of previous basins. The different events clearly broke the orogenic wedge into different sections, allowing the appearance of different sources reflected in the stratigraphic record. Subsidence was, probably, the most important control regarding gravel and coarse facies progradation. The group also records mostly arid to semi-arid conditions during its deposition, with only slight fluctuations, as seen in proposed climatic models for the Late Cretaceous.

These common characteristics allow the formations to be grouped under the name Muriacala Group.

In a regional context, these results are in accordance with the age of compression seen elsewhere in north-central Chile and the western margin of South America, and provide new information for the Mesozoic to Cenozoic evolution of the northern Central Andes.

VI REFERENCES

- Amilibia, A.; Sàbat, F.; McClay, K.R.; Muñoz, J.A.; Roca, E.; Chong, G. 2008. The role of inherited tectono-sedimentary architecture in the development of the central Andean mountain belt: Insights from the Cordillera de Domeyko. *Journal of Structural Geology* 30 (12): 1520-1539.
- Andriessen, P.A.M.; Reutter, K.J. 1994. K-Ar and fission track mineral age determination of igneous rocks related to multiple magmatic arc systems along the 23°S latitude of Chile and NW Argentina. *In* *Tectonics of the Southern Central Andes: Structure and Evolution of an Active Continental Margin* (Reutter, K.J.; Scheuber, E.; Wigger, P.; editors). Springer: 141 – 154. New York.
- Armitage, J.J.; Duller, R.A.; Whittaker, A.C.; Allen, P.A. 2011. Transformation of tectonic and climatic signals from source to sedimentary archive. *Nature Geoscience* 4: 231-235. <http://dx.doi.org/10.1038/ngeo1087>
- Armitage, J.J.; Dunkley Jones, T.; Duller, R.A.; Whittaker, A.C.; Allen, P.A. 2013. Temporal buffering of climate-driven sediment flux cycles by transient catchment response. *Earth and Planetary Science Letters* 369-370: 200-210.
- Arriagada, C. 1999. Geología y Paleomagnetismo del Borde Oriental de la Cordillera de Domeyko entre los 22°45' y 23°30' latitud Sur. II Región, Chile. MSc thesis (Unpublished), Universidad de Chile: 1-176 p.
- Arriagada, C.; Roperch, P.; Mpodozis, C. 2000. Clockwise block rotations along the eastern border of the Cordillera de Domeyko, northern Chile (22°45'–23°30'S). *Tectonophysics* 326: 153 – 171.
- Arriagada, C.; Roperch, P.; Mpodozis, C.; Dupont-Nivet, G.; Cobbold, P.R.; Chauvin, A.; Cortés, J. 2003. Paleogene clockwise tectonic rotations in the forearc of central Andes, Antofagasta region, northern Chile. *Journal of Geophysical Research* 18, B1 2032. doi:10.1029/2001JB001598
- Arriagada, C.; Cobbold, P.R.; Roperch, P. 2006. The Salar de Atacama basin: a record of Cretaceous to Paleogene compressional tectonics in the Central Andes. *Tectonics* 25: TC1008, doi:10.1029/2004TC001770.
- Arriagada, C.; Roperch, C.; Mpodozis, C.; Fernandez, R. 2006b. Paleomagnetism and tectonics of the southern Atacama Desert (25-28°S), northern Chile. *Tectonics* 25: TC4001, doi: 10.1029/2005TC001923.
- Bahlburg, H.; Vervoort, J.D.; Du Frane, S.A.; Bock, B.; Augustsson, C.; Reimann, C. 2009. Timing of crust formation and recycling in accretionary orogens: Insights learned from the western margin of South America. *Earth-Science Reviews* 97: 215-241.

- Basso, M.; Mpodozis, C. 2012. Carta Cerro Quimal, Región de Antofagasta. Servicio Nacional de Geología y Minería, Carta Geológica de Chile, Serie Geología Básica 143: 46 p. 1 mapa escala 1:100.000. Santiago, Chile.
- Blair, T.C.; Bilodeau, W.L. 1988. Development of tectonic cyclothems in rift, pull-apart and foreland basins: Sedimentary response to episodic tectonism. *Geology* 16: 517-520.
- Breitkreuz, C.; Helmdach, F.F.; Kohring, R.; Mosbrugger, V. 1992. Late Carboniferous Intra-arc sediments in the north Chilean Andes: Stratigraphy, Paleogeography and Paleoclimate. *Facies* 26: 67-80.
- Breitkreuz, C. 1995. The Late Permian Peine and Cas Formations at the eastern margin of the Salar de Atacama, Northern Chile: stratigraphy, volcanic facies, and tectonics. *Revista Geológica de Chile* 22: 3-23.
- Breitkreuz, C.; van Schmus, W.R. 1996. U-Pb geochronology and significance of Late Permian ignimbrites in Northern Chile. *Journal of South American Earth Sciences* 9 (5/6): 281– 293.
- Bridge, J.S. 2003. Rivers and floodplains, Form, Processes and Sedimentary Record. Blackwell Publishing Company: 1-486. Oxford.
- Brüggen, J. 1934. Las Formaciones de Sal y Petróleo de la Puna de Atacama. *Boletín de Minas y Petróleo* 32: 105-122. Santiago, Chile.
- Brüggen, J. 1942. Geología de la Puna de San Pedro de Atacama y sus formaciones areniscas y arcillas rojas. *In Congreso Panamericano de Ingeniería de Minas y Geológica, Actas* 2: 342-467. Santiago, Chile.
- Brüggen, J. 1950. Fundamentos de la Geología de Chile. Instituto Geográfico Militar: 1 – 374. Santiago, Chile.
- Burbank, D.W.; Beck, R.A.; Reynolds, R.G.H.; Hobbs, R.; Tahirkheli, R.A.K. 1988. Thrusting and gravel progradation in foreland basins: A test of post-thrusting gravel dispersal. *Geology* 16: 1143-1146.
- Carrapa, B.; DeCelles, P.G. 2008. Eocene exhumation and basin development in the Puna of northwestern Argentina. *Tectonics* 27: TC1015, doi: 10.1029/2007TC002127.
- Carrapa, B.; Bywater-Reyes, S.; DeCelles, P.G.; Mortimer, E.; Gehrels, G.E. 2012. Late Eocene–Pliocene basin evolution in the Eastern Cordillera of northwestern Argentina (25°–26°S): regional implications for Andean orogenic wedge development. *Basin Research* 24: 249–268. doi: 10.1111/j.1365-2117.2011.00519.x
- Charrier, R.; Reutter, K.J., 1990. The Purilactis group of Northern Chile: link between arc and backarc during Late Cretaceous and Paleogene. *In Proceedings I ORSTOM-ISAG*: 249–252. Grenoble, France.

- Charrier, R.; Muñoz, N. 1994. Jurassic-Cretaceous Paleogeographic evolution of the Chilean Andes at 23°-24°S.L. and 34°-35°S.L.: a comparative analysis. *In* Tectonics of the Southern Central Andes: Structure and Evolution of an Active Continental Margin (Reutter, K.J.; Scheuber, E.; Wigger, P.; editors). Springer: 233 – 242. New York.
- Charrier, R.; Reutter, K.J. 1994. The Purilactis group of northern Chile: Boundary between arc and backarc from Late Cretaceous to Eocene. *In* Tectonics of the Southern Central Andes: Structure and Evolution of an Active Continental Margin (Reutter, K.J.; Scheuber, E.; Wigger, P.; editors). Springer: 189 – 202. New York.
- Charrier, R.; Pinto, L.; Rodríguez, M.P. 2007. Tectonostratigraphic evolution of the Andean Orogen in Chile. *In* The Geology of Chile (Moreno, T.; Gibbons, W.; editors). The Geological Society: 21-114. London.
- Charrier, R.; Farías, M.; MaksaeV, V. 2009. Evolución tectónica, paleogeográfica y metalogénica durante el Cenozoico en los Andes de Chile norte y central e implicaciones para las regiones adyacentes de Bolivia y Argentina. *Revista de la Asociación Geológica Argentina* 65 (1): 5-35.
- Cobbold, P.R.; Rossello, E.A. 2003. Aptian to recent compressional deformation, foothills of the Neuquén Basin, Argentina. *Marine and Petroleum Geology* 20: 429-443.
- Cobbold, P.R.; Rossello, E.A.; Roperch, P.; Arriagada, C.; Gómez, L.A.; Lima, C. 2006. Distribution and timing of Andean deformation across South America. *In* Global Tectonic Processes: The legacy of Mike Coward (Ries, A.; Graham, R.H.; Butler, R.W.; editors). Geological Society Special Publications. In Press.
- Coira, B.; Davidson, J.; Mpodozis, C.; Ramos, V. 1982. Tectonic and Magmatic Evolution of the Andes of Northern Argentina and Chile. *Earth-Science Reviews* 18: 303-332.
- Coira, B.; Koukharsky, M.; Ribeiro Guevara, S.; Cisterna, C.E. 2009. Puna (Argentina) and northern Chile Ordovician Basic Magmatism: A contribution to the tectonic setting. *Journal of South American Earth Sciences* 27: 24-35.
- Cornejo, P.; Mpodozis, C.; Ramírez, C.; Tomlinson, C.F. 1993. Estudio Geológico de la Región de El Salvador y Potrerillos. Servicio Nacional de Geología y Minería, Informe Registrado IR-93-1: 1-258. Santiago, Chile.
- Cornejo, P.; Matthews, S.; Pérez, C. 2003. The “K-T” compressive deformation event in northern Chile (24°-27°S). *In* Proceedings 10th Congreso Geológico Chileno. Concepción, Chile.
- Cornejo, P.; Mpodozis, C.; Tomlinson, A. 1998. Hoja Salar de Maricunga. Servicio Nacional de Geología y Minería, Mapas Geológicos 7. 1 mapa escala 1:100.000.
- Cortés, J. 2000. Hoja Palestina, Región de Antofagasta. Servicio Nacional de Geología y Minería, Mapas Geológicos 19. 1 mapa escala 1:100.000. Santiago, Chile.
- Damm, K.W.; Pichowiak, S.; Harmon, R.S.; Todt, W.; Kelley, R.; Omarini, R.; Niemeyer, H. 1990. Pre-Mesozoic evolution of the central Andes: The basement revisited. *Geological Society of America Special Papers* 241: 101-126.

- DeCelles, P.G.; Gilles, K.A. 1996. Foreland basin systems. *Basin Research* 8: 105-123.
- DeCelles, P.G.; Carrapa, B.; Horton, B.K.; Gehrels, G.E. 2011. Cenozoic foreland basin system in the central Andes of northwestern Argentina: Implications for Andean geodynamics and modes of deformation. *Tectonics* 30: TC6013. 2011 doi:10.1029/2011TC002948
- Dickinson, W.R. 1970. Interpreting detrital modes of greywacke and arkose. *Journal of Sedimentary Petrology* 40: 695-707.
- Dickinson, W.R.; Suczek, C.A. 1979. Plate tectonics and sandstone composition. *American Association of Petroleum Geologists Bulletin* 63: 2164-2182.
- Dickinson, W.R.; Beard, L.S.; Brakenridge, G.R.; Erjavec, J.L.; Ferguson, R.C.; Inman, K.F.; Knepp, R.A.; Lindberg, A.; Ryberg, P.T. 1983. Provenance of North American Phanerozoic sandstones in relation to tectonic. *Geological Society of America Bulletin* 94: 222-235.
- Dickinson, W.R. 1985. Interpreting provenance relation from detrital modes of sandstones. *In Provenance of Arenites* (Zuffa, G.G.; editor). D. Reidel: 333-363. Dordrecht, Netherlands.
- Dietrich, W.E.; Bellugi, D.G.; Sklar, L.S.; Stock, J.D.; Heimsath, A.M.; Roering, J.J. 2003. Geomorphic transport laws for predicting landscape form and dynamics. *In Prediction in Geomorphology*, Geophysical Monograph Series v. 135 (Wilcock, P.R.; Iverson, R.M.; editors). American Geophysical Union: 103-32. Washington D.C., U.S.A. doi: 10.1029/135GM09
- Dingman, R.J., 1963. Cuadrángulo Tular. Instituto de Investigaciones Geológicas, Carta Geológica de Chile 11:1-35. 1 mapa escala 1:50.000. Santiago, Chile.
- Dingman, R.J. 1967. Geology and Groundwater Resources of the Northern part of the Salar de Atacama, Antofagasta Province, Chile. U.S. Geological Survey Bulletin 1219: 1-49 p.
- Döbel, R. 1989. Geochemie und Geochronologie Alttertiärer Vulkanite aus der Prakordillere Nordchiles Zwischen 21° und 23°30'S. Unpublished PhD thesis, Freie Universität, Berlin, Germany, 152 p.
- Flint, S.; Hartley, A.; Rex, D.; Guise, P.; Turner, P. 1989. Geochronology of the Purilactis Formation, Northern Chile: an insight into Late Cretaceous/Early Tertiary basin dynamics of the Central Andes. *Revista Geológica de Chile* 16: 241-246.
- Flint, S.; Turner, P.; Jolley, E.J.; Hartley, A.J. 1993. Extensional tectonics in convergent margin basins: An example from the Salar de Atacama, Chilean Andes. *Geological Society of America Bulletin* 105: 603-617.
- Götze, H.J.; Krause, S. 2002. The central Andean gravity high, a relic of an old subduction complex?. *Journal of South American Earth Sciences* 14: 799-811.
- Hammerschmidt, K.; Döbel, R.; Friedrichsen, H. 1992. Implication of $^{40}\text{Ar}/^{39}\text{Ar}$ dating of Early Tertiary volcanic rocks from the north-Chilean Precordillera. *Tectonophysics* 202: 55-81.

- Hartley, A.; Flint, S.; Turner, P. 1988. A proposed lithostratigraphy for the Cretaceous Purilactis Formation, Antofagasta Province, northern Chile. *In* Congreso Geológico Chileno, No. 5, Actas 3: H83–H99. Santiago.
- Hartley, A.J.; Flint, S.; Turner, P.; Jolley, E.J. 1992. Tectonic controls on the development of a semiarid, alluvial basin as reflected in the stratigraphy of the Purilactis Group (upper Cretaceous-Eocene), northern Chile. *Journal of South American Earth Sciences* 5: 275-296.
- Hartley, A.J. 1993. Sedimentological response of an alluvial system to source area tectonism: the Seilao Member of the Late Cretaceous to Eocene Purilactis Formation of northern Chile. *In* Alluvial Sedimentation: International Association of Sedimentologists Special Publication 17 (Marzo, M.; Puigdefabregas, C.; editors). Blackwell Publishing Ltd.: 489-500. Oxford, London.
- Hein, F.J. 1984. Deep-sea and fluvial braided channel conglomerates: A comparison of two case studies. *In* Sedimentology of Gravels and Conglomerates, Memoir 10 (Koster, E.H.; Steel, R.J.; editors). Canadian Society of Petroleum Geologists.: 33-49. Calgary, Alberta, Canada.
- Heller, P.; Paola, C. 1992. The Large-scale dynamics of grain-size variation in alluvial basins, 2: Application to syntectonic conglomerate. *Basin Research* 4: 91-102.
- Henríquez, S.M. 2012. Estructura del Salar de Atacama: Implicancias en la estructura cortical de los Andes Centrales. MSc thesis (Unpublished). Universidad de Chile, Santiago: 1-97 p.
- Henríquez, S.M.; Arriagada, C.; Becerra, J. In prep. Geología del área San Pedro de Atacama, Región de Antofagasta. Servicio Nacional de Geología y Minería. Carta Geológica de Chile, Serie Geología Básica. 1 mapa escala 1:100.000. Santiago, Chile.
- Hervé, F.; Faundez, V.; Calderón, M.; Massone, H.J.; Willner, A.P. 2007. Metamorphic and plutonic basement complexes. *In* The Geology of Chile (Moreno, T.; Gibbons, W.; editors). The Geological Society: 5-20. London.
- Ingersoll, R.V.; Bullard, T.F.; Ford, R.L.; Grimm, J.P.; Pickle, J.D.; Sares, S.W. 1984. The effect of grain size on detrital modes: A test of the Gazzi-Dickinson point-counting method. *Journal of Sedimentary Research* 54: 103-116.
- Ingersoll, R.V. 2012. Composition of modern sand and Cretaceous sandstone derived from the Sierra Nevada, California, USA, with implications for Cenozoic and Mesozoic uplift and dissection. *Sedimentary Geology* 280: 195-207.
- Isacks, B.L. 1988. Uplift of the central Andean plateau and bending of the Bolivian orocline. *Journal of Geophysical Research* 93: 3211 – 3231.
- Jaillard, E. 1992. La Fase Peruana (Cretáceo Superior) en la Margen Peruana. *Boletín de la Sociedad Geológica del Perú* 83: 81-87.
- Jaillard, E. 1993. L'évolution tectonique de la marge péruvienne au Sénonien et Paléocène et ses relations avec la géodynamique. *Bulletin de la Société Géologique de France* 164, n°6: 819-830.

- Jaillard, E.; Bengtson, P.; Dhondt, A.V. 2005. Late Cretaceous marine transgressions in Ecuador and northern Peru: a refined stratigraphic framework. *Journal of South American Earth Sciences* 19: 307-323.
- Jaimes, E.; de Freitas, M. 2006. An Albian-Cenomanian unconformity in the northern Andes: evidence and tectonic significance. *Journal of South American Earth Sciences* 21: 466-492.
- Jokat, W.; Boebel, T.; König, M.; Meyer, U. 2003. Timing and geometry of early Gondwana breakup. *Journal of Geophysical Research* 108: B9, 2428. doi: 10.1029/2002JB001802.
- Jolley, E.J.; Turner, P.; Williams, G.D.; Hartley, A.J.; Flint, S. 1990. Sedimentological response of an alluvial system to Neogene thrust tectonics, Atacama Desert, northern Chile. *Journal of the Geological Society, London* 147: 769-784.
- Jordan, T.E.; Muñoz, N.; Hein, M.; Lowenstein, T.; Godfrey, L.; Yu, J. 2002. Active faulting and folding without topographic expression in an evaporite basin, Chile. *Geological Society of America Bulletin* 114: 1406-1421.
- Kocurek, G. 1981. Significance of interdune deposits and bounding surfaces in aeolian dune sands. *Sedimentology* 28: 753-780.
- Kocurek, G. 1991. Interpretation of ancient eolian sand dunes. *Annual Reviews Earth Planetary Science Letters* 19: 43-75.
- Le Roux, J.P. 1991. Paleocurrent analysis using Lotus 1-2-3. *Computers & Geosciences* 17, no. 10: 1465-1468.
- Le Roux, J.P. 2012. A review of Tertiary climate changes in southern South America and the Antarctic Peninsula. Part 2: continental conditions. *Sedimentary Geology* 247-248: 21-38.
- Lucassen, F.; Becchio, R.; Wilke, H.G.; Franz, G.; Thirlwall, M.F.; Viramonte, J.; Wemmer, K. 2000. Proterozoic-Paleozoic development of the basement of the Central Andes (18-26°S) – a mobile belt of the South American craton. *Journal of South American Earth Sciences* 13: 697-715.
- Ludwig, K.R. 2008. Isoplot 3.6. Berkeley Geochronology Center Special Publication 4. 77 p.
- Macellari, C.E.; Su, M.J.; Townsend, F. 1991. Structure and seismic stratigraphy of the Atacama Basin (northern Chile). *In Congreso Geológico Chileno, No. 6, Actas* 1: 133-137. Viña del Mar, Chile.
- Maksaev, V.; Zentilli, M. 1999. Fission track thermochronology of the Domeyko Cordillera, northern Chile: Implications for Andean tectonics and porphyry copper metallogenesis. *Exploration and Mining Geology* 8: 65-89.
- Maksaev, V.; Munizaga, F.; Valencia, V.; Barra, F. 2009. LA-ICP-MS zircon U-Pb geochronology to constrain the age of post-Neocomian continental deposits of the Cerrillos Formation, Atacama Region, northern Chile: tectonic and metallogenic implications. *Andean Geology* 36 (2): 264-287.

- Marinovic, N.; Lahsen, A. 1984. Hoja Calama. Servicio Nacional de Geología y Minería, Carta Geológica de Chile 58: 140 p. 1 mapa escala 1:250.000. Santiago, Chile.
- Marinovic, N.; García, M. 1999. Hoja Pampa Unión. Región de Antofagasta. Servicio Nacional de Geología y Minería, Mapas Geológicos 9. 1 mapa escala 1:100.000. Santiago, Chile.
- Martínez, F.; Arriagada, C.; Mpodozis, C.; Peña, M. 2012. The Lautaro Basin: a record of inversión tectónicas in northern Chile. *Andean Geology* 39 (2): 258-278.
- Martínez, F.; Arriagada, C.; Peña, M.; Del Real, I.; Deckart, K. 2013. The structure of the Chañarcillo Basin: An example of tectonic inversión in the Atacama region, northern Chile. *Journal of South American Earth Sciences* 42: 1-16.
- Marzo, M.; Steel, R.J. 2000. Unusual features of sediment supply-dominated, transgressive-regressive sequences: Paleogene clastic wedges, SE Pyrenean foreland basin, Spain. *Sedimentary Geology* 138: 3-15.
- Mégard, F. 1978. The Andean orogenic period and its major structures in central and northern Peru. *Journal of the Geological Society of London* 141: 893-900.
- Merino, R.; Salazar, E.; Mora-Franco, C.; Creixell, C.; Coloma, F.; Oliveros, V. 2013. Fluvial deposition and retro-arc volcanism in a Late Cretaceous foreland basin and the unroofing of the Early Cretaceous arc in the Chilean Frontal Cordillera at 28°30'S, Atacama Region. *Bolletino di Geofisica: teorica ed applicata* Vol.54, Supplement 2, GeoSur 2013, Proceedings: p. 237-238.
- Miall, A.D. 1985. Architectural element analysis: A new method of facies analysis applied to fluvial deposits. *Earth Science Reviews* 22: 261-308.
- Miall, A.D. 1996. *The Geology of Fluvial Deposits. Sedimentary Facies, Basin Analysis and Petroleum Geology*. Springer-Verlag: 582 p. New York.
- Monaldi, C.R.; Salfity, J.A.; Kley, J. 2008. Preserved extensional structures in an inverted Cretaceous rift basin, northwestern Argentina: Outcrop examples and implications for fault reactivation. *Tectonics* 27: TC1011. doi:10.1029/2006TC001993
- Montaño, J.M. 1976. Estudio geológico de la zona de Caracoles y áreas vecinas, con énfasis en el Sistema Jurásico, Provincia de Antofagasta, II Región, Chile. Bsc. Thesis (Unpublished). Universidad de Chile, Santiago: 1-168 p.
- Morandé, J.; Mpodozis, C.; Valencia, V.; Arriagada, C.; Marquardt, C. 2012. Las Diamictitas de Sierra Limón Verde, Antofagasta: Evidencias de Glaciación Neoproterozoica en el Norte de Chile?. *In Congreso Geológico Chileno XIII, Actas T2: 271-273*. Antofagasta, Chile.
- Morandé, J. in prep. Basamento pre-Mesozoico de la Sierra Limón Verde: Implicancias para la evolución tectónica del norte de Chile. MSc thesis (Unpublished), Universidad de Chile: 1-114 p.
- Mpodozis, C.; Marinovic, N.; Smoje, I. 1993. Eocene Left Lateral Strike Slip Faulting and Clockwise Block Rotations in the Cordillera de Domeyko, West of the Salar de Atacama, Northern Chile. *Proceedings II ORSTOM-ISAG: 225– 228*. Oxford.

- Mpodozis, C.; Arriagada, C.; Roperch, P. 1999. Cretaceous to Paleogene geology of the Salar de Atacama basin, northern Chile: A reappraisal of the Purilactis Group stratigraphy. *In Proceedings IV IRD-ISAG*: 523-526. Göttingen.
- Mpodozis, C.; Clavero, J. 2002. Tertiary tectonic evolution of the southwestern edge of the Puna Plateau: Cordillera Claudio Gay (26°-27°S), Northern Chile. *In Proceedings V IRD-ISAG*: 445-448. Toulouse.
- Mpodozis, C.; Arriagada, C.; Basso, M.; Roperch, P.; Cobbold, P.; Reich, M. 2005. Late Mesozoic to Paleogene stratigraphy of the Salar de Atacama basin, Antofagasta, northern Chile: Implications for the tectonic evolution of the central Andes. *Tectonophysics* 399: 125-154.
- Mundaca, P. 2002. Geología de los cuadrángulos Aguada de la Teca y Barros Arana, II Región, Antofagasta. BSc. thesis (Unpublished). Universidad de Chile, Santiago: 1-69 p.
- Muñoz, N.; Charrier, R.; Reutter, K. 1997. Evolución de la cuenca Salar de Atacama: Inversión tectónica y relleno de una cuenca de antepaís de retroarco. *In Congreso Geológico Chileno*, No. 8, Actas, Vol. 1, p. 195-199. Antofagasta.
- Muñoz, N.; Jordan, T.E.; Charrier, R. 2002. Interactions between basement and cover during the evolution of the Salar de Atacama basin, northern Chile. *Revista Geológica de Chile* 29: 3-29.
- Nalpas, T.; Dabard, M.P.; Ruffet, G.; Vernon, A.; Mpodozis, C.; Loi, A.; Hérail, G. 2008. Sedimentation and preservation of the Miocene Atacama Gravels in the Pedernales Chañaral area, Northern Chile: climatic or tectonic control?. *Tectonophysics* 459: 161–173.
- Narea, K. In prep. Análisis Paleomagnético y Estructural de las unidades paleozoicas y mesozoicas del Cuadrángulo Barros Arana, Región de Antofagasta, Chile. BSc. thesis (Unpublished). Universidad de Chile, Santiago: 1-53 p.
- Nemec, W.; Steel, R.J. 1984. Alluvial and coastal conglomerates: their significant features and some comments on gravelly mass-flow deposits. *In Sedimentology of Gravels and Conglomerates* (Koster, E.H.; Steel, R.J.; editors). Canadian Society of Petroleum Geologists, Memoir 10: 1-31.
- Niemeyer, R.H. 1989. El Complejo Ígneo-Sedimentario del Cordón de Lila, Región de Antofagasta: significado tectónico. *Revista Geológica de Chile* 16(2): 163-181.
- Niemeyer, H. In prep. Geología del área Cerro Lila-Peine, Región de Antofagasta. Servicio Nacional de Geología y Minería. Carta Geológica de Chile, Serie Geología Básica. 1 mapa escala 1:100.000. Santiago, Chile.
- Noble, D.C.; McKee, E.H.; Mégard, F. 1979. Early Tertiary “Incaic” tectonism, uplift, and volcanic activity, Andes of central Peru. *Geological Society of America Bulletin* 90: 903-907.
- Noblet, C.; Lavenu, A.; Marocco, R. 1996. Concept of continuum as opposed to periodic tectonism in the Andes. *Tectonophysics* 255: 65-78.
- North American Commission on Stratigraphic Nomenclature. 2005. North American Stratigraphic Code. *The American Association of Petroleum Geologists Bulletin* 89, no. 11: 1547-1591.

- Oliveros, V.; Féraud, G.; Aguirre, L.; Fornari, M.; Morata, D. 2006. The Early Andean Magmatic Province (EAMP): $^{40}\text{Ar}/^{39}\text{Ar}$ dating on Mesozoic volcanic and plutonic rocks from the Coastal Cordillera, northern Chile. *Journal of Volcanology and Geothermal Research* 157: 311-330.
- Pananont, P.; Mpodozis, C.; Blanco, N.; Jordan, T.E.; Brown, L.D. 2004. Cenozoic evolution of the northwestern Salar de Atacama Basin, northern Chile. *Tectonics* 23: TC6007, doi: 10.1029/2003TC001595.
- Paola, C.; Heller, P.L.; Angevine, C.L. 1992. The large-scale dynamics of grain-size variation in alluvial basins, 1: Theory. *Basin Research* 4: 73-90.
- Parada, M.A.; Féraud, G.; Fuentes, F.; Aguirre, L.; Morata, D.; Larrondo, P. 2005. Ages and cooling history of the Early Cretaceous Caleu pluton: testimony of a switch from a rifted to a compressional continental margin in central Chile. *Journal of the Geological Society of London* 162: 273-287.
- Pichowiak, S.; Buchelt, M.; Damm, K.W. 1990. Magmatic activity and tectonic setting of the early stages of the Andean cycle in northern Chile. *Geological Society of America Special Papers* 241: 127-144. doi: 10.1130/SPE241-p127
- Raczynnski, A. 1963. Geología del distrito minero de Tuina. BSc. thesis (Unpublished). Universidad de Chile, Santiago: 1-117 p.
- Ramírez, C. F.; Gardeweg, M. 1982. Hoja Toconao. *Carta Geológica de Chile* 54: 122 pp. 1 mapa escala 1:250.000.
- Ramos, V.A. Zapata, T. Cristallini, E. Introcaso, A. 2004. The Andean thrust system- Latitudinal variations in structural styles and orogenic shortening. *In Thrust tectonics and hydrocarbon Systems: AAPG Memoir 82* (McClay, K.R.; editor). AAPG: 30-50. Tulsa.
- Ramos, V.A. 2008. The Basement of the Central Andes: The Arequipa and Related Terranes. *Annual Review of Earth and Planetary Sciences* 36: 289-324.
- Ramos, V.A. 2010. The tectonic regime along the Andes: Present-day and Mesozoic regimes. *Geological Journal* 45: 2-25.
- Ramos, V.A. 2010. The tectonic regime along the Andes: Present-day and Mesozoic regimes. *Geological Journal* 45: 2-25.
- Reutter, K.J.; Charrier, R.; Götze, H.J.; Schurr, B.; Wigger, P.; Scheuber, E.; Giese, P.; Reuther, C.D.; Schmidt, S.; Rietbrock, A.; Chong, G.; Belmonte-Pool, A. 2006. The Salar de Atacama Basin: a Subsiding Block within the Western Edge of the Altiplano-Puna Plateau. *In The Andes Active Subduction Orogeny* (Oncken, O.; editor). Springer: 303-325. Berlin.
- Scheuber, E.; Bogdanic, T.; Jensen, A.; Reutter, K.J. 1994. Tectonic Development of the North Chilean Andes in Relation to Plate Convergence and Magmatism Since the Jurassic. *In Tectonics of the Southern Central Andes: Structure and Evolution of an Active Continental Margin* (Reutter, K.J.; Scheuber, E.; Wigger, P.; editors). Springer: 121 – 139. New York.

- Sellwood, B.W.; Valdes, P.J. 2006. Mesozoic climates: General circulation models and the rock record. *Sedimentary Geology*: 269-287.
- Siks, B.; Horton, B.K. 2011. Growth and fragmentation of the Andean foreland basin during eastward advance of fold-thrust deformation, Puna plateau and Eastern Cordillera, northern Argentina. *Tectonics*: doi:10.1029/2011TC002944, in press.
- Skarmeta, J. 1983. The structural geology of the Sierra de Moreno, northern Chile. Thesis, University of London.
- Smith, G.A. 1994. Climatic influences on continental deposition during late-stage filling of an extensional basin, southeastern Arizona. *Geological Society of America Bulletin* 106, no.9: 1212-1228.
- Somoza, R.; Ghidella, M.E. 2005. Convergencia en el margen occidental de América del Sur durante el Cenozoico: subducción de las placas de Nazca, Farallón y Aluk. *Revista de la Asociación Geológica Argentina* 60 (4): 797-809.
- Somoza, R.; Tomlinson, A.J.; Caffè, P.J.; Vilas, J.F. 2012. Paleomagnetic evidence of earliest Paleocene deformation in Calama (~22°S), northern Chile: Andean-type or ridge-collision tectonics? *Journal of South American Earth Sciences* 37: 208-213.
- Solari, L.A.; Gómez-Tuena, A.; Bernal, J.P.; Pérez-Arvizu, O.; Tanner, M. 2010. U-Pb zircon geochronology by an integrated LA-ICPMS microanalytical workstation: achievements in precision and accuracy. *Geostandards and Geoanalytical Research* 34-1: 5-18.
- Steinman, G. 1929. *Geologie von Peru*. Carl Winters Universitats-Buchhandlung. 448 pp.
- Tomlinson, A.J.; Blanco, N.; Makshev, V.; Dilles, J.; Grunder, A.L.; Ladino, M. 2001. Geología de la Precordillera Andina de Quebrada Blanca-Chuquicamata, Regiones I y II (20°30'-22°30'S). Servicio Nacional de Geología y Minería, Informe Registrado IR-01-20: 1-444. Santiago, Chile.
- Tunik, M.; Folguera, A.; Naipauer, M.; Pimentel, M.; Ramos, V.A. 2010. Early uplift and orogenic deformation in the Neuquén Basin: Constraints on the Andean uplift from U-Pb and Hf isotopic data of detrital zircons. *Tectonophysics* 489: 258-273.
- Weltje, G.J. 2006. Ternary sandstone composition and provenance: an evaluation of the 'Dickinson model'. Geological Society, London, Special Publications 264: 79-99.
- Yang, Y.; Miall, A.D. 2010. Migration and stratigraphic fill of an underfilled foreland basin: Middle-Late Cenomanian Belle Fourche Formation in southern Alberta. *Sedimentary Geology* 227: 51-64.
- Yang, Y. 2011. Tectonically-driven underfilled-overfilled cycles, the middle Cretaceous in the northern Cordilleran foreland basin. *Sedimentary Geology* 233: 15-27.
- Yuan, X.; Sobolev, S.; Kind, R. 2002. Moho topography in the central Andes and its geodynamic implications. *Earth Planetary Science Letters* 199: 389-402.

Zahid, K.M.; Barbeau, D.L. 2011. Constructing sandstone provenance and classification ternary diagrams using electronic spreadsheet. *Journal of Sedimentary Research* 81: 702-707.

Zimmermann, U.; Niemeyer, H.; Meffre, S. 2009. Revealing the continental margin of Gondwana: The Ordovician arc of the Cordón de Lila (northern Chile). *International Journal of Earth Sciences*: doi: 10.1007/s00531-009-0483-811

VII APPENDIX

A. Stratigraphic columns

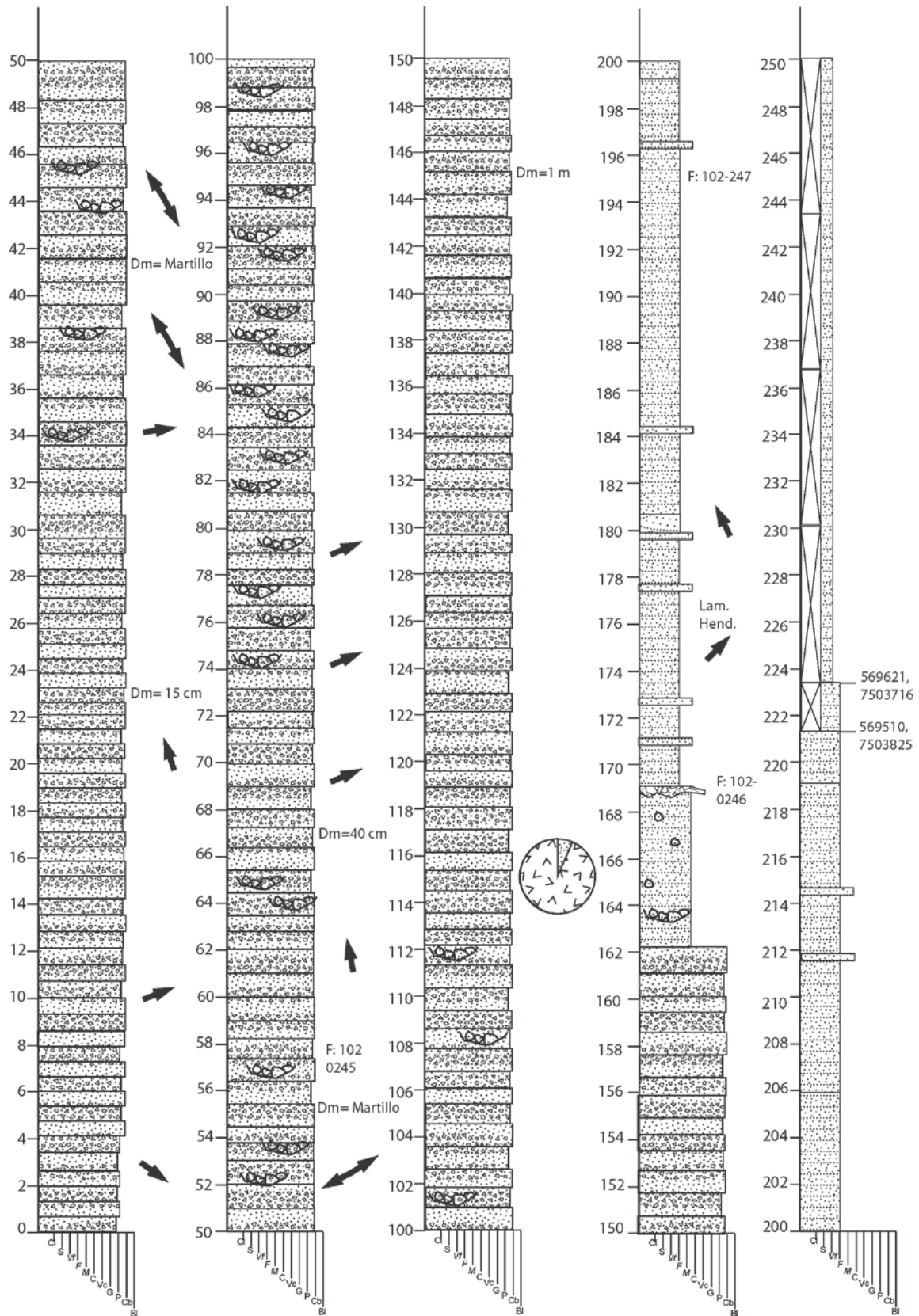


Figure A.1: Measured section of the Tonel Formation.

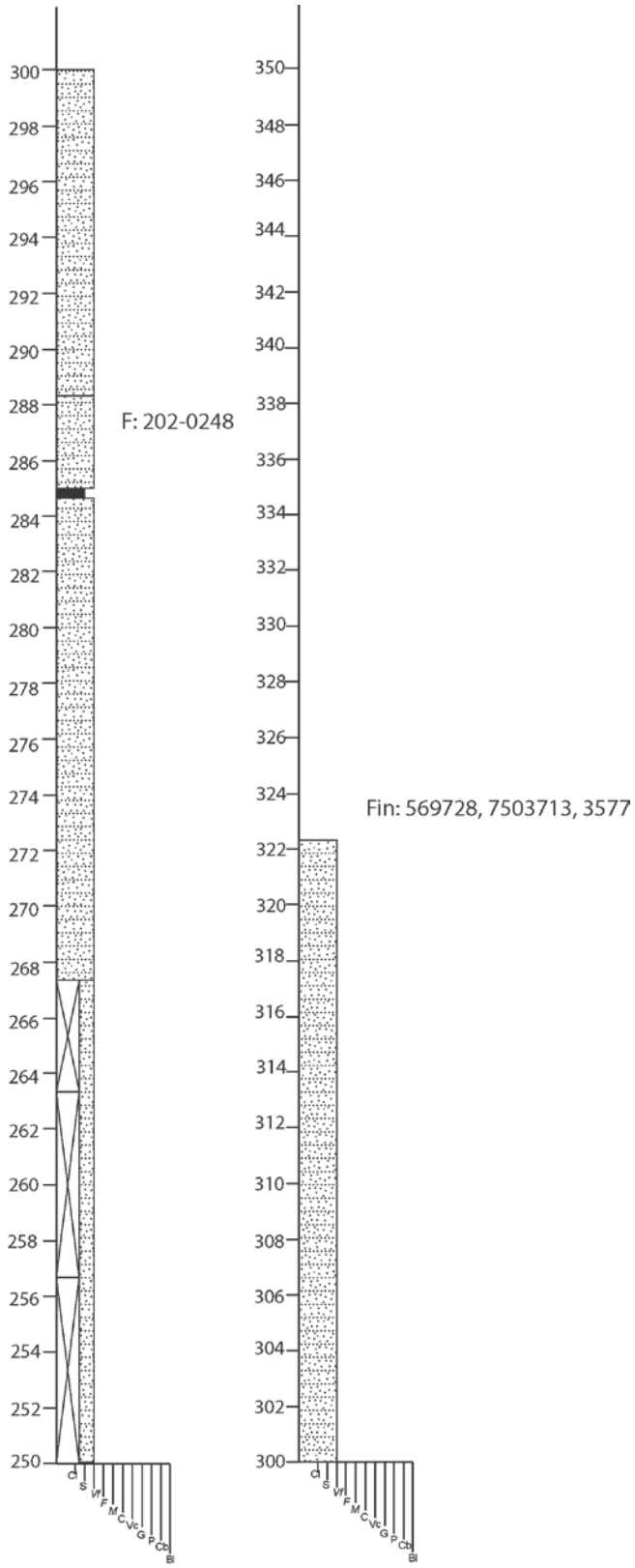


Figure A.1: (continued).

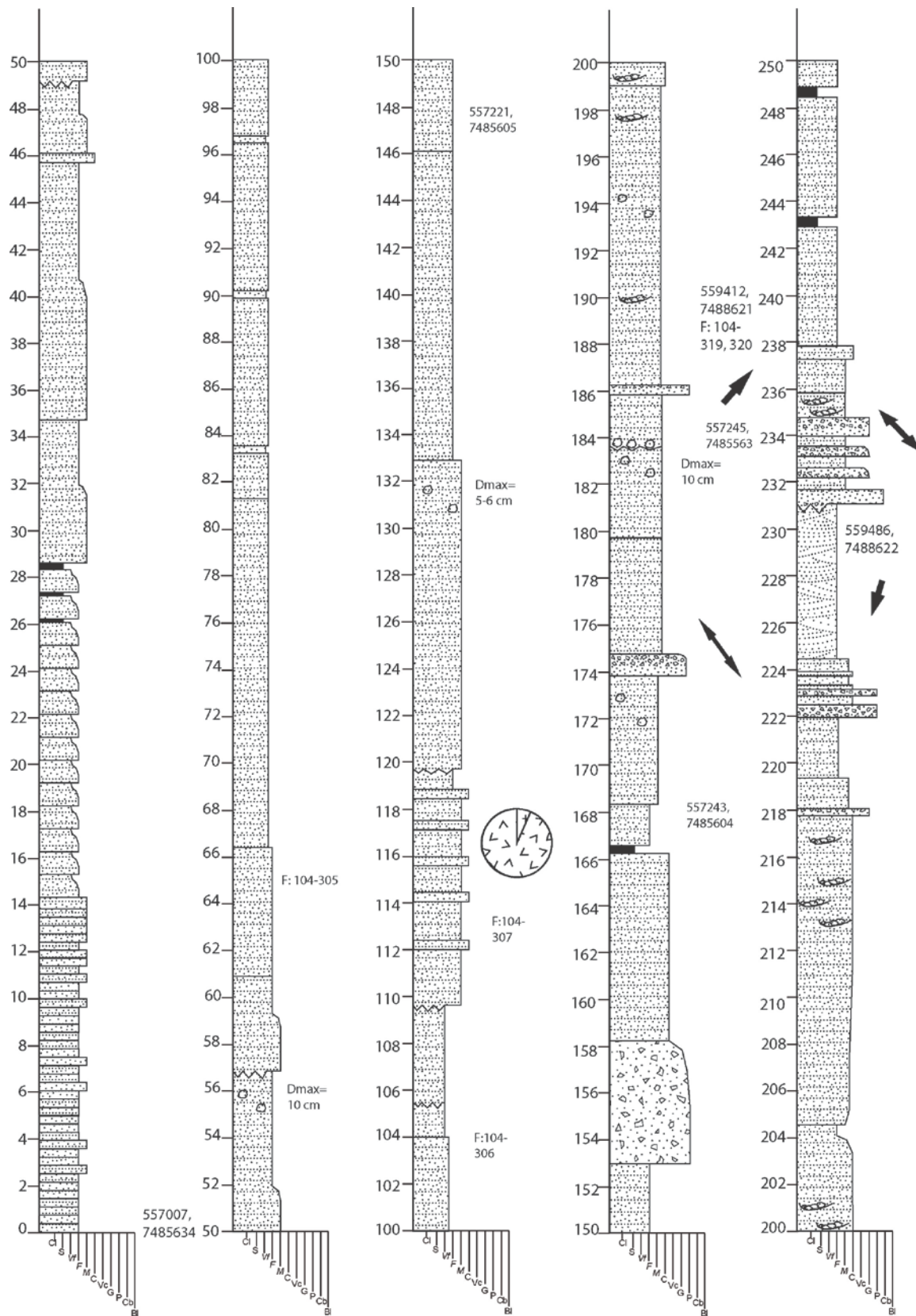


Figure A.2: Measured section of the Limón Verde Member.

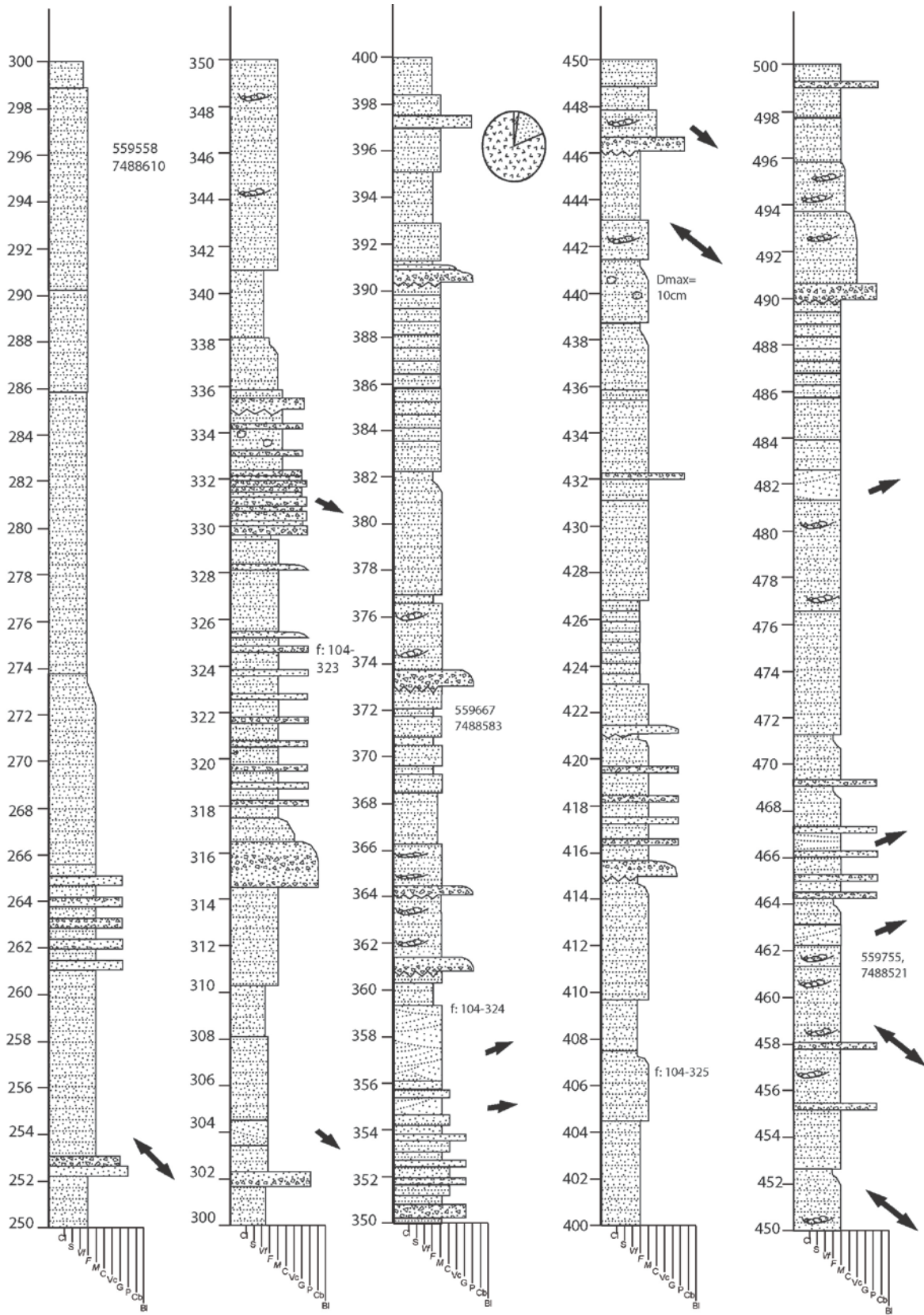


Figure A.2: (continued).

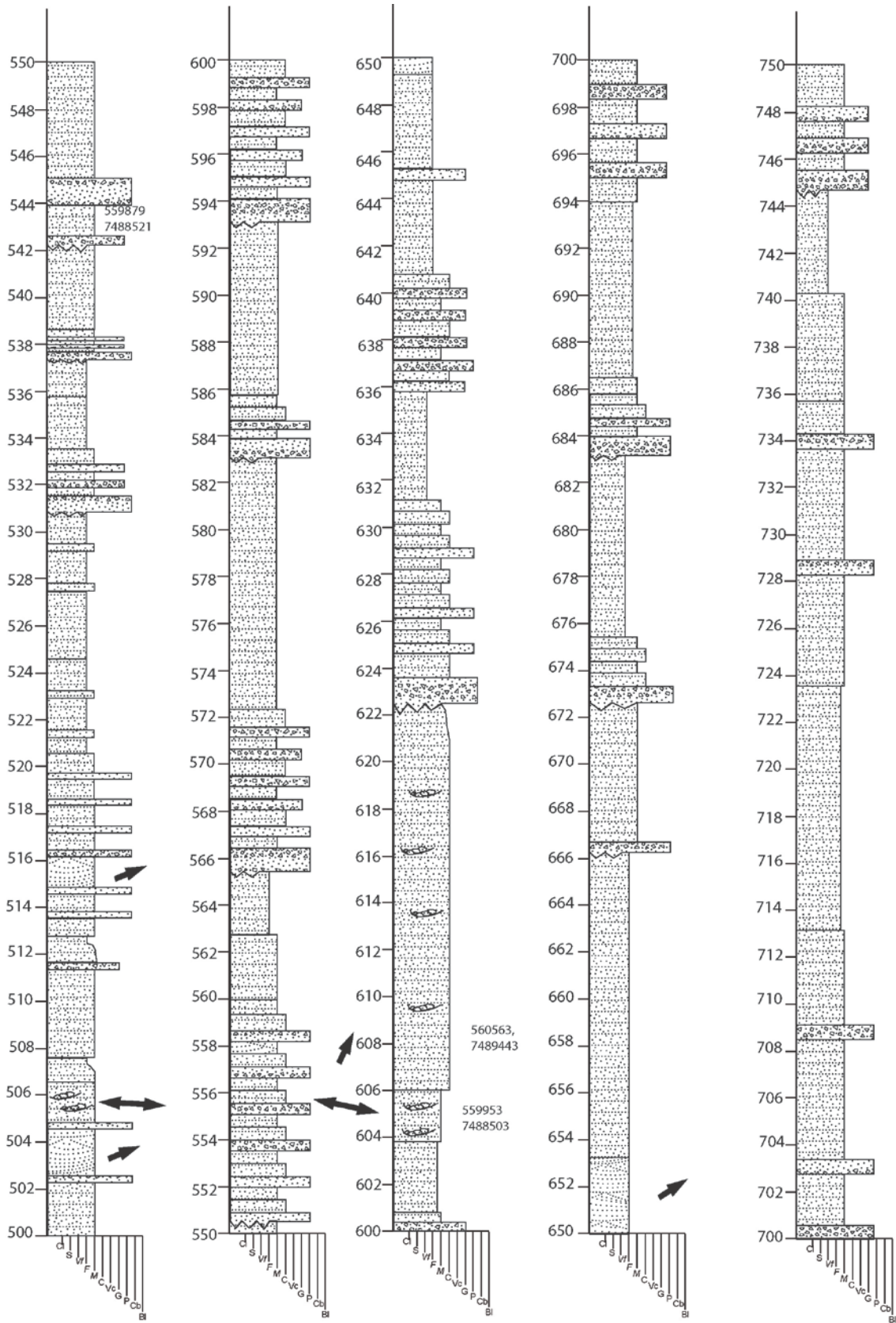


Figure A.2: (continued).

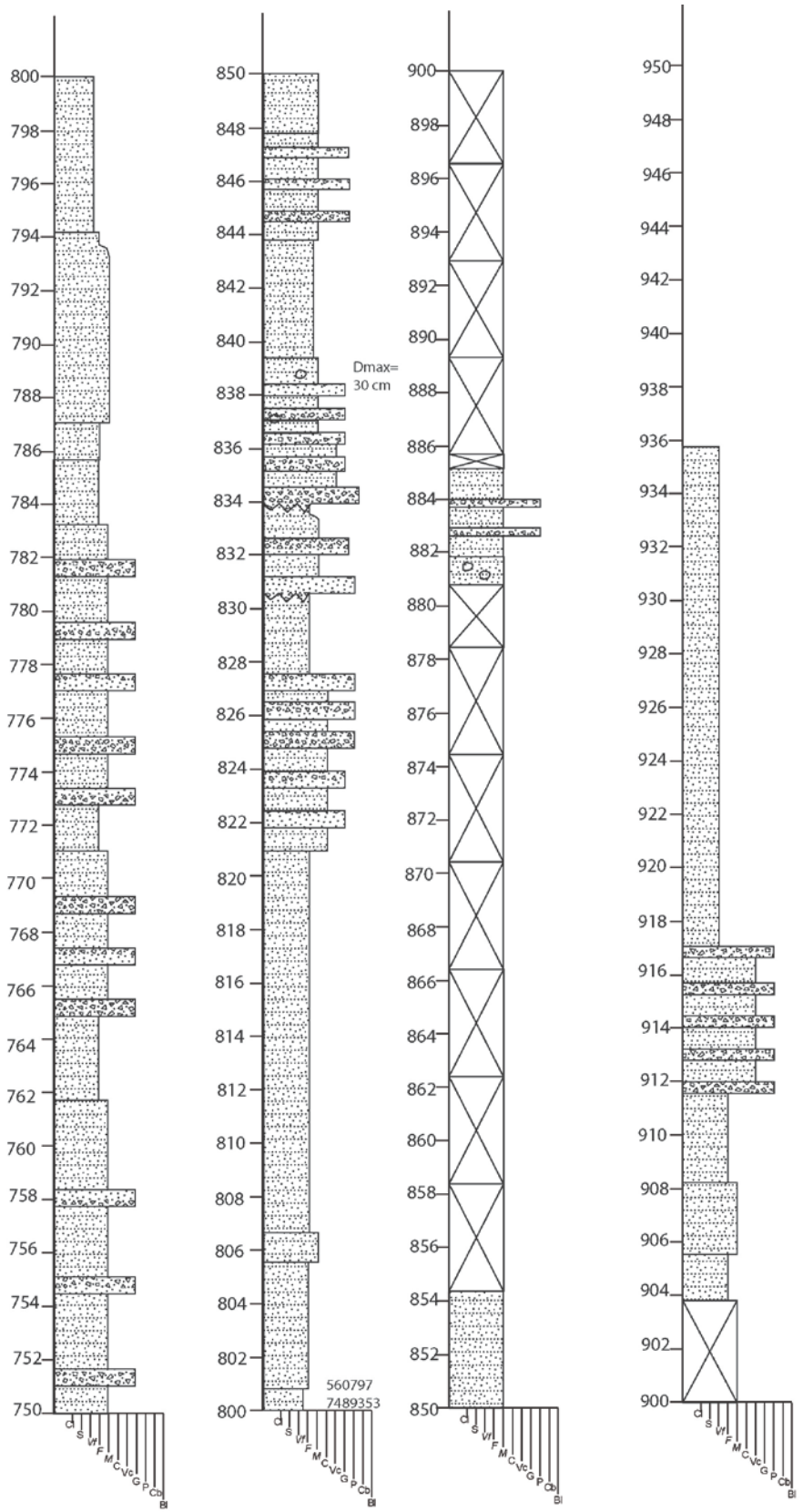


Figure A.2: (continued).

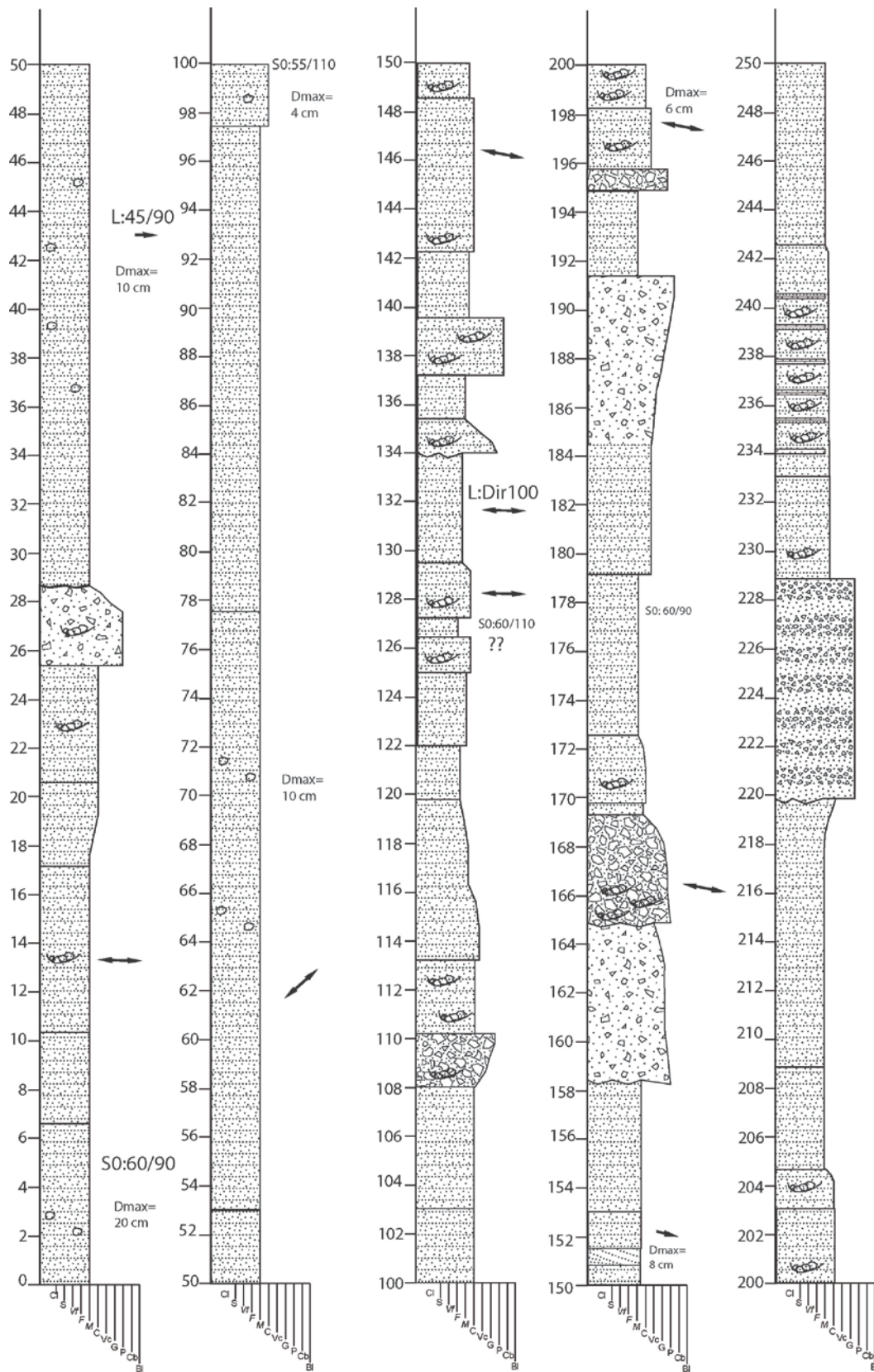


Figure A.3: Measured section of the Lampallar Member.

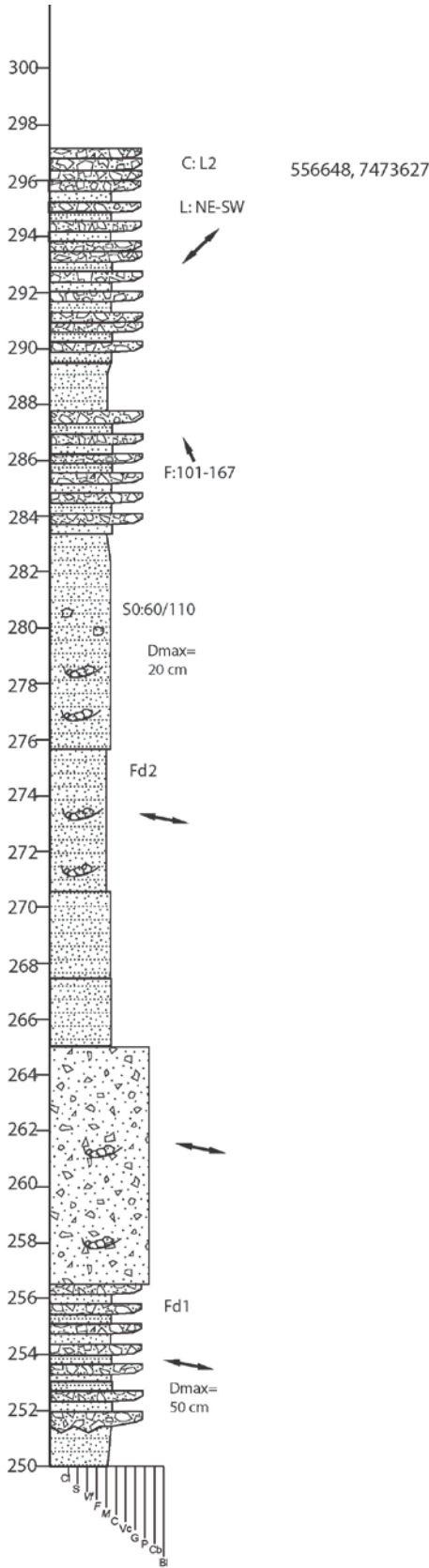


Figure A.3: (continued).

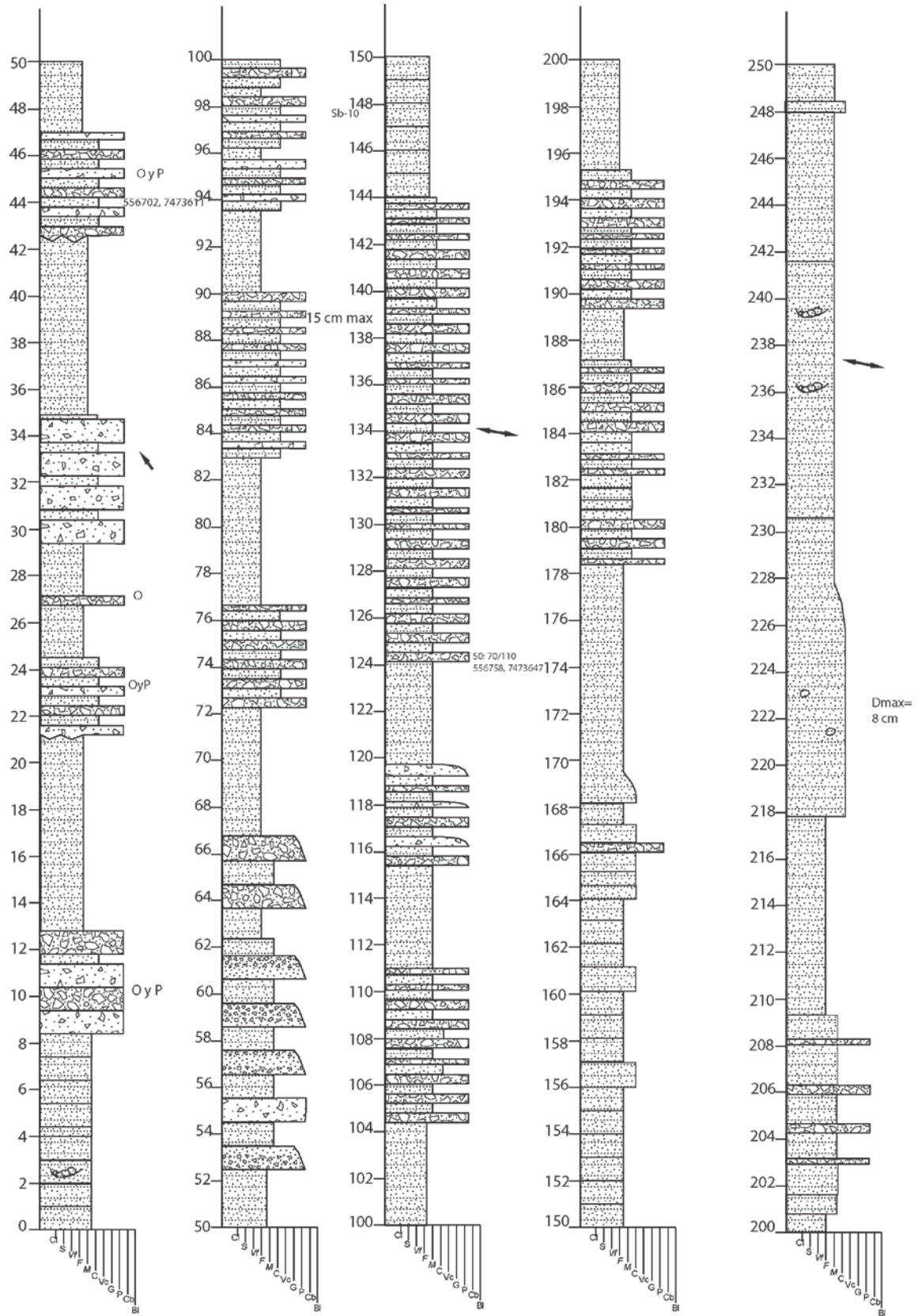


Figure A.4: Measured section of the Licán Member.

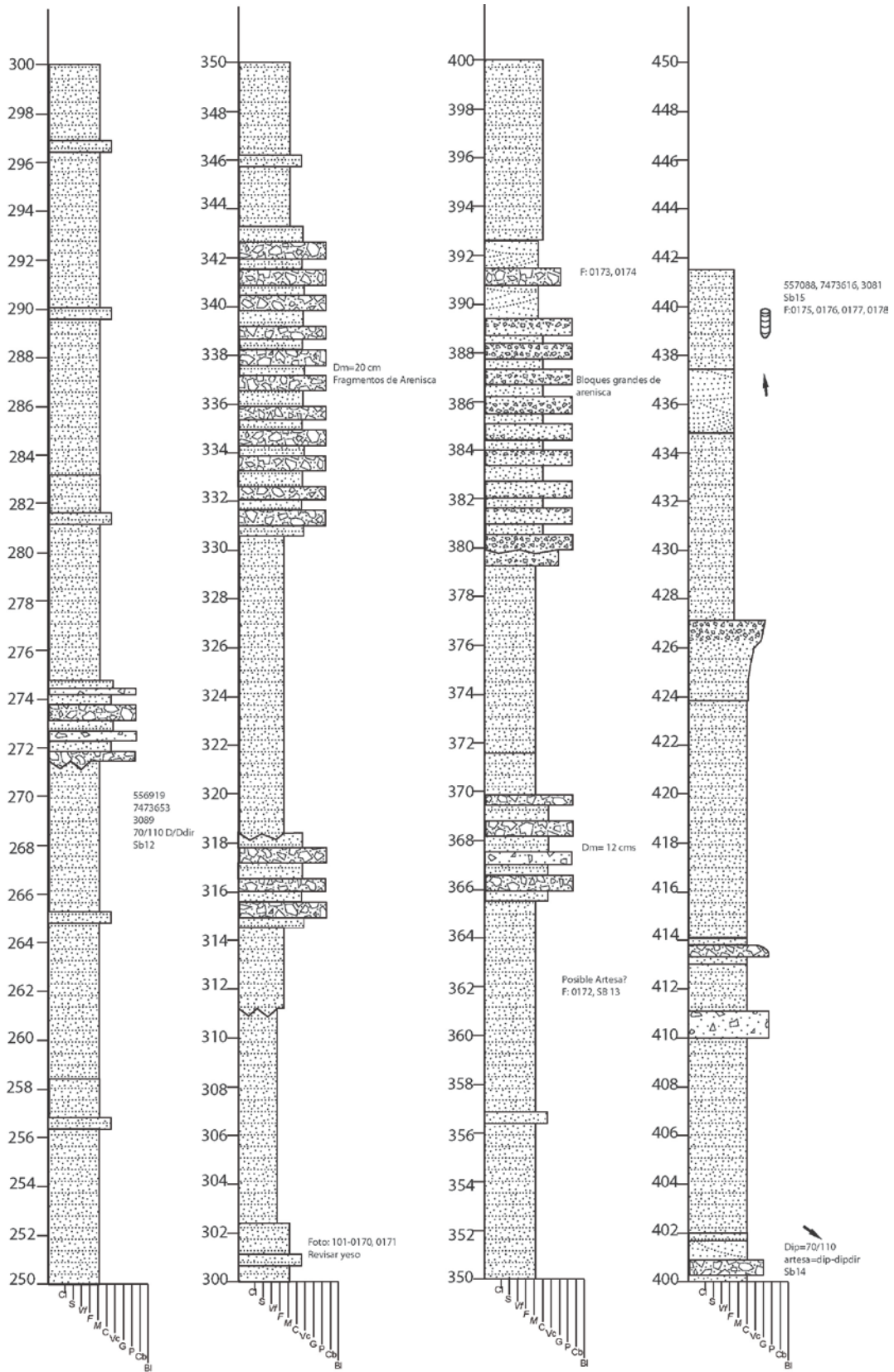


Figure A.4: (continued).

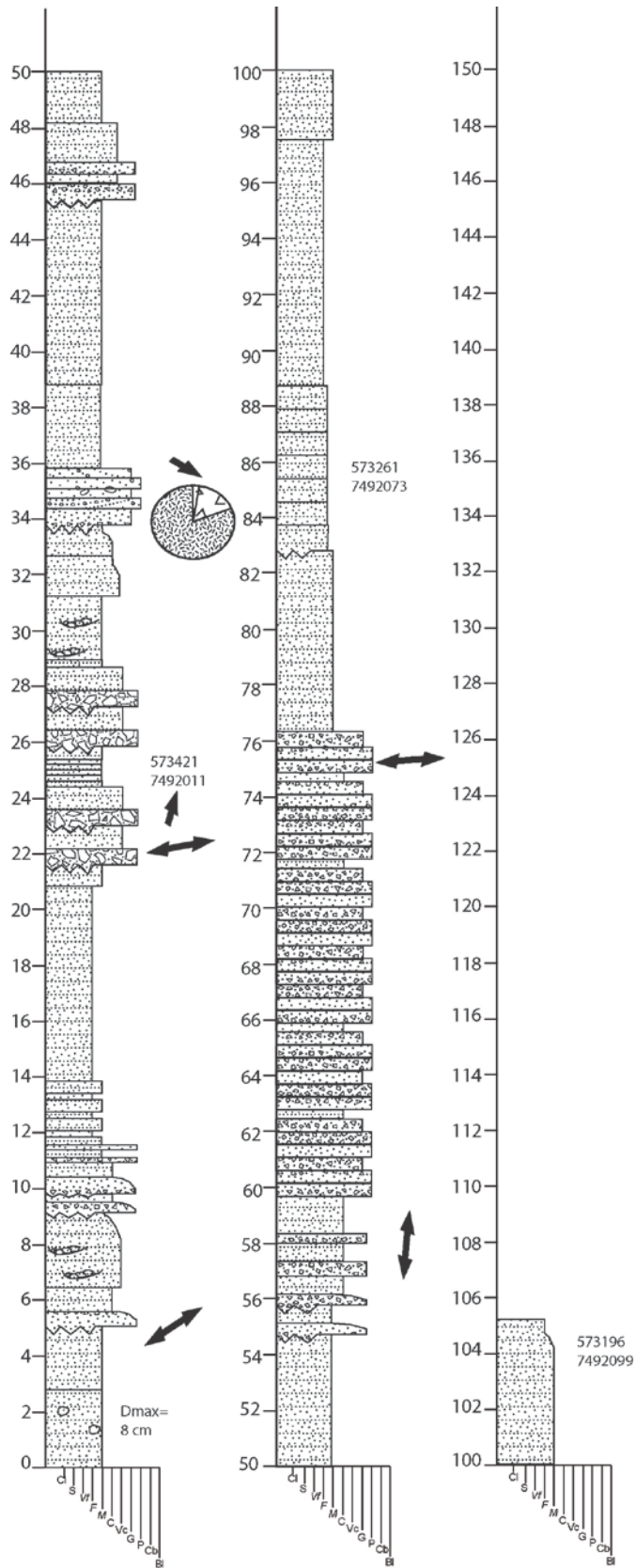


Figure A.5: Measured section of the Pajarito Member.

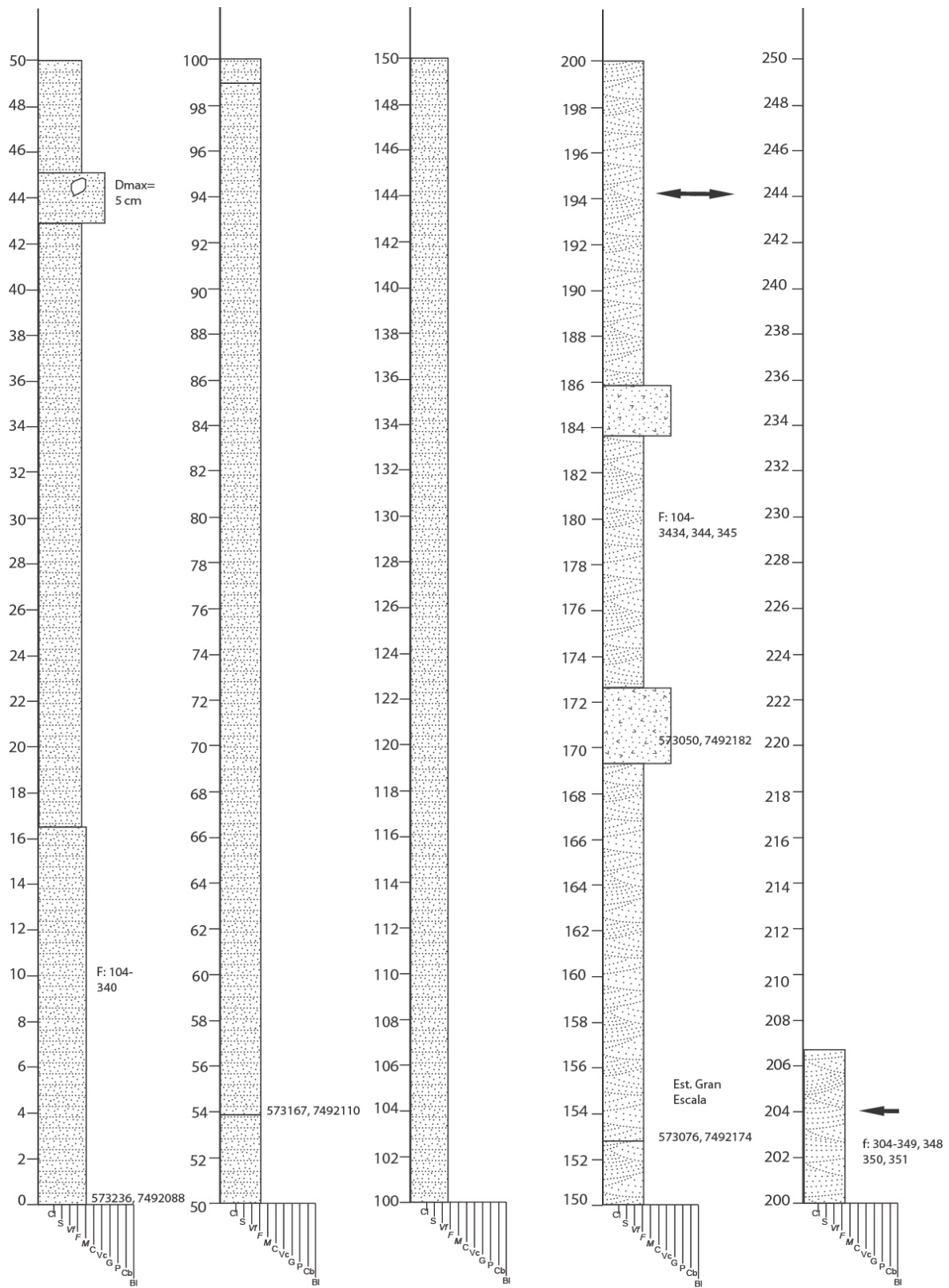


Figure A.6: Measured section of the Vizcachita Member.

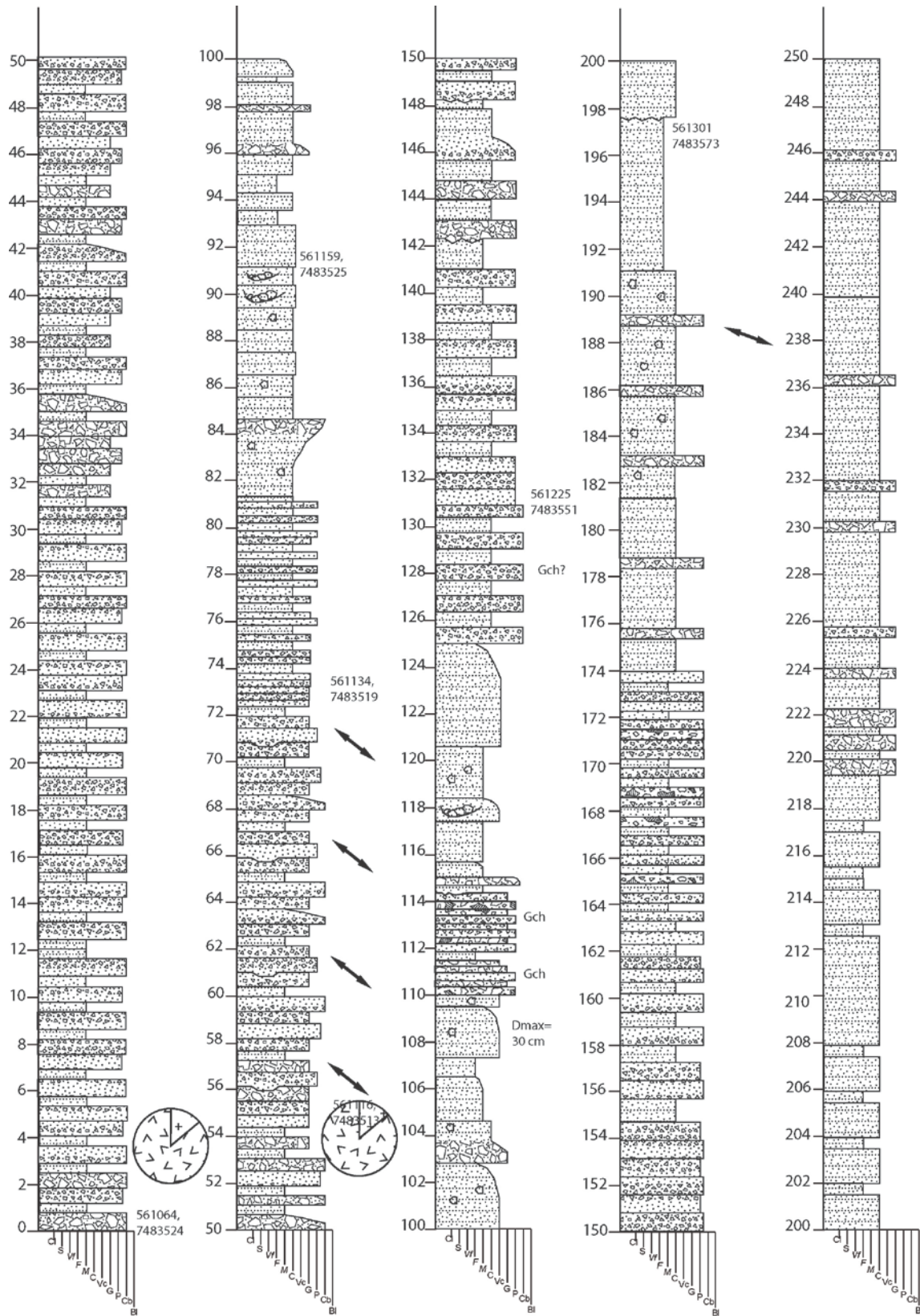


Figure A.7: Measured section of the Seilao Member.

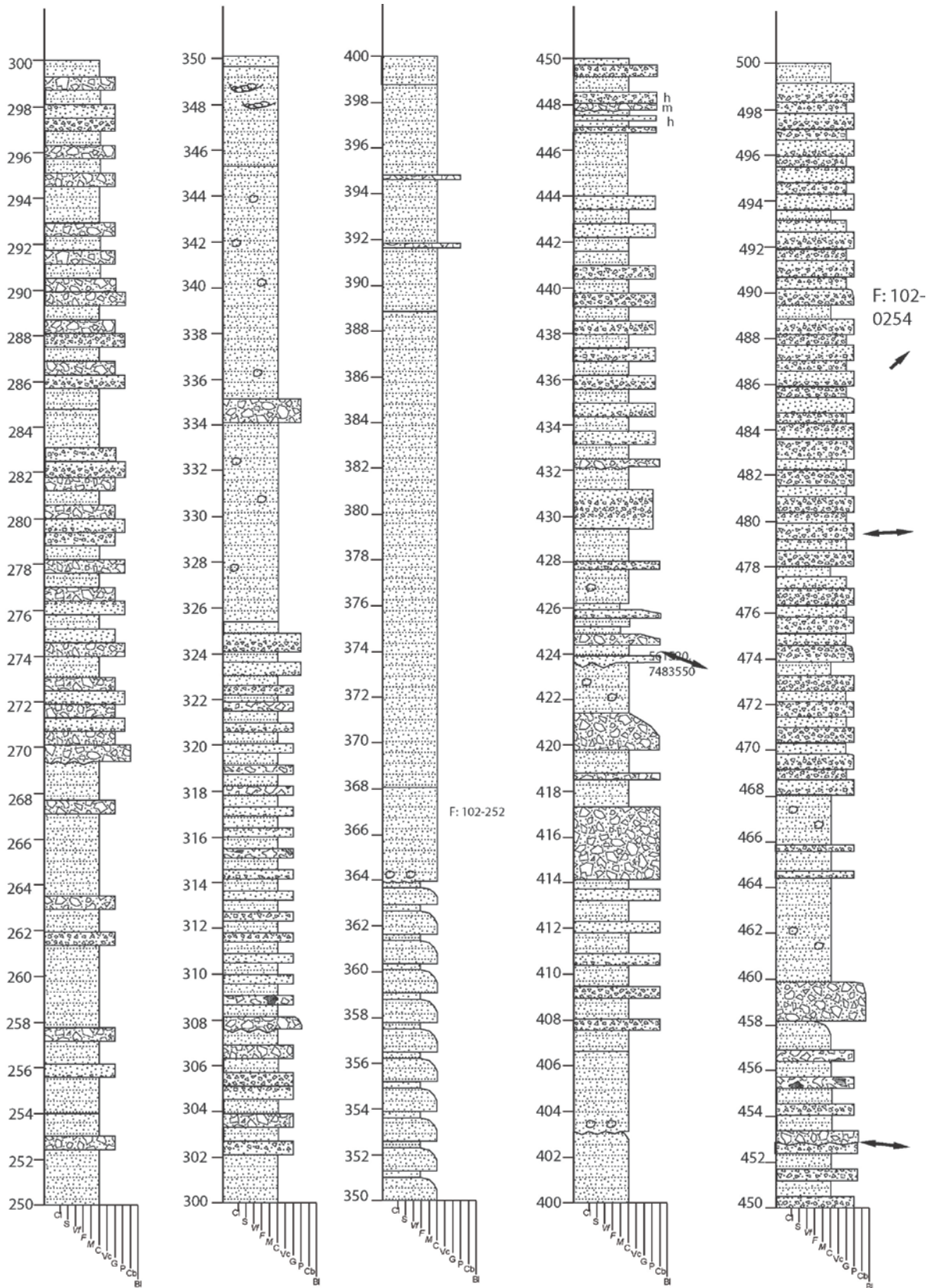


Figure A.7: (continued).

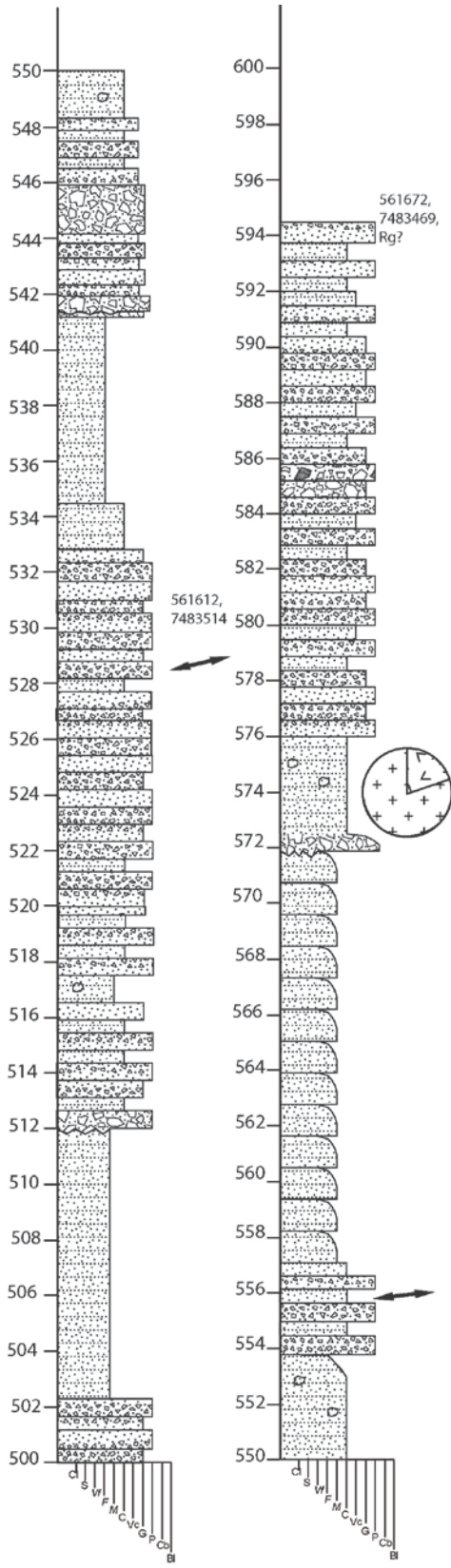


Figure A.7: (continued).

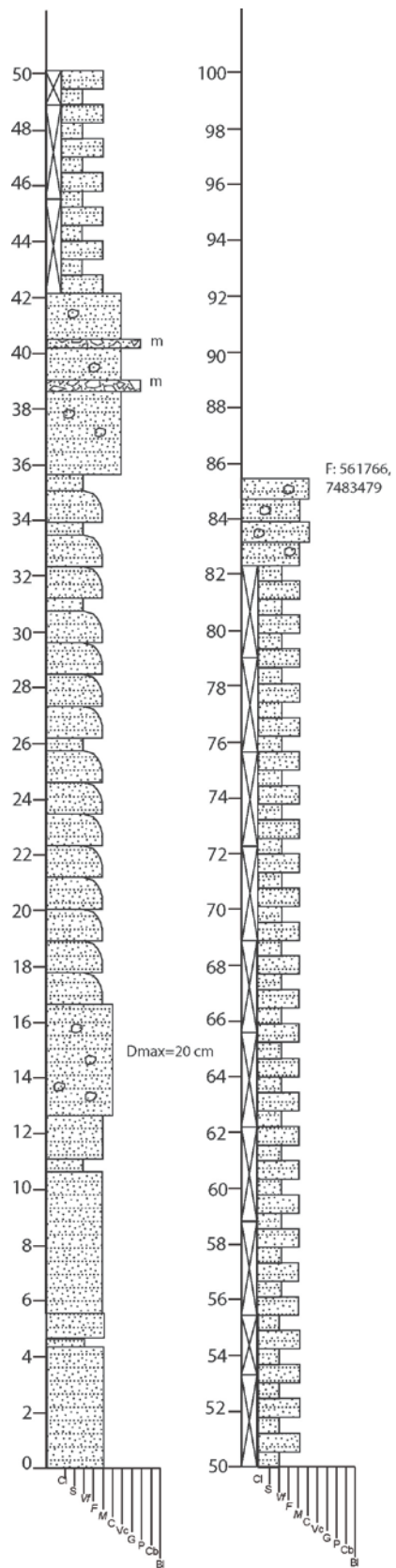


Figure A.8: Measured section of the Río Grande Member.

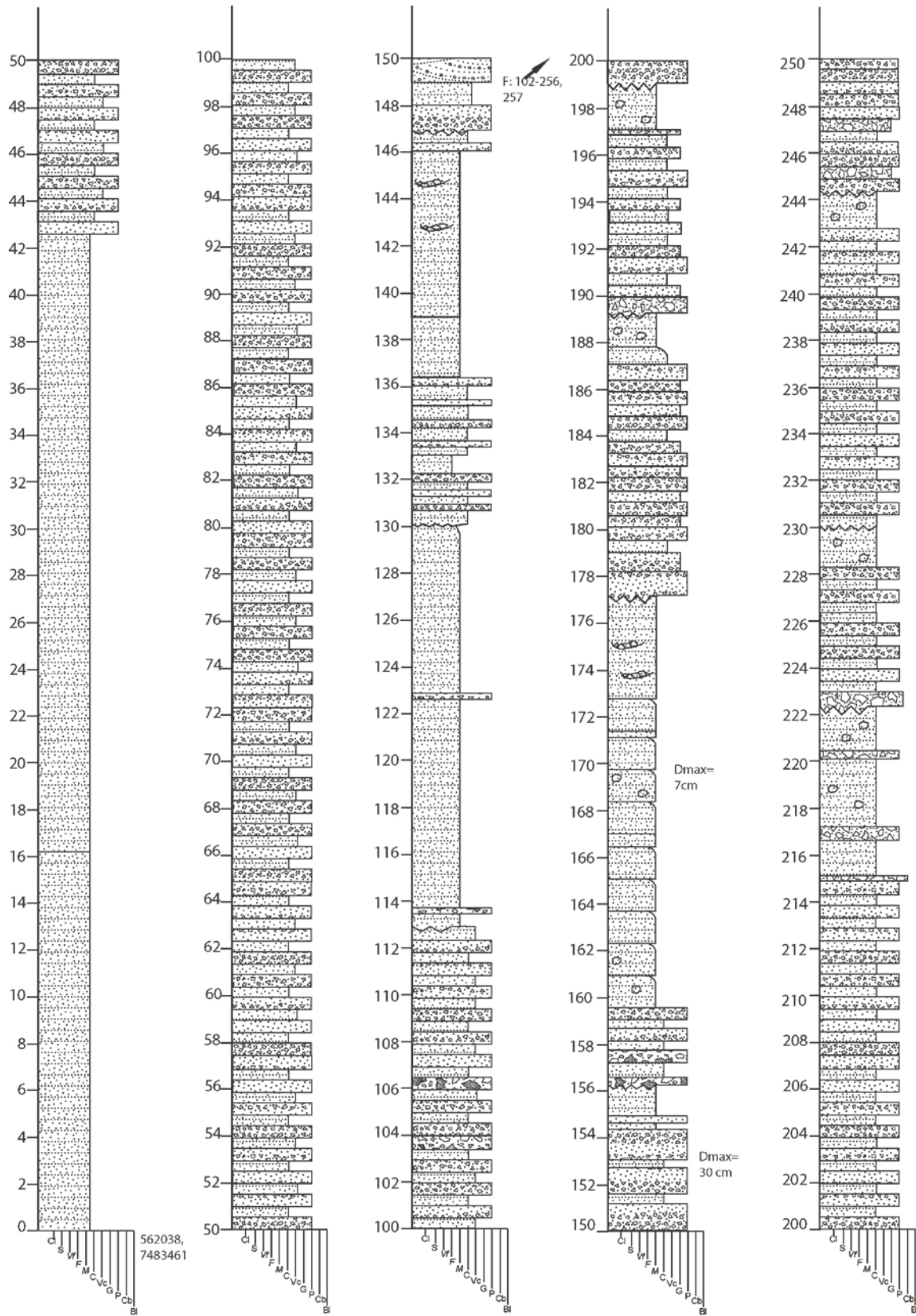


Figure A.9: Measured section of the Barros Arana Formation.

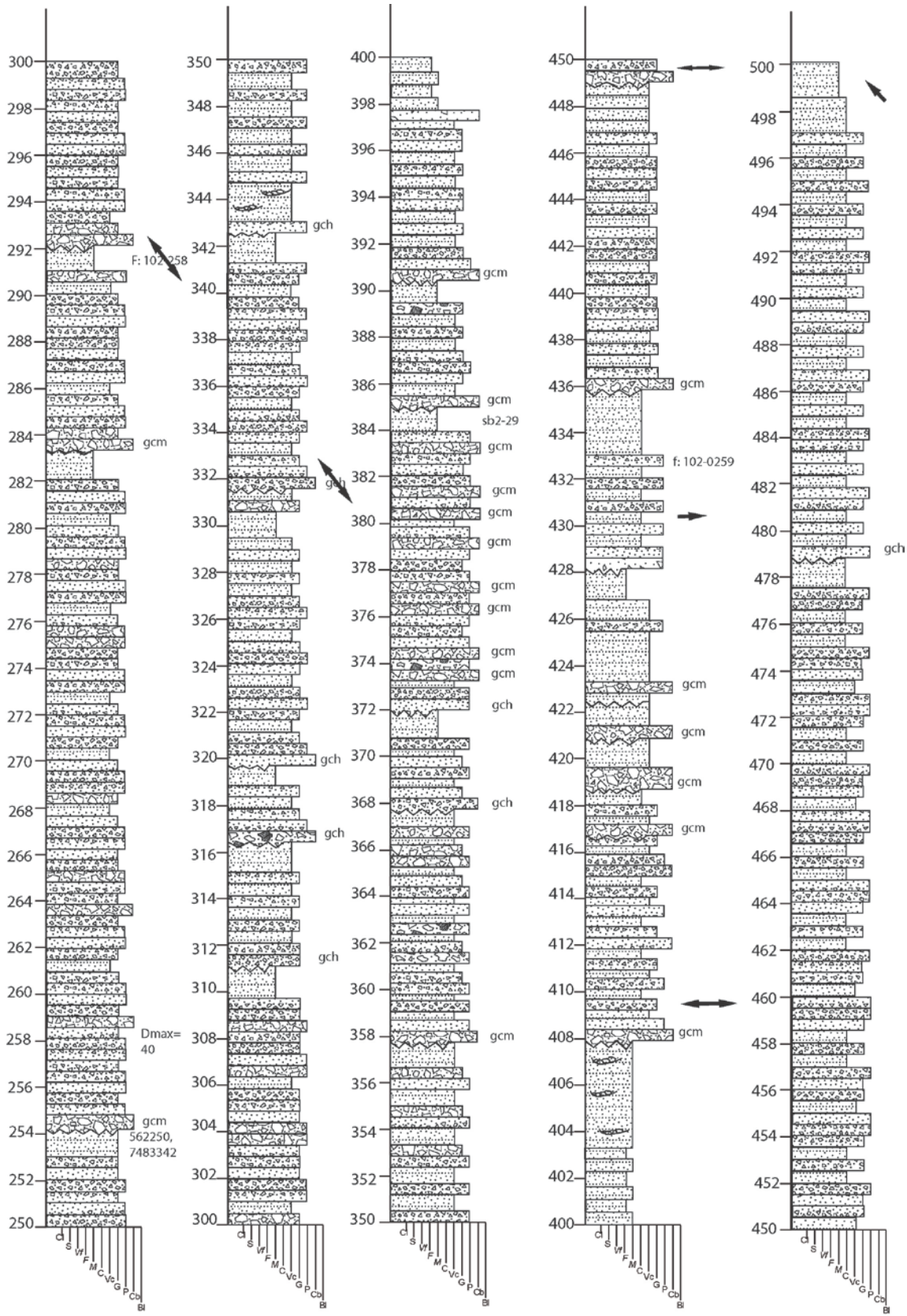


Figure A.9: (continued).

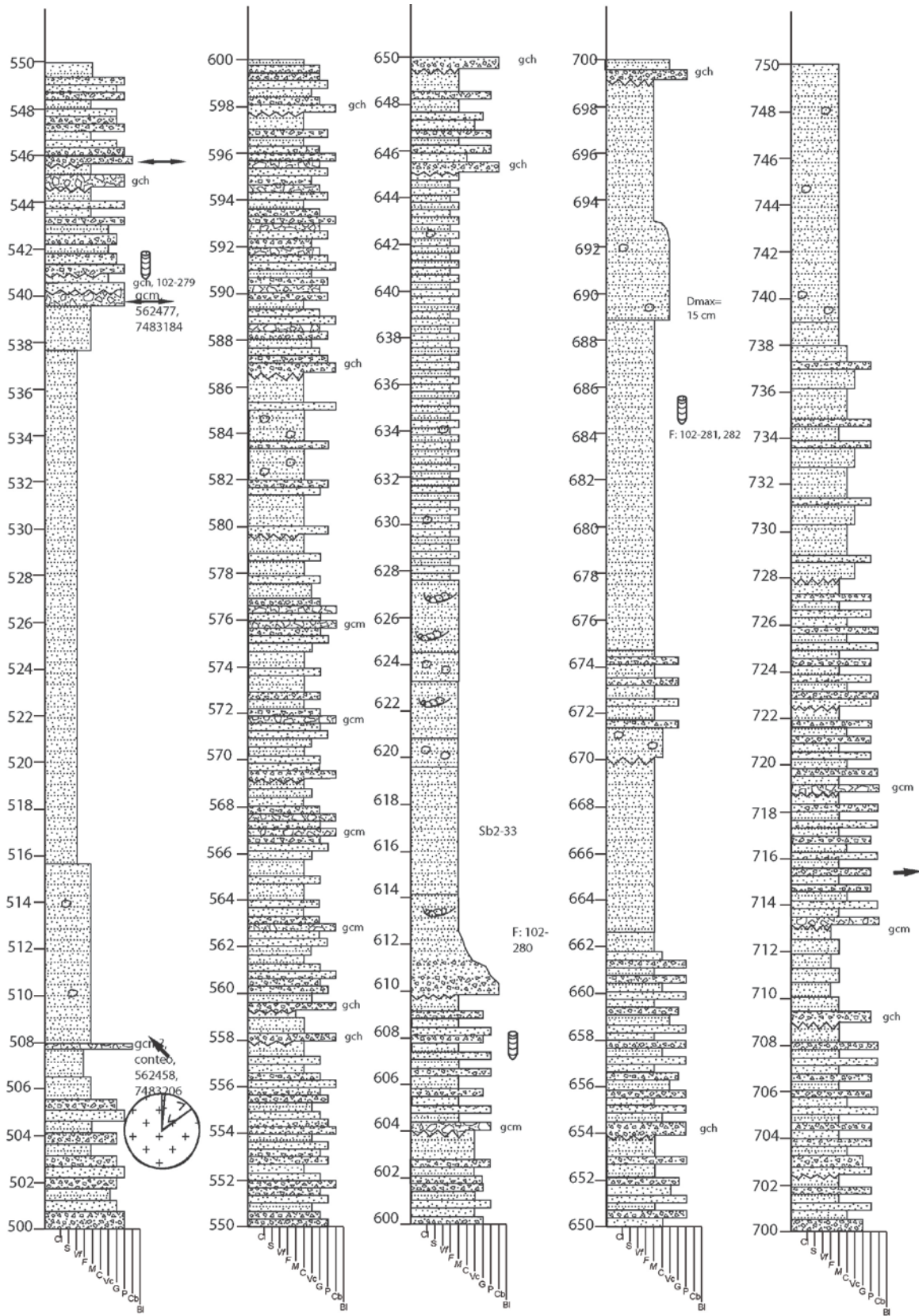


Figure A.9: (continued).

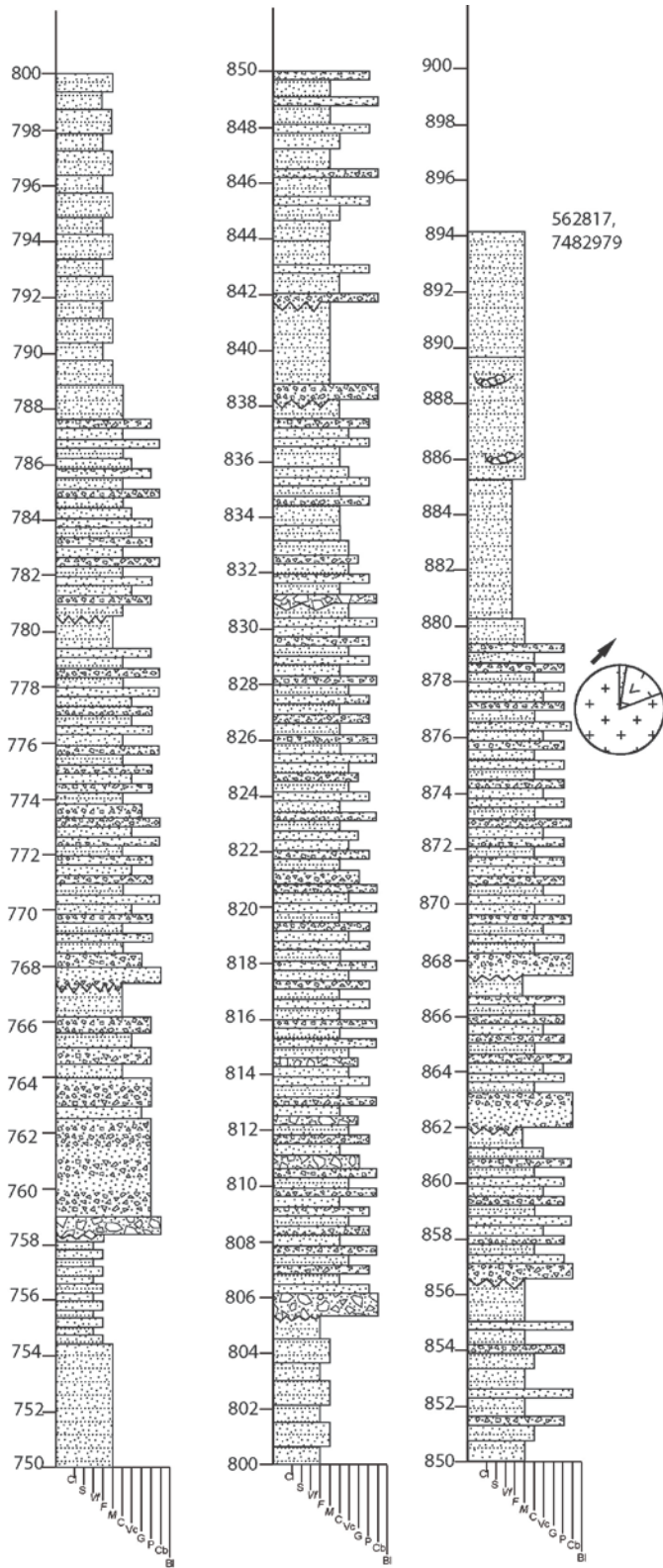


Figure A.9: (continued).

Legend

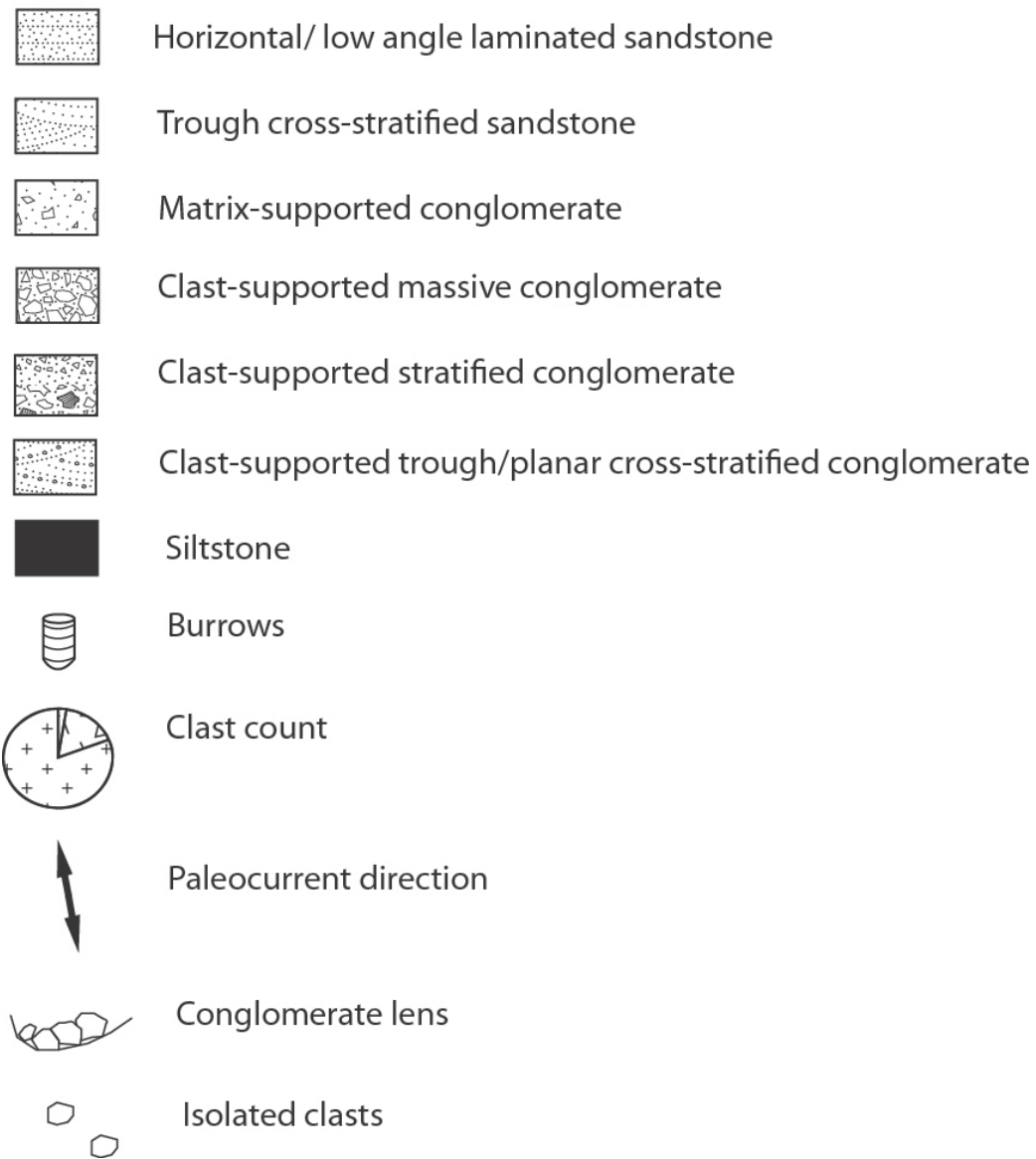


Figure A.10: Legend for the columns.

B. Provenance Data

B.1 First Count

Component	Samples										
	SP3-90	SP3-89	SP2-04	SP3-91	SP3-87	SP3-92	SP3-85	SP3-88	SBP3-1	SP3-86	SP3-94
Monoc. Qtz	130	105	59	32	26	5	74	49	55	27	5
Polyc. Qtz	0	0	0	0	0	0	0	12	4	4	1
Chert	2	14	0	0	0	0	0	0	0	0	0
Mono. Qtz	130	105	59	32	26	5	74	49	55	27	5
Plagioclase	14	19	19	44	68	107	85	102	173	153	190
Feldspar	189	203	255	208	185	185	154	154	108	159	109
Total Feldspar	203	222	274	252	253	292	239	256	281	312	299
Volcanic Fragment	5	6	4	52	48	54	44	38	33	27	30
Sedimentary Fragment	0	4	0	0	0	0	0	0	2	0	0
Metamorphic Fragment	0	0	0	0	0	0	0	0	0	0	0
Total Frag.	7	24	4	52	48	54	44	50	39	31	31
Heavy Minerals	28	33	28	17	12	6	10	4	3	10	14
Amphibole	0	0	0	0	0	0	0	0	0	0	0
Piroxene	0	0	0	0	29	3	0	0	2	7	12
Matrix and Cement	42	126	45	57	42	50	43	148	30	23	49
Qz %	38,2352941	29,91453	17,50742	9,52381	7,95107	1,424501	20,72829	13,80282	14,66667	7,297297	1,492537
F%	59,7058824	63,24786	81,30564	75	77,37003	83,19088	66,94678	72,11268	74,93333	84,32432	89,25373
L%	2,05882353	6,837607	1,186944	15,47619	14,6789	15,38462	12,32493	14,08451	10,4	8,378378	9,253731
Data ID	KsLv1	KsL2	Kst	KsLv2	KsRg	KsL3	KsS	KspBa	KsL1	KsV	KsV

Component	Samples										
	SP3-90	SP3-89	SP2-04	SP3-91	SP3-87	SP3-92	SP3-85	SP3-88	SBP3-1	SP3-86	SP3-94
Monoc. Qtz	130	105	59	32	26	5	74	49	55	27	5
Polyc. Qtz	0	0	0	0	0	0	0	12	4	4	1
Chert	2	14	0	0	0	0	0	0	0	0	0
Total Qtz	132	119	59	32	26	5	74	61	59	31	6
Plagioclase	14	19	19	44	68	107	85	102	173	153	190
Feldspar	189	203	255	208	185	185	154	154	108	159	109
Total Feldspar	203	222	274	252	253	292	239	256	281	312	299
Volcanic Fragment	5	6	4	52	48	54	44	38	33	27	30
Sedimentary Fragment	0	4	0	0	0	0	0	0	2	0	0
Metamorphic Fragment	0	0	0	0	0	0	0	0	0	0	0
Total Frag.	5	10	4	52	48	54	44	38	35	27	30
Heavy Minerals	28	33	28	17	12	6	10	4	3	10	14
Amphibole	0	0	0	0	0	0	0	0	0	0	0
Olivine	0	0	0	0	29	3	0	0	2	7	12
Matrix and Cement	42	126	45	57	42	50	43	148	30	23	49
Qz %	38,8235294	33,90313	17,50742	9,52381	7,95107	1,424501	20,72829	17,1831	15,73333	8,378378	1,791045
F%	59,7058824	63,24786	81,30564	75	77,37003	83,19088	66,94678	72,11268	74,93333	84,32432	89,25373
L%	1,47058824	2,849003	1,186944	15,47619	14,6789	15,38462	12,32493	10,70423	9,333333	7,297297	8,955224
Data ID	KsLv1	KsL2	Kst	KsLv2	KsRg	KsL3	KsS	KspBa	KsL1	KsV	KsV

B.2 Second Count

Component	Samples										
	SP3-90	SP3-89	SP2-04	SP3-91	SP3-87	SP3-92	SP3-85	SP3-88	SBP3-1	SP3-86	SP3-94
Monoc. Qtz	200	137	124	68	46	32	137	142	115	79	14
Polyc. Qtz	1	8	22	2	3	2	10	6	7	4	8
Chert		26	7	2	2	18	6	9	8	2	2
Mono. Qtz	200	137	124	68	46	32	137	142	115	79	14
Plag in Lv		27	8	148	180	153	41	42	136	126	150
Plagioclase	194	27	164	94	115	127	146	102	66	111	88
Feldspar	21	103	96	13	8	11	25	33	12	43	42
Total Feldspar	215	157	268	255	303	291	212	177	214	280	280
Volcanic Fragment		5	1	88	54	60	23	35	76	53	119
Sedimentary Fragment		93	1								0
Metamorphic Fragment	1			1	1			3		1	
Total Frag.	2	132	31	93	60	80	39	53	91	60	129
Heavy Minerals	1			2	24	4	3				4
Amphibole											
Olivine											
Matrix and Cement	32	24	29	32	17	40	59	78	30	21	18
Qz %	47,9616307	32,15962	29,31442	16,34615	11,24694	7,940447	35,30928	38,17204	27,38095	18,85442	3,309693
F%	51,558753	36,85446	63,35697	61,29808	74,08313	72,20844	54,63918	47,58065	50,95238	66,82578	66,19385
L%	0,47961631	30,98592	7,328605	22,35577	14,66993	19,85112	10,05155	14,24731	21,66667	14,31981	30,49645
Data ID	KsLv1	KsL2	Kst	KsLv2	KsRg	KsL3	KsS	KspBa	KsL1	KsV	KsV

Component	Samples										
	SP3-90	SP3-89	SP2-04	SP3-91	SP3-87	SP3-92	SP3-85	SP3-88	SBP3-1	SP3-86	SP3-94
Monoc. Qtz	200	137	124	68	46	32	137	142	115	79	14
Polyc. Qtz	1	8	22	2	3	2	10	6	7	4	8
Chert		26	7	2	2	18	6	9	8	2	2
Total Qtz	201	171	153	72	51	52	153	157	130	85	24
Plag in Lv	0	27	8	148	180	153	41	42	136	126	150
Plagioclase	194	27	164	94	115	127	146	102	66	111	88
Feldspar	21	103	96	13	8	11	25	33	12	43	42
Total Feldspar	215	157	268	255	303	291	212	177	214	280	280
Volcanic Fragment		5	1	88	54	60	23	35	76	53	119
Sedimentary Fragment		93	1								0
Metamorphic Fragment	1			1	1			3		1	
Total Frag.	1	98	2	89	55	60	23	38	76	54	119
Heavy Minerals	1			2	24	4	3				4
Amphibole											
Olivine											
Matrix and Cement	32	24	29	32	17	40	59	78	30	21	18
Qz %	48,2014388	40,14085	36,17021	17,30769	12,46944	12,90323	39,43299	42,2043	30,95238	20,2864	5,673759
F%	51,558753	36,85446	63,35697	61,29808	74,08313	72,20844	54,63918	47,58065	50,95238	66,82578	66,19385
L%	0,23980815	23,00469	0,472813	21,39423	13,44743	14,88834	5,927835	10,21505	18,09524	12,88783	28,13239
Data ID	KsLv1	KsL2	Kst	KsLv2	KsRg	KsL3	KsS	KspBa	KsL1	KsV	KsV

C. Zircon data

C.1. Sample SP3-88

	U (ppm) ¹	Th (ppm) ¹	Th/U	CORRECTED RATIOS ²			CORRECTED ACES (M.L.)											
				²⁰⁷ Pb/ ²⁰⁹ Pb ±2. abs	²⁰⁷ Pb/ ²³⁵ U ±2. abs	²⁰⁶ Pb/ ²³⁸ U ±2. abs	²⁰⁶ Pb/ ²³⁵ U ±2. abs	²⁰⁷ Pb/ ²³⁵ U ±2.	²⁰⁷ Pb/ ²⁰⁶ Pb ±2.									
Zircon_001_SP3-88	465	352	0.76	0.0534	0.0034	0.339	0.024	0.0461	0.00665	0.0146	0.0017	0.20	290.6	4	296	18	390	150
Zircon_002	832	1498	1.8	0.0522	0.0032	0.327	0.023	0.04525	0.00064	0.0143	0.0017	0.28	285.3	3.9	287	17	300	140
Zircon_003	171.2	142.9	0.83	0.0546	0.0053	0.165	0.018	0.02149	0.00041	0.00652	0.0009	0.17	137	2.6	154	15	390	180
Zircon_004	394.2	183.2	0.46	0.0531	0.0043	0.34	0.032	0.04614	0.00092	0.0141	0.0019	0.21	290.8	5.7	297	23	400	160
Zircon_005	560	305.7	0.55	0.0488	0.004	0.0836	0.0073	0.01225	0.00019	0.0037	0.00046	0.23	78.5	1.2	81.4	6.8	320	160
Zircon_006	390.6	282.7	0.72	0.0535	0.0034	0.326	0.023	0.04404	0.00062	0.0136	0.0016	0.09	277.8	3.8	287	18	340	150
Zircon_007	614	226	0.37	0.0522	0.0031	0.343	0.023	0.04725	0.00073	0.0157	0.0019	0.55	297.6	4.5	300	17	290	130
Zircon_008	136.3	108.1	0.79	0.0555	0.0056	0.348	0.039	0.04494	0.00088	0.0155	0.0019	0.12	283.4	5.4	303	28	490	200
Zircon_009	64.8	35.2	0.54	0.06	0.044	0.22	0.036	0.04774	0.00052	0.0096	0.0045	0.44	414.4	3.3	408	30	4580	340
Zircon_010	420.6	489	1.16	0.0592	0.0035	0.334	0.024	0.04122	0.00094	0.0106	0.0015	0.36	280.4	5.8	293	18	570	140
Zircon_011	779	961	1.23	0.0523	0.0042	0.345	0.028	0.04677	0.00071	0.0147	0.0016	0.07	294.6	4.4	301	20	320	150
Zircon_012	286.3	240	0.84	0.0533	0.0074	0.158	0.026	0.02108	0.00056	0.0069	0.0012	0.28	134.5	3.5	148	22	450	210
Zircon_013	97.9	50.2	0.51	0.056	0.012	0.098	0.025	0.01342	0.00039	0.00387	0.00074	0.11	86	2.5	95	22	790	340
Zircon_014	199	130.5	0.66	0.0535	0.0035	0.352	0.026	0.04752	0.00067	0.015	0.0018	0.19	299.3	4.1	306	19	380	150
Zircon_015	190.5	115.3	0.61	0.0522	0.0035	0.345	0.026	0.04727	0.00084	0.0148	0.0018	0.36	297.7	5.1	300	20	360	140
Zircon_016	222.8	94.3	0.42	0.0449	0.0044	0.134	0.014	0.02171	0.00040	0.006	0.00029	0.21	438.5	3.1	425	42	220	170
Zircon_017	161.4	124.14	0.77	0.0541	0.0045	0.361	0.032	0.04783	0.0007	0.0149	0.0019	0.10	301.2	4.3	312	23	370	170
Zircon_018	48.9	29.76	0.61	0.0593	0.0068	0.357	0.043	0.04221	0.0008	0.0124	0.0015	0.18	266.5	5	315	31	770	230
Zircon_019	93.3	40.4	0.43	0.069	0.052	0.14	0.27	0.0146	0.0019	0.0059	0.0087	0.07	93	12	130	110	940	260
Zircon_020	252.3	265.1	1.05	0.0497	0.0066	0.085	0.012	0.01222	0.00025	0.00375	0.0005	0.09	78.3	1.6	82	11	630	220
Zircon_021	470.1	407.4	0.86	0.07	0.044	0.107	0.024	0.04085	0.00033	0.00436	0.00098	0.18	66.6	2.4	402	24	4000	330
Zircon_022	394.7	460.5	0.48	0.0428	0.0052	0.133	0.018	0.01438	0.00023	0.00491	0.00044	0.15	78.7	1.3	69	7.9	340	240
Zircon_023	150.1	97	0.65	0.0665	0.0081	0.406	0.034	0.0465	0.00071	0.0159	0.002	0.09	92	2.1	126	16	880	200
Zircon_024	212.8	160.2	0.75	0.0637	0.0046	0.406	0.034	0.0465	0.00071	0.0159	0.002	0.09	293	4.4	350	24	730	150
Zircon_025	1761	2688	1.53	0.0701	0.005	0.345	0.027	0.036	0.0012	0.0111	0.0013	0.38	227.8	7.3	301	19	910	130
Zircon_026	717	543	0.76	0.0509	0.0059	0.0749	0.0098	0.01051	0.0002	0.0034	0.00049	0.15	67.4	1.3	73.2	9	410	200
Zircon_027	294.4	212.5	0.72	0.0508	0.0032	0.324	0.023	0.04618	0.00068	0.0142	0.0017	0.21	291	4.2	285	17	220	140
Zircon_028	546	274	0.5	0.0451	0.0037	0.0809	0.0071	0.01291	0.00022	0.00366	0.00042	0.19	82.7	1.4	78.9	6.7	260	150
Zircon_029	80	56.9	0.71	0.0577	0.0073	0.357	0.049	0.0459	0.0011	0.0148	0.002	0.10	289.2	6.5	313	36	750	240
Zircon_030	631	337	0.53	0.05	0.0043	0.0978	0.0093	0.01416	0.00025	0.00469	0.00055	0.08	90.6	1.6	94.7	8.9	290	160
Zircon_031	153.9	113	0.73	0.0504	0.0077	0.103	0.018	0.01474	0.00032	0.00423	0.0007	0.09	94.3	2	99	15	610	270
Zircon_032	244	189	0.77	0.0513	0.0071	0.138	0.02	0.01956	0.00047	0.00573	0.00084	0.05	124.9	3	130	18	470	250
Zircon_033	295.5	107.9	0.37	0.0479	0.0036	0.143	0.012	0.02155	0.00057	0.00659	0.0008	0.27	137.4	3.6	135	11	330	160
Zircon_034	207.5	103.9	0.5	0.046	0.011	0.07	0.017	0.01093	0.00022	0.00323	0.00055	0.02	70.1	1.4	68	16	760	340
Zircon_035	143.5	104	0.72	0.078	0.014	0.53	0.11	0.0487	0.0011	0.019	0.0034	0.31	306.4	6.7	427	61	1170	240
Zircon_036	306	257	0.84	0.0662	0.0049	0.426	0.036	0.04662	0.00066	0.0154	0.002	0.06	293.7	4.1	360	25	870	140
Zircon_037	237	242	1.02	0.0537	0.0093	0.115	0.046	0.04062	0.0003	0.00384	0.00056	0.20	68.4	1.9	414	44	4490	200
Zircon_038	107.7	109.6	1.02	0.0537	0.0044	0.342	0.03	0.04615	0.00078	0.0141	0.0016	0.26	290.8	4.8	298	23	350	170
Zircon_039	471	337	0.72	0.0495	0.0034	0.213	0.016	0.03117	0.00047	0.0096	0.0011	0.20	197.8	2.9	196	13	210	140
Zircon_040	928	1430	1.54	0.0527	0.0031	0.329	0.022	0.04517	0.00062	0.0135	0.0015	0.23	284.8	3.8	288	17	350	130
Zircon_041	286	313	1.09	0.0521	0.0037	0.311	0.025	0.04329	0.00073	0.0131	0.0015	0.38	273.2	4.5	275	19	300	150
Zircon_042	71.5	45.4	0.63	0.076	0.012	0.405	0.074	0.03893	0.00097	0.0157	0.0032	0.28	246.2	6	342	45	1080	210
Zircon_043	361.3	265.3	0.73	0.0478	0.0037	0.125	0.01	0.01918	0.00031	0.00569	0.00066	0.02	122.5	1.9	119.8	9.4	250	150
Zircon_044	308.7	218.5	0.71	0.057	0.0036	0.358	0.026	0.04555	0.00067	0.0147	0.0018	0.45	287.1	4.1	310	18	500	130
Zircon_045	496.9	419.3	0.84	0.0517	0.0031	0.328	0.022	0.04598	0.00065	0.0143	0.0016	0.19	289.8	4	288	17	300	150
Zircon_046	354.3	318.1	0.9	0.0648	0.004	0.416	0.028	0.04858	0.00064	0.0156	0.0018	0.12	293.5	3.9	353	20	760	140
Zircon_047	539	41.48	0.08	0.0566	0.0033	0.585	0.039	0.07478	0.00098	0.026	0.0031	0.05	464.9	5.9	467	25	490	120
Zircon_048	34.2	13.54	0.4	0.0825	0.0083	1.92	0.21	0.1732	0.0031	0.0573	0.0093	0.10	1030	17	1095	63	1280	160
Zircon_049	74.5	49.9	0.67	0.059	0.019	0.133	0.037	0.01491	0.00047	0.00567	0.00084	0.00	95.4	3	123	32	1080	430
Zircon_050	294	202.4	0.69	0.053	0.0034	0.348	0.024	0.04711	0.00071	0.0142	0.0017	0.22	296.8	4.4	303	18	370	140

		CORRECTED RATIOS ²					CORRECTED AGES (Ma)									
U (ppm) ¹	Th (ppm) ¹	²⁰⁷ Pb/ ²¹⁰ Pb ±2. abs	²⁰⁷ Pb/ ²³⁵ U ±2. abs	²⁰⁶ Pb/ ²³⁸ U ±2. abs	²⁰⁸ Pb/ ²³² Th ±2. abs	Rho	²⁰⁶ Pb/ ²³⁸ U ±2. abs	²⁰⁷ Pb/ ²³⁵ U ±2. abs	²⁰⁷ Pb/ ²¹⁰ Pb ±2. abs							
Zircon_051	336.5	0.0544	0.0035	0.331	0.024	0.04401	0.00063	0.0136	0.0016	0.22	277.7	3.9	290	18	380	130
Zircon_052	412	0.0528	0.0035	0.325	0.023	0.0449	0.00066	0.0142	0.0016	0.21	283.1	4.1	285	18	350	140
Zircon_053	287.2	0.0541	0.0034	0.344	0.024	0.04647	0.00066	0.0142	0.0016	0.20	292.8	4.1	300	18	370	150
Zircon_054	190	0.0556	0.0039	0.341	0.027	0.04575	0.00067	0.014	0.0016	0.18	288.4	4.1	303	20	450	150
Zircon_055	67.5	0.0613	0.0055	0.356	0.033	0.04149	0.00085	0.0131	0.0016	0.12	262.5	5.2	307	25	740	200
Zircon_056	222.9	0.0541	0.004	0.342	0.028	0.04656	0.00079	0.0148	0.0019	0.69	293.4	4.9	299	21	370	150
Zircon_057	406.9	0.0563	0.0037	0.351	0.025	0.04536	0.00061	0.0144	0.0016	0.19	286.3	3.8	305	19	480	140
Zircon_058	340	0.0538	0.0037	0.335	0.025	0.04526	0.00065	0.0145	0.0017	0.19	285.4	4	293	19	420	140
Zircon_059	313	0.0523	0.0034	0.335	0.024	0.04668	0.00065	0.0137	0.0016	0.09	294.1	4	295	19	330	150
Zircon_060	311	0.0522	0.0034	0.327	0.024	0.04591	0.00092	0.0137	0.0016	0.31	289.4	5.7	289	18	310	150
Zircon_061	233.4	0.0529	0.0039	0.336	0.027	0.04644	0.00068	0.0144	0.0017	0.22	292.6	4.2	294	20	310	160
Zircon_062	574	0.0735	0.0041	1.85	0.12	0.182	0.0023	0.051	0.0063	0.56	1078.13	1062	41	1020	120	
Zircon_063	302	0.0547	0.0036	0.344	0.024	0.04632	0.00067	0.0146	0.0017	0.01	291.9	4.1	299	18	370	140
Zircon_064	342.9	0.0518	0.0034	0.329	0.024	0.04567	0.00063	0.0141	0.0017	0.19	287.9	3.9	289	18	300	130
Zircon_065	453	0.0514	0.003	0.324	0.021	0.04599	0.00061	0.0142	0.0016	0.01	289.9	3.8	285	16	240	140
Zircon_066	433.6	0.0489	0.0041	0.144	0.014	0.02114	0.00061	0.00708	0.00085	0.54	134.9	3.9	136	12	310	170
Zircon_067	88.6	0.0566	0.025	0.457	0.098	0.02342	0.00082	0.0405	0.003	0.65	449.2	5.2	438	74	4530	460
Zircon_068	108.3	0.0526	0.0064	0.234	0.029	0.03248	0.00066	0.0108	0.0016	0.06	206.1	4.1	211	24	570	230
Zircon_069	189.8	0.0491	0.0087	0.092	0.015	0.01308	0.00034	0.00431	0.00061	0.08	83.8	2.2	89	14	610	300
Zircon_070	279	0.0505	0.0033	0.272	0.02	0.0394	0.00056	0.0119	0.0014	0.27	249.1	3.5	244	16	300	140
Zircon_071	266	0.0555	0.004	0.347	0.029	0.04602	0.00068	0.0146	0.0017	0.07	290.4	2	302	20	430	150
Zircon_072	214.1	0.0598	0.0037	0.6	0.04	0.0722	0.001	0.026	0.0031	0.12	449.5	6.2	477	26	620	140
Zircon_073	78.1	0.115	0.012	0.379	0.043	0.02393	0.00067	0.0174	0.0024	0.07	153.5	4.2	340	30	2000	170
Zircon_074	321	0.0533	0.0035	0.341	0.024	0.04652	0.00067	0.0148	0.0018	0.20	293.1	4.2	299	18	360	140
Zircon_075	55.8	0.0751	0.0048	1.82	0.13	0.1768	0.0026	0.0527	0.0062	0.13	1050.14	1050	48	1070	130	
Zircon_076	270.2	0.0526	0.0034	0.348	0.024	0.04771	0.00072	0.0145	0.0017	0.22	300.4	4.4	303	18	360	140
Zircon_077	336.9	0.0522	0.0049	0.336	0.033	0.04641	0.0007	0.0144	0.0019	0.15	292.5	4.3	294	24	280	170
Zircon_078	111	0.0636	0.0075	0.421	0.053	0.04792	0.0009	0.0171	0.0027	0.15	301.7	5.6	356	38	720	210
Zircon_079	110.3	0.059	0.0098	0.114	0.018	0.01402	0.0004	0.00474	0.00077	0.17	89.7	2.5	110	16	920	270
Zircon_080	271.4	0.0492	0.005	0.097	0.01	0.01417	0.00024	0.00466	0.00054	0.77	90.7	1.6	93.4	9.7	260	210
Zircon_081	154.1	0.0545	0.0045	0.353	0.033	0.04673	0.00091	0.0149	0.0018	0.04	294.4	5.6	307	24	430	170
Zircon_082	39.52	0.091	0.016	0.216	0.038	0.04744	0.00062	0.005	0.0013	0.20	411.2	3.9	495	31	1430	340
Zircon_083	366.7	0.0496	0.0046	0.0822	0.0079	0.01207	0.00022	0.00385	0.00044	0.19	77.3	1.4	80.1	7.4	300	170
Zircon_084	73.8	0.054	0.0061	0.349	0.039	0.04395	0.00084	0.0132	0.0016	0.17	277.3	5.2	301	29	580	220
Zircon_085	39.5	0.062	0.015	0.196	0.044	0.02211	0.00068	0.0052	0.0012	0.14	141.4	4.3	177	35	1070	380
Zircon_086	94.2	0.0564	0.0092	0.127	0.019	0.01513	0.0004	0.00465	0.00086	0.18	96.8	2.5	120	17	710	290
Zircon_087	436	0.0584	0.0036	0.648	0.048	0.0818	0.0014	0.0233	0.0029	0.00	507.8	1	507	28	540	130
Zircon_088	209	0.0542	0.0039	0.349	0.027	0.04722	0.00093	0.0148	0.0017	0.20	297.4	5.7	306	20	380	150
Zircon_089	102.9	0.056	0.01	0.094	0.017	0.01241	0.00028	0.00324	0.00052	0.12	79.5	1.8	91	16	870	320
Zircon_090	305	0.069	0.0055	0.421	0.038	0.04427	0.0007	0.0173	0.0022	0.12	279.3	4.3	356	26	920	140
Zircon_091	95.6	0.052	0.0051	0.325	0.033	0.04525	0.00086	0.0141	0.0018	0.13	285.3	5.3	284	25	450	200
Zircon_092	208.6	0.0826	0.0084	0.174	0.02	0.04544	0.00063	0.0079	0.0044	0.44	98.7	2.1	462	47	1130	470
Zircon_093	259.2	0.0655	0.0075	0.131	0.016	0.01456	0.00025	0.00668	0.00081	0.03	93.2	1.6	124	14	880	200
Zircon_094	108.4	0.0665	0.0051	0.416	0.035	0.04538	0.00079	0.0156	0.0018	0.10	286.1	4.9	352	25	860	140
Zircon_095	496.1	0.0498	0.0033	0.313	0.023	0.04583	0.00084	0.0135	0.0016	0.38	288.9	5	275	47	290	450
Zircon_096	133	0.0525	0.0077	0.104	0.015	0.01448	0.00033	0.00463	0.00065	0.16	92.7	2.1	100	14	490	270
Zircon_097	97.4	0.0553	0.0064	0.172	0.021	0.02261	0.00043	0.00717	0.00085	0.16	144.1	2.7	160	18	720	230
Zircon_098	181.5	0.0518	0.006	0.1	0.012	0.01414	0.00027	0.00417	0.00055	0.28	90.5	1.7	96	11	520	240
Zircon_099	92.5	0.0571	0.0052	0.344	0.034	0.04395	0.00081	0.0132	0.0017	0.19	277.2	5	304	26	550	190
Zircon_100	409	0.0521	0.0031	0.317	0.021	0.04405	0.00062	0.0137	0.0016	0.21	277.9	3.8	279	16	330	140

C.2. Sample SP3-89

	U (ppm)		Th (ppm)		Th/U		CORRECTED RATIOS ³						CORRECTED AGES (Ma)						
	U	Th	U	Th	$^{207}\text{Pb}/^{235}\text{U}$	$^{207}\text{Pb}/^{238}\text{U}$	$^{206}\text{Pb}/^{235}\text{U}$	$^{206}\text{Pb}/^{238}\text{U}$	$^{208}\text{Pb}/^{232}\text{Th}$	Rho	$^{206}\text{Pb}/^{238}\text{U}$	$^{207}\text{Pb}/^{235}\text{U}$	$^{206}\text{Pb}/^{238}\text{U}$	$^{207}\text{Pb}/^{235}\text{U}$	$^{206}\text{Pb}/^{238}\text{U}$	$^{207}\text{Pb}/^{235}\text{U}$			
Zircon_001_SP3-89	205.1	239	1.17		0.0554	0.003	0.349	0.019	0.04608	0.00055	0.0123	0.0017	0.51068	290.4	3.4	303	14	446	87
Zircon_002	237	176.1	0.74		0.058	0.0061	0.183	0.018	0.02303	0.00053	0.007	0.0012	0.23397	146.8	3.4	171	16	560	170
Zircon_003	136.5	166	1.22		0.0565	0.0062	0.396	0.043	0.05134	0.00077	0.0142	0.0019	0.138122	322.7	4.7	344	32	482	82
Zircon_004	235.5	213.8	0.91		0.0587	0.0038	0.38	0.026	0.04746	0.00072	0.0132	0.0019	0.45932	298.9	4.4	326	19	566	97
Zircon_005	273.6	173.7	0.63		0.0564	0.0028	0.375	0.021	0.04796	0.00051	0.0137	0.0019	0.41168	302	3.1	326	14	517	97
Zircon_006	69.9	38.21	0.55		0.058	0.011	0.259	0.048	0.03231	0.00082	0.0093	0.0023	0.033222	205	5.1	230	38	830	180
Zircon_007	352	236.3	0.67		0.0552	0.0029	0.359	0.019	0.04735	0.00054	0.0127	0.0018	0.38958	298.3	3.3	311	14	419	75
Zircon_008	420.7	443	0.94		0.0849	0.0056	0.388	0.026	0.0333	0.00062	0.0102	0.0016	0.26925	241.2	3.9	333	49	4300	410
Zircon_009	203.6	187.1	0.92		0.0646	0.0037	0.44	0.026	0.04932	0.00076	0.014	0.0019	0.25344	310.3	4.7	369	18	750	87
Zircon_010	173.6	128.6	0.74		0.0542	0.003	0.355	0.02	0.04704	0.00071	0.0125	0.0017	0.10349	296.3	4.4	308	15	446	85
Zircon_011	323.5	302	0.93		0.0515	0.0027	0.338	0.016	0.047	0.00059	0.013	0.0018	0.265186	296.1	3.6	295	13	256	61
Zircon_012	288	156.9	0.54		0.0679	0.0054	0.124	0.01	0.01312	0.00024	0.0039	0.0011	0.018843	84	1.5	118.8	9	890	110
Zircon_013	225.9	163.9	0.73		0.0546	0.0029	0.362	0.02	0.04776	0.00068	0.0131	0.0018	0.38359	300.8	4.2	313	15	385	66
Zircon_014	670.1	479	0.71		0.0506	0.0037	0.0924	0.0071	0.01332	0.00022	0.00371	0.00046	0.43049	85.3	1.4	89.6	6.6	300	130
Zircon_015	420.3	76.5	0.64		0.118	0.014	0.488	0.063	0.02824	0.00078	0.0028	0.0004	0.44864	482.7	4.9	404	43	2000	460
Zircon_016	345.6	391.8	1.13		0.0558	0.0049	0.315	0.029	0.04093	0.00084	0.0121	0.0017	0.17534	258.6	5.2	277	22	450	130
Zircon_017	163.6	65.84	0.4		0.072	0.0031	1.555	0.065	0.1574	0.0023	0.0462	0.0067	0.2399	94.3	1.3	956	29	967	63
Zircon_018	320.1	438.3	1.37		0.0583	0.0034	0.384	0.021	0.04752	0.00088	0.0142	0.0024	0.57502	299.3	5.4	330	15	552	46
Zircon_019	249	160.85	0.65		0.0545	0.0069	0.111	0.013	0.01488	0.0003	0.00472	0.00065	0.174492	93.9	1.9	107	12	400	98
Zircon_020	237.1	228.6	0.96		0.0562	0.0054	0.287	0.031	0.03657	0.00061	0.0109	0.0013	0.51864	231.5	3.8	256	24	480	120
Zircon_021	186.5	101.2	0.54		0.0536	0.0072	0.149	0.02	0.0202	0.00049	0.00648	0.00089	0.089635	128.9	3.1	141	18	400	120
Zircon_022	261.2	206.2	0.79		0.0514	0.0038	0.221	0.016	0.03113	0.00059	0.0091	0.0014	0.1333	197.6	3.7	202	14	313	54
Zircon_023	152.2	181	1.19		0.0541	0.0043	0.362	0.03	0.048	0.0011	0.0142	0.002	0.22697	302.4	6.5	318	23	400	100
Zircon_024	104.6	55.5	0.53		0.0753	0.0032	1.929	0.084	0.186	0.0024	0.0566	0.0078	0.46857	1100	13	1093	30	1076	37
Zircon_025	198.8	150.6	0.76		0.0532	0.0036	0.349	0.025	0.0473	0.00072	0.0148	0.002	0.37231	297.9	4.4	303	18	410	100
Zircon_026	271	325	1.2		0.0477	0.0048	0.0764	0.0081	0.01121	0.00022	0.00347	0.00042	0.44197	71.9	1.4	74.5	7.7	400	140
Zircon_027	290	238	0.82		0.0509	0.0025	0.338	0.016	0.04694	0.00063	0.0143	0.0016	0.1212	295.7	3.9	296	12	275	49
Zircon_028	88.64	35.98	0.41		0.0586	0.0039	0.812	0.049	0.0993	0.0012	0.0295	0.0043	0.040233	610.1	7.2	602	28	567	96
Zircon_029	169.4	107.4	0.63		0.0539	0.0047	0.363	0.033	0.04788	0.00081	0.016	0.0023	0.079712	300.2	5	313	24	420	120
Zircon_030	241.1	202.3	0.84		0.0518	0.0025	0.337	0.016	0.04726	0.00056	0.0145	0.002	0.026923	297.6	3.5	294	12	277	63
Zircon_031	209.4	173	0.83		0.0626	0.0034	0.388	0.024	0.04532	0.00067	0.0151	0.0018	0.63676	285.7	4.1	332	18	680	110
Zircon_032	431.4	411	0.95		0.0578	0.0026	0.375	0.016	0.04639	0.00068	0.0148	0.0021	0.22793	292.3	4.2	323	12	511	51
Zircon_033	198.8	136.5	0.69		0.0747	0.0031	1.918	0.078	0.1857	0.0025	0.0554	0.0076	0.337041	1098	13	1087	27	1047	53
Zircon_034	423.7	213.4	0.5		0.0692	0.0028	1.251	0.055	0.1302	0.0021	0.0428	0.0061	0.71124	789	12	824	25	905	51
Zircon_035	481.6	411.2	0.61		0.0794	0.0041	0.505	0.026	0.04587	0.00074	0.0194	0.0025	0.18951	289.1	4.6	412	42	4206	68
Zircon_036	744	791	1.06		0.0484	0.0029	0.0787	0.0042	0.01191	0.00019	0.00364	0.0005	0.298928	76.4	1.2	76.9	3.9	193	71
Zircon_037	117.8	77.5	0.66		0.0517	0.0047	0.24	0.021	0.03371	0.00065	0.0104	0.0017	0.220387	213.7	4.1	218	17	264	76
Zircon_038	111.1	59.29	0.53		0.0555	0.0086	0.176	0.026	0.02288	0.00062	0.0077	0.0019	0.183432	145.8	3.9	164	23	490	150
Zircon_039	132.5	95.4	0.72		0.0494	0.0059	0.0815	0.009	0.01211	0.00028	0.00368	0.00053	0.209377	77.6	1.8	79.2	8.4	416	98
Zircon_040	361.9	232.3	0.64		0.0544	0.0052	0.0957	0.0089	0.01256	0.00029	0.00408	0.0062	0.15628	80.5	1.9	92.8	8.3	380	130
Zircon_041	462	440	0.95		0.0527	0.0023	0.342	0.015	0.04696	0.00055	0.0144	0.0017	0.23872	295.2	3.4	299	11	336	55
Zircon_042	352.9	143.3	0.41		0.0568	0.0032	0.0966	0.0058	0.01223	0.00025	0.00435	0.0005	0.34984	78.3	1.6	93.6	5.4	497	88
Zircon_043	192	141.7	0.74		0.0565	0.0058	0.372	0.039	0.04738	0.00079	0.0148	0.0021	0.23402	298.4	4.8	320	29	470	90
Zircon_044	113	63.5	0.56		0.0546	0.004	0.372	0.028	0.0491	0.0011	0.0137	0.0017	0.28317	308.9	6.5	320	21	425	75
Zircon_045	414	297.3	0.72		0.053	0.0026	0.353	0.018	0.04782	0.00051	0.0145	0.002	0.209152	301.1	3.1	307	13	343	60
Zircon_046	456	431	0.95		0.058	0.0031	0.39	0.022	0.04891	0.0007	0.0161	0.0022	0.37225	307.8	4.3	339	18	550	100
Zircon_047	559	235.2	0.42		0.0452	0.0035	0.0867	0.0063	0.01398	0.00022	0.00391	0.00055	0.19937	87	1.4	84.3	5.9	148	59
Zircon_048	227	310	1.37		0.0545	0.0035	0.359	0.022	0.04749	0.00081	0.0142	0.0021	0.11108	299.1	5	311	16	448	79
Zircon_049	1656	424	0.26		0.0569	0.0022	0.524	0.021	0.06626	0.0008	0.0215	0.003	0.61712	413.6	4.8	428	14	482	34
Zircon_050	232.1	162.4	0.7		0.0525	0.0033	0.352	0.025	0.04763	0.00078	0.0144	0.0021	0.067373	299.9	4.8	306	18	366	79

	U (ppm) ¹	Th (ppm) ¹	Th/U	CORRECTED RATIOS ²				CORRECTED AGES (Ma)										
				²⁰⁷ Pb/ ²¹⁰ Pb ±2.1 abs	²⁰⁷ Pb/ ²³⁵ U ±2.1 abs	²⁰⁶ Pb/ ²³⁸ U ±2.1 abs	²⁰⁸ Pb/ ²³² Th ±2.1 abs	Rho	²⁰⁶ Pb/ ²³⁸ U ±2.1	²⁰⁷ Pb/ ²³⁵ U ±2.1	²⁰⁷ Pb/ ²¹⁰ Pb ±2.1							
Zircon_051	143	70.75	0.49	0.0533	0.0034	0.356	0.022	0.0482	0.0007	0.0144	0.002	0.15764	303.5	4.3	309	17	356	86
Zircon_052	454	329	0.72	0.0524	0.0023	0.347	0.015	0.04772	0.00051	0.0145	0.002	0.15289	300.5	3.2	303	11	303	54
Zircon_053	216.2	128.3	0.59	0.0551	0.0064	0.195	0.023	0.05043	0.00043	0.0173	0.0011	0.19854	163.6	2.7	181	19	380	120
Zircon_054	432.1	331.2	0.77	0.0698	0.0026	0.476	0.021	0.0488	0.0011	0.0173	0.0024	0.74278	307.3	7	395	15	961	85
Zircon_055	227.5	126	0.55	0.0687	0.0028	0.843	0.036	0.0893	0.0014	0.0264	0.0039	0.11353	551.3	8.3	621	20	865	62
Zircon_056	367.6	199.2	0.54	0.0563	0.0026	0.36	0.017	0.04599	0.0007	0.0143	0.002	0.041164	289.9	4.3	312	12	474	36
Zircon_057	819.2	1024	1.25	0.0507	0.0031	0.0805	0.0047	0.01141	0.00022	0.00357	0.00054	0.101822	73.2	1.4	78.6	4.4	264	87
Zircon_058	263.6	196.8	0.75	0.0542	0.0034	0.357	0.021	0.04767	0.00066	0.0149	0.0021	0.235368	300.2	4.1	309	16	371	96
Zircon_059	180.2	255.3	1.42	0.1112	0.0044	5.26	0.21	0.3383	0.0047	0.097	0.013	0.63455	1879	23	1862	34	1826	30
Zircon_060	473	312.8	0.66	0.0622	0.0028	0.399	0.018	0.04667	0.00071	0.0143	0.0023	0.36308	294.1	4.4	343	14	696	38
Zircon_061	1199	1888	1.57	0.0479	0.002	0.1532	0.0063	0.02298	0.00026	0.00679	0.00079	0.015539	146.4	1.7	144.7	5.6	121	42
Zircon_062	926	817	0.88	0.0582	0.0022	0.707	0.027	0.08752	0.00095	0.0275	0.0031	0.3722	140.8	5.6	54.3	16	544	57
Zircon_063	211.8	159.2	0.75	0.0589	0.0012	0.179	0.024	0.04596	0.00044	0.00659	0.00099	0.26646	96.3	2.6	162	48	1360	140
Zircon_064	313	253	0.81	0.0576	0.0028	0.369	0.019	0.04746	0.0007	0.0151	0.002	0.286446	298.9	4.3	319	14	500	43
Zircon_065	4180	728	0.17	0.0472	0.0028	0.0699	0.0041	0.01076	0.00019	0.00387	0.00049	0.301047	69	1.2	68.6	3.9	155	92
Zircon_066	291	220.4	0.76	0.053	0.0029	0.332	0.017	0.04582	0.00056	0.0135	0.0019	0.005863	288.8	3.4	293	13	347	63
Zircon_067	158.2	123.4	0.78	0.0546	0.0059	0.354	0.034	0.04629	0.00063	0.0169	0.0024	0.141703	291.7	3.9	307	23	400	140
Zircon_068	262.9	191.8	0.73	0.0526	0.0026	0.325	0.017	0.04484	0.00063	0.0147	0.0017	0.4472	282.7	3.9	286	13	289	56
Zircon_069	389	362	0.93	0.0486	0.0028	0.1553	0.009	0.02302	0.00041	0.0076	0.001	0.14024	146.7	2.6	146.4	7.9	230	71
Zircon_070	315	148.8	0.47	0.052	0.011	0.092	0.017	0.01304	0.00061	0.0049	0.0012	0.253158	83.5	3.9	90	15	217	86
Zircon_071	326	172.4	0.53	0.0489	0.0029	0.1551	0.0093	0.02288	0.00031	0.0075	0.001	0.16306	145.8	2	146.2	8.2	237	85
Zircon_072	297	244	0.82	0.0567	0.0024	0.625	0.027	0.079	0.001	0.025	0.0034	0.47166	490.3	6.1	493	17	517	42
Zircon_073	265.2	300	1.13	0.0539	0.0043	0.337	0.023	0.0454	0.0011	0.0143	0.002	0.11685	286.1	6.6	295	18	416	69
Zircon_074	74.9	38	0.51	0.0512	0.0058	0.163	0.02	0.02326	0.00056	0.00601	0.00096	0.12034	148.2	3.5	156	17	540	130
Zircon_075	605	526	0.87	0.0499	0.0039	0.0875	0.0072	0.01275	0.00019	0.00417	0.00049	0.11751	81.7	1.2	85.2	6.7	223	82
Zircon_076	156.8	101.6	0.65	0.0518	0.0062	0.226	0.027	0.03169	0.00055	0.0102	0.0015	0.027452	201.1	3.4	207	23	310	130
Zircon_077	402	103.5	0.26	0.0671	0.0026	1.314	0.054	0.1408	0.0022	0.0426	0.006	0.68762	849	12	852	24	848	46
Zircon_078	732	353.9	0.48	0.0763	0.0035	0.301	0.015	0.02862	0.00094	0.0143	0.0022	0.71856	181.9	5.9	269	10	1109	50
Zircon_079	430.6	76.7	0.59	0.136	0.013	0.458	0.047	0.02467	0.00085	0.0153	0.0046	0.20259	166.5	5.3	382	32	2160	100
Zircon_080	274	256.7	0.94	0.0473	0.0029	0.0803	0.0047	0.01248	0.00021	0.00371	0.00051	0.081526	79.9	1.4	78.3	4.7	271	81
Zircon_081	228.2	162.5	0.71	0.0619	0.0039	0.395	0.027	0.04631	0.00063	0.0155	0.0026	0.21372	291.8	3.9	337	19	635	89
Zircon_082	351.9	293.2	0.83	0.0542	0.003	0.328	0.016	0.04459	0.00074	0.0134	0.0019	0.11812	281.2	4.6	288	12	400	67
Zircon_083	221.2	186.3	0.84	0.0547	0.0028	0.353	0.018	0.04716	0.00047	0.0147	0.002	0.195446	297.1	2.9	308	14	375	62
Zircon_084	68.6	62.7	0.91	0.057	0.011	0.318	0.06	0.0404	0.001	0.0125	0.0018	0.075825	255.6	6.4	278	46	540	170
Zircon_085	339	229	0.68	0.0627	0.003	0.408	0.021	0.04749	0.0007	0.0163	0.0023	0.54973	299.1	4.3	347	15	687	48
Zircon_086	132.1	66.8	0.51	0.0659	0.0049	0.301	0.024	0.03288	0.00062	0.0126	0.0015	0.13589	208.5	3.9	266	19	910	150
Zircon_087	178.8	96.6	0.54	0.0581	0.006	0.101	0.01	0.01258	0.00029	0.00435	0.00058	0.34928	80.6	1.8	97.1	9.5	599	93
Zircon_088	217	145.9	0.67	0.0558	0.0031	0.368	0.022	0.04909	0.0008	0.0154	0.0021	0.046053	308.9	4.9	318	16	395	73
Zircon_089	351.4	244.5	0.7	0.053	0.003	0.335	0.019	0.04606	0.00068	0.0143	0.002	0.20908	290.3	4.2	293	15	343	65
Zircon_090	356	214.2	0.6	0.0577	0.0046	0.33	0.028	0.04123	0.00042	0.015	0.0021	0.44432	280.5	2.6	289	21	500	110
Zircon_091	286.3	193.9	0.68	0.0634	0.0062	0.103	0.01	0.01118	0.00022	0.00429	0.0005	0.41509	75.6	1.4	99.7	9.5	710	160
Zircon_092	341.6	325	0.95	0.0554	0.0032	0.345	0.021	0.04527	0.0006	0.0143	0.002	0.34055	285.4	3.7	301	16	462	71
Zircon_093	954	1800	1.89	0.0709	0.0031	0.345	0.018	0.03355	0.0011	0.0093	0.0013	0.76997	224.9	6.8	301	14	966	58
Zircon_094	485	224.6	0.46	0.0524	0.0027	0.317	0.015	0.03368	0.00055	0.0139	0.0017	0.266102	275.6	3.4	280	11	315	54
Zircon_095	154.8	90.3	0.58	0.0658	0.0049	0.302	0.023	0.03324	0.00067	0.013	0.0021	0.23783	210.8	4.2	268	18	860	110
Zircon_096	420.2	378.1	0.9	0.0571	0.0027	0.382	0.019	0.04921	0.00063	0.0157	0.0022	0.10302	309.7	3.9	328	14	488	64
Zircon_097	720	278	0.39	0.0507	0.0038	0.0814	0.0065	0.01166	0.00021	0.00401	0.00067	0.24068	74.7	1.4	79.4	6.1	241	75
Zircon_098	109.8	53.2	0.48	0.0597	0.004	0.485	0.034	0.0587	0.0011	0.0193	0.0026	0.17763	367.6	6.7	401	23	600	110
Zircon_099	179	121	0.68	0.0506	0.0038	0.159	0.011	0.02284	0.00046	0.0072	0.0011	0.29116	145.5	2.9	149.5	9.8	278	76
Zircon_100	449	305	0.68	0.0518	0.0024	0.225	0.011	0.03179	0.00038	0.01	0.0014	0.091775	201.7	2.4	206.2	8.8	315	72

C.3. Sample SP3-90

	U (ppm)		Th (ppm)		Th/U		$^{207}\text{Pb}/^{209}\text{Pb}$		$^{207}\text{Pb}/^{235}\text{U}$		$^{206}\text{Pb}/^{238}\text{U}$		$^{206}\text{Pb}/^{235}\text{U}$		CORRECTED RATIOS ²		$^{206}\text{Pb}/^{232}\text{Th}$		CORRECTED AGES (Ma)	
							± 2 , abs	± 2 , abs	± 2 , abs	± 2 , abs	± 2 , abs	± 2 , abs	± 2 , abs	± 2 , abs	± 2 , abs	± 2 , abs	± 2 , abs	± 2 , abs	± 2 , abs	± 2 , abs
Zircon_001_SP3-90	185.3	115.4	0.62	0.62	0.108	0.108	0.0061	0.108	0.01	0.01246	0.00026	0.00443	0.00022	0.225361	79.8	1.6	103.7	9.4	770	200
Zircon_002	167.2	122.3	0.73	0.73	0.112	0.112	0.0066	0.112	0.016	0.01268	0.00033	0.00417	0.00022	0.182177	81.2	2.1	107	14	950	230
Zircon_003	261.7	248.7	0.95	0.95	0.099	0.099	0.0084	0.099	0.011	0.01254	0.00025	0.00427	0.00019	0.179426	80.3	1.6	95.8	9.8	580	190
Zircon_004	476	394	0.83	0.83	0.09	0.09	0.0074	0.09	0.014	0.01255	0.00023	0.0041	0.00018	0.33716	80.4	1.5	88	12	360	220
Zircon_005	236	291	1.23	1.23	0.0518	0.0518	0.0019	0.0518	0.011	0.0397	0.00071	0.01245	0.00018	0.461736	251	4.4	253.4	9.1	354	79
Zircon_006	71	48	0.68	0.68	0.0591	0.0591	0.003	0.0591	0.033	0.0686	0.0017	0.01858	0.00061	0.37815	428	10	448	21	580	110
Zircon_007	77.4	42	0.54	0.54	0.0757	0.0757	0.0023	1.435	0.047	0.1386	0.0026	0.028	0.00071	0.28673	837	15	902	20	1062	63
Zircon_008	240.1	62.1	0.26	0.26	0.0542	0.0542	0.0019	0.394	0.017	0.0527	0.001	0.01454	0.00068	0.439781	331	6.2	337	12	364	78
Zircon_009	218.8	146.5	0.67	0.67	0.0488	0.0488	0.0041	0.0891	0.0071	0.01327	0.00025	0.00393	0.00012	0.236422	85	1.6	86.5	6.2	370	160
Zircon_010	449	249	0.55	0.55	0.0718	0.0718	0.0015	1.599	0.042	0.1626	0.0034	0.0438	0.0021	0.51199	971	19	969	17	980	43
Zircon_011	329.3	254.2	0.77	0.77	0.052	0.052	0.0033	0.8883	0.0053	0.01271	0.00024	0.00392	0.00012	0.314594	81.4	1.5	85.8	4.9	390	140
Zircon_012	76.4	54.81	0.72	0.72	0.106	0.106	0.012	0.108	0.02	0.01292	0.0004	0.00376	0.00031	0.15486	82.7	2.5	102	18	1030	330
Zircon_013	296.4	136.5	0.46	0.46	0.0751	0.0751	0.0016	1.869	0.046	0.1817	0.0029	0.0545	0.00061	0.22326	1076	16	1070	16	1051	44
Zircon_014	195	81.1	0.42	0.42	0.0572	0.0572	0.0017	0.699	0.024	0.0872	0.0017	0.02635	0.00042	0.599681	539.1	9.8	532	14	514	73
Zircon_015	190.7	98.2	0.51	0.51	0.0556	0.0556	0.0059	0.964	0.095	0.01268	0.0003	0.00478	0.00026	0.24008	81.2	1.9	93	8.6	480	190
Zircon_016	340.2	28.43	0.08	0.08	0.0726	0.0726	0.0014	1.739	0.04	0.1733	0.0024	0.053	0.0013	0.22867	1030	13	1023	15	987	41
Zircon_017	111.6	129.5	1.16	1.16	0.1107	0.1107	0.0023	5.13	0.13	0.3352	0.0055	0.0933	0.0011	0.015671	1863	26	1841	21	1810	36
Zircon_018	274.5	457	1.66	1.66	0.0524	0.0524	0.0026	0.302	0.015	0.04186	0.00075	0.01283	0.00022	0.360726	264.3	4.7	267	12	330	100
Zircon_019	49.8	29.9	0.60	0.60	0.059	0.059	0.0034	0.715	0.041	0.0871	0.0015	0.02705	0.00091	0.300328	538.5	9	553	22	610	110
Zircon_020	330	286.6	0.87	0.87	0.159	0.159	0.0029	10.09	0.24	0.4627	0.008	0.1232	0.0021	0.74812	2451	35	2443	23	2442	31
Zircon_021	142.6	84.8	0.59	0.59	0.0629	0.0629	0.0018	0.825	0.025	0.0952	0.0017	0.03019	0.00058	0.1575	585.9	9.9	610	14	720	62
Zircon_022	323.8	225.5	0.70	0.70	0.0621	0.0621	0.0046	0.12	0.011	0.01462	0.0005	0.00481	0.00021	0.006905	93.5	3.2	114.8	9.5	700	160
Zircon_023	250	182	0.73	0.73	0.0539	0.0539	0.002	0.364	0.014	0.04954	0.00075	0.01492	0.00042	0.393621	311.7	4.6	315	11	361	80
Zircon_024	240.1	178.8	0.74	0.74	0.0498	0.0498	0.0035	0.905	0.062	0.01306	0.0027	0.00391	0.00014	0.32263	83.6	1.7	87.8	5.8	330	150
Zircon_025	259.2	166.2	0.64	0.64	0.0543	0.0543	0.0026	0.1759	0.0083	0.02278	0.00042	0.00754	0.00017	0.24597	145.2	2.7	164.1	7.2	390	100
Zircon_026	127.3	91.1	0.72	0.72	0.0557	0.0557	0.0038	0.299	0.02	0.03997	0.00068	0.01301	0.00031	0.254341	252.7	4.2	272	15	440	140
Zircon_027	207.5	207.3	1.00	1.00	0.0496	0.0496	0.006	0.988	0.01	0.01277	0.00027	0.00394	0.00015	0.196061	81.8	1.7	85.3	9.4	430	210
Zircon_028	321.3	53.6	0.17	0.17	0.0727	0.0727	0.0017	1.649	0.042	0.1646	0.0023	0.0471	0.0031	0.012514	982	13	989	17	1000	47
Zircon_029	277	279	1.01	1.01	0.0528	0.0528	0.002	0.286	0.011	0.03922	0.00068	0.01254	0.00019	0.45079	248	4.2	255.6	8.9	336	82
Zircon_030	376	101.1	0.27	0.27	0.0559	0.0559	0.0014	0.586	0.016	0.0747	0.0011	0.02335	0.00055	0.12273	464.6	6.9	469	10	448	58
Zircon_031	350.6	62.4	0.18	0.18	0.0747	0.0747	0.0015	1.949	0.049	0.1864	0.0036	0.0541	0.0012	0.7339	1102	20	1098	17	1053	42
Zircon_032	342	184	0.54	0.54	0.1058	0.1058	0.002	4.64	0.1	0.3141	0.0048	0.08994	0.00091	0.4318	1761	24	1756	18	1726	33
Zircon_033	216.2	170	0.79	0.79	0.0544	0.0544	0.0024	0.344	0.015	0.04646	0.00076	0.01482	0.00031	0.375147	292.7	4.7	300	11	390	100
Zircon_034	161	253.2	1.57	1.57	0.0822	0.0822	0.0017	2.471	0.073	0.2145	0.0044	0.063	0.0013	0.21579	1253	24	1263	21	1260	40
Zircon_035	184.6	99.6	0.54	0.54	0.1201	0.1201	0.0024	5.77	0.14	0.3425	0.0057	0.0893	0.0014	0.43277	1899	28	1941	21	1952	36
Zircon_036	149.4	130.6	0.87	0.87	0.0706	0.0706	0.0033	0.714	0.03	0.0733	0.0013	0.01787	0.00044	0.44176	455.8	7.9	545	18	923	94
Zircon_037	943	674	0.71	0.71	0.0522	0.0522	0.0022	0.282	0.015	0.0391	0.00072	0.01178	0.00027	0.54379	247.2	4.5	252	11	318	84
Zircon_038	470	263.3	0.56	0.56	0.0546	0.0546	0.0028	0.36	0.016	0.0471	0.0021	0.01372	0.00042	0.44557	297	13	312	12	403	93
Zircon_039	360	95.8	0.27	0.27	0.0551	0.0551	0.0017	0.346	0.011	0.04558	0.00084	0.01634	0.00057	0.22969	287.3	5.2	301.3	8.7	450	64
Zircon_040	488	283	0.58	0.58	0.0555	0.0555	0.0015	0.512	0.015	0.0667	0.001	0.0218	0.00058	0.28775	416.2	6.3	421	10	453	59
Zircon_041	162.2	173.7	1.07	1.07	0.0532	0.0532	0.0022	0.343	0.014	0.04643	0.00095	0.01424	0.00023	0.501292	292.6	5.9	299	11	344	88
Zircon_042	456	376	0.82	0.82	0.0492	0.0492	0.0022	0.0817	0.004	0.0122	0.00022	0.003797	0.00081	0.26082	78.2	1.4	81.4	3.8	252	93
Zircon_043	915	18.32	0.02	0.02	0.0598	0.0598	0.0012	0.851	0.022	0.1021	0.002	0.043	0.001	0.304339	627	12	625	12	587	43
Zircon_044	150.6	194	1.29	1.29	0.1045	0.1045	0.002	4.405	0.099	0.3034	0.005	0.08371	0.00095	0.52277	1708	25	1713	17	1713	35
Zircon_045	215	346	1.61	1.61	0.0573	0.0573	0.0018	0.589	0.019	0.0749	0.0012	0.02288	0.0003	0.496662	465.7	7.4	470	12	487	69
Zircon_046	752.3	197	0.26	0.26	0.0607	0.0607	0.0015	0.754	0.026	0.092	0.0034	0.0235	0.001	0.3634	588	20	571	16	620	53
Zircon_047	85	40.8	0.48	0.48	0.0502	0.0502	0.0085	0.163	0.027	0.02313	0.0005	0.00904	0.00066	0.58396	147.4	3.1	152	22	610	270
Zircon_048	68.08	41.2	0.61	0.61	0.0865	0.0865	0.003	1.99	0.066	0.1668	0.0027	0.0428	0.00031	0.12359	994	15	1116	24	1361	67
Zircon_049	375.3	284.5	0.76	0.76	0.0548	0.0548	0.0008	0.094	0.015	0.01246	0.00029	0.004	0.00037	0.145853	79.8	1.8	91	13	420	220
Zircon_050	168.6	152.7	0.91	0.91	0.0531	0.0531	0.0032	0.286	0.016	0.03903	0.00082	0.01242	0.00038	0.375544	246.8	5.1	259	13	440	130

	U (ppm) ¹		Th/U	²⁰⁷ Pb/ ²⁰⁶ Pb		²⁰⁷ Pb/ ²³⁵ U		CORRECTED RATIOS ²		Rho	²⁰⁶ Pb/ ²³⁸ U	CORRECTED AGES (Ma)					
	Th (ppm) ¹	U (ppm) ¹		± 2 , abs	± 2 , abs	± 2 , abs	± 2 , abs	± 2 , abs	± 2 , abs			²⁰⁷ Pb/ ²³⁵ U	± 2	²⁰⁷ Pb/ ²⁰⁶ Pb	± 2		
Zircon_051	306	71.3	0.23	0.09	0.0024	2.98	0.17	0.239	0.011	0.0722	0.0032	59	1402	53	1434	55	
Zircon_052	244.9	157.8	0.64	0.0604	0.002	6.48	0.023	0.0777	0.0014	0.02275	0.00066	8.4	506	15	636	70	
Zircon_053	243.8	50.6	0.21	0.0635	0.0016	1.006	0.03	0.115	0.0019	0.0253	0.0014	701	11	707	15	740	50
Zircon_054	272.7	210.2	0.77	0.0584	0.0043	0.0961	0.008	0.01264	0.00031	0.0041	0.00016	81	2	93.1	7.3	540	160
Zircon_055	296	96.4	0.33	0.0647	0.0016	1.064	0.031	0.1192	0.0022	0.02877	0.00067	726	13	735	15	769	48
Zircon_056	322	119.6	0.37	0.0597	0.0018	0.63	0.023	0.0772	0.0016	0.01752	0.00043	479.5	9.8	496	15	527	65
Zircon_057	496	217	0.44	0.058	0.0015	0.609	0.017	0.0761	0.0012	0.02213	0.00047	472.8	7.1	483	11	585	58
Zircon_058	333	553.4	1.66	0.06	0.0014	7.05	0.02	0.0847	0.0014	0.02537	0.00025	524	8.5	541	12	605	56
Zircon_059	1081	1645	1.51	0.0488	0.0014	1.494	0.0048	0.0222	0.00045	0.00675	0.00016	141.5	2.9	141.4	4.3	145	61
Zircon_060	603	22.3	0.04	0.0563	0.0013	0.566	0.017	0.0726	0.0013	0.0245	0.00016	451.8	8	455	12	468	52
Zircon_061	405	312.1	0.77	0.0637	0.0016	7.04	0.022	0.0802	0.0017	0.01975	0.0004	497	10	541	13	735	57
Zircon_062	166.2	105.8	0.64	0.0562	0.0027	0.31	0.015	0.04045	0.00072	0.01292	0.00031	255.6	4.5	274	11	490	110
Zircon_063	40.1	33.7	0.84	0.075	0.0027	1.713	0.063	0.1662	0.0028	0.0497	0.0011	991	15	1011	23	1033	75
Zircon_064	82.9	63.2	0.76	0.061	0.003	0.871	0.072	0.1034	0.0045	0.0298	0.00057	634	26	634	36	682	87
Zircon_065	125.3	68.2	0.54	0.0544	0.0038	0.399	0.03	0.0534	0.0011	0.01708	0.00069	335.3	6.5	340	21	390	150
Zircon_066	263.5	212	0.80	0.0556	0.0022	4.98	0.033	0.0652	0.0024	0.0196	0.0012	407	14	410	21	550	79
Zircon_067	264	121.5	0.46	0.0661	0.0021	7.95	0.025	0.0879	0.0016	0.031	0.00069	543.2	9.4	593	14	809	64
Zircon_068	249.4	194.5	0.78	0.0665	0.0024	7.91	0.031	0.0866	0.0014	0.02792	0.00073	535.6	8.4	591	17	852	72
Zircon_069	763	193.7	0.25	0.0563	0.0013	6.19	0.019	0.0789	0.0017	0.01698	0.00072	489	10	489	11	552	47
Zircon_070	94.6	60.2	0.64	0.0705	0.0041	7.97	0.056	0.0831	0.0015	0.02538	0.00091	514.8	9.1	594	30	940	110
Zircon_071	294	105	0.36	0.0591	0.0021	6.66	0.024	0.0824	0.0019	0.02205	0.00085	510	12	514	14	565	73
Zircon_072	984	554.2	0.56	0.0602	0.0013	7.87	0.019	0.0957	0.0015	0.03023	0.00057	589.3	9.1	589	11	613	50
Zircon_073	90.2	69.6	0.77	0.0654	0.0052	0.206	0.017	0.02325	0.00059	0.00715	0.00035	148.2	3.7	189	14	740	160
Zircon_074	89.8	49.8	0.55	0.0788	0.0022	1.9	0.13	0.178	0.012	0.0545	0.0019	1055	69	1080	59	1170	60
Zircon_075	1288	24.6	0.02	0.0598	0.0012	8.23	0.019	0.101	0.0015	0.0379	0.0019	620.4	8.9	610	11	605	45
Zircon_076	140.1	86.4	0.62	0.1154	0.0023	5.63	0.14	0.3556	0.006	0.1019	0.0011	1961	28	1920	22	1886	36
Zircon_077	538.9	61.4	0.11	0.0544	0.0013	4.97	0.013	0.0665	0.001	0.0205	0.00063	415.2	6.1	409.5	9.1	403	55
Zircon_078	465.4	424	0.75	0.0501	0.0064	0.152	0.04	0.0268	0.00028	0.00509	0.00025	81.2	4.8	443.3	9.7	4320	450
Zircon_079	282	176	0.62	0.0576	0.0021	6.12	0.058	0.0777	0.0012	0.02416	0.00041	478	7.3	485	14	537	77
Zircon_080	84.3	98.3	1.17	0.066	0.0028	1.109	0.058	0.1235	0.0027	0.03632	0.00077	751	15	756	26	807	82
Zircon_081	641	860	1.34	0.049	0.0024	0.082	0.0036	0.0123	0.00024	0.003642	0.00007	78.8	1.5	80	3.4	340	100
Zircon_082	107.1	82.3	0.77	0.0674	0.0089	0.2	0.028	0.02319	0.00071	0.00692	0.00094	147.8	4.5	195	23	840	230
Zircon_083	1187	260	0.22	0.0571	0.0012	6.66	0.015	0.0846	0.0013	0.02457	0.00053	523.5	7.8	518	9.2	489	48
Zircon_084	319	163.3	0.51	0.0928	0.0023	3.14	0.16	0.249	0.01	0.0731	0.0039	1431	52	1440	32	1463	48
Zircon_085	755	594	0.79	0.0788	0.0023	2.097	0.054	0.1924	0.005	0.058	0.0018	1134	28	1148	18	1174	51
Zircon_086	309.4	89.9	0.29	0.0734	0.0018	1.599	0.044	0.1575	0.0028	0.0539	0.0014	943	16	969	17	1029	48
Zircon_087	87.1	23.93	0.27	0.085	0.0025	2.746	0.083	0.2323	0.0038	0.0686	0.0018	1346	20	1340	23	1337	49
Zircon_088	338	183.6	0.54	0.1637	0.0032	6.93	0.28	0.3079	0.0087	0.0982	0.0022	1730	43	2102	33	2493	33
Zircon_089	681	59.1	0.09	0.1223	0.0022	5.26	0.14	0.3088	0.0062	0.0843	0.0034	1734	30	1861	22	1992	32
Zircon_090	360	323	0.90	0.1113	0.0022	3.578	0.09	0.233	0.004	0.06756	0.00087	1350	21	1544	20	1827	37
Zircon_091	247.1	251	1.02	0.0585	0.0025	0.376	0.016	0.0463	0.00084	0.01268	0.00021	291.8	5.2	323	12	575	93
Zircon_092	160.9	75.06	0.47	0.065	0.0027	8.19	0.033	0.0919	0.0014	0.02848	0.00048	566.7	8.5	606	18	782	79
Zircon_093	166	40.9	0.25	0.0613	0.0021	7.24	0.033	0.0853	0.0027	0.02893	0.00019	528	16	552	19	737	78
Zircon_094	136	209	1.54	0.0572	0.0042	6.24	0.044	0.0798	0.0013	0.02349	0.00048	488.9	8	491	26	520	150
Zircon_095	87.8	109.8	1.25	0.0621	0.0083	0.198	0.025	0.02286	0.00049	0.00767	0.0003	145.7	3.1	181	20	820	260
Zircon_096	192	112.3	0.58	0.1119	0.0024	4.27	0.14	0.2808	0.0079	0.0737	0.0027	1595	40	1688	30	1829	39
Zircon_097	200	119.7	0.60	0.0629	0.0041	1.139	0.074	0.01324	0.00029	0.00481	0.00023	84.8	1.9	109.3	6.7	650	150
Zircon_098	154.2	92	0.60	0.0632	0.0053	0.1059	0.0087	0.01233	0.00028	0.00426	0.00028	79	1.8	102	8.3	800	180
Zircon_099	325.3	166	0.51	0.0484	0.0032	0.0821	0.0057	0.01235	0.00025	0.00406	0.00019	79.1	1.6	80	5.3	380	130
Zircon_100	225	353	1.57	0.1126	0.0022	5.09	0.12	0.3288	0.0056	0.0945	0.002	1832	27	1833	20	1844	35

C.4. Sample SP3-91

	U (ppm) ¹	Th (ppm) ¹	Th/U	CORRECTED RATIOS ²				Rho	CORRECTED AGES (Ma)									
				²⁰⁷ Pb/ ²⁰⁶ Pb ±2. abs	²⁰⁷ Pb/ ²³⁵ U ±2. abs	²⁰⁸ Pb/ ²³² Th ±2. abs	²⁰⁶ Pb/ ²³⁸ U ±2. abs		²⁰⁶ Pb/ ²³⁸ U ±2.	²⁰⁷ Pb/ ²³⁵ U ±2.	²⁰⁸ Pb/ ²³² Th ±2.	²⁰⁶ Pb/ ²⁰⁶ Pb ±2.						
Zircon_001_SP3-91	720	322.8	0.45	0.0502	0.0041	0.0887	0.0063	0.01287	0.00032	0.00417	0.00033	0.03313	82.5	2	86.2	5.9	390	120
Zircon_002	388	189	0.49	0.0515	0.0022	0.2019	0.0085	0.02821	0.00052	0.00865	0.00063	0.437842	179.4	3.2	186.6	7.2	288	65
Zircon_003	117.1	83.5	0.71	0.0518	0.0073	0.173	0.023	0.02438	0.00055	0.00725	0.00066	0.169686	155.2	3.5	161	20	480	160
Zircon_004	990	448	0.45	0.0504	0.0032	0.0874	0.0051	0.01275	0.00042	0.004	0.00037	0.48258	81.7	2.7	85	4.8	202	55
Zircon_005	361.3	186.8	0.52	0.0615	0.0059	0.1139	0.0095	0.01353	0.00032	0.0046	0.00023	0.283565	86.6	2.1	109.3	8.7	630	110
Zircon_006	126.2	75.4	0.60	0.0643	0.0099	0.127	0.018	0.01443	0.00054	0.00564	0.00053	0.264033	92.4	3.5	121	16	820	170
Zircon_007	846	517	0.61	0.0506	0.0047	0.0921	0.0091	0.01311	0.00021	0.00416	0.00032	0.61666	83.9	1.3	89.4	8.5	290	110
Zircon_008	526.9	432.8	0.82	0.0514	0.0036	0.0836	0.0056	0.01202	0.00022	0.00388	0.00029	0.11917	77	1.4	81.4	5.3	359	86
Zircon_009	410	283.1	0.69	0.0495	0.004	0.0862	0.0076	0.01253	0.0003	0.00406	0.00036	0.38822	80.3	1.9	83.8	7.1	248	95
Zircon_010	268.5	184.8	0.69	0.0654	0.0072	0.118	0.012	0.0129	0.00026	0.00443	0.00042	0.198191	82.6	1.7	113	11	890	170
Zircon_011	225.7	181.4	0.80	0.061	0.0035	0.389	0.012	0.04632	0.00086	0.0149	0.0011	0.074278	291.9	5.3	334	14	660	70
Zircon_012	282.1	226	0.80	0.0524	0.0097	0.514	0.013	0.01446	0.00033	0.00509	0.00035	0.2271	92.6	2.1	101	12	440	120
Zircon_013	62	39	0.63	0.0752	0.0097	0.514	0.013	0.01446	0.00033	0.00509	0.00035	0.2271	319	10	418	40	1170	140
Zircon_014	70.9	37.88	0.53	0.0535	0.0093	0.201	0.033	0.02758	0.0007	0.008	0.001	0.154592	175.4	4.4	183	28	850	230
Zircon_015	263.2	127.3	0.48	0.0528	0.0061	0.089	0.011	0.01276	0.00042	0.00402	0.0004	0.266315	81.7	2.6	87	10	580	170
Zircon_016	196	119	0.61	0.0491	0.0074	0.094	0.014	0.01343	0.0003	0.00459	0.00045	0.28347	86	1.9	90	13	590	160
Zircon_017	300	1980	6.60	0.0657	0.006	0.134	0.012	0.01473	0.00027	0.00395	0.0003	0.08943	94.3	1.7	128	11	820	120
Zircon_018	335.4	308.3	0.92	0.0463	0.005	0.0845	0.0086	0.01352	0.00024	0.00408	0.00032	0.156846	86.6	4.4	82.4	8	460	460
Zircon_019	336.2	158.4	0.47	0.0494	0.0043	0.0862	0.0075	0.01289	0.00027	0.00466	0.00044	0.240745	82.6	1.7	83.7	7	370	100
Zircon_020	63.86	79.24	1.24	0.1068	0.0072	2.26	0.16	0.1563	0.0027	0.0469	0.0038	0.28941	936	15	1199	50	1759	36
Zircon_021	376.4	218	0.58	0.0606	0.0069	0.105	0.012	0.01254	0.00028	0.00417	0.00038	0.095098	80.3	1.8	101	11	760	130
Zircon_022	43.08	21.02	0.49	0.044	0.018	0.174	0.069	0.02858	0.00098	0.0063	0.0023	0.32162	181.6	6.1	178	59	1230	250
Zircon_023	128	40.4	0.32	0.0551	0.0071	0.389	0.052	0.0511	0.001	0.013	0.0017	0.26147	321.2	6.3	331	37	460	120
Zircon_024	296	36.38	0.14	0.058	0.0024	0.741	0.035	0.0934	0.0027	0.0286	0.0019	0.60552	576	16	562	20	536	42
Zircon_025	492.6	238.5	0.48	0.0471	0.0033	0.0829	0.0057	0.01273	0.0002	0.00388	0.00035	0.228497	81.6	1.3	80.7	5.3	153	52
Zircon_026	82.8	41.67	0.50	0.045	0.0097	0.211	0.045	0.03253	0.00079	0.0091	0.0014	0.42289	206.3	4.9	203	37	860	260
Zircon_027	58.11	41.32	0.71	0.053	0.024	0.22	0.11	0.0302	0.0014	0.0086	0.0016	0.42289	191.5	8.5	194	86	810	260
Zircon_028	214	174	0.81	0.068	0.019	0.142	0.04	0.01503	0.00057	0.00655	0.00056	0.077859	96.2	3.6	134	35	870	360
Zircon_029	75.1	158.7	2.11	0.1113	0.0043	5.21	0.18	0.3423	0.0057	0.0932	0.006	0.095008	1898	27	1859	32	1830	17
Zircon_030	462	514	1.11	0.0574	0.0029	0.372	0.019	0.04695	0.00077	0.01498	0.00077	0.21711	295.8	4.7	321	14	532	74
Zircon_031	300.3	121.7	0.41	0.057	0.012	0.136	0.026	0.01859	0.00045	0.00649	0.00054	0.27314	118.7	2.8	129	23	600	200
Zircon_032	476	75.9	0.43	0.143	0.045	0.207	0.027	0.04345	0.00032	0.00092	0.001	0.090283	86.4	2.3	490	23	4940	440
Zircon_033	73.9	46.7	0.63	0.0914	0.0081	1.98	0.18	0.1557	0.0028	0.0544	0.0043	0.16169	933	16	1124	48	1463	72
Zircon_034	111.3	71.9	0.65	0.046	0.013	0.08	0.022	0.01272	0.00034	0.00308	0.00066	0.097198	81.5	2.2	80	20	790	220
Zircon_035	268	167	0.62	0.0491	0.0047	0.159	0.017	0.02293	0.00048	0.00692	0.00053	0.49065	146.1	3	149	15	318	74
Zircon_036	37.27	46.23	0.44	0.193	0.039	0.478	0.092	0.0474	0.0005	0.0205	0.0034	0.31649	411.4	8.7	382	65	2930	170
Zircon_037	460.3	427.7	0.90	0.0073	0.0028	0.558	0.047	0.04172	0.00079	0.0188	0.0047	0.38432	263.5	4.9	448	30	4525	89
Zircon_038	193	102.6	0.53	0.0509	0.0055	0.169	0.018	0.02393	0.00057	0.00804	0.00074	0.20213	152.4	3.6	158	16	320	120
Zircon_039	456	405	0.89	0.0517	0.0023	0.336	0.014	0.04698	0.00067	0.0145	0.0011	0.012072	295.9	4.1	294	11	308	45
Zircon_040	259.7	150.4	0.58	0.0622	0.0087	0.12	0.016	0.01403	0.00041	0.00483	0.00052	0.219173	89.8	2.6	115	14	640	110
Zircon_042	265.7	381.5	0.78	0.0625	0.0022	0.837	0.03	0.0972	0.0014	0.0301	0.0024	0.21047	598.2	8.1	617	16	707	42
Zircon_043	279	207.8	0.74	0.0504	0.0079	0.096	0.016	0.01379	0.00037	0.00405	0.00037	0.37833	88.3	2.4	93	14	530	200
Zircon_044	268.6	113.9	0.42	0.052	0.011	0.094	0.021	0.01287	0.00047	0.0049	0.00051	0.40041	82.4	3	91	20	730	340
Zircon_046	531	129	0.24	0.0518	0.0029	0.1152	0.006	0.01587	0.00036	0.00685	0.00066	0.15841	151.3	3.1	160	16	440	180
Zircon_047	204	99.6	0.49	0.0672	0.0045	0.438	0.027	0.0472	0.0011	0.0175	0.0019	0.37806	297.6	6.7	368	19	905	84
Zircon_048	44.74	23.22	0.56	0.157	0.063	0.4	0.12	0.0472	0.0012	0.0464	0.0025	0.60208	442.9	7.8	320	420	2360	300
Zircon_049	174.7	111.2	0.64	0.0634	0.0049	0.429	0.034	0.0494	0.0011	0.0174	0.0015	0.36252	311	6.5	361	25	716	59
Zircon_050	582	320	0.55	0.0581	0.0039	0.1154	0.0079	0.01463	0.00027	0.00513	0.0005	0.089463	93.6	1.7	110.8	7.6	501	70

Zircon ID	U (ppm) ¹	Th (ppm) ¹	Th/U	CORRECTED RATIOS ²					CORRECTED AGES (Ma)									
				²⁰⁷ Pb/ ²⁰⁶ Pb	²⁰⁷ Pb/ ²³⁵ U	²⁰⁷ Pb/ ²³⁸ U	²⁰⁶ Pb/ ²³² Th	Rho	²⁰⁶ Pb/ ²³⁸ U	²⁰⁷ Pb/ ²³⁵ U	²⁰⁷ Pb/ ²⁰⁶ Pb							
Zircon_051	192	154	0.80	0.0495	0.0076	0.112	0.02	0.01515	0.00042	0.00435	0.00047	0.33213	96.9	2.7	107	18	540	150
Zircon_052	430.5	93.1	0.74	0.066	0.024	0.181	0.045	0.01367	0.00048	0.0048	0.004	0.15847	86.9	3.1	167	39	4740	230
Zircon_053	46	29.49	0.64	0.104	0.033	0.183	0.055	0.01381	0.00049	0.00085	0.0009	0.204792	88.4	5.4	176	51	4730	340
Zircon_054	114	66	0.58	0.068	0.0096	0.185	0.031	0.0232	0.00065	0.00789	0.00069	0.035397	147.8	4.1	171	26	620	150
Zircon_055	302.6	130.1	0.43	0.052	0.0047	0.207	0.018	0.02894	0.00044	0.01028	0.00074	0.11405	183.9	2.8	191	15	360	140
Zircon_056	309.2	175.3	0.57	0.0585	0.0055	0.112	0.013	0.01459	0.00032	0.00444	0.00042	0.15446	93.3	2.1	111.7	9.7	530	130
Zircon_057	101.5	84.9	0.84	0.058	0.01	0.182	0.031	0.02379	0.00095	0.00735	0.00069	0.234444	151.5	6	168	27	600	190
Zircon_058	999	353.1	0.35	0.0503	0.0038	0.0956	0.0663	0.01387	0.0004	0.00449	0.00034	0.437624	88.8	2.6	92.7	5.9	251	46
Zircon_059	139.8	77.9	0.56	0.0547	0.0029	0.384	0.02	0.05111	0.0009	0.0159	0.0012	0.0529	321.3	5.5	330	15	456	83
Zircon_060	178	91	0.51	0.0525	0.004	0.294	0.021	0.04056	0.00076	0.0132	0.0011	0.262327	256.3	4.7	264	15	386	61
Zircon_061	516	173.2	0.34	0.0435	0.0034	0.0786	0.0057	0.01309	0.00021	0.00388	0.00036	0.221222	83.8	1.3	76.8	5.4	45	41
Zircon_062	48.8	21.32	0.44	0.162	0.039	0.42	0.092	0.01835	0.0008	0.0242	0.0032	0.199029	417.2	5.4	364	64	2520	490
Zircon_063	186.7	91.5	0.49	0.062	0.012	0.203	0.04	0.02383	0.00089	0.011	0.0012	0.39242	151.8	5.6	187	35	750	190
Zircon_064	284	275	0.97	0.0504	0.0067	0.162	0.02	0.02317	0.00056	0.00839	0.00066	0.19577	147.7	3.5	152	18	410	170
Zircon_065	279.6	321.7	1.15	0.061	0.015	0.114	0.028	0.01376	0.00065	0.0044	0.0014	0.19575	88.1	4.2	109	25	740	130
Zircon_066	28.07	10.28	0.37	0.076	0.031	0.31	0.13	0.0293	0.0014	0.0045	0.0022	0.32478	186.3	8.7	256	99	1550	330
Zircon_067	33.55	52.4	1.56	0.069	0.012	0.377	0.071	0.0461	0.0017	0.0138	0.0013	0.195808	290	11	318	53	820	170
Zircon_068	213.7	140.7	0.66	0.0497	0.0047	0.0929	0.0085	0.01356	0.00031	0.00362	0.00032	0.072854	86.8	2	89.9	7.9	460	120
Zircon_069	335	188	0.80	0.0547	0.0069	0.341	0.047	0.0452	0.0013	0.014	0.0033	0.73321	284.9	8.2	296	34	400	200
Zircon_070	385	357.9	0.93	0.054	0.01	0.092	0.016	0.01249	0.0006	0.00392	0.00024	0.276221	80	3.8	89	15	520	190
Zircon_071	386	169.5	0.44	0.073	0.011	0.149	0.021	0.01496	0.00054	0.00099	0.00062	0.32452	95.7	3.4	140	19	4030	260
Zircon_072	271	124.1	0.46	0.0516	0.0089	0.092	0.015	0.01322	0.00038	0.00462	0.00046	0.176299	84.6	2.4	89	14	480	170
Zircon_073	1041	752.3	0.72	0.0516	0.0037	0.0932	0.0065	0.01315	0.00018	0.00409	0.0004	0.196268	84.2	1.2	90.4	6.1	254	61
Zircon_074	67.4	21.69	0.32	0.0645	0.0051	1.211	0.092	0.137	0.0024	0.0374	0.0031	0.031741	828	13	802	42	762	53
Zircon_075	138.3	77.5	0.56	0.056	0.0055	0.384	0.034	0.0498	0.0011	0.0155	0.0011	0.249468	313.1	6.9	329	26	550	150
Zircon_076	119.1	97.6	0.82	0.0573	0.0078	0.225	0.03	0.02856	0.00081	0.00885	0.00064	0.10984	181.6	5.1	205	25	570	130
Zircon_077	707	260.4	0.37	0.0498	0.0031	0.0883	0.0052	0.0129	0.00023	0.00401	0.00021	0.302758	82.6	1.4	85.9	4.8	342	68
Zircon_078	989	338	0.34	0.0498	0.0019	0.092	0.0036	0.0135	0.00021	0.00446	0.00033	0.1765	86.5	1.4	89.4	3.4	208	52
Zircon_079	527	235.7	0.45	0.0496	0.0027	0.0925	0.0049	0.01361	0.00024	0.00432	0.00033	0.072061	87.1	1.5	89.8	4.6	239	77
Zircon_080	24.5	8.1	0.33	0.0796	0.0043	2.06	0.11	0.1902	0.0037	0.0593	0.0052	0.11208	1123	20	1136	37	1227	51
Zircon_081	266.6	125.7	0.47	0.0528	0.0055	0.0902	0.0084	0.01243	0.00032	0.00391	0.00038	0.276443	79.6	2.1	90.4	9.4	540	140
Zircon_082	72.12	30.17	0.42	0.064	0.016	0.2	0.047	0.0233	0.001	0.0093	0.0012	0.085066	148.2	6.6	182	40	770	240
Zircon_083	994	399	0.40	0.0497	0.0021	0.0882	0.0037	0.01287	0.00019	0.00428	0.00032	0.02632	82.5	1.2	85.8	3.5	247	92
Zircon_084	107	94.7	0.89	0.058	0.013	0.195	0.039	0.0236	0.0012	0.00806	0.00067	0.254237	150.6	7.4	191	28	790	350
Zircon_085	781	265.3	0.34	0.0486	0.0021	0.0861	0.0037	0.01284	0.0002	0.00404	0.0003	0.362465	82.2	1.3	83.8	3.4	259	60
Zircon_086	251	163.3	0.65	0.0523	0.0046	0.0956	0.0084	0.01319	0.00037	0.00417	0.00038	0.15155	84.5	2.3	92.5	7.8	446	91
Zircon_087	120.8	93.1	0.77	0.061	0.012	0.113	0.022	0.01298	0.00049	0.0046	0.00043	0.1939	83.1	3.1	107	19	970	230
Zircon_088	90.4	84.6	0.94	0.0548	0.0045	0.354	0.028	0.04683	0.00096	0.0146	0.0011	0.259175	295	5.9	307	21	560	150
Zircon_089	136.2	79.9	0.59	0.051	0.011	0.089	0.019	0.01335	0.00049	0.00412	0.00041	0.5374	85.5	3.1	86	18	450	180
Zircon_090	385.2	44.3	0.12	0.0512	0.0021	0.285	0.012	0.0399	0.00059	0.0125	0.0011	0.15809	252.2	3.7	254.4	9.4	226	62
Zircon_091	233	64.5	0.28	0.0751	0.0023	1.877	0.06	0.1809	0.0025	0.0491	0.0036	0.33439	1072	13	1073	22	1068	15
Zircon_092	636	270.2	0.42	0.0596	0.0021	0.812	0.029	0.099	0.0015	0.029	0.002	0.10111	608.5	8.7	603	14	573	26
Zircon_093	791	464.5	0.59	0.0529	0.0038	0.0916	0.0063	0.0126	0.00023	0.00398	0.0003	0.265407	80.7	1.5	88.9	5.9	342	88
Zircon_094	220.5	178.6	0.81	0.058	0.01	0.096	0.015	0.01283	0.00031	0.00438	0.00036	0.154638	82.2	2	98	16	620	190
Zircon_095	52.7	23.8	0.45	0.066	0.017	0.171	0.049	0.01833	0.00095	0.0071	0.001	0.54906	117.1	6	157	43	1330	180
Zircon_096	368	328	0.89	0.0518	0.0046	0.1138	0.0091	0.01615	0.00035	0.0051	0.00036	0.271017	103.3	2.2	109.3	8.3	290	100
Zircon_097	121.9	62.5	0.51	0.0651	0.0062	0.151	0.014	0.01694	0.00036	0.00635	0.00061	0.228212	108.3	2.3	142	13	900	120
Zircon_098	171	34.13	0.20	0.0579	0.0021	0.629	0.024	0.0792	0.0012	0.0247	0.002	0.13101	491.3	7.1	495	15	526	50
Zircon_099	121.6	57.7	0.47	0.061	0.016	0.133	0.033	0.01591	0.00059	0.00584	0.00058	0.15239	101.8	3.7	126	30	1010	310
Zircon_100	1000	1176	1.18	0.0487	0.0022	0.0867	0.004	0.01287	0.00018	0.00401	0.00022	0.29349	83.1	1.1	84.4	3.7	194	56

C.5. Sample SP3-87

	U (ppm) ¹	Th (ppm) ¹	Th/U	CORRECTED RATIOS ²			CORRECTED AGES (Ma)											
				²⁰⁷ Pb/ ²⁰⁶ Pb ±2. abs	²⁰⁷ Pb/ ²³⁵ U ±2. abs	²⁰⁶ Pb/ ²³⁸ U ±2. abs	²⁰⁶ Pb/ ²³⁵ U ±2. abs	²⁰⁷ Pb/ ²³⁵ U ±2. abs	²⁰⁷ Pb/ ²⁰⁶ Pb ±2. abs									
Zircon_001_SP3-87	333.3	233.5	0.70	0.0542	0.004	0.346	0.026	0.0465	0.00099	0.0143	0.0011	0.057808	293	6.1	302	20	378	92
Zircon_002	295.8	150.79	0.51	0.0529	0.0035	0.347	0.024	0.04749	0.00089	0.0152	0.0012	0.10468	299.1	5.5	302	18	333	98
Zircon_003	328.1	216	0.66	0.0537	0.0036	0.36	0.025	0.04875	0.00093	0.0149	0.0012	0.028926	306.9	5.7	314	17	367	85
Zircon_004	248.4	146.5	0.59	0.0613	0.0044	0.388	0.029	0.046	0.0011	0.0144	0.0011	0.39567	289.6	6.5	332	22	660	110
Zircon_005	318.6	202.9	0.64	0.0525	0.0034	0.35	0.024	0.04825	0.00092	0.0145	0.0012	0.027112	303.8	5.7	305	18	322	77
Zircon_006	251	152.7	0.61	0.0554	0.0037	0.366	0.026	0.04842	0.00094	0.0149	0.0012	0.62501	304.8	5.8	316	20	431	80
Zircon_007	324.7	188.1	0.58	0.0575	0.0043	0.381	0.029	0.04857	0.00097	0.0152	0.0012	0.12348	305.7	6	327	24	540	110
Zircon_008	80.8	58.5	0.72	0.0639	0.0049	0.41	0.031	0.0468	0.0011	0.0147	0.0012	0.310863	294.7	6.5	348	22	720	120
Zircon_009	301.9	156.8	0.52	0.0535	0.006	0.144	0.014	0.01967	0.00055	0.0604	0.00055	0.287603	125.6	3.5	136	13	363	98
Zircon_010	351	228.8	0.65	0.0679	0.0047	0.451	0.032	0.04818	0.00089	0.0171	0.0014	0.260345	303.4	5.5	377	22	880	110
Zircon_011	334.5	192.2	0.57	0.0542	0.0038	0.354	0.026	0.04745	0.00093	0.0152	0.0012	0.30466	298.9	5.7	307	20	410	120
Zircon_012	311.5	186.6	0.60	0.0606	0.0043	0.382	0.028	0.04633	0.00096	0.0159	0.0012	0.26192	291.9	5.9	329	21	650	140
Zircon_013	187	109.2	0.58	0.0555	0.005	0.371	0.031	0.0478	0.0011	0.0145	0.0012	0.275408	300.8	6.6	320	23	400	110
Zircon_014	260.7	413	1.58	0.0622	0.0042	0.931	0.064	0.1073	0.002	0.0322	0.0027	0.19375	657	11	667	39	714	97
Zircon_015	408.5	80.4	0.24	0.0602	0.0042	0.189	0.033	0.04463	0.00044	0.0666	0.00066	0.172249	93.6	2.8	475	28	4560	240
Zircon_016	366	250.8	0.69	0.0567	0.0045	0.353	0.028	0.0456	0.001	0.0137	0.0011	0.097395	287.7	6.3	306	21	470	100
Zircon_017	185.1	112.7	0.61	0.0602	0.0043	0.4	0.028	0.0489	0.0011	0.0151	0.0012	0.321356	307.5	7	342	20	620	120
Zircon_018	567	382	0.67	0.0542	0.0039	0.365	0.026	0.04936	0.00099	0.0156	0.0027	0.056977	310.6	6.1	315	19	379	79
Zircon_019	316	276	0.87	0.0531	0.0037	0.346	0.025	0.04747	0.00097	0.0147	0.0012	0.097498	299	6	301	19	380	100
Zircon_020	168.7	106.8	0.63	0.0558	0.0046	0.396	0.033	0.052	0.0012	0.0168	0.0013	0.276923	326.7	7.3	338	24	481	90
Zircon_021	249.5	147.3	0.59	0.0556	0.0045	0.363	0.031	0.04739	0.00088	0.0142	0.0012	0.46311	298.5	5.4	314	23	462	83
Zircon_022	170	126.7	0.75	0.0578	0.0048	0.383	0.031	0.0481	0.0011	0.0152	0.0013	0.282543	302.8	6.7	328	23	549	95
Zircon_023	298	429	1.44	0.0546	0.0048	0.341	0.028	0.0464	0.001	0.0138	0.0011	0.262469	292.3	6.2	298	21	390	130
Zircon_024	138.2	94.8	0.69	0.0537	0.0047	0.363	0.033	0.0469	0.0011	0.0159	0.0013	0.008823	307.6	6.9	314	25	400	130
Zircon_025	179.2	203.7	1.14	0.0568	0.0066	0.367	0.042	0.0471	0.0013	0.0143	0.0012	0.241179	296.7	8.2	317	31	530	72
Zircon_026	604	360.8	0.60	0.054	0.0036	0.345	0.024	0.04685	0.00095	0.0151	0.0012	0.079884	295.2	5.8	303	18	376	84
Zircon_027	228.8	128.2	0.56	0.0552	0.0042	0.367	0.03	0.0489	0.0011	0.0147	0.0016	0.275187	307.9	6.5	321	20	376	83
Zircon_028	299.8	195.9	0.65	0.0524	0.0036	0.339	0.024	0.04691	0.00087	0.0148	0.0011	0.16507	295.5	5.4	296	18	310	100
Zircon_029	655	364	0.56	0.0525	0.0032	0.347	0.023	0.04784	0.00085	0.0149	0.0012	0.10932	301.2	5.2	302	17	316	85
Zircon_030	100.6	71.3	0.71	0.0565	0.006	0.393	0.04	0.0517	0.0012	0.0171	0.0014	0.18697	324.8	7.3	335	29	540	150
Zircon_031	152.1	164.3	1.08	0.0544	0.0045	0.354	0.029	0.048	0.00099	0.0154	0.0012	0.251767	302.2	6.1	307	22	366	91
Zircon_032	581	340.5	0.59	0.0544	0.0043	0.346	0.031	0.04643	0.00089	0.0154	0.0012	0.55459	292.5	5.5	302	23	379	40
Zircon_033	222	158.8	0.72	0.0648	0.0066	0.42	0.042	0.04702	0.00097	0.016	0.0014	0.078043	296.2	6	355	30	690	110
Zircon_034	340.3	216.7	0.64	0.0678	0.0053	0.442	0.042	0.0487	0.0011	0.0179	0.0032	0.035972	306.7	6.7	371	30	778	76
Zircon_035	275	140.7	0.51	0.0566	0.0062	0.335	0.033	0.04437	0.0009	0.0151	0.0012	0.205913	279.9	5.5	293	25	530	100
Zircon_036	448	373.9	0.83	0.0617	0.0042	0.398	0.028	0.0467	0.00098	0.016	0.0012	0.14732	294.2	6.1	340	20	660	110
Zircon_037	127	114	0.90	0.0563	0.0052	0.394	0.037	0.0516	0.0015	0.0164	0.0016	0.4508	324.3	9.1	336	27	490	120
Zircon_038	507.8	502.6	0.99	0.0504	0.0042	0.134	0.012	0.01959	0.00038	0.0626	0.00046	0.216607	125.1	2.4	127	11	375	75
Zircon_039	499	460	0.92	0.0526	0.0038	0.323	0.024	0.04603	0.00086	0.0141	0.0012	0.046067	279.6	5.3	284	19	298	87
Zircon_040	380.8	416.9	1.09	0.0545	0.0045	0.34	0.028	0.04549	0.00087	0.0143	0.0011	0.232233	286.8	5.4	297	21	430	110
Zircon_041	234	209	0.89	0.0749	0.009	0.462	0.048	0.04572	0.00053	0.06638	0.0002	0.303435	400.6	3.4	453	46	660	240
Zircon_042	674.2	444.5	0.66	0.0566	0.0052	0.0992	0.0089	0.01278	0.00028	0.00468	0.00038	0.244202	81.9	1.8	95.9	8.3	480	130
Zircon_043	196	113.6	0.58	0.0527	0.0045	0.334	0.029	0.04609	0.00096	0.0149	0.0012	0.23989	290.4	5.9	292	22	380	110
Zircon_044	231.9	198.7	0.86	0.053	0.0038	0.344	0.025	0.0475	0.00099	0.0154	0.0012	0.32481	295.1	6.1	300	19	359	94
Zircon_045	271	131.6	0.49	0.0794	0.0092	0.514	0.07	0.0474	0.0014	0.0212	0.0017	0.78864	298.8	8.8	418	45	1260	220
Zircon_046	417	279	0.67	0.0544	0.0036	0.357	0.024	0.04765	0.00095	0.0163	0.0013	0.296563	300.1	5.8	310	18	540	310
Zircon_047	206	105.7	0.51	0.0541	0.0056	0.351	0.036	0.0479	0.001	0.0165	0.0013	0.24914	301.3	6.4	304	27	360	130
Zircon_048	644	493	0.77	0.058	0.0041	0.1106	0.0085	0.014	0.00028	0.00496	0.00043	0.27793	89.6	1.8	106.5	7.8	490	110
Zircon_049	235	161	0.69	0.053	0.0044	0.352	0.03	0.04813	0.00099	0.0157	0.0014	0.241346	303	6.1	305	23	450	120
Zircon_050	144.1	103.2	0.72	0.0535	0.0064	0.352	0.043	0.04767	0.00095	0.0159	0.0015	0.42165	300.2	5.8	310	33	372	94

	CORRECTED RATIOS ²				CORRECTED RATIOS ²				CORRECTED AGES (Ma)								
	U (ppm) ¹	Th (ppm) ¹	²⁰⁷ Pb/ ²⁰⁶ Pb ±2.1 abs	²⁰⁷ Pb/ ²³⁵ U ±2.1 abs	²⁰⁶ Pb/ ²³⁸ U ±2.1 abs	²⁰⁶ Pb/ ²³² Th ±2.1 abs	Rho	²⁰⁶ Pb/ ²³⁸ U ±2.1	²⁰⁷ Pb/ ²³⁵ U ±2.1	²⁰⁷ Pb/ ²⁰⁶ Pb ±2.1							
Zircon_051	257.5	156.9	0.0521	0.0039	0.339	0.026	0.04743	0.00092	0.016	0.0012	0.18097	298.7	5.6	296	20	272	94
Zircon_052	393.1	263.7	0.0511	0.0043	0.355	0.04	0.0479	0.0015	0.0163	0.002	0.096487	301.4	9.3	308	30	350	300
Zircon_053	273.5	151.8	0.0499	0.0048	0.326	0.032	0.04725	0.00097	0.0158	0.0012	0.2622	297.6	6	285	24	300	110
Zircon_054	231.1	191.7	0.053	0.013	0.168	0.04	0.02295	0.00059	0.00856	0.0008	0.23102	146.3	3.7	156	35	800	300
Zircon_055	275.3	181.7	0.0582	0.0064	0.361	0.032	0.0469	0.0012	0.0168	0.0013	0.288646	295.5	7.1	313	35	550	100
Zircon_056	341	260.5	0.0805	0.0061	0.537	0.04	0.04808	0.0009	0.0202	0.0015	0.2513	302.7	5.5	436	26	1198	30
Zircon_057	202.6	117	0.0538	0.0076	0.334	0.048	0.0453	0.0012	0.0152	0.0015	0.184327	285.5	7.4	291	37	460	170
Zircon_058	313	301	0.063	0.0047	0.359	0.033	0.04997	0.00096	0.0163	0.0015	0.57179	314.3	5.9	310	24	510	230
Zircon_059	227.5	211.3	0.0567	0.009	0.372	0.056	0.0476	0.0011	0.0154	0.0012	0.153511	299.8	6.7	319	43	530	130
Zircon_060	280.8	157.6	0.0474	0.006	0.086	0.011	0.01317	0.00032	0.00362	0.00043	0.065445	84.4	2	83	10	348	87
Zircon_061	403.8	76.3	0.0492	0.0076	0.332	0.056	0.048	0.0012	0.0138	0.0013	0.63194	302.3	7.4	286	42	530	280
Zircon_062	712.1	641	0.0579	0.0044	0.388	0.028	0.0463	0.001	0.015	0.0012	0.283863	291.7	6.2	318	21	510	120
Zircon_063	348	320	0.0989	0.0064	0.682	0.046	0.04985	0.00095	0.0204	0.0017	0.16197	313.6	5.8	527	28	4605	46
Zircon_064	288.3	231.7	0.054	0.01	0.352	0.063	0.04706	0.00089	0.0145	0.0013	0.105667	296.4	5.5	306	47	390	180
Zircon_065	413.4	249.7	0.0685	0.0054	0.451	0.038	0.04785	0.00095	0.0185	0.0019	0.48072	301.3	5.8	377	27	870	130
Zircon_066	164.7	88.4	0.0534	0.0064	0.352	0.043	0.0477	0.001	0.0152	0.002	0.25513	300.4	6.4	302	31	460	220
Zircon_067	462	333.5	0.051	0.004	0.339	0.026	0.0486	0.0011	0.0144	0.0011	0.295109	305.9	6.7	296	20	185	77
Zircon_068	236.1	183.5	0.0528	0.0038	0.34	0.026	0.04704	0.00091	0.015	0.0012	0.50179	296.3	5.6	297	20	330	100
Zircon_069	325.5	322.1	0.051	0.0045	0.326	0.031	0.04605	0.00087	0.0141	0.0011	0.51073	290.2	5.4	286	24	270	120
Zircon_070	213.3	163.4	0.0536	0.0048	0.352	0.032	0.0476	0.001	0.0148	0.0014	0.088396	300	6.2	305	24	410	100
Zircon_071	67.2	38.83	0.09	0.017	0.6	0.11	0.0474	0.0016	0.0216	0.002	0.2364	298.3	9.2	468	72	4500	450
Zircon_072	207.1	402.4	0.076	0.022	0.418	0.034	0.04136	0.00099	0.0047	0.0068	0.070243	72.8	2.5	112	31	410	230
Zircon_073	235.3	274.1	0.0521	0.0042	0.331	0.027	0.04671	0.0009	0.0145	0.0011	0.090677	294.3	5.5	289	20	410	120
Zircon_074	222.9	130.7	0.0548	0.0056	0.357	0.035	0.0475	0.001	0.0142	0.0012	0.214737	298.9	6.4	310	26	474	98
Zircon_075	120	94.6	0.0552	0.0051	0.371	0.036	0.0491	0.0012	0.0153	0.0013	0.09827	308.8	7.4	320	26	410	77
Zircon_076	353.9	232.5	0.0535	0.0043	0.357	0.032	0.0472	0.001	0.0147	0.0012	0.14845	297	6.3	309	24	416	96
Zircon_077	358	304	0.0536	0.0038	0.358	0.027	0.0485	0.001	0.0149	0.0012	0.48598	305.3	6.2	311	20	367	80
Zircon_078	215.4	125.9	0.0608	0.0074	0.402	0.047	0.0479	0.0011	0.0153	0.0014	0.19642	301.4	6.8	343	34	704	65
Zircon_079	70	60.4	0.049	0.019	0.082	0.031	0.01124	0.0005	0.00341	0.00069	0.13033	72.1	3.2	76	29	1600	350
Zircon_080	166.5	87.71	0.0621	0.009	0.126	0.019	0.0147	0.00037	0.00468	0.00058	0.31061	94.1	2.4	120	17	750	200
Zircon_081	134	75.2	0.0591	0.0054	0.4	0.035	0.0497	0.001	0.0159	0.0016	0.229951	312.6	6.4	341	25	620	110
Zircon_082	190	122.9	0.0539	0.0042	0.358	0.029	0.04822	0.00094	0.0141	0.0011	0.24065	303.6	5.8	315	24	430	180
Zircon_083	126	63.5	0.056	0.013	0.085	0.017	0.01164	0.00051	0.00353	0.00049	0.219072	74.6	3.2	83	16	870	230
Zircon_084	179.9	103.7	0.0515	0.0042	0.325	0.028	0.0456	0.0011	0.0144	0.0012	0.279997	287.8	6.7	285	22	320	110
Zircon_085	597	634	0.0525	0.0032	0.328	0.021	0.04538	0.00087	0.0133	0.0011	0.12945	286.1	5.3	288	16	317	62
Zircon_086	84.6	112	0.0591	0.0089	0.405	0.057	0.0503	0.0018	0.0141	0.0013	0.254264	316	11	343	42	610	210
Zircon_087	265	443	0.0535	0.0043	0.357	0.029	0.04856	0.00093	0.0142	0.0011	0.15018	305.7	5.7	310	22	386	65
Zircon_088	231	140.8	0.0517	0.0038	0.339	0.025	0.0476	0.00089	0.0143	0.0012	0.253538	299.7	5.5	296	19	309	88
Zircon_089	81.9	37.7	0.06	0.013	0.358	0.067	0.0462	0.0014	0.0132	0.0015	0.1295	290.8	8.5	308	50	680	190
Zircon_090	216.7	126.1	0.0533	0.0045	0.348	0.027	0.0475	0.001	0.0142	0.0011	0.271345	298.9	6.3	303	21	410	150
Zircon_091	160.5	106.7	0.0556	0.0046	0.364	0.03	0.0477	0.001	0.0141	0.0012	0.055333	300.3	6.4	314	22	447	90
Zircon_092	101.4	48.2	0.06	0.02	0.093	0.031	0.01117	0.00073	0.00464	0.00083	0.196061	71.6	4.6	89	29	910	270
Zircon_093	211.9	118.1	0.0543	0.005	0.355	0.034	0.0476	0.0011	0.0155	0.0014	0.51278	299.6	6.8	308	26	470	200
Zircon_094	359	186.6	0.0545	0.0041	0.34	0.027	0.04537	0.00085	0.0133	0.0011	0.33156	286.1	5.2	297	20	420	140
Zircon_095	369.5	358	0.0719	0.005	0.456	0.033	0.0461	0.001	0.0153	0.0012	0.38443	290.3	6.3	381	23	971	80
Zircon_096	136.4	93.51	0.0546	0.0067	0.338	0.041	0.04533	0.00091	0.0136	0.0013	0.165496	285.8	5.6	295	31	560	180
Zircon_097	287.5	107.9	0.0606	0.0037	0.835	0.054	0.1	0.002	0.0328	0.0027	0.46803	614	12	616	32	628	90
Zircon_098	713	653	0.0606	0.0038	0.387	0.025	0.04661	0.00096	0.0141	0.0012	0.318833	293.6	5.9	332	19	616	92
Zircon_099	491	454	0.0542	0.0037	0.361	0.026	0.04839	0.00095	0.0144	0.0011	0.22974	304.6	5.9	313	20	371	97
Zircon_100	178.1	92.9	0.0575	0.0051	0.376	0.032	0.0482	0.0011	0.0153	0.0012	0.084931	303.7	7	323	24	479	88

C.6. Sample K-4

	U (ppm) ¹	Th (ppm) ¹	Th/U	²⁰⁷ Pb/ ²⁰⁶ Pb ±2.1 abs	²⁰⁷ Pb/ ²³⁵ U ±2.1 abs	²⁰⁶ Pb/ ²³⁸ U ±2.1 abs	²⁰⁶ Pb/ ²³⁵ Th ±2.1 abs	Rho	²⁰⁶ Pb/ ²³⁸ U ±2.1	²⁰⁷ Pb/ ²³⁵ U ±2.1	CORRECTED AGES (Ma) ²⁰⁷ Pb/ ²⁰⁶ Pb ±2.1							
Zircon_001_01	135	107	0.71	0.05463	0.00502	0.29632	0.02404	0.03979	0.00122	0.01245	0.00088	-0.19	252	8	264	18	397	202
Zircon_002_01	52	28	0.48	0.04733	0.00964	0.11799	0.024	0.01807	0.00096	0.00648	0.00072	0.13	115	6	113	22	66	406
Zircon_003_01	1328	2580	1.74	0.04999	0.0026	0.25708	0.01334	0.03724	0.00086	0.01109	0.00062	0.22	236	6	232	10	195	118
Zircon_004_01	132	168	1.44	0.05468	0.01018	0.296	0.06038	0.03926	0.00128	0.01226	0.0004	0.05	248	8	263	48	399	412
Zircon_005_01	186	89	0.43	0.05289	0.0042	0.2386	0.01894	0.03275	0.00086	0.01002	0.00072	0.16	208	6	217	16	324	176
Zircon_006_02	145	172	1.06	0.05669	0.00812	0.31749	0.05252	0.04062	0.00136	0.01263	0.00034	0.3	257	8	280	40	479	314
Zircon_007_02	608	382	0.56	0.05232	0.00294	0.26346	0.01482	0.03649	0.00084	0.01118	0.00064	0.21	231	6	237	12	299	124
Zircon_008_02	423	96	0.70	0.04746	0.00406	0.27442	0.0242	0.04473	0.00104	0.01264	0.00076	0.28	264	6	246	20	342	182
Zircon_009_02	90	36	0.36	0.06115	0.0085	0.13847	0.01874	0.01666	0.00058	0.00547	0.0005	0.02	107	4	132	16	645	296
Zircon_010_02	75	58	0.69	0.05185	0.00516	0.28338	0.02814	0.03991	0.0011	0.01303	0.00092	0.13	252	6	253	22	279	224
Zircon_011_02	278	145	0.47	0.05147	0.0039	0.23552	0.01786	0.03314	0.00084	0.01056	0.00064	0.17	210	6	215	14	262	170
Zircon_012_02	402	425	1.05	0.06664	0.007	0.25596	0.038	0.04888	0.0012	0.01243	0.00078	0.2	245	8	249	28	327	216
Zircon_013_02	102	75	0.66	0.05539	0.0048	0.33911	0.02994	0.04437	0.00116	0.01338	0.00088	0.21	280	8	296	22	428	190
Zircon_014_03	83	60	0.64	0.05261	0.00484	0.28679	0.02636	0.03977	0.00122	0.01251	0.00086	0.16	251	8	256	20	312	206
Zircon_015_03	95	66	0.62	0.05288	0.00476	0.26477	0.02434	0.03628	0.00092	0.01167	0.00098	0.21	230	6	239	20	324	200
Zircon_016_03	361	428	1.06	0.05563	0.00366	0.35679	0.02462	0.04613	0.00108	0.01445	0.00084	0.3	291	6	310	18	438	142
Zircon_017_03	155	123	0.71	0.05312	0.0035	0.34948	0.02354	0.04759	0.0011	0.01452	0.00088	0.23	300	6	304	18	334	146
Zircon_018_03	176	139	0.71	0.05455	0.01274	0.30916	0.08122	0.04111	0.00122	0.01284	0.00046	0.92	260	8	274	62	394	510
Zircon_020_03	154	103	0.60	0.05237	0.0038	0.2395	0.01694	0.03324	0.00082	0.01105	0.00082	0.1	211	6	218	14	302	162
Zircon_021_04	180	211	1.05	0.05388	0.00456	0.258	0.02186	0.03477	0.00102	0.01061	0.00074	0.18	220	6	233	18	366	186
Zircon_022_04	76	60	0.71	0.05426	0.0053	0.35594	0.03272	0.04768	0.00132	0.01499	0.001	-0.06	300	8	309	24	382	216
Zircon_023_04	44	23	0.46	0.06399	0.01102	0.20856	0.03346	0.02423	0.00104	0.00824	0.00114	-0.15	154	6	192	28	741	364
Zircon_024_04	180	175	0.87	0.05448	0.00432	0.29501	0.02342	0.03911	0.00096	0.01196	0.00072	0.16	247	6	262	18	391	174
Zircon_025_04	173	83	0.43	0.05509	0.00516	0.12939	0.01214	0.01717	0.00056	0.0057	0.00046	0.18	110	4	124	10	416	206
Zircon_026_04	342	227	0.59	0.05299	0.00366	0.26041	0.01798	0.03561	0.00082	0.01124	0.00066	0.17	226	6	235	14	328	154
Zircon_027_04	284	172	0.54	0.05307	0.00316	0.35631	0.02168	0.0484	0.00124	0.01591	0.00098	0.26	305	8	309	16	332	132
Zircon_028_05	130	154	1.06	0.05508	0.00448	0.28956	0.02298	0.03811	0.00098	0.01201	0.00076	0.08	241	6	258	18	415	178
Zircon_030_05	59	39	0.60	0.05262	0.00762	0.25886	0.03452	0.03614	0.00118	0.01003	0.0009	-0.24	229	8	234	28	312	318
Zircon_031_05	228	232	0.91	0.04933	0.0085	0.28036	0.05318	0.04122	0.0012	0.01303	0.00088	0.34	260	8	251	42	164	372
Zircon_032_05	106	53	0.45	0.05174	0.00572	0.11981	0.01302	0.01681	0.00052	0.00557	0.00044	0.08	107	4	115	12	274	244
Zircon_033_05	168	186	0.99	0.05011	0.0033	0.26451	0.01782	0.03819	0.00094	0.0124	0.00074	0.24	242	6	238	14	200	148
Zircon_034_05	306	161	0.47	0.05139	0.00306	0.05139	0.02138	0.04942	0.00136	0.01562	0.00094	0.27	311	8	306	16	258	132
Zircon_035_05	67	33	0.44	0.05718	0.00918	0.19211	0.0312	0.02433	0.00092	0.00866	0.00084	0.17	155	6	178	26	499	346
Zircon_036_06	78	53	0.61	0.06316	0.00604	0.42494	0.03908	0.04866	0.00142	0.01592	0.0011	0.03	308	8	360	28	714	198
Zircon_037_06	116	76	0.59	0.05651	0.00448	0.26785	0.02032	0.03456	0.00096	0.0106	0.0007	0.06	219	6	241	16	472	170
Zircon_038_06	62	32	0.46	0.05063	0.01036	0.16808	0.03804	0.02408	0.00096	0.00759	0.001	0.39	153	6	158	34	224	436
Zircon_039_06	252	55	0.20	0.08038	0.00386	2.2697	0.10882	0.2043	0.0045	0.06032	0.00342	0.23	1198	24	1203	34	1206	92
Zircon_040_06	218	143	0.59	0.05389	0.004	0.25519	0.01848	0.03446	0.00086	0.01198	0.00074	0.1	218	6	231	14	366	162
Zircon_041_06	52	31	0.54	0.05533	0.00694	0.27386	0.03286	0.03653	0.00126	0.01174	0.00088	-0.03	231	8	246	26	417	274
Zircon_042_07	161	103	0.57	0.0536	0.00388	0.3004	0.02176	0.04069	0.001	0.01267	0.00078	0.17	257	6	267	16	354	158
Zircon_043_07	57	36	0.57	0.06264	0.00812	0.1921	0.02342	0.0226	0.00078	0.0073	0.00064	-0.09	144	4	178	20	696	270
Zircon_044_07	282	221	0.70	0.05171	0.00316	0.30347	0.01846	0.04248	0.001	0.01278	0.0007	0.18	268	6	269	14	773	136
Zircon_045_07	482	100	0.19	0.05478	0.00286	0.47249	0.02452	0.06245	0.00146	0.01967	0.00114	0.21	391	8	393	16	403	114
Zircon_046_07	168	134	0.71	0.05533	0.0041	0.38114	0.02826	0.04994	0.0013	0.01566	0.00094	0.18	314	8	328	20	426	160
Zircon_047_07	13	11	0.72	0.06463	0.00812	0.9701	0.11824	0.11008	0.00416	0.03377	0.00312	0.05	673	24	689	60	762	258
Zircon_048_07	343	237	0.62	0.05302	0.0034	0.29112	0.01818	0.04006	0.00104	0.01285	0.00076	0.14	253	6	259	14	330	140
Zircon_050_08	140	137	0.88	0.05901	0.0086	0.28431	0.04556	0.03494	0.00118	0.01081	0.00034		221	8	254	36	567	310

	U (ppm)	Th (ppm)	Th/U	$^{207}\text{Pb}/^{206}\text{Pb}$	$^{207}\text{Pb}/^{235}\text{U}$	$^{206}\text{Pb}/^{238}\text{U}$	$^{206}\text{Pb}/^{235}\text{U}$	$^{206}\text{Pb}/^{232}\text{Th}$	Rho	$^{206}\text{Pb}/^{238}\text{U}$	$^{207}\text{Pb}/^{235}\text{U}$	CORRECTED AGES (Ma)						
				$\pm 2\%$ abs	$\pm 2\%$ abs	$\pm 2\%$ abs	$\pm 2\%$ abs	$\pm 2\%$ abs		$\pm 2\%$	$\pm 2\%$	$\pm 2\%$						
Zircon_051_08	162	124	0.69	0.05584	0.0064	0.27164	0.03498	0.03528	0.00106	0.01099	0.0003	0.1	224	6	244	28	446	248
Zircon_052_08	495	256	0.46	0.06833	0.00438	0.77493	0.04132	0.08304	0.00208	0.02491	0.00156	-0.24	514	12	583	24	879	128
Zircon_053_08	108	51	0.43	0.05365	0.00634	0.12104	0.01338	0.01665	0.00054	0.00568	0.00046	-0.1	106	4	116	12	356	260
Zircon_054_08	620	935	1.35	0.05282	0.00306	0.26686	0.0154	0.0367	0.00082	0.01125	0.00062	0.18	232	6	240	12	321	128
Zircon_055_08	151	456	2.70	0.05181	0.00402	0.14305	0.01844	0.03996	0.00088	0.01036	0.00058	0.1	215	6	221	16	277	172
Zircon_056_09	91	55	0.54	0.05931	0.01126	0.15298	0.02842	0.01908	0.00072	0.00635	0.00005	-0.01	122	4	145	26	579	406
Zircon_057_09	98	74	0.68	0.05422	0.00422	0.37704	0.0306	0.05032	0.00148	0.01626	0.0011	0.29	316	10	325	22	380	170
Zircon_058_09	162	140	0.78	0.05612	0.00756	0.33689	0.05188	0.04354	0.00134	0.01355	0.00034	0.41	275	8	295	40	457	292
Zircon_059_09	59	47	0.72	0.05366	0.00644	0.24887	0.02938	0.03333	0.00114	0.01008	0.00076	0.09	211	8	226	24	357	262
Zircon_060_09	247	222	0.80	0.05483	0.00334	0.35176	0.02086	0.0464	0.00108	0.01397	0.00008	0.13	292	6	306	16	405	132
Zircon_061_09	131	97	0.66	0.0551	0.0039	0.3593	0.02602	0.04732	0.00124	0.01441	0.001	0.24	298	8	312	20	416	154
Zircon_062_09	66	60	0.81	0.06222	0.0095	0.35294	0.06024	0.04114	0.00138	0.01265	0.00038	0.23	260	6	307	46	682	320
Zircon_063_09	66	30	0.41	0.05792	0.00652	0.13524	0.01572	0.01694	0.00064	0.00564	0.00052	0.26	108	4	129	14	527	240
Zircon_064_10	470	1124	2.14	0.05183	0.00316	0.15496	0.00918	0.0217	0.00054	0.00653	0.00036	0.14	138	4	146	8	278	136
Zircon_065_10	170	132	0.69	0.05636	0.00326	0.58347	0.0337	0.07508	0.00176	0.02284	0.0013	0.2	467	10	467	22	467	124
Zircon_066_10	543	214	0.35	0.06873	0.0033	1.6549	0.07934	0.17432	0.00388	0.05044	0.00278	0.23	1036	22	991	30	891	96
Zircon_067_10	82	58	0.63	0.05376	0.00504	0.2888	0.02602	0.03955	0.0011	0.01193	0.00074	0.02	250	6	258	20	361	206
Zircon_068_10	79	50	0.57	0.05785	0.0049	0.31509	0.02612	0.03952	0.00102	0.01247	0.00082	0.08	278	6	278	20	524	180
Zircon_069_10	307	172	0.50	0.04905	0.00356	0.13391	0.00946	0.01982	0.00048	0.00644	0.0004	0.09	127	4	128	8	150	162
Zircon_070_10	335	25	0.07	0.04983	0.00362	0.16488	0.01166	0.02406	0.0006	0.00871	0.00078	0.1	153	4	155	10	187	138
Zircon_071_11	240	99	0.37	0.05357	0.00336	0.33757	0.02108	0.04568	0.00106	0.01437	0.0006	0.02	288	6	295	16	353	138
Zircon_072_11	601	83	0.12	0.06197	0.00384	0.54544	0.03396	0.06383	0.00174	0.01964	0.0006	0.07	399	10	442	22	673	128
Zircon_074_11	76	40	0.47	0.05453	0.00562	0.35534	0.03594	0.0472	0.0013	0.01517	0.00102	0.07	297	8	309	26	393	224
Zircon_075_11	70	48	0.61	0.0534	0.00462	0.29605	0.02454	0.04052	0.00126	0.01262	0.00094	0.07	256	8	263	20	346	190
Zircon_076_11	558	455	0.73	0.05343	0.00294	0.26795	0.01468	0.03636	0.00082	0.01159	0.00097	0.2	230	6	241	12	347	120
Zircon_077_11	109	70	0.58	0.05117	0.00328	0.33676	0.02212	0.04786	0.00124	0.01555	0.00092	0.26	301	8	295	16	248	142
Zircon_078_12	309	197	0.57	0.06832	0.01176	0.57729	0.03162	0.06796	0.0027	0.02239	0.0013	-5.76	424	16	463	20	878	384
Zircon_079_12	221	185	0.75	0.0604	0.00314	0.67884	0.03524	0.08129	0.00182	0.02428	0.00138	0.21	504	10	526	22	618	118
Zircon_080_12	81	53	0.59	0.05696	0.00462	0.28768	0.02386	0.03644	0.00094	0.01148	0.00078	0.23	231	6	257	18	490	188
Zircon_081_12	131	129	0.88	0.06447	0.00536	0.31615	0.02454	0.03606	0.00084	0.01277	0.0008	-0.1	228	6	279	18	757	184
Zircon_082_12	199	193	0.87	0.05128	0.00354	0.26998	0.01864	0.03814	0.0009	0.01164	0.00068	0.17	241	6	243	14	253	166
Zircon_084_12	223	151	0.61	0.05419	0.00356	0.30282	0.0189	0.04051	0.00102	0.01267	0.00076	0.07	256	6	269	14	379	156
Zircon_085_12	132	103	0.70	0.05959	0.00392	0.60238	0.03858	0.07338	0.00192	0.02302	0.00138	0.14	456	12	479	24	589	150
Zircon_086_13	147	86	0.52	0.05569	0.00414	0.35674	0.02768	0.04659	0.00122	0.01449	0.00088	0.29	294	8	310	20	440	174
Zircon_087_13	182	182	0.89	0.05511	0.0038	0.29822	0.0191	0.03934	0.001	0.01259	0.00074		249	6	265	14	417	162
Zircon_088_13	64	44	0.44	0.07257	0.0133	0.36248	0.06846	0.06277	0.00146	0.01111	0.0005	-0.6	233	10	348	50	402	402
Zircon_089_13	194	130	0.60	0.05319	0.0056	0.29113	0.03378	0.0397	0.0011	0.01244	0.00034	0.05	251	6	259	26	337	252
Zircon_091_13	78	57	0.65	0.05395	0.00506	0.29701	0.0273	0.04005	0.00124	0.01313	0.00088	0.11	253	8	264	22	369	224
Zircon_092_13	237	290	1.10	0.05922	0.00334	0.37775	0.02068	0.04599	0.00116	0.01477	0.00086	0.16	290	8	325	16	575	128
Zircon_093_13	69	52	0.67	0.05322	0.00404	0.31842	0.02416	0.04343	0.00134	0.01389	0.00106	0.2	274	8	281	18	338	180
Zircon_094_13	20	20	0.87	0.07813	0.00566	0.26613	0.15636	0.1911	0.00558	0.06097	0.00412	0.31	1127	30	1136	52	1150	152
Zircon_095_14	116	74	0.58	0.05687	0.00674	0.24704	0.03172	0.0315	0.00098	0.00979	0.0003	-0.03	200	6	224	26	487	278
Zircon_096_14	323	442	1.22	0.05401	0.00296	0.343	0.01878	0.04609	0.0011	0.01435	0.00082	0.22	290	6	299	14	371	130
Zircon_097_14	62	29	0.41	0.08189	0.00438	2.4105	0.132	0.21311	0.0052	0.06283	0.00366	0.28	1245	28	1246	40	1243	110
Zircon_098_14	140	300	1.91	0.07517	0.00392	1.6874	0.08996	0.16269	0.00416	0.04791	0.00264	0.27	972	24	1004	34	1073	110
Zircon_099_14	180	127	0.63	0.0537	0.00354	0.30345	0.01994	0.04078	0.00094	0.01243	0.00078	0.18	258	6	269	16	358	156
Zircon_100_14	52	49	0.85	0.06015	0.01076	0.30729	0.05956	0.03705	0.0013	0.01144	0.0004	0.07	235	8	272	46	609	416

	U (ppm) ¹	Th (ppm) ¹	Th/U	²⁰⁷ Pb/ ²⁰⁶ Pb	CORRECTED RATIOS ²		Rho	²⁰⁶ Pb/ ²³⁸ U	²⁰⁷ Pb/ ²³⁵ U	CORRECTED AGES (Ma)								
					²⁰⁷ Pb/ ²³⁵ U ±2 abs	²⁰⁶ Pb/ ²³⁸ U ±2 abs				²⁰⁶ Pb/ ²³⁸ U ±2	²⁰⁷ Pb/ ²³⁵ U ±2							
Zircon_051_083	129	125	0.97	0.05941	0.0035	0.69648	0.04512	0.08501	0.00232	0.02597	0.00194	0.42	526	14	537	28	582	124
Zircon_052_084	497	49	0.10	0.05779	0.00266	0.61621	0.03218	0.0771	0.00192	0.02427	0.0019	0.47	479	12	487	20	522	98
Zircon_053_085	113	139	1.23	0.05416	0.00526	0.28578	0.02906	0.0383	0.00116	0.01181	0.00086	0.3	242	8	255	22	378	212
Zircon_054_086	103	64	0.62	0.0603	0.0045	0.72321	0.05692	0.08756	0.00218	0.02729	0.00206	0.32	541	12	553	34	614	156
Zircon_055_087	533	139	0.26	0.06212	0.00294	0.68262	0.03842	0.07972	0.00248	0.0217	0.00162	0.54	494	14	528	24	678	98
Zircon_056_090	66	56	0.84	0.06951	0.0127	0.21035	0.04166	0.02195	0.00078	0.00667	0.00022	0.25	140	4	194	34	914	376
Zircon_057_091	73	33	0.46	0.05656	0.00548	0.35855	0.03612	0.04637	0.00126	0.01575	0.00148	0.27	292	8	311	26	474	210
Zircon_058_092	286	336	1.18	0.05718	0.00376	0.28306	0.03612	0.00092	0.00092	0.01123	0.0008	0.36	229	6	253	16	499	140
Zircon_059_093	113	66	0.59	0.06096	0.0038	0.79931	0.05346	0.09587	0.00236	0.02752	0.00228	0.36	590	14	596	30	638	130
Zircon_060_094	48	104	2.15	0.08585	0.00626	1.3387	0.10414	0.11611	0.00316	0.03632	0.00262	0.35	708	18	863	46	1335	138
Zircon_061_097	346	61	0.18	0.05954	0.00274	0.73016	0.03742	0.08909	0.00202	0.02715	0.00198	0.44	550	12	557	22	587	98
Zircon_063_099	317	133	0.42	0.06496	0.0035	0.59224	0.03986	0.06673	0.0027	0.02168	0.00174	0.6	416	16	472	26	773	110
Zircon_066_104	164	37	0.22	0.0594	0.00328	0.75403	0.04562	0.09217	0.00224	0.03099	0.00244	0.41	568	14	571	26	582	116
Zircon_067_105	277	136	0.49	0.0773	0.00344	1.7995	0.09078	0.16892	0.00402	0.04408	0.00318	0.47	1006	22	1045	32	1129	86
Zircon_068_106	384	191	0.50	0.05467	0.00312	0.35413	0.02192	0.04713	0.00114	0.015	0.00108	0.39	297	8	308	16	399	124
Zircon_070_108	151	74	0.49	0.08655	0.00398	2.4703	0.12982	0.2072	0.0053	0.0461	0.00388	0.48	1214	28	1263	38	1350	86
Zircon_071_111	185	195	1.05	0.0917	0.00408	2.6141	0.13842	0.20768	0.00598	0.02378	0.00184	0.54	1216	32	1305	38	1461	82
Zircon_072_112	193	138	0.71	0.06232	0.00376	0.6813	0.04468	0.07993	0.00204	0.02327	0.0018	0.39	496	12	528	26	685	126
Zircon_073_113	290	87	0.30	0.07361	0.00338	1.6513	0.08462	0.16281	0.0037	0.04754	0.00336	0.44	972	20	990	32	1031	90
Zircon_074_114	117	98	0.84	0.06453	0.00484	0.43744	0.10906	0.04917	0.00196	0.01506	0.00056	0.29	309	12	368	78	759	482
Zircon_075_115	275	93	0.34	0.07447	0.00354	1.1995	0.06366	0.11675	0.00278	0.05951	0.00422	0.44	712	16	800	30	1054	94
Zircon_076_118	40	920	22.88	0.07847	0.00434	2.1858	0.13642	0.20244	0.00582	0.05852	0.00408	0.46	1188	32	1177	44	1159	108
Zircon_077_119	140	156	1.11	0.05952	0.0033	0.71097	0.04322	0.08692	0.00218	0.02546	0.00184	0.41	537	12	545	26	586	118
Zircon_078_120	112	39	0.35	0.0984	0.00438	3.5524	0.1776	0.26203	0.006	0.07937	0.00562	0.46	1500	30	1539	40	1594	82
Zircon_079_121	180	100	0.56	0.06423	0.00324	1.0205	0.05766	0.11541	0.00292	0.03564	0.00252	0.45	704	16	714	28	749	106
Zircon_080_122	163	91	0.56	0.06383	0.00327	1.0031	0.05994	0.11412	0.00364	0.04678	0.00474	0.54	697	22	705	30	736	106
Zircon_081_124	253	161	0.63	0.05912	0.00378	0.29325	0.02004	0.03605	0.00086	0.00977	0.00072	0.35	228	6	261	16	572	138
Zircon_082_125	122	138	1.14	0.0795	0.01404	0.52133	0.10332	0.04756	0.00176	0.01423	0.00042	0.37	300	10	426	68	1185	350
Zircon_083_126	212	134	0.63	0.06292	0.0037	0.55957	0.03622	0.06472	0.00176	0.01104	0.00092	0.42	404	10	451	24	706	124
Zircon_085_128	54	94	1.73	0.06063	0.01562	0.83199	0.2371	0.09952	0.00392	0.0307	0.00108	0.37	612	22	615	132	626	556
Zircon_087_131	84	71	0.84	0.06347	0.0079	0.8488	0.12064	0.097	0.00302	0.02976	0.0008	0.43	597	18	624	66	724	262
Zircon_088_132	336	154	0.46	0.0493	0.00298	0.32409	0.02118	0.04808	0.00118	0.01411	0.00108	0.37	303	8	286	16	162	140
Zircon_089_133	153	76	0.50	0.07157	0.00384	0.92005	0.05514	0.09332	0.00248	0.02853	0.0022	0.45	575	14	662	30	974	108
Zircon_090_134	166	174	1.04	0.10867	0.00452	4.5627	0.21714	0.30449	0.007	0.08476	0.0059	0.49	1714	34	1742	40	1777	74
Zircon_091_136	170	91	0.53	0.05846	0.00344	0.58155	0.03766	0.0724	0.00198	0.02048	0.0015	0.42	451	12	465	24	547	134
Zircon_092_137	156	117	0.75	0.0826	0.00404	1.6995	0.10254	0.14864	0.00524	0.04509	0.00348	0.59	893	30	1008	38	1260	100
Zircon_093_138	96	76	0.79	0.0898	0.01104	0.96429	0.1351	0.07788	0.00242	0.023	0.00066	0.36	483	14	686	70	1421	244
Zircon_094_139	225	236	1.05	0.05456	0.0032	0.36405	0.0232	0.04847	0.0012	0.01529	0.00108	0.39	305	8	315	18	394	136
Zircon_095_140	174	41	0.23	0.06322	0.0034	0.97014	0.0568	0.11178	0.0026	0.03714	0.00286	0.4	683	16	689	30	716	118
Zircon_096_142	116	57	0.49	0.06697	0.0037	1.004	0.06266	0.10965	0.00316	0.0309	0.00222	0.47	671	18	706	32	837	120
Zircon_098_144	73	23	0.31	0.06067	0.00356	0.74325	0.04792	0.08927	0.00238	0.02525	0.0021	0.41	551	14	564	28	628	132
Zircon_099_145	65	30	0.46	0.0665	0.016	0.20147	0.05114	0.02197	0.00094	0.00671	0.0003	0.2	140	6	186	44	822	534
Zircon_100_146	189	107	0.57	0.06051	0.00356	0.64298	0.04068	0.07735	0.00182	0.02479	0.00184	0.37	480	10	504	26	622	132